KfK 3514 B
April 1983

General and Special Engineering Materials Science — Ciencia General y Especial de los Materiales —

Vol. III
- Special Engineering Materials Science - Nuclear Materials under Off-normal Reactor Operation Conditions

P. Hofmann, G. Ondracek
Institut für Material- und Festkörperforschung

Kernforschungszentrum Karlsruhe

KERNFORSCHUNGSZENTRUM KARLSRUHE

Institut für Material- und Festkörperforschung

KfK 3514 B

General and special engineering materials science
- Ciencia General y Especial de los Materiales -

Vol. III - Special engineering materials science - Nuclear Materials under off-normal reactor operation conditions

P. Hofmann, G. Ondracek

Kernforschungszentrum Karlsruhe GmbH, Karlsruhe

Pt UB-Berichte

Die Kernforschungszentrum Karlsruhe GmbH hat im Auftrag des Bundesministers für Forschung und Technologie die Durchführung der Projektträgerschaft für die Aufgabengebiete Universitätsforschung zum nuklearen Brennstoffkreislauf/Stillegung von Nuklearanlagen (Pt UB/SN) übernommen. Im Rahmen dieses Auftrages betreut sie fachlich und administrativ von der Bundesregierung geförderte F + E-Vorhaben an Universitäten/Hochschulen und an wissenschaftlichen Forschungsinstituten der Privatwirtschaft im Bereich des nuklearen Brennstoffkreislaufs sowie F + E-Vorhaben zur Stillegung von Nuklearanlagen. Hierbei arbeitet sie eng mit den an F + E-Arbeiten beteiligten Hochschulen und Firmen der kerntechnischen Industrie zusammen.

Der Projektträger gibt in beiden Arbeitsbereichen eine Schriftenreihe heraus, um alle Beteiligten umgehend über Zwischen- und Endergebnisse der durchgeführten Arbeiten zu informieren.

Der vorliegende Pt UB-Bericht dokumentiert Stand und Ergebnisse der F + E-Vorhaben im Bereich des nuklearen Brennstoffkreislaufs und setzt damit die Berichterstattung der bisherigen Projektbegleitung „F + E-Entsorgung" (PBE-Berichte 1-20) fort. Der Bericht ist nicht zitierfähig. Eine Weitergabe des Berichtes bzw. seines Inhalts kann erst nach Rücksprache mit dem Projektträger UB/SN erfolgen.

Verantwortlich für den Inhalt sind die Autoren. Die Kernforschungszentrum Karlsruhe GmbH übernimmt keine Gewähr insbesondere für die Richtigkeit, Genauigkeit und Vollständigkeit der Angaben sowie die Beachtung privater Rechte Dritter.

Druck und Verbreitung:

Kernforschungszentrum Karlsruhe GmbH
Postfach 3640, 7500 Karlsruhe 1

Printed in Western-Germany

Preface and Summary

The present report about general and special engineering materials science is the result of lectures given by the authors in two terms in 1982 at Instituto Balseiro, San Carlos de Bariloche, the graduated college of the Universidad de Cuyo and Comision Nacional de Energia Atomica, Republica Argentina. These lectures were organised in the frame of the project "nuclear engineering" (ARG/78/020) of the United Nations Development Program (UNDP) by the International Atomic Energy Agency (IAEA).

Some chapters of the report are written in English, others in Spanish. The report is subdivided into three volumes:
Volume I treats general engineering materials science in 4 capital chapters on

- the structure of materials
- the properties of materials
- materials technology
- materials testing and investigation

supplemented by a selected detailed chapter about elasticity plasticity and rupture mechanics.
Volume II concerns special engineering materials science with respect to nuclear materials under normal reactor operation conditions including

- reactor clad and structural materials
- nuclear fuels and fuel elements
- nuclear waste as a materials viewpoint

Volume III - also concerning special engineering materials science - considers nuclear materials with respect to off-normal ("accident") reactor operation conditions including

- nuclear materials in loss-of-coolant accidents
- nuclear materials in core melt accidents.

December 1982 Gerhard Ondracek

P R O L O G O

La presente serie de tres informes procede de un curso de dos semestres sobre ciencias de los materiales en que los autores participaron como docentes invitados en el Instituto Balseiro, para estudiantes de la carrera de Ingenieros Nucleares de la Universidad de Cuyo en San Carlos de Bariloche, dentro del proyecto "Nuclear Engineering" (ARG/78/020) del Organismo Internacional de Energía Atómica (OIEA), United Nations Development Program (UNDP). Los diferentes capítulos están escritos en idioma inglés o español.

El primer informe trata de la ciencia general de los materiales y está subdividido en capítulos sobre:

- la estructura de los materiales
- la tecnología de los materiales y
- el ensayo de materiales

y se completa mediante un capítulo selecto donde se profundiza el tema de las características mecánicas: elasticidad, plasticidad y mecánica de la fractura.

El segundo informe sobre ciencia especial de los materiales trata de los materiales de reactores bajo condiciones normales de funcionamiento del reactor:

- materiales de vaina y de estructura del reactor,
- combustibles nucleares y elementos combustibles,
- desecho nuclear como problema de material.

El tercer informe - también sobre ciencia especial de los materiales - trata de los materiales de reactores bajo condiciones de accidente:

- materiales de reactores en el accidente con pérdida de refrigerante
- materiales de reactores en el accidente de fusión del núcleo del reactor.

Diciembre de 1.982 Gerhard Ondracek

Vorwort und Zusammenfassung

Allgemeine und spezielle Werkstoffkunde

Der vorliegende Report über allgemeine und spezielle Werkstoffkunde ist das Ergebnis von Vorlesungen, die die Autoren über zwei Semester 1982 am Institut Balseiro, dem Graduierten-College der Universität von Cuyo und der Kommission Nacional de Energia Atomica in San Carlos de Bariloche, Argentinien, gehalten haben. Die Vorlesungen wurden im Rahmen des Projektes Kerntechnik (ARG/78/020) des Entwicklungsprogramms der Vereinten Nationen (UNDP) veranstaltet und von der Internationalen Atomenergiebehörde (IAEA) in Wien organisiert.

Einige Kapitel des Reports sind in Englisch geschrieben, andere in Spanisch. Der Report gliedert sich in drei Bände:
Band 1 behandelt die Grundlagen der allgemeinen Werkstoffkunde in 4 Kapiteln über

- den Aufbau von Werkstoffen
- die Eigenschaften von Werkstoffen
- die Werkstofftechnologie
- die Werkstoffprüfung und -untersuchung,

die ergänzt werden durch ausgewählte Kapitel über Elastizität, Plastizität und Bruchmechanik.
Band 2 betrifft spezielle Werkstoffkunde und zwar Reaktorwerkstoffe unter normalen Betriebsbedingungen eines Kernreaktors und behandelt

- Reaktorhüll- und Strukturwerkstoffe
- Nukleare Brennstoffe und Brennelemente
- Nuklearen Abfall und seine Behandlung als Werkstoff

Band 3 betrifft ebenfalls spezielle Werkstoffkunde und behandelt Reaktorwerkstoffe unter Störfallbedingungen, wie den Kühlmittelverlust-Unfall und dem Core-Schmelzunfall.

Dezember 1982 Gerhard Ondracek

Content/Indice

PART I: Behaviour of LWR, HWR and LMFBR oxide fuel rods under normal and off-normal operation conditions

(P. Hofmann)

1) LWR: Light Water Reactor
2) HWR: Heavy Water Reactor

3) LMFBR: Liquid Metal Fast Breeder Reactor

PARTE II: El material y el accidente de fusión del núcleo (seguridad nuclear)

(G. Ondracek)

PART I

Behaviour of LWR, HWR and LMFBR oxide fuel rods under normal and off-normal (accidential)operation conditions

P. Hofmann

N O T E

This report is to provide a general survey of the fuel rod behaviour in LWRs, HWRs and LMFBRs, both under normal reactor operating conditions and under off-normal conditions. The different parameters are described which determine the fuel rod behavior. The individual chapters do not claim to be complete. The fuel rod behavior is described in qualitative terms only. The reader interested in a detailed quantitative description of the fuel rod behavior is referred to the literature listed at the end of the relevant chapters.

A. IRRADIATION AND BURNUP EFFECTS IN LWR AND HWR FUEL RODS

1. Irradiation and burnup effects during steady state reactor operation conditions

1.1 Cladding Irradiation Damage

1.2 Fuel-Cladding Gap Closure and Mechanical Interactions

1.3 Fission Product Effects

1.4 Additional Effects

2. Simulation of Irradiation and Burnup Effects

2.1 Cladding Irradiation Damage

2.2 Fuel-Cladding Mechanical Interactions

2.3 Fission Product Effects

2.4 Additional Phenomena

H. IRRADIATION AND BURNUP EFFECTS IN LWR FUEL RODS DURING STEADY STATE REACTOR OPERATION CONDITIONS

Table 1 presents a general summary of factors affecting fuel rod behaviour. The term "irradiation effect" is applied to these phenomena since all are environmental-service caused, if not directly influenced by the neutron flux-itself.

The effect of probable importance may be grouped in the following categories:

1.1. Cladding Irradiation Damage
1.2 Fuel-Cladding Gap Closure and Mechanical Interaction
1.2.1 Burnup related causes
1.2.1.1. Fuel pellet cracking
1.2.1.2. Cladding creepdown and collapse
1.2.1.3. Internal cladding oxidation
1.2.2. Effects of fuel density and density changes
1.2.3. Results of mechanical interactions
1.2.3.1. Cladding ridging
1.2.3.2. Incipient cladding cracking
1.2.3.3. Rod growth and bowing
1.3. Fission Product Effects
1.3.1. Gas release
1.3.2. Stress corrosion cracking
1.4. Additional Effects
1.4.1. Fuel restructuring
1.4.2. Crud and oxide formation
1.4.3. Oxygen to metal ratio

These effects are briefly discussed in the above order.

1.1. Cladding Irradiation Damage

Neutron irradiation produces substantial increases in the yield and ultimate tensile strengths of zircaloy cladding, accompanied by equally substantial decreases in uniform and total elongations and strain hardenability.

Point defects - vacancies and interstitial atoms - and their aggregates are produced by neutron irradiation. The particular form these defects take depends upon the irradiation temperature. Self-interstitials are

mobile far below room temperature, but vacancies in zircaloy require temperatures on the order of 150°C in order to migrate freely. At irradiation temperatures allowing significant mobility several reactions are possible. Vacancies and interstitials will cluster with their own kind or otherwise become trapped at impurities or dislocations, or will annihilated in another. The dislocation density, as determined by the degree of cold work, then becomes an important factor in determining the damage state. The kind and concentration of impurities is also a significant factor.

As the defect density increases, so does the probability that newly created interstitials and vacancies will be immediately annihilated by previously created nearby defects. The rate of damage production in zircaloy cladding is then greater for fresh material. As exposure continues, the damage rate steadily decreases, as do the accompanying changes in material properties. A saturation level in defect concentration and material properties is reached.

Cladding properties that exhibit saturation include yield stress, ultimate tensile stress, uniform and total elongation, and strain hardenability. The influence required to achieve saturation depends upon material properties of composition, cold work level, specimen orientation (texture) and other fabrication variables. This accounts for the variation in reported results. Strength changes saturate between 10^{21} and 10^{22} n/cm^2 ($E > 1$ MeV), with ductility saturating between 3×10^{19} and 10^{20} n/cm^2.

1.2. Fuel-Cladding Gap Closure and Mechanical Interaction

Gap closure is influenced by the five phenomena discussed below - cladding creepdown, fuel pellet cracking, fuel densification, fuel swelling, and internal cladding oxidation. All of these effects contribute to increased fuel-cladding mechanical interactions.

When a LWR fuel rod is brought to power for the first time, the radial clearance between the pellet stack and the cladding will decrease with increased specific power due to the greater relative thermal expansion

of the fuel and also due to the development of fuel cracks. Cladding creepdown will contribute to gap closure with increasing burnup. Fuel densification is also a factor since it delays swelling, increases the fuel density, and may cause severe fuel-cladding mechanical interactions.

The relative importance of these phenomena varies with rod design and the inreactor environment. Creepdown can be significant in PWR service, but in BWR reactors, the lower system pressure and cladding temperature results in lower creep rates. In extreme cases, for unpressurized PWR fuel rods, fuel stack have occured and complete flattening of the cladding in the gap was observed. Complete collaps has not been observed in prepressurized PWR rods, although creepdown into the fuel is expected for such rods late in life. Fuel swelling is another effect that varies with environment.

In the design of fuel rods, a large gap will delay fuel-cladding interaction but it will also decrease gap conductance. An optimum choice involves a compromise between these effects. Experiments has shown that diametral gaps on the order of 1.5 to 2.5% of the fuel diameter provide satisfactory performance at linear heat generation rates of 33 KW/m or greater.

1.2.1. Burnup Related Causes of Gap Closure and Fuel-Cladding Mechanical Interaction

1.2.1.1. Fuel Pellet Cracking - Fuel pellet cracking is commonly observed in all light water reactors. Out-of-pile experiments have shown that a temperature difference from center to surface of approximately 100°C will initiate cracking. Temperature differences under irradiation are usually more than 400°C, and so cracking is assured.

Fuel pellet cracking is probably one if the principal causes of fuel-cladding gap closure. In fact, it is thought to be the main reason for closure at substantially lower levels than predicted solely by thermal expansion considerations. A thermal expansion mechanism would lead to a direct relationship between initial gap size and the onset of mechanical interactions. The lack of experimental support for a thermal expansion correlation gives credence to the belief that fuel cracking and gap closure are

closely related.

During power increases, tensile stresses occuring in the outer regions of a fuel pellet cause a number of radial cracks to develop from the surface toward the center. Continuing burnup produces swelling in the fuel material which increases the stresses on the pellet fragments as they press against the cladding and each other. At temperatures above approximately 1300-1400°C, the crack will eventually close through plastic flow and resisting of the fuel.

Characterizing the fracture strength of a given oxide fuel composition is not a simple task. In the brittle range, the fracture strength is sensitive to material and environmental conditions, including temperature, stress state, strain rate porosity, grain size, specimen dimensions, surface conditions, and atmosphere.

Attempts have been made to predict fuel cracking based on mechanical data of the fuel. Recent information indicates that there is a possible linear relationship between the average number of radial cracks and the linear heat generation rate and that power cycling does not seem to affect crack patterns.

1.2.1.2 Cladding Creepdown - One of the problems with the use of zirconium alloys as cladding is the increase in creep rate during reactor operation. This enhancement is apparently due to the interaction of irradiation-induced point defects with dislocations. It has been proposed that the creep rate is controlled by the absorption of vacancies and interstitials at dislocations.

Recent work on the inreactor creep of biaxially stressed (by internal pressure) cold-worked zircaloy tubing has given linear relationship between log strain and log time. This implies that

$$\varepsilon = \beta t^{m},$$

where ε is the creep strain, β is a constant for a particular experiment and the power function m is the slope of the log-log curve. There was no significant difference between the unirradiated and the thermal-neutron irradiated tubes, each giving a slope m of 0.24 to 0.27. The samples in a fast flux of 3×10^{13} n/cm^2-sec (E > 1 MeV) gave an increased slope of 0.42 to 0.47. In addition to the significant fast effect, this

result indicates that as test time is double, the creep rate decreases by about 30 per cent.

1.2.1.3. Internal Cladding Oxidation and Fuel Bonding

Oxygen released from fission in the UO_2 fuel is generally thought to be responsible for the buildup of oxide in zircaloy cladding surfaces. These internal cladding oxide layers increase the resistance to heat transfer (slightly) change the surface emissivity characteristics, and later the friction coefficient between the fuel and the cladding.

Bonding will most likely influence the severity of fuel-cladding mechanical interaction, especially during a power increase.

1.2.2 Effects on Fuel Density and Density Changes

Density and porosity substantially affect UO_2 fuel mechanical properties. As a result, fuel density will partially determine the consequences of fuel-cladding mechanical interactions. During reactor service fuel densification and swelling occur. Initial fuel density affects the rate if these processes as well as the magnitude of potential changes.

During reactor operation, both densification and swelling can affect fuel-cladding interactions - densification by causing increased localized cladding stresses upon gap closure, and swelling by contribution to gap closure. Densification is also believed to increase the fuel thermal conductivity and decrease the gap conductance. Swelling has the opposite effects in gap conductance by causing gap closure. The extent to which swelling occurs in LWR fuel is somewhat uncertain.

The rate of densification appears to be dependent upon such things as pore size, grain and stoichiometry. The end result is a pellet or pellet fragments occupying less volume and possessing the thermal and mechanical characteristics of fuel having initially higher fuel density.

1.2.3 Results of Mechanical Interactions.

Fuel-cladding mechanical interactions, occuring due to the effects discussed above (Sections 1.2.1 and 1.2.2), are most certainly involved in fuel rod failures. The role may be direct as, for example, in ridge production, or it may be more indirect, as a partner in stress corrosion cracking (see Section 1.3.2), for example. Four phenomena will be discussed below: Cladding ridging, fuel-cladding bonding, cladding cracking, rod growth and bowing.

1.2.3.1 Cladding Ridging

Cladding ridges are produced by greater radial expansion of the fuel pellet ends than of the pellet centres due to a nonuniform temperature distribution. Nonuniform restrain between the centre and the ends of the pellet can also contribute to this effect.

The amount of ridging depends on the rod power level and on fuel rod design parameter such as fuel density, diametral gap, pellet length, and pellet end shape. Experiments have shown the ridges to consist of a plastic and elastic strain component. The ridges develope during an initial power ramp and increase in height with increasing rod linear power.

Three types of strain concentrations meet at the ridges and make that part of the cladding most susceptible to failure. There are: (a) hoop strain from ridging, (b) axial strain from rod elongation, and (c) hoop strain from longitudinal cracks in the fuel surface. Failure may take place in an axial or transverse direction, depending upon the relative magnitude of these strains. Cladding cracks have been observed to originate at cladding ridges over the pellet-interfaces, and some failure have been reported in which there is a close correlation between failure and pellet cracks.

1.2.3.2 Incipient Cladding Cracking

Incipient cladding cracks are defined to be partially penetrating cracks originating on the inner cladding surface. Some failed rods from test reactors have revealed this phenomenon along with through-cracks. Whether incipient or penetrating, however, cracks are normally found opposite cracks in a fuel pellet, The existence of incipient cracks in unfailed power reactor fuel rods has been disputed, as have the fundamental causes of cracking.

One cracking mechanism has been frequently supported - that involving localized stress concentrations opposite a fuel crack causing overstrain of the embrittled cladding. Another stress-aided mechanism involves the presence of a fission product such as as cesium or iodine (as discussed in Section 1.3.2 - stress corrosion cracking).

1.2.3.3 Rod Growth and Bowing

Cladding axial length changes occur during reactor service and have been attributed to various causes including anisotropic creep, fuel-cladding interactions, and irradiation growth.

Since the fuel pellets do not fill the length of the cladding, axial deformation of the cladding due to fuel-cladding mechanical interaction require large frictional forces. A ratcheting mechanism can provide a means for extensive axial growth. The phenomenon has been observed at powers as low as 6,5 Kw/m and depends upon cladding properties, pellet shape, density, dimensions, and intitial fuel-cladding gap as well as heat load.

Irradiation-induced dimensional changes (irradiation growth) are a function of material anisotropy, fluence, temperature and degree of cold work. The growth mechanism involves selective precipitation of vacancies and interstitials causing shrinkage in one crystallographic direction and elongation in another.

1.3. Fission Product Effects

1.3.1 Gas Release

Fission product gas release results from the inability of uranium dioxide to accumulate within its structure all of the fission product gas atoms that are generated. The pressure developed within a fuel rod by the released gases is a potential performance-limiting phenomenon that must be allowed for in the design of fuel rods. The pressure is determined by a complicated interaction between the release process, the initial gas content of the rod, the space available to accommodate released gas. Consequently, it is not feasible to describe the fission gas pressure quantitatively except by taking into account the detailed operating history of the fuel rod.

Most gas is released discontinuously during power changes and the amount of released gas is highly temperature dependent. Below approximately 1300°C less than 1% of the fission gases are released. Regions of the fuel heated above about 1800°C release 80 to 90% of the generated fission gases. Between 1300 and 1800°C, the gas release fraction is nearly proportional to temperature.

1.3.2 Stress Corrosion Cracking

Stress corrosion cracking (SCC) has received widespread attention as a means of explaining failure of zircaloy clad fuel rods at low to intermediate burnup levels. Brittle cracks have been found on rods subjected to power increases after having operated for sustained periods at low power levels. Extensive out-of-pile experiments have confirmed that zircaloy is susceptible to SCC in iodine environments.

Phenomenogically, SSC is stress-induced cracking with the assistance of one ore more active chemical species. Once crack initiation occurs (see Section 1.2.3.2), the chemical agent accelerates its propagation.

With respect to SCC in fuel elements, it is conjectured that the stress-concentrator occurs in the vicinity of ridges induced by fuel-cladding mechanical interaction, and that the chemically active species is a fission-product (Cs, Te, I, Br, etc) which becomes released during an increase in rod power . The following observations support these conclusions:

1. Fuel failures occur a few minutes to a few hours after increases in rod power
2. I_2 plus other species are released during power increases
3. I_2 and stress caused out-of-reactor failure at lower stress levels than in the absence of I_2.
4. A stress threshold exists in SCC simulation tests below which no cracking occurs.
5. Increased cladding strains from brief operation at high power reduce the stress threshold for SCC at subsequent intermediate power operations. As discussed in Sections 1.2.2 there are a number of different fuel rod design characteristics that may be releated to the occurance or nonoccurence of stress corrosion cracking. Because of these design differences, SCC, even if responsible for the above observed failures, may not produce failures in commercial LWR designs.

1.4. Additional Phenomena

Neutron irradiation and service in a reactor environment produces many additional effects not explicitly discussed above. Topic of current and future interest in modeling efforts are irradiation induced changes in fuel creep, UO_2 melting point, UO_2 and cladding elastic properties, and other thermal and mechanical characteristics.

1.4.1 Fuel Restructuring

High temperatures in UO_2 fuel cause fuel restructuring - a change in grain size and orientation and in fuel density. Due to the large temperature gradient across the fuel, the outer surface region will generally remain unrestructured. The core region with the highest temperatures will undergo columnar grain growth at temperatures above 1800°C depending on initial fuel density and structure. In the intermediate region, equiaxed grain growth will occur at temperatures from 1200-1300°C to °1650 C.

The presence of restructured fuel will produce somewhat different fuel temperature profiles across a fuel pellet, as well as a different thermal and mechanical influence upon the cladding. This is especially true if a central void forms due to operation at high power levels. Only short time at the appropriate temperatures are needed for these restructuring processes to occur.

For commercial LWR fuel, the operating power level combined with the thermal design characteristics are such that central voids should not be present. In fact, columnar grain growth is usually not expected even in the rods experiencing maximum power.

1.4.2 Crud and Oxide Formation

Crud deposits are observed to form in all water-cooled nuclear fuel rods. These deposits are normally soft and porous films up to 75 μm thick, consisting mainly of hydrated iron oxides. Upon removal of the crud, the cladding does not show any adverse effects from its presence.

Zircaloy oxidation is a continuous function of time at temperature in the coolant environment. This environmental-service caused effect results in slightly increased declining power level of the fuel rod as burnup is accumulated.

The slight temperature rise that is expected due to the surface crud and oxide films as burnup proceeds may also slightly affect cladding strength and ductility due to increased thermal recovery of irradiation damage.

1.4.3 Oxygen to Metal Ratio

The ratio of oxygen to metals atoms is of little concern in uranium dioxide fuel, but is of more importance in mixed oxide fuels since surplus oxygen can cause undesirable reactions. In the former case as-sintered pellets have a stoichiometric oxygen to uranium (O/U) ratio of 2.00. Storage and handling procedures are normally carried out under inert atmosphere conditions and oxygen pickup of pellets of greater than 90% density is insignificant even in dry air, so the O/U ratio at the beginning of irradiation will be 2.00.

During irradiation, some oxygen will become available to either oxidize the cladding or the fuel. Only part of the fission products have an affinity to oxygen high enough to bind the oxygen atoms released by the fissioning of the heavy metal atoms. Depending on the reaction rate with the cladding at the rather low cladding temperatures during operation the oxygen will be picked up by the cladding or will oxidize the fuel to higher O/U levels. However, the increase in O/U ratio will not be high for burnup levels usually reached by commercial water reactor fuel rods if only uranium fission is involved.

In the case of mixed fuels the oxygen to metal (O/M) ratio is of more concern. For plutonium fission the available amount of surplus oxygen is almost twice as high as for uranium fission. In a fuel rod under irradiation, it is very likely that any surplus oxygen will be picked up by the cladding material. If this is the case, mixed oxide fuel can be reduced by the zircaloy to O/M ratios well below 2.00 (depending upon the plutonium concentration), resulting in cladding oxidation and embrittlement. As a consequence it will be especially important to consider the O/M ratio when examining or simulating mixed oxide fuels.

2. SIMULATION OF IRRADIATION AND BURNUP EFFECTS

In reactor investigations of irradiation effects would be facilitated by the ability to simultate the effects of reactor service. Successful simulation approaches would aid in the isolation and study of separate failure-influencing phenomena such as stress-corrosion cracking or cladding embrittlement. Handling and instrumentation possibilities would also be favorably affected by use of simulated materials.

Possibilities for inreactor simulations focus in the three primary areas of irradiation and burnup phenomena. These categories are:

2.1 Cladding Irradiation Damage

2.1.1 "Simulation" by use of previously cladding

2.1.1.1 Previously fueled cladding

2.1.1.2 Previously unfueled cladding "water tubes"

2.1.2 Simulation by cold-wotking

2.1.3 Simulation by addition strengthening agent

2.1.4 Simulation by rapid quenching from a high temperature

2.2 Fuel cladding Mechanical Interaction Causes and Effects

2.2.1 Simulation of fuel pellet cracking

2.2.2 Simulation of fuel cladding gap closure and bonding

2.3 Fission Product Effects

In addition , several effects of varying importance are discussed in a fourth category, "Additional Phenomena": cladding ridging and cracking, rod growth and bowing, densification and restructuring, crudding and oxygen to metal ratio.

Cladding irradiation damage is believed to be of potential major significance but its simulation is found to lack sufficient plausibility for a continued major development effort.

Mechanical interactions between fuel and cladding can easily be achieved by inreactor thermally-induced pellet cracking and by use of small fuel-cladding gaps. Fission gas effects are perhaps less adequately simulated, with prepressurization and introduction of corrosive gases among the possible approaches.

2.1. Cladding Irradiation Damage

Cladding with a prior irradiation history my be utilized directly, but the plausibility of simulating irradiation damage with unirradiated material should also be investigated.

2.1.1 "Simulation" by Use of Previously Irradiated Cladding

2.1.1.1 - Use of Previously Fueled and Irradiated Zircaloy Cladding.
The use of cladding from previously irradiated fuel rods will provide the most literally correct "simulation". Removal of fuel from irradiated rods will be difficult, however, due to a need for hot cell handling. The presence of cracked pellets and possible fuel-cladding bonding also increases the difficulty of fuel removal and raises the possibility of creating scratches during fuel removal.

Previous cladding exposure to an environment involving both neutron irradiation and fuel burnup effects may give maximum confidence in the typicality of the cladding response: both irradiation and burnup phenomena cause increased cladding brittleness and potential for failure. While ductility losses may be primarily due to neutron damage, the relative contribution to failure of the many coupled effects may depend upon in-reactor history in complex ways that are not completely predictable. Changes caused by fuel-cladding mechanical interactions, fission gas effects and corrosion will be most accurately reflected by use of pre-irradiated fueled cladding.

2.1.1.2 - Use of Previously Unfueled but Irradiated Zircaloy Cladding

The use of preirradiated unfueled "water tubes" may be satisfactory simulation approach, although this cladding lacks environmental service-caused effects that may increase the propensity for cladding failure. Some fabrication advantages are present in comparison to use of cladding from fueled and irradiated rods, but the material must still be handled remotely. A slight difference in irradiation effects is expected since there will be lower effective temperatures due to the lack of fuel, producing greater irradiation-induced defect retention and a higher equilibrium saturation damage level.

2.1.2 Simulation by Cold Working

Cladding irradiation damage may be simulated by employing cold work and/or by hydride additions to unirradiated cladding.

One of the basic difference between cold-worked and irradiated materials lies in the defect structure responsible for mechanical property changes - lengthy extended line defects (dislocations) and twin interfaces in the former case and point defect clusters in the latter. Transmission electron microscopy of Zircaloy-4 shows that the defects introduced by irradiation at 290°C have a size range from about 7 Å to 22 Å, far differentfrom the 10.000 Å length typical of diclocations on cold-worked materials. These differnces result in a disparity both in thermal recovery behaviour and in the degree of associated ductility loss. Cold working could not be expected to duplicate the effects of point defects and defect clusters. Increased strength due to irradiation anneals at lower isothermal temperatures than that due to cold work. The differences in ductility are perhaps more important, however, : cold worked cladding

expansion at failure often averages nearly twice that of irradiated tubing for identical temperature and internal pressure conditions.

2.1.3 Simulation by Addition of a Strengthening Agent

The addition of hydrogen to zircaloy is an other possibility to simulate cladding irradiation damage. Zirconium alloys have a large affinity for hydrogen and are strengthened by its addition. While the strengthening effects are negligible up to about 300 ppm significant increases are found with larger concentrations. The phenomenon does depend upon hydride platelet orientation in relation to the applied stress and upon the distribution of hydrogen, but drastic room temperature embrittlement can be caused by well dispersed concentrations in excess of 400 ppm. In addition, the activation energy for diffusion of hydrogen in zircaloy is small - about 1o.6 kcal/mole - so that relatively low temperatures can be applied on fabrication, and hydridging can be accomplished in a LiOH solution, by electrolysis, and by gaseous diffusion.

The primary disadvantage in irradiation damage simulation by hydriding is the increase in ductility found at higher temperatures. At temperatures above about 150°C, surface hydride layers appear to have little effects on rupture ductility, although large reductions are found at lower temperatures.

The burst strength of hydrided tube decreases by about 50% from 20°C to 400°C but at that higher temperature is still affected by hydrogen content, and of course can be made comparable to the failure strength of cold worked specimens. In fact, the failure stress has been found to be unaffected by an outside hydride layer between 20°C and 300°C. Burst temperature, again,may be well simulated by hydriding,but expansion at failure will tend to be greater than found with irradiated tubes. Due to the importance of circumferential expansion with respect to potential flow blockage,development of a damage simulation technique superior in this regard would be desirable.

2.1.4 Simulation By Quenching

Very rapid cooling of metals from elevated temperatures typically results in mechanical strengthening and ductility loss. Quenching strains and impurity (solute) effects are thought to be partly responsible. During a quench, thermal gradients exist in the specimen. The cooler surface region contracts more than the inner region and is in tension while the center is in compression. When the temperature is again uniform, residual stresses may remain to affect mechanical properties. A rapid

quench of zircaloy through the beta to alpha transformation may also contribute to mechanical property changes.

Some strengthening and ductility loss may be expected upon quenching from the high alpha phase. Quenching zirconium from 700°C has produced an apparent defect concentration of 10^{-4}. This effect was thought to be partly due to quenching strains and partly to redissolution of impurities.

If quenching is performed from temperatures much greater than 800°C, a principal question it the effect of the β to α transformation (from about 970 to 830°C). Rapid cooling through the transition can result in a martensitic structure in Zircaloy-4. Microhardness increases have been observed in Zircaloy-4, possibly due to the size of martensite needles (which are finer the faster the quenching rate), so β stabilizing agent are not necessarily involved in the effect.

2.2. Fuel-Cladding Mechanical Interaction - Causes and Effects

2.2.1 Fuel Pellet Cracking

Fuel pellet cracking can be easily achieved. As discussed in Section 1, UO_2 pellets crack when the center to edge temperature difference exceeds approximately 100°C, a magnitude reached at very low heat ratings.

2.2.2 Fuel-Cladding Gap Closure

As discussed in Section 1, gap closure results from a combination of cladding creepdown, pellet cracking, internal oxidation, and fuel swelling. Cladding creepdown can best be simulated by sizing the pellets to reduce the diametral gap. This is preferable to using a high pressure and temperature autoclave to cause creepdown since the cladding metallurgical state will not be affected by this method.

In service, internal fuel porosity accomodates most of the fission products produced during early burnup; after the internal porosity is filled, a volume increase of the fuel pellets occurs. A small gap will then provide an adequate simulation of fuel swelling, with use of the relatively high density pellets adding validity. Internal oxidation can be simulated by prior heating of the cladding at low temperatures in air or steam. At high temperatures (for example 1100°C) oxidation in air is found to be more severe than in steam.

Gap closure my also be caused by an exreactor technique in which hollow UO_2 pellets are threaded onto a metal tube that is internally pressurized to creep, producing radial cracks in the pellets, causing the cracks to expand, and locally streching the cladding. A similar technique is, utilizing a ceramic pellet and a compressible mandrel. An apparatus to similate the behaviour of fuel elements during power increases consists of an aluminium cylinder and a ceramic annulus contained in zircaloy cladding. The aluminium cylinder is axially compressed with a plugger which expands and cracks the brittle ceramic annulus. With further compression if the aluminum core, the cracked ceramic presses radially against the cladding, deforming and eventually fracturing it.

Increased local strains due to fuel-cladding bonding could be partially simulated by roughening the inner cladding surface. This might have the undesirable effect of weakening the cladding, however, and a more reproducible simulation may be possible. Simply oxidizing the internal cladding surface will not produce bonding during short test durations, but inasmuch as graphite has been employed to reduce Fuel-cladding friction a substance could be added to the inner surface to increase friction.

The criteria for choice of such a material are: (1) chemical compatibility with the fuel and cladding, (2) survival to high temperature, (3) manageable and known pressure addition in vaporization, and (4) ease of application. However, the introduction of additional chemical species into a fuel rod can cause undesirable effects, especially at high temperatures. Graphite provides an example, carbon having a strong affinity for zirconium at high temperatures.

Fuel-cladding bonding can also be simulated by out-of-pile heating (of zircaloy in contact with the UO_2 fuel), although the temperatures required for sifnificant reaction rates would cause at least some recrystallization of the cladding material. An isostatic bonding approach could also be employed at elevated temperatures.

2.3. Fission Product Effects

2.3.1 Simulation of Gas Release

Gaseous fission products produce fuel swelling, degrade the fill gas thermal conductivity, and affect cladding stresses upon release. A simulation of steady-state conditions at moderate or high burnup can be performed by prepressurization with gases of the appropriate composition (or at minimum, with gases of the correct thermal conductivity).

2.3.2 Simulation of Corrosion Effects

Stresses due to fuel-cladding mechanical interactions in a corrosive atmosphere of fission products may lead to stress-corrosion cracking (SCC) of the cladding. Reproduction of the potential causes of SCC will involve the introduction of iodine and cesium into a simulated fuel rod with either uniform stress due to prepressurization, or more localized interactions due to stress concentrators. For an exreactor experiment, stress may also be caused by using a tightly fitting mandrel; a differential mandrel-cladding thermal expansion upon heating in iodine vapor causes a potential for SCC.

Another approach involves fabrication of pellets with simulated fission products (i.e., I_2, Cs, Br_2, Te) combined with hyperstoichiometric fuel. These can be used with either stressconcentrators or uniform stress techniques. It should be noted that the kind and distribution of the fission products under irradiation are very complex. The distribution of fission products depend upon temperature profiles, oxygen potential in the fuel pellets, and precursor half life. For example, ^{137}Cs remains within a mixed oxide fuel matrix having an oxygen/metal ratio greater than 1.95 (dependingon the Pu content) and is deposited in the cooler regions of the fuel pellets. (In UO_2 fuels the O/M ratio is normally 2.00 or larger). On the other hand, ^{134}Cs has precursors (^{133}I and ^{133}Xe) with longer lives so that it is formed only after greater diffusion times and occurs preferentially in the gas plenum end of the fuel blanket. The species ^{106}Rh is concentrated near the center of the fuel column. Since temperature and pellet composition do control some aspects of the fission product distribution it may be possible to employ a direct electrical heating apparatus to redistribute species introduced during pellet fabrication.

2.4. Additional Phenomena

Several additional phenomena fall in categories that should either not be simulated at all or that will be either: (1) simulated by default or (2) tested in exreactor studies. These effects, only some of which are observed and which have varying degrees of importance, are: (1) cladding ridging and ratcheting, (2) incipient cladding cracking, (3) rod growth and bowing, (4) fuel densification and restructuring, and (5) crudding of cladding, and (6) oxygen to metal ratio in the fuel.

2.4.1 Cladding Ridging

The simulation of cladding ridges is not easily accomplished. The cladding ridge shape can probably be achieved by using an internal, expanding madrel, but the ridge must also coincide with the pellet end faces when fuel-cladding hard ineraction occurs at high powers.

2.4.2 Incipient Cladding Cracking

Vendor information indicates that cladding cracking (due to a stress corrosion environment) is not an often observed irriadiation effect in PWR fuel; partially penetrating cracks occasionally exist, but are very rare.

2.4.3 Rod Growth and Bowing

A potential ex- or in-reactor simulation techniques involves restraining the ends during a test.

2.4.4 Fuel Densification and Restructuring

Simulation of fuel-cladding gap closure has been discussed in Section 2.2.2 above. The effects of fuel densification on fuel cladding mechanical interactions can be simulated by the use of higher density test fuel.

2.4.5 Oxygen to Metal Ratio

As pointed out in Section 1.4.3 the oxygen to metal ratio of the fuel has some significance in the simulation of irradiated mixed oxide fuel rods. Simulation of the surplus amount of oxygen due to burnup could be carried out by pre-oxidation of the cladding or by utilization of a fuel with O/M ratio above 2.00 or by introduction of oxide compounds of fission products such as MoO_2 or Cs_2UO_4. The mode of simulating excess oxygen effects depends upon the reactions that take place in a water reactor fuel rod under normal operating conditions. The zircaloy-oxygen reaction is dependent on the oxygen potential in the fuel, and the mechanical properties of the cladding will vary according to its oxygen content or its state of oxidation.

REFERENCE

L.B. Thompson et al.
LWR Fuel Behavior Program Description; Irradiation Effects Experiment Requirements ANC Report SRD-57-76 (1976)

Table 1: SUMMARY OF IRRADIATION EFFECTS IN LWR FUEL RODS

Irradiation Effects	Relative time of Occurrence during Irradiation	Transients during which Effects are Important(1)	Comment
Cladding irrad.damage	Saturates at $\sim 1 \times 10^{21}$ n/cm^2	All	Reduces cladding strain to failure margin
Incipient cladding cracks (nonpenetrating)	Middle to end-of-life	All	Medium to low importance because of low frequently of occurrence
Cladding ridging	At high power	Overpower	Stress concentrations occur at ridges
Cladding axial growth	Continious	Overpower	Important only if bowing results
Cladding creepdown	Beginning to middle-of-life	All	Results in more interaction but improved gap conductance
Cladding internal oxidation	Continuous	All	Influences fuel-cladding bonding
Cladding external oxidation	Continuous	None	Causes a small temperature increase
Cladding hydrogen pick-up from coolant	Continuous	None (?)	Pickup is generally low but the of transient effects is untested
Cladding crud accumulation	Continuous	None	Modern water chemistry control precludes massive crud accumulation
Fuel-cladding bonding between ZrO_2 and fuel	Middle to end-of-life	All	May increase mechanical interaction or restrict the redistribution of internal gases
Fuel swelling	Middle to end-of-life	All	Causes increades cladding stress and improved gap conductance. May restrict gas flow.
Fuel cracking	Beginning-of-life	All	Causes stress concentration in the cladding and degraded thermal conductivity. May improve gap conductance but restrict gas flow
Fuel restructuring	At high temp., increasing with temp.	All	Increases fuel density and improves thermal conductivity

Fuel densification	Early in life	All	Postpone the swelling effect but may cause greater stresses in fuel cladding interactions
Fuel stoichiometric ratio	Indeterminate	None	Affects UO_2 thermal conductivity, but not observed to be significant
Melting point change	Continuous	None	Melting point is reduced slightly with neutron damage and burnup
Steady-state fission gas release	Continuous	All	Affects cladding stresses and reduces gap conductance.
Transient fission gas release	Early to end-of life	All	Affects cladding stresses and decreases gap conductance
Fission product attack of cladding (stress corrosion)	Indeterminate but probably middle to late-life	Overpower	Never actually proven to occur in a reactor, but well demonstrate in out-pile tests. May not be significant during fast transients.

(1) Transient are divided into two categories: (1) overpower where insuffient cooling exists, and (2) loos-of-coolant where inadequate cooling occurs followed by a power reduction limited by decay heating.

B. THE BEHAVIOR OF FISSION PRODUCTS INSIDE LWR AND HWR FUEL RODS

1. Internal Fuel Rod Chemistry from Equilibrium Thermodynamics

2. Preliminary Assessment of the Chemical States of the Fission Products

3. Detailed Oxygen Balance Calculation

4. Shift of Fuel O/M-Ratio during Burnup

5. Valatilities of the Fission Products

6. Conclusions

B) THE BEHAVIOR OF FISSION PRODUCTS INSIDE LWR AND HWR FUEL RODS

1. INTERNAL FUEL ROD CHEMISTRY FROM EQUILIBRIUM THERMODYNAMICS

The interaction between fission products and cladding depends on their chemistry as follows. Fission products must be transported from the fuel to the cladding to interact. The rate and mechanism of transport will depend on the temperature, temperature gradient, and oxygen potential gradient. The oxygen potential effectively sets the chemical states of the fission products. Then the reactivity of the fission products with the cladding will depend on their chemical states.

The chemistry of the system involving the fuel fission products and cladding of light-water-reactor (LWR) and heavy-water-reactor (HWR) fuel rods is treated below on the basis of available thermodynamic information. The treatment is similar to those for fast-breeder-reactor (FBR) fuel Rods. The present treatment will concentrate attention on interactions with cladding and, therefore, consider primarily the fission products that migrate to the cladding. Fission products that do not migrate will interact through their effect on the oxygen potential of the fuel.

2. Preliminary Assessment of the Chemical States of Fission Products

The distribution anticipated for the fission products in a fuel rod depends on chemical states of the fission products. Assessment of the chemical states can be made from a comparison of the free energies of formation of the oxides of the fission products relative to the oxygen potential of the fuel during irradiation. Such an assessment provides a useful criterion because it, in effect, indicates how the available oxygen will be partitioned among the metallic elements present. A more sophisticated approach, which considers more complex compounds such as ternary oxide compounds, can only be applied adequately for a few of the fission products, since no thermodynamic data are available.

The standard free energies of formation of fission-product oxides, according to available thermodynamic data, are shown in Figure 1. The

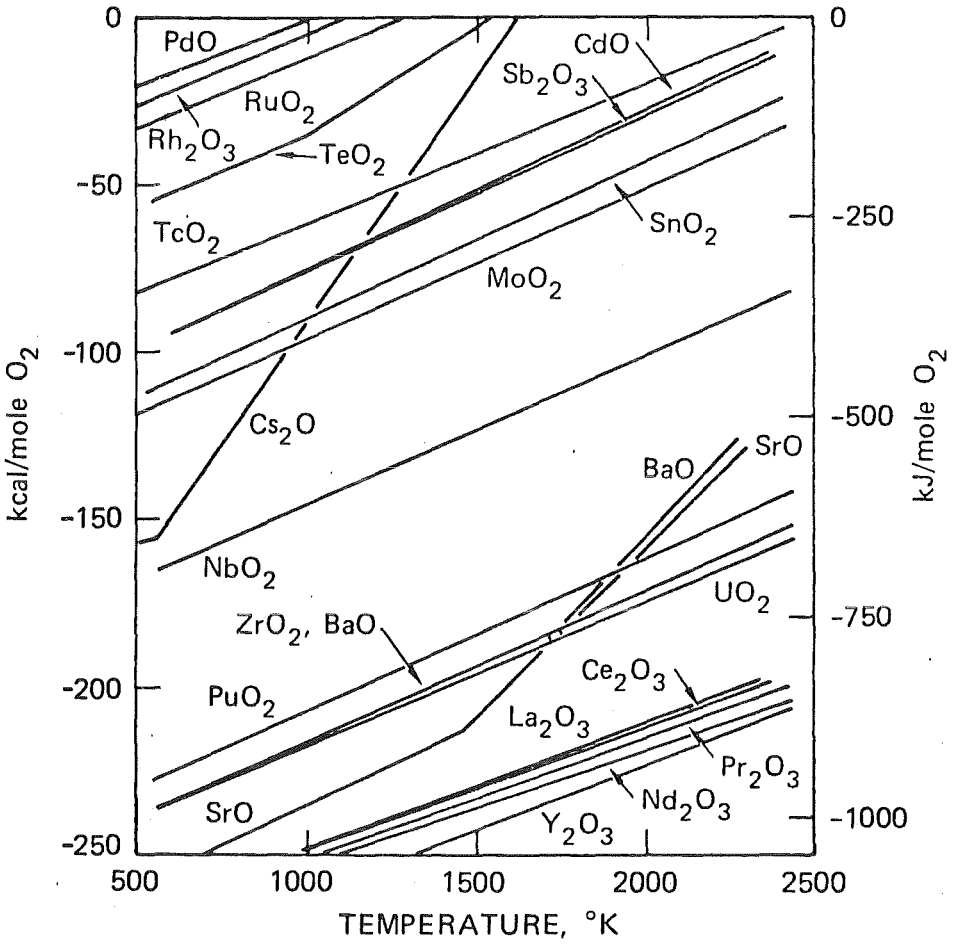

Figure 1: Standard free energies of formation of pure solid metal oxides

values represent the free-energy change associated with the reaction between the pure metal with oxygen at one atmosphere to form the pure oxide. That situation is very different from conditions of interest, namely, fission products formed in a UO_2 matrix. In that case, oxides can dissolve in UO_2 or form compounds with it. The metals can alloy with one another, and local conditions can vary because of impurities in the UO_2. Therefore, the information provided in Figure 1 can only give a rough approximation to fission-product behavior.

In the LWR and HWR fuel rods the oxygen potential is roughly -460 to -540 kJ/mol O_2 (110 - 130 kcal/mol O_2) over the whole range of operating temperatures. The majority of the fission products should thus fall into two categories: Those with free energies of formation more positive than the fuel and are expected to be in the form of elements, and those with free energies of formation more negative than the fuel and expected to be combined as oxides. In the thermodynamic calculations it will generally assumed that the oxygen potential of fuel lies in the range of -460 to -540 kJ/mol.

A second important criterion is the volatility of the fission product. Presumably volatile forms can be transported to the cladding and be available for reaction with the cladding while the involatile ones will remain in the body of the fuel. The volatilities of ternary oxides, such as Cs_2MoO_4, also need to be considered.

Those two criteria lead to the preliminary classification of the fission products shown in Table 1.

A more careful assessment of the chemical states of the fission products is made below. The way that oxygen, released by fission from the UO_2, combines with the fission products formed is evaluated in a detailed balance of the amount of oxygen available and the possible chemical combinations with fission products based on relative stabilities. To make that detailed balance, it is necessary to make the preliminary considerations given in the sections below.

Table 1: Preliminary classification of fission products (Percent fission yields in parantheses)

A. Noble Gases

Xe, Kr (24)

B. Volatile Elements

Cs, Rb (21)
I, Br (1.3)
Te, Se (3)
Cd, Sb (0.2)
Ag, Sn (0.3)
Pd, (1.4) Moderately volatile

C. Relatively Involatile Elements

Ru, (9)
Rh, Tc (11)
Mo, Nb (25)

D. Relatively Involatile Oxides

Rare Earths (55)
Ba, Sr (13)
Mo, Nb (25), Cs_2MoO_4 is moderately volatile
U, Pu

2.1 Background Information for Detailed Assessment

2.2 Fission-Product Inventory

The exact amount of each fission product present in a fuel at any time is, beside the fissile atoms (U-235, Pu-239), a function of the power history; however, a reasonable approximation can be obtained from the cumulative yields of the long-lived and stable isotopes. Table 2 gives the yields by element.

Table 2: Stable (or long lived) fission product yields for thermal fission of U-235

	% Yield[a]		% Yield[a]
Se	0.4	Sn	0.1
Br	0.3	Sb	0.1
Kr	3.8	Te	2.5
Rb	1.3	I	1.0
Sr	6.2	Xe	20
Y	4.8	Cs	20
Zr	36.9	Ba	6.7
Nb		La	6.6
Mo	25	Ce	12.3
Tc	6.1	Pr	5.9
Ru	9.3	Nd	20.5
Rh	4.9	Pm	2.3
Pd	1.4	Sm	1.9
Ag	0.2	Eu	0.2
Cd	0.1	Pu	23.

[a] Number of atoms per 100 fissions.

The percent of each stable fission product element in the fuel for long irradiations can be calculated from the product of the burnup and fission yield. Thus, at 1% burnup (1% of uranium atoms fissioned, or 820 GJ/kgU, i.e., 9500 MWd/MTU) the Zr content of the fuel should be 0.37 x 1% = 0.37 atom % of the uranium.

2.3 Oxidation of Zircaloy

During reactor irradiation, oxygen is slowly transferred from the fuel to the inner surface of the cladding. From thermodynamic considerations zirconium should react with the oxygen of the UO_2; however, the rate apparently limited by processes such as release of oxygen from the UO_2, transport across the fuel-clad gap, and diffusion in the zirconia scale. It appears that the arrival of oxygen at the

Zircaloy surface is not rate limiting because the rate of oxidation of the cladding seems to be the same as in the plentiful supply of oxygen (at normal reactor operating temperatures of the cladding).

Little is known about the rate of oxidation of cladding under the conditions that exist inside fuel rods. The few available PIE measurements of oxide thickness indicate that its rate of formation in the absence of fuel-clad bonding is about the same as that on Zircaloy exposed to oxygen gas. When deposits of fission products give rise to bonding between the fuel and the cladding, the zirconium oxide layer is distinctly thicker.

Initially the inner oxidation of Zircaloy by the fuel follows a parabolic law until the oxide layer reaches a certain thickness (about 2 μm) and then the reaction becomes linear in time. The effect of radiation on the oxidation influences the oxidation. The higher the temperature the smaller the effect; at 675 K the radiation effect is negligible.

Quantitative literature information about the thickness of oxides on the inner surfaces of irradiated fuel rod cladding is scarce. Over the majority of the surface where fuel had not bonded, the oxide thickness at the end of a burnup of about 20000 MWd/MTU ranged from 1 to 5 μm. At the end of a burnup of about 34000 MWd/MTU it ranged from 5 to 9 μm with an average of 8 μm. In areas where the fuel has bonded to the cladding the ZrO_2 layer there was thicker (apparently in the range of 6 to 10 μm).

2.4 Oxygen Potential of UO_{2+x}

The oxygen potential of a system is given by the expression:

$$\overline{\Delta G}(O)_2 = RT\ell np(O_2 \text{ atm})$$

For a two-component system containing two solid phases, the oxygen potential depends only on the temperature. For example, the pressure of oxygen in equilibrium with uranium metal and the equilibrium oxide in equilibrium with uranium metal (approximately UO_2), as represented

by the equation,

$$O_2 + U(\text{metal}) = UO_{2\pm x} \text{ (solid)}$$

depends only on temperature. The oxygen potential is equal to the standard free energy of formation of the oxide as given in Figure 1. The composition of the oxide, $UO_{2\pm x}$, in equilibrium with U metal depends on temperature but is close to $UO_{2.00}$.

Uranium dioxide not in equilibrium with metal can dissolve excess oxygen, in which case its oxygen potential is a function of its composition as well as temperature. Values calculated for various O/U ratios are shown in Figure 2.

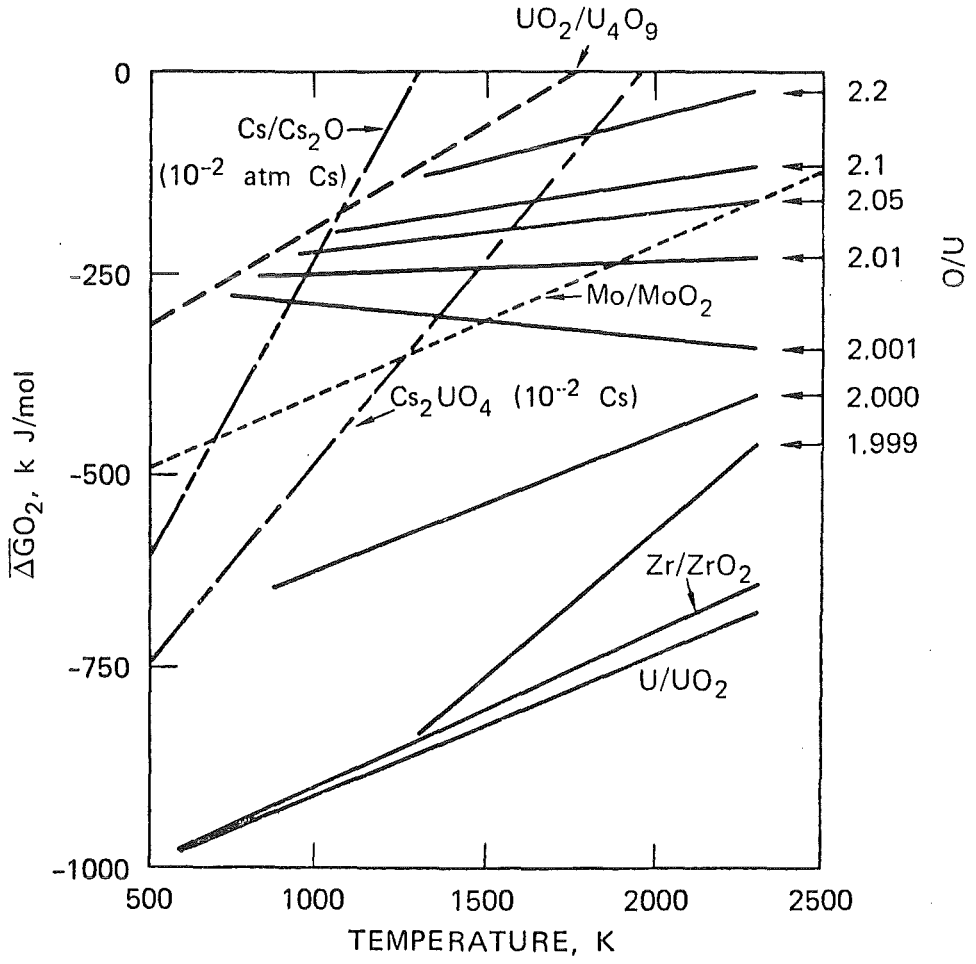

Figure 2: Oxygen potentials for UO_{2+x} (full lines) and for formation of some solid oxides and for the reaction $2\,Cs(g) + O_2 + UO_2(s) = Cs_2UO_4(s)$
(Uncertainties are of the order of ±50 kJ.)

The initial O/U of LWR fuel is in the range of 2.001 to 2.003. The oxygen potential of that material can be approximated by a line slightly above the 2.001 line of Figure 2. As burnup proceeds, the oxygen potential becomes somewhat more negative. During the first stages of burnup, oxygen in excess of stoichiometry (i.e., x in UO_{2x}) tends to redistribute radially because of the temperature gradients in the fuel.

3. Detailed Oxygen Balance Calculation

To understand the chemical states of the fission products, it is necessary to assess the way that oxygen recombines inside a fuel rod because of fission. The calculation is based on the following considerations. Each fission event annihilates a uranium atom, releasing two oxygen atoms that oxidize the reactive fission products formed (and to some extend the cladding and the fuel). The released oxygen is assigned to the fission products in order of their reactivity. The oxygen potential of the system is then estimated from the reactivity of the remaining fission products. Comparison with the few available measurements can be made to evaluate the validity of the calculation. The calculation is only approximate mainly because it is based on free energies of formation of pure oxides as separate phases rather than solutions of the oxides in UO_2 matrix.

The calculation is summarized in Table 3. In the detailed calculation, it is convenient to consider the situation at 1% burnup (1% of U atoms fissioned, which occurs at 820 GJ/kgU or 9500 MWd/MTU). The results can be scaled to other burnups. The amount of 1% burnup is about 0.001 O/U units,* and is shown as item 1 in Table 3. The rate of oxygen pickup by the cladding is nonlinear with burnup, but because it is only a small part of the inventory it does not affect the calculation very strongly.

The next oxygen assignment is to the fission products that form the very stable oxides. The amount of oxygen is the product of the amount of the fission product (fission yield x burnup fraction)

* In this discussion, including Table 3, the amounts of oxygen are presented in O/U units, defined as a number of atoms of oxygen involved per atom of uranium.

Table 3: Oxygen Inventory calculation

Oxygen Sink			Amount of Oxygen Used at 1% Burnup in O/U units
1. Cladding oxidation			0.001
2. Fission products completely oxidized:			
Oxides	Fission Yield	Oxygen per metal**	
RE_2O_3*, Y_2O_3	0.55	1.5	0.0083
BaO, SrO	0.13	1.0	0.0013
ZrO_2	0.37	2.0	0.0074
NbO_2	0.006	2.0	0.0001
		Total combined =	0.018
3. Fission products partially oxidized			
Cs + Rb:	0.21		
	-0.013 (amount combined as iodide and bromide)		
	-0.058 (amount combined as Cs_2Te and Cs_2Se)		
	0.14		
Cs_2O		0.5	0.0007
Cs_2UO_4		1.0	0.0014
$Cs_2U_2O_7$		1.5	0.0021
$Cs_2U_4O_{12}$		2.0	0.0028
Mo	0.25	2	0.005
4. Fission products not oxidized			
Sn, Sb, Cd	0.003		
Tc	0.061		
Ru	0.093		
Rh	0.049		
Pd, Ag	0.016		
Xe, Kr	0.238		

* RE represents the rare earth elements.

**This column gives the number of oxygen atoms reacted per fission product metal atom to give the oxide in the first column. Note that in ternary oxides containing U, each U initially has 2 oxygen atoms.

times the atomic ratio of oxygen to metal in the oxide formed. The calculation is shown in Table 3, Item 2. There is some indication in the literature that the rare-earth oxides dissolved in UO_2 act like +4 ions; however, that occurs only at relatively high oxygen potentials. It is justified in assuming a +3 state because the oxygen potential of irradiated fuel is quite negative. Ba and Sr might also behave similarly except that the oxygen potential of the fuel is too low for that to occur. If the Ba and Sr form separate zirconate phases, as sometimes observed, their valence states will be as assumed in Table 3.

After the most stable oxides are accounted for, the total oxygen combined (items 1 and 2 of Table 3) amounts to 0.018 O/U units. Because 0.020 O/U units are released by fission, there are 0.002 left for further distribution. ** The next most oxygen-reactive fission products are either Cs (and Rb) or Mo. Figure 3 presents the oxygen potentials for which MoO_2 and Cs_2UO_4 are formed. Also the formation of Cs-Molybdates has to be considered.

Cesium should form CsI and CsBr in preference to Cs_2UO_4 or Cs_2MoO_4 at low oxygen potentials. The net fission yield of Cs (and Rb) after allowance for I and Te is about 0.14, as indicated in Item 3 of Table 3, since Cs_2Te and Cs_2Se probably form in preference to Cs_2UO_4 and Cs_2MoO_4. It is not certain how much oxygen will be combined per atom of Cs (and Rb). The number can range from 0.5 to 2 for the compounds indicated in Table 3. Figure 2 indicates that Cs_2UO_4 should form at lower oxygen potentials than Cs_2O. Therefore most of the oxygen should go to form Cs-U-O compounds except near the hot fuel center where MoO_2 may form (Cs_2MoO_4 is even thermodynamically more stable than Cs_4UO_4). Therefore the inventory calculation indicates that the last oxygen combines to form either cesium uranates or MoO_2 and they buffer the oxygen potential of the fuel.

** In this assessment it is not considered the initial amount of oxygen excess of stoichiometric in the fuel (i.e., x in UO_{2+x}). That quantity ($\sim$0.002) should be added to the amount of oxygen available to react with fission products and become significant for smaller burnups.

The remaining fission products will be in an unoxidized state. They are listed in Item 4 of Table 3 roughly in order of decreasing reactivity with oxygen.

4. Shift of Fuel O/M-Ratio during Burnup

The oxygen potential of UO_2 is determined by the oxygen gettering of the Zry-cladding material. In power reactors the cladding temperature is sufficiently high so that part of the oxygen released during nuclear fission of UO_2 gets bound by the cladding material. However, if the fuel/fission product system is considered separate from the cladding, the O/U ratio of UO_2 will always increase during irradiation because the fission products cannot bind the entire oxygen released by nuclear fission. Therefore, an average stoichiometric shift can be determined which, besides on the fissile isotope and the neutron energy, depends on the state of oxidation of the fission products. However, the estimate of the stoichiometric shift is complicated by the inadequate knowledge of the oxidation state of some fission products and by the plutonium fission increasing with burnup. Figure 3 represents the change of the O/U ratio as a function of the burnup for different oxidation states of the fission products Cs, Mo and the lanthanides. The most probable case is that Cs and Mo largely occur in a nonoxidized state in UO_2; the formation of Cs_2MoO_4 and/or Cs_2UO_4 or other oxygen containing complex compounds was not considered in the calculations.

Depending on the valency of the rare earth metals (lanthanides) the stoichiometric shift of MO_2 (M = U,Pu) as a function of the burnup for U-235 and Pu-239 fission is presented in Figure 4. The rare earth metals were assumed to be trivalent or tetravalent. In this way, a scatter band is obtained in which the O/M-increase of the oxide fuel takes place. A higher amount of oxygen release can be expected from Pu-239 fission because less oxygen binding fission products are formed. However, the oxygen in excess estimated in this way is completely gettered at sufficiently high cladding material temperatures as encountered in power reactors so that the O/M-ratio of the fuel takes the value 2.000.

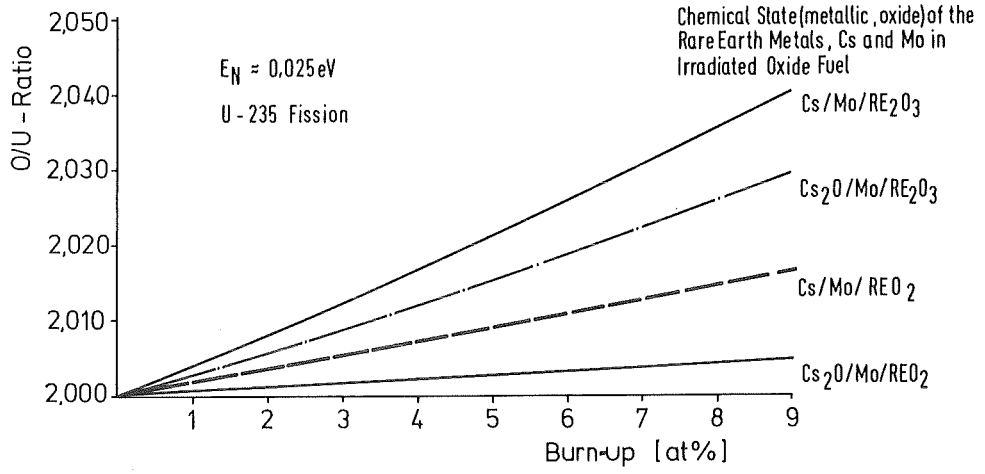

Figure 3: O/U-shift of UO_2 as a function of the burnup for different states of oxidation of Cs, Mo and the lanthanides (rare earth metals)

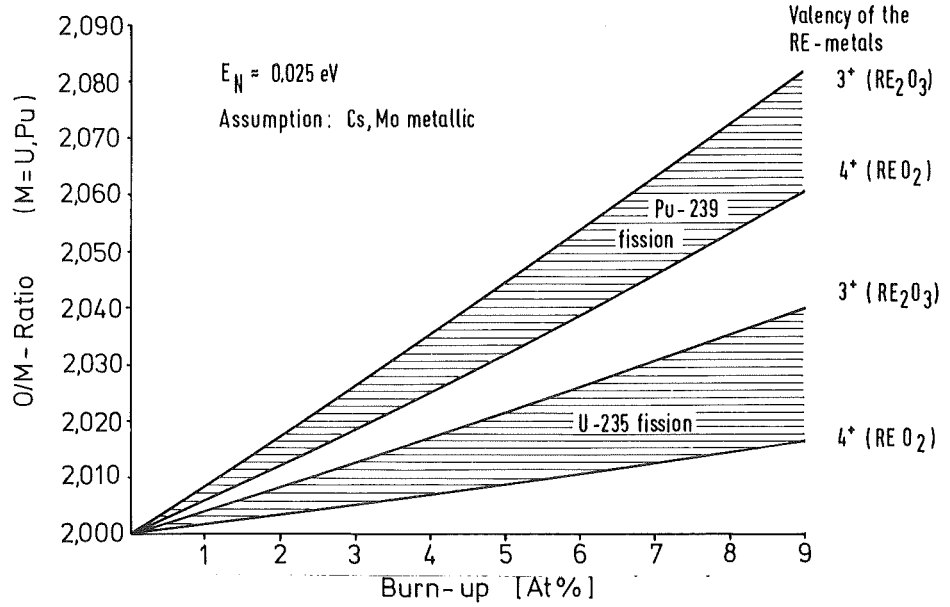

Figure 4: O/M-shift of the oxide fuel as a function of the burnup for the fission of U-235 and Pu-239

Therefore, using these estimates, the maximum oxygen uptake of the Zry-cladding can be determined and, consequently, the maximum thickness of the oxide layers to be expected on the cladding inner surface can be estimated which is significant for the performance of simulation experiments (1 μm ZrO_2 $\hat{=}$ $-\Delta O/M \approx 0.001$; ID of the cladding: 9.3 mm).

5. Volatilities of the fission products

The fission product compounds, as indicated in Table 1, are classified according to their valatilities in more detail in Table 4. Substances in Classes I and II are sufficiently volatile to be vapor transported from the fuel during normal operation (fuel temperatures ∿1500 K at the center to ∿1000 K at the outer surface). Those in Class III might be expected to be transported if the fuel operated at temperatures higher than normal. Substances in Class IV would not be expected to be vapor transported during reactor operation.

The release of even the very volatile noble gases (Xe, Kr) does not occur during normal rod operation or is rather small even to relatively large burnups. That is, the kinetics of release of fission products must be a controlling factor. We will assume that the release of volatile fission products is comparable to that of the fission gases and the fraction released will be the same for all the compounds in Classes I and II.

6. Conclusions

The oxygen balance calculations indicate that the oxygen potential of the fuel is in the neighborhood of -500 kJ/mol. Fission product cesium is combined in ternary compounds with uranium and oxygen; molybdenum oxide probably buffers the oxygen potential.

The fission products that might be expected to reach the cladding by vaporization are: Cs (Rb) in compounds; I (Br), Te (Se) in compounds with Cs; elemental Cd, Sb, Ag, Sn, and Pd; Ba, as BaO; and possibly MoO_2.

Table 4: Chemical States and Volatilities of Fission Products

Compound Classification	Vapor Pressure (Atm) 1000K	2000 K
I Very volatile (permanent gases)		
Xe, Kr		
II Moderately volatile		
CsI, RbI, CsBr, RbBr	10^{-3}	1
Cs_2Te, Cs_2Se[2]	10^{-3}	1
Cd	0.5	>>1
Sb	10^{-3}	1
Ag	10^{-8}	0.1
(Cs pressure over Cs_2UO_4)[3]	10^{-3}	>>1
III Moderately nonvolatile		
Sn	$\sim 10^{-10}$	$10^{-3.3}$
Pd	$\sim 10^{-10}$	10^{-3}
BaO	$\sim 10^{-10}$	$10^{-3.5}$
MoO_2	$< 10^{-10}$	10^{-4}
IV Nonvolatile (pressure < 10^{-4} atm at 2000 K)		
Ru, Rh, Tc, Mo		
Rare-earth oxides		
SrO		
ZrO_2, NbO_2		

Fission products and impurities observed at the fuel-cladding interface of irradiated LWR rods (indicated as elements without implying the chemical compound) are: Cs, Te, I, Pd, Ba, Fe, Cl, Si, Al, Ag, Na, and Ca.

As regards the chemical interactions with the Zry-cladding material, the fission products iodine and tellurium as well as cadmium, in addition to oxygen, have found to be aggressive with respect to Zry from thermodynamic estimates and laboratory scale experiments. It should be further noted that even the UO_2/Zry initial system, which is free from fission products, is not stable thermodynamically. However, since the normal cladding material temperatures are sufficiently low, the chemical interactions with the cladding material can be tolerated. Nevertheless, the question arises to which extent the mechanical properties of Zry are influenced accordingly. The impact of iodine on Zry has appeared as a special problem since iodine can cause stress corrosion cracking.

References

/1/ D. Cubicciotti, R.L.Jones
EPRI-NASA Cooperative Project on SCC of Zircaloys, EPRI NP-717 (1978)

/2/ D.Cubicciotti, J.E.Sanecki
Characterization of Deposits on Inside Surfaces of LWR Cladding, J.Nucl.Mat., 78 (1978) 96-111

/3/ H.Holleck, H.Kleykamp
Zur Stöchiometrieverschiebung in einem oxidischen Brennelement bei hohem Abbrand, KfK 1181 (1970)

/4/ H.Kleykamp
The chemical state of LWR High Power Rods Under Irradiation, KfK 2696

/5/ P.Hofmann
Fission Product Yield for the Fission of U-235 and Pu-239, KfK-Ext./IMF 6/70-2 (1970)

/6/ P.Hofmann
Simulation of the Chemical State of Irradiated Oxide Fuel, KfK 2785 (1979)

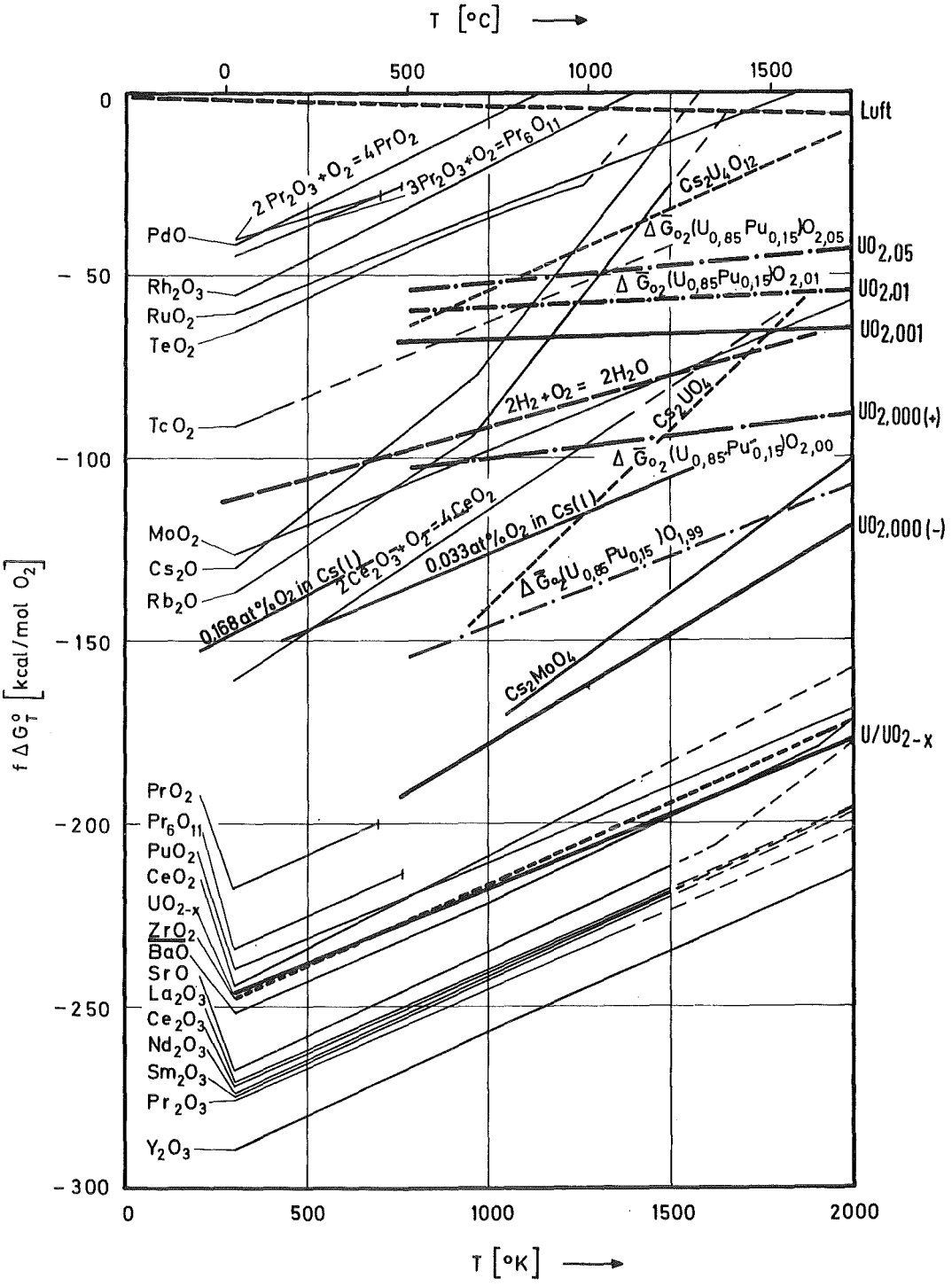

Oxygen potential of UO_2, $(U,Pu)O_2$ and fission product oxides as a function of the temperature [3].

C. FUEL SWELLING AND FISSION GAS RELEASE FROM UO_2

1. INTRODUCTION
2. STEADY-STATE CONDITIONS
3. TRANSIENT CONDITIONS
4. CONCLUSIONS

C. FUEL SWELLING AND FISSION GAS RELEASE FROM UO_2

1. Introduction

The fuel swelling and the pressure developed by the released fission gas in a fuel element are the most important clad-straining mechanisms under steady-state and transient conditions. Therefore, the knowledge of these phenomena and their dependence on temperature, burnup, and external restraint is important for fuel element design. Beyond this the quantitative knowledge of the fission gas retention is necessary for the development of models of fuel behaviour under transient conditions because the state and the location of fission gas affects the way in which the fuel reacts to an overpower transient.

The fission gas release from the UO_2 and the fuel swelling were therefore determined in in-pile experiments for steady-state and transient (large break LOCA) conditions. In addition, out-of-pile annealing experiments were performed with irradiated UO_2 in hot cells to investigate the fission gas and fuel behaviour under "Severe Fuel Damage" (small break LOCA) conditions.

Fission gas determinations were carried out after irradiation and after LOCA-testing. The amount of fission gas was measured in the three steps as

(1) released fission gas,
(2) fission gas retained in pores and bubbles and
(3) fission gas retained in the matrix.

The released fission gas was removed from the capsules or fuel rods by puncturing the cladding. The quantities of xenon and krypton were evaluated by gas chromatography. Because of the cladding defects in the LOCA-tested

fuel pins it was not possible to measure exactly the fission gas release during the LOCA. The release values could only be deduced from the measurements of the retained fission gas. To evaluate the retained fission gas the fuel was ground in a ball mill to particle sizes smaller than 1 µm. The fission gas released during grinding is called "gas in pores". It orginates from pores and bubbles and from grain boundaries. After grinding the powdered fuel was dissolved in nitric acid. The fission gas released in this step was in fission-induced solution and in very small intragranular bubbles. This gas is called "gas in the matrix".

2. Steady-state conditions

Fig. 1 shows the volume increase as a function of burnup for different temperatures. The unrestrained swelling is presented by the full lines. There is a very strong dependence on temperature. The unrestrained swelling rate varies from 1.2 % per 1 % burnup at 1250 K to approximately 20 % per 1 % burnup at 2000 K at the beginning of the irradiation. At all temperatures the burnup dependence is characterized by a linear increase of swelling with burnup at low and medium burnups, respectively. With increasing burnup, however, the swelling rate diminishes and that the sooner the higher the temperature. At 1250 K the swelling rate is virtually independent of burnup up to 8 % burnup.

Taking into account a swelling rate of about 0.65 vol. % per 1 % burnup induced by solid fission products the fission gas swelling seems to be saturated at about 5 vol. % for temperatures up to 1250 K. At 2000 K the swelling rate decreases already at burnups below 1 %. At burnups above 4 % it is reduced to a value below 0.5 % per 1 % burnup.

The mean unrestrained swelling rates of UO_2 in various burnups ranges are plotted in Fig. 2 as a function of temperature. These values are only valid, if there is no gross bubble migration in the fuel because bubble migration reduces the swelling. Fig. 2 shows a very strong temperature dependence of the swelling at low burnups. However, with increasing burnup the temperature dependence diminishes due to the saturation of fission gas swelling at high temperatures.

The restrained volume increase is represented by the shaded area in Fig. 1. In comparison with the unrestrained swelling there is a marked decrease of the restrained swelling. The temperature dependence decreases, too. At burnups above 4 % the mean swelling rate is between 0.4 and 0.6 % per 1 % burnup at temperatures between 1500 and 1900 K /5/.

The strong dependence of the swelling on temperature and burnup is primarily caused by the behaviour of the fission gas. This behaviour is determined by the irradiation-induced solution of the gas atoms in the matrix and by the growth of bubbles. Dependent on the temperature one of these processes predominates. At low temperature it is the irradiation-induced solution and at high temperature it is the growth of the bubbles.

The fission gas behaviour can be explained qualitatively by means of Fig. 3 showing the concentration of the retained fission gas and of its fraction in UO_2 at a temperature of 1500 K as a function of burnup. At the beginning of the irradiation most of the fission gas remains in the grains in irradiation-induced solution. By and by some of the gas precipitates in bubbles in the matrix. The size of these bubbles is determined by the equilibrium between resolution rate and growth rate. It is in the order of 2 nm as pointed out by Cornell /6/ and Speight /7/. The concentration of this gas is represented by the curve A in Fig. 3. With increasing burnup a new population of bubbles builds up at favoured sites in the fuel, e.g. at dislocations and at subgrain boundaries. The size of these bubbles ranges from 10 to 40 nm as shown by Ronchi and Matzke /8/. With increasing gas content in the grains the gas transport to the grain boundaries increases, too. The concentration of the gas in grain boundaries and of the gas in intragranular bubbles with diameteres greater then 10 nm is shown by the curve B in Fig. 3. Curve C represents the sum of the fission gas in the matrix and of the gas in bubbles and grain boundaries.

The concentration of the fission gas in bubbles and grain boundaries at burnups above 3 % is shown in Fig. 4, where it is plotted versus the fuel temperature. The concentration of the fission gas in the matrix and its temperature dependence are shown in Fig. 5. The sum of the fission gas in pores and of that in the matrix is the retained fission gas. At low temperatures

there is a high fission gas retention. Based on the concentration of the retained fission gas and on the actual values of the released gas the fission gas release is plotted in Fig. 6 as a function of burnup for different temperatures.

Fig. 7 shows the release of Cs-137 as a function of burnup. Compared with the fission gas release the Cs-137 release is delayed. It is much lower at low burnups, but it increases markedly at higher burnups resulting in high temperature release values similar to those of the fission gas. Cs makes a large contribution to the swelling by solid fission products. Therefore, the quantitative knowledge of the release behaviour of Cs is necessary for the evaluation of the burnup dependent local swelling rate due to solid fission products.

3. Transient conditions

Fission gas release from UO_2 and fuel swelling were determined for the pre-irradiated test rods exposed to an in-pile LOCA transient, and for the test rods with the same steady state preirradiation that were not exposed to the transient.

Fission gas release during steady state irradiation was always below 10 %. The additional fission gas release during the LOCA transient was less than 6 %.

The fuel density had increased during steady-state irradiation up to about 3 at.% burnup. This was due to a volume averaged swelling rate of about 1 % per 1 at.% burnup and an irradiation-induced densifiation to about 2 % residual porosity. There was no noticeable swelling during the LOCA tests.

In order to investigate fission gas and fuel behaviour under "small break LOCA" conditions fuel samples of the preirradiated but not LOCA-tested fuel pins were annelaed out-of-pile for various times at temperatures between 1200 and 1600°C. The observed effects were small at temperatures up to 1400°C. After a 3 hours annealing at 1400°C the swelling was 0.5 % and the fission gas release was 3 %. With increasing temperature fission gas release

and swelling increase. Fig. 8 shows the fission gas release during the annealing tests at 1500 and 1600°C as a function of annealing time.

The time dependence of the fission gas release during the LOCA and the annealing tests supports the conclusion that different release mechanisms are effective:

- microcrack formation,
- grain boundary separations caused by bubble growth and coalescence,
- diffusion, i.e. transport of single gas atoms or small bubbles to free surfaces or grain boundaries.

The fission gas fractions, i.e. the released gas, the gas in pores, and the gas in the matrix, in fuel samples of a test serie after different treatments are shown in Fig. 9.

4. Summary and Conclusions

The fission gas behaviour in UO_2 is primarily determined by the irradiation temperature. With increasing temperature the mobility of the gas increases resulting in higher fission gas release and higher swelling. At all temperatures there is also a burnup dependence of the fission gas release and the swelling which is caused by the limited capacity of the fuel to retain the fission gas. The higher the temperature the lower is the saturation level of the retained fission gas and the earlier it is attained.

A strong cladding restraint reduces the fission gas swelling to a maximum value of about 7 vol. % even at high temperatures. This is presumably caused by preventing the formation of large grain boundary bubbles as a result of fuel deformation.

At temperatures above 1250 K the swelling rate induced by solid fission products diminishes with increasing burnup due to the release of cesium.

Fission gas release during a large break LOCA transient is smaller than 6 %. Fuel swelling was negligible. During a small break LOCA the fission gas release depends strongly on temperature and amounts to about 25 % at 1873 K after 1 hour.

5. References

/1/ H.E. Häfner, J. Nucl. Mat. 65 (1977) 65

/2/ H. Häfner und K. Philipp, KFK 1389 (1971)

/3/ D. Brucklacher and W.Dienst, J. Nucl. Mat. 36 (1970) 244

/4/ H.E. Häfner and H. Will, Kerntechnik 10 (1971) 454

/5/ H. Zimmermann, KFK 2467 (1977)

/6/ R.M. Cornell, J. Nucl. Mat. 38 (1971) 319

/7/ M.W. Speight, J. Nucl. Mat. 38 (1971) 236

/8/ C. Ronchi and Hj. Matzke, Fuel and Fuel Elements for Fast Reactors, IAEA, Vienna, 1974

/9/ J.A. Turnbull, BNES Conf. Nuclear Fuel Performance, London, Oct. 1973

General Literature

H. Zimmermann,
Investigations on swelling and fission gas release in UO_2,
J. Nucl. Mat., 75 (1978) 154-161

D.R. Olander,
Fundamental aspects of nuclear reactor fuel elements,
TID-26711-PL (1976), Technical Information Center, ERDA

C.E. Beyer, C.R. Hann,
Prediction of fission gas release from UO_2,
BNWL-1875 (1973)

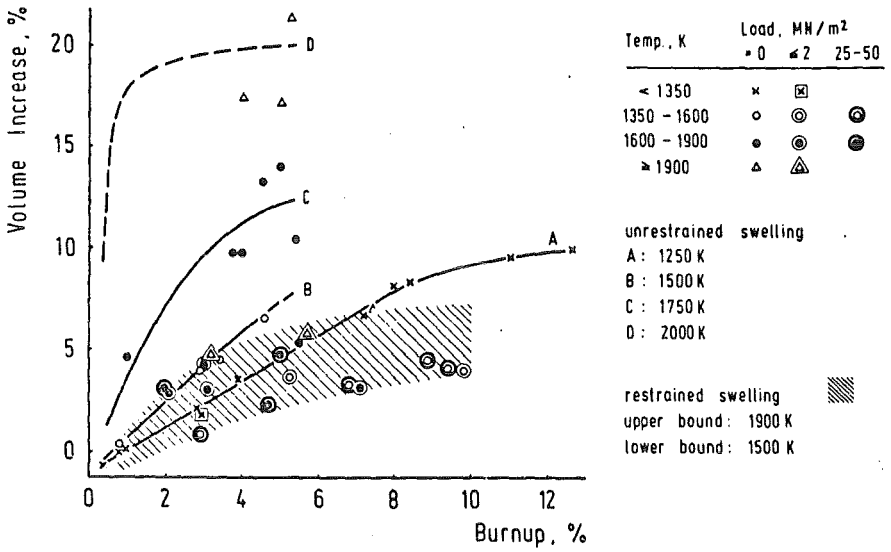

Fig. 1: Volume increase of UO_2 as a function of burnup.

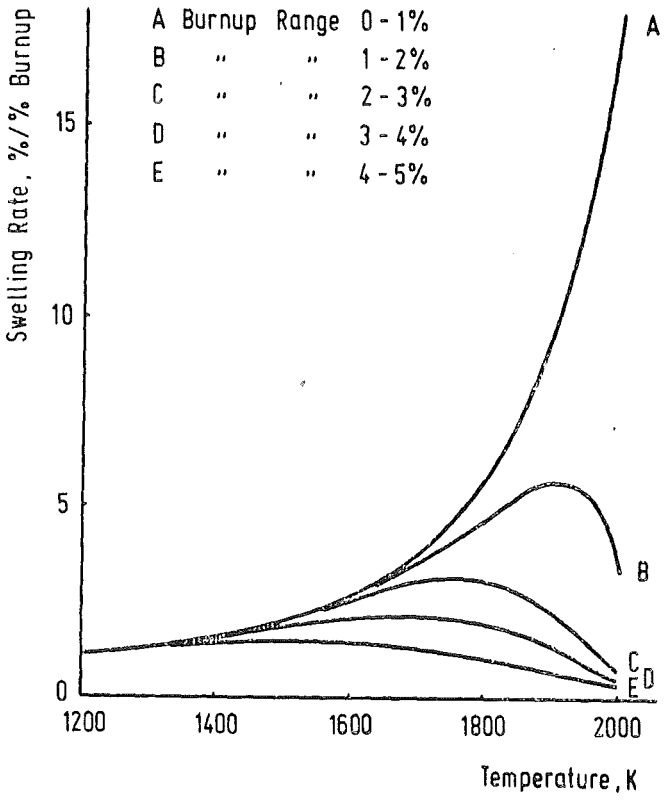

Fig. 2: Mean unrestrained swelling rates of UO_2 (without extensive bubble migration) as a function of temperature for various burnup ranges.

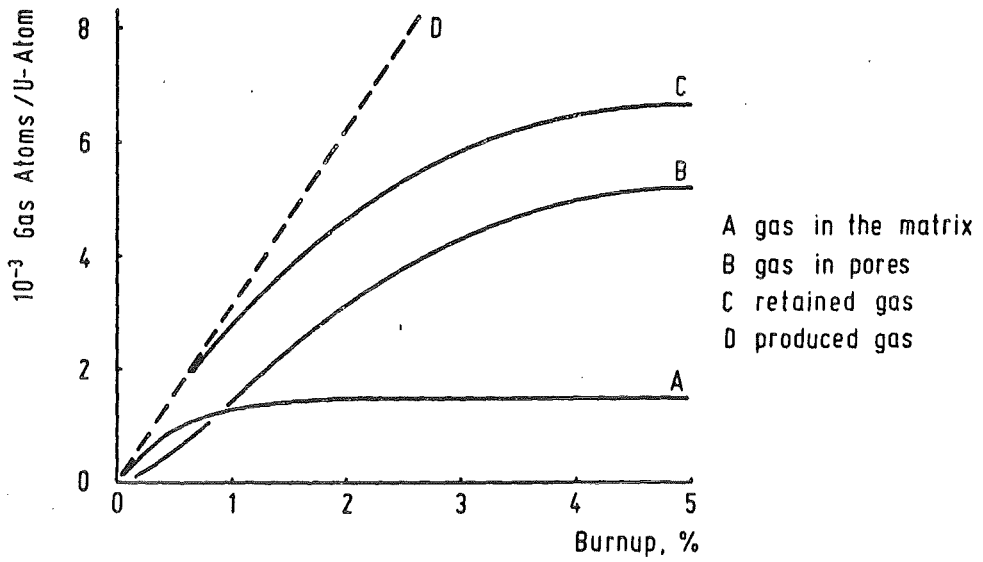

Fig. 3: Fission gas concentrations in UO_2 as a function of burnup at 1500 K.

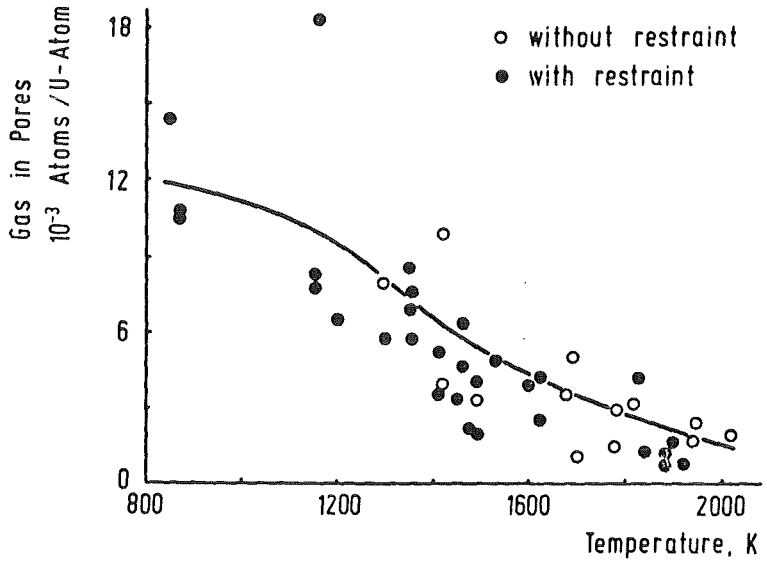

Fig. 4: Fission gas in pores as a function of fuel temperature for burnups $\geq$ 3 at.%.

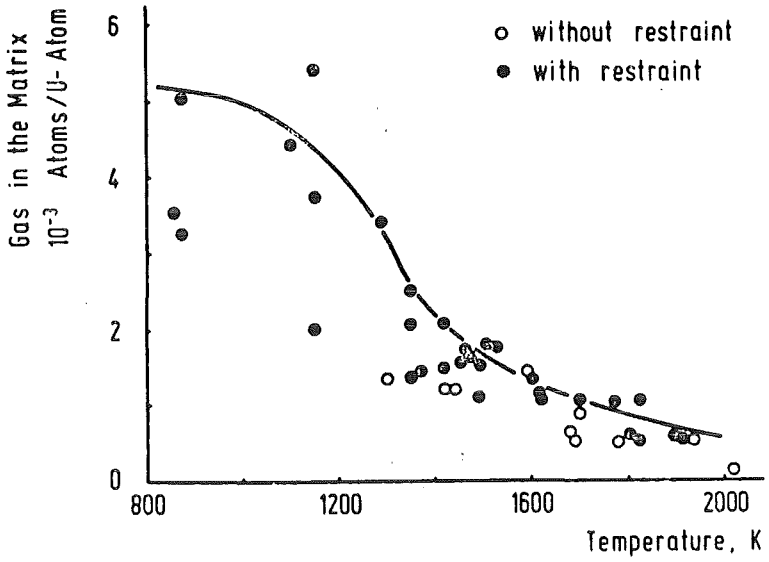

Fig. 5: Fission gas in the UO_2 matrix as a function of temperature for burnups $\geq$ 3 at.%.

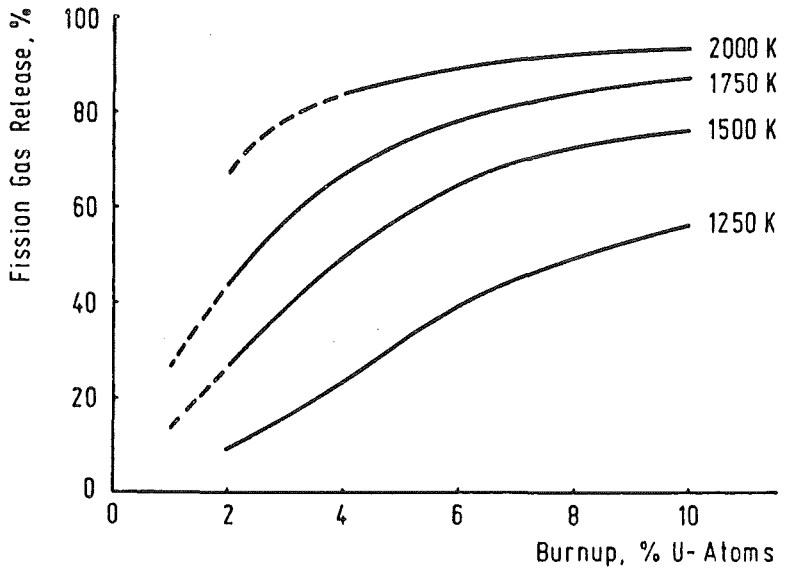

Fig. 6: Fission gas release from UO_2 as a function of burnup.

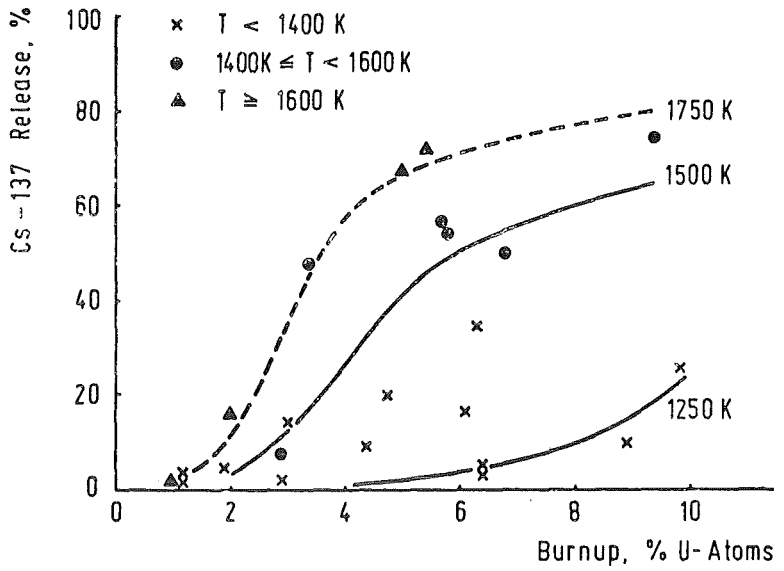

Fig. 7: Cs-137 release from UO_2 as a function of burnup.

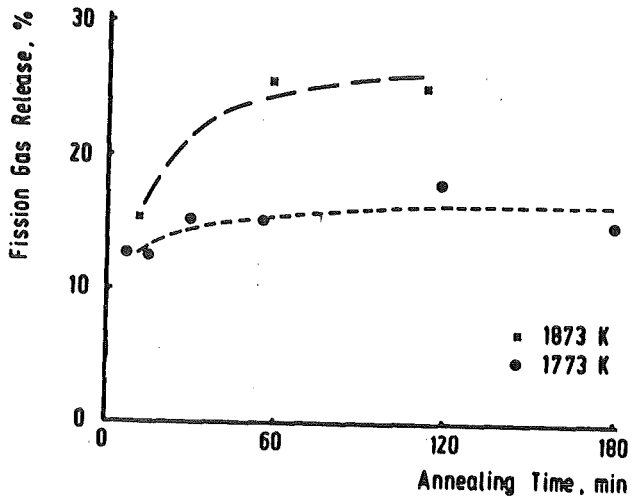

Fig. 8: Fission gas release during annealing as a function of time. Burnup: 2.4 at.%.

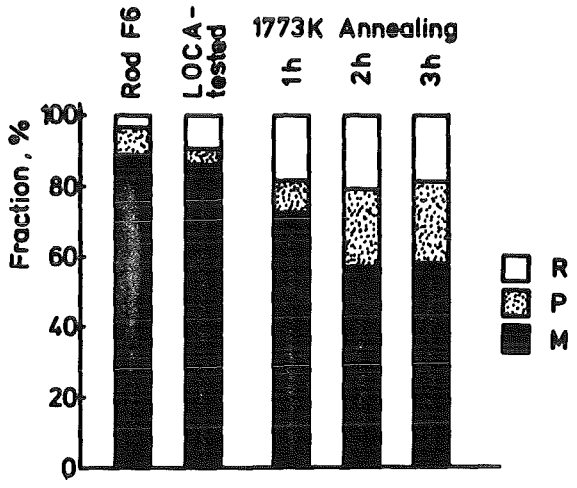

Fig. 9: Fission gas fractions in fuel samples with a burnup of about 2.4 at.% after various heat treatments. R = released gas, P = gas in pores, M = gas in matrix.

D. LWR AND HWR FUEL ROD BEHAVIOR UNDER NORMAL CONDITIONS

1. Pellet-Cladding Interaction (PCI)
2. Zircaloy Stress Corrosion Cracking (SCC)
3. Pellet-Cladding Interaction Remedies
4. Conclusions

D. LWR AND HWR FUEL ROD BEHAVIOR UNDER NORMAL CONDITIONS

1. PELLET-CLADDING INTERACTION IN LWR AND HWR FUEL RODS

The phenomenon responsible for Pellet-Cladding Interaction (PCI) failures is the stress corrosion cracking (SCC) of the Zircaloy cladding. SCC is the degradation of susceptible materials under the combined action of both an applied stress and an aggressive chemical environment where either of these factors acting independently would pose little threat to the integrity of the material. In a fuel rod, the fuel pellets create a load on the inner surface of the cladding, and the aggresive environment is provided by the release of volatile fission products from the fuel pellets.

PCI is recognized as a major mechanism for cladding rupture during normal operation /1/. It is also being evaluated as a possible clad failure mechansim during off normal power transients /2,3/. To understand this phenomenon one must first consider the processes that occur in a fuel rod in a reactor.

When the power is raised initially the Zircaloy cladding is ductile and the as-fabricated gap between the fuel pellets and the cladding is sufficient to accommodate the larger thermal expansion of the fuel pellets. The pellets also crack and relocate outwards to contribute to gap closure. Later in life, however, the Zircaloy cladding becomes somewhat embrittled due to its exposure in the intense neutron environment, while the pellet-clad gap continues to decrease due to dimensional increases (fission product swelling) in the fuel pellets and, in the case of PWRs, inward motion or creepdownof the thin-walled cladding in response to the applied coolant pressure. Under such conditions, if the fuel rod power is increased, local power changes may be of sufficient magnitude to cause direct interaction between the UO_2 pellet and the Zircaloy cladding with the resulting straining and possible fracture of the cladding.

Both the presence of aggressive chemical species and high localized stress (strains) are prerequisites for power-ramp-induced PCI failures, although the relative contributions of these two factors remains to be resolved /1/. This synergism between stress or strain concentrations at pellet crack and/or pellet-pellet interface locations and the harmful species is schematically illustrated in Fig. 1.

The principal basis for concluding that PCI fracture of Zircaloy cladding is the result of stress corrosion is the large body of data on the shape and morphology on the cracks found in both power reactor /4, 5/ and test reactor /6,7/ fuel rods, which exhibit similar characteristics to those found for cracks induced in laboratory SCC experiments using iodine (a known fission product) as the embrittling agent /8,9/. The key features in common are listed as follows /10/:

1. Cladding cracks are normal to the cladding surface (i.e., 90^{o} to the hoop stress).
2. A number of partially penetrating (incipient) cracks are observed.
3. Incipient cracks are tight, i.e., openings are small compared to their length.
4. Fully penetrating cracks are characterized by an absence of general deformation or necking of the cladding.
5. Fracture surfaces are essentially macroscopically flat with little evidence of extended 45^{o} shear fracture segments except perhaps near the outer cladding surface.
6. At the microscopic level, fracture surfaces exhibit flat cleavage planes and fluted regions.

Figures 2 and 3 illustrate some of these features.

The SCC phenomenon in Zircaloy appears to be the operative failure mode over a broad range of reactor operating conditions. PCI failures have occurred in Zircaloy-2 BWR and Zircaloy-4 PWR cladding, operated under quite different conditions but within the normal range for fuel rod linear heat generation rates in power reators (26 to 43 kW/m); similar failures are also seen in test reactor fuel rods that are power ramped outside the normal power reactor domain (e.g., to powers 60 > kW/m at ramp rates up to $\sim$ 0.16 kW/m/s). The implication of this conclusion is that stress corrosion cracks can form and propagate under a broad range of mechanical/chemical conditions, extending from high stress - low fission product (iodine) availability to low stress-high fission product availability situations. Thus, fission product availability and stress can be considered to be reciprocal in the Zircaloy PCI-SCC process.

2. ZIRCALOY STRESS CORROSION CRACKING

Mechanistic studies of Zircaloy SCC have been, and still are, involved in

(a) characterizing the steps involved in iodine SCC and the role, if any, of Zircaloy's metallurgical properties;
(b) identifying the rate-limiting or critical steps in the process; and
(c) establishing the mechanical/chemical conditions for SCC, in particular the existence of "thresholds".

The majority of the data is from unirradiated Zircaloy-2 and-4, but sufficient data have been obtained on irradiated cladding to show the major effects of irradiation /11,12/. The current data base supports a threshold-stress concept; that is, a sustained critical tensile stress in a sustained environment of aggressive fission-product species /11/. The threshold stress is associated with the formation of a crack at inhomogeneities in the Zircaloy surface (e.g., FeNiCr or Al/Si rich particles) /9/. If the ID oxide film is cracked, small intergranular cracks will form below the threshold stress, but these are nonpropagating. The threshold stress is influenced, as expected, by iodine availability, a well-defined iodine concentration threshold, of $1\text{-}3 \times 10^{-2}$ g I_2/m^2, was measured below which no cracking was observed /13/ (Fig. 4). The iodine concentration threshold (critical iodine concentration) depends strongly on temperature /3/. An influence of iodine on the mechanical properties of Zircaloy cladding can be observed up to about 800°C /3/. Times to failure above the iodine concentration thresholds were reduced by about an order of magnitude for each order-of-magnitude increase in iodine concentration, and failure strains dropped to near zero ($\leq$ 400°C). This work also indicates a temperature influence such that a temperature increase from 623 to 673 K produced two orders of magnitude reduction in time to rupture. Similar behavior was observed in tests on irradiated Zircaloy.

The effect of metallurgical variables on Zircaloy SCC does not appear to be strong /9,11,14/. Data on unirradiated Zircaloys indicate a slight effect of microstructure, and there is an influence due to either Zircaloy surface condition, surface texture, or internal stress, or a complex combination of these features /14/. By far the strongest effect on threshold stress, however,

is that of irradiation, which tend to override any small differences in microstructure or chemical compositions /11,15/. Results from pressurized-tube tests on power reactor irradiated Zircaloys (from which the fuel was removed before testing), shown in Fig. 5, clearly show the large reduction in threshold stress (when compared as a fraction of the yield strength) at long times to failure, which is observed after 5 x 10^{24} n/m^2 fast neutron fluence. SCC can therefore occur at stresses ranging from close-to-yield stress to a fraction ($\sim \frac{1}{3}$) of the yield stress (i.e., in the elastic range!). At the high stresses short, axial splits result, wheras at the low stresses pinhole failures were most common. Cracks of both type have also been observed in defected power reactor fuel rods /4,5/.

2.1. Role of Zircaloy Plastic Deformation

Although there is a general consensus that plastic tensile strain is needed for SCC to occur, there is some doubt as to whether a macroscopic critical strain is a prerequisite for SCC. Rather, the data support a threshold stress concept as discussed above.

Due to a combination of anisotropic properties and varying axial and circumferential stress and temperature profiles, the strain distribution in a fuel rod cladding is irregularly distributed even on a macroscopic scale, as is evidenced by the observation of both creep ovalization (particularly in PWR CLADDING) and circumferential ridge formation. The former, as noted earlier, is partially responsible for closure of the fuel-clad gap - ovalization generally results is point contact between fuel and cladding. The latter form as a result of a "ratcheting" process - cyclic stretching of the cladding by the fuel - principally during power cycling /16/. There is clear evidence from test reactor data that ridges form or grow during power ramps /17,18/. These ridges are the location of the PCI-induced cracks, but since this is also the region of maximum fission product concentration, it is not clear whether the high stress (or strain) concentration at ridges is responsible for crack initiation.

2.2. Role of the Fuel Pellet

The fuel pellet is both the source of clad loading and of fission-product chemical environment. In the former role, it is the cracking, and relocation of the cracked fuel segments, that provides the principal source of cladding stress, with fission-product swelling making a smaller contribution. At higher fuel rod powers and hence fuel temperatures, fuel pellet plasticity can of course relax part of these stresses, but, in general, operating conditions minimize this effect. Stresses (and hence strains) are concentrated over fuel pellet cracks at pellet-pellet interfaces, due to the "wheatsheafing" expansion characteristics of the fuel pellet. Fig. 6 illustrates the "theoretical" picture of a cracked fuel pellet at operating temperature /19/. Utilizing such a model, hoop stress concentrations of factors of 2 or more have been calculated in PCI situations /16,19/.

The second key aspect of the PCI process is the availability of aggressive fission products at the cladding inner surfaces. Current information about fission product availability in fuel rods is very limited and is only sufficient to indicate a correspondence between the occurrence of PCI cracks and the presence of fission products at the cladding inner surfaces /20/.

The species most aggressive to Zircaloy are iodine, cesium and cadmium (in that order) which are released in vapor form from regions of the fuel that operate at high temperatures. These vapors then migrate and form compounds (e.g., CsI) that condense on the cooler inner surface of the cladding. In calculating the release of the aggressive volatile fission products (VFP) the assumption is typically made that the fraction released is equal to the fraction of inert fission gases released by the fuel.

A recent "first generation" model for the behavior of VFP provides a more detailed picture of their behavior. As schematically represented in Fig. 7, several different regimes, and hence behavior patterns, are expected /21,22/.

(1) For low fuel temperatures, the VFP do not redistribute.
(2) For steady-state operation at higher temperatures or for slow temperature increases, the VFP migrate readily toward the fuel periphery and for the most part remain in the UO_2 (a small fraction find crack surfaces and hence an easy path to the rod free volume).
(3) For low burnups or small increases in burnup after the most recent temperature rise, the VFP will migrate radially to the fuel periphery and remain in the UO_2 even for fast temperature increases.
(4) For fast temperature increases after some burnup (larger than that of Item 3) at low temperature, the VFP will be released and deposited on cladding inner surfaces and will be available to cause SCC or PCI failures.
(5) The fractional release of VFP during the operational mode identified in Item 4 above will be approximately equal to the fractional fission gas release.
(6) The fractional release of VFP during operational modes 1,2 and 3 above is expected to be smaller than the fractional fission gas release.

The interesting feature of this model is that it can explain the effects of duty cycle on PCI failure probability strictly in terms of the availability of VFP at the cladding inner surface, and hence downgrades the importance of mechanical loading of the cladding.

3. PELLET-CLADDING INTERATION REMEDIES

The understanding of PCI is advanced but incomplete. Nevertheless, design and operating remedies have been introduced in an attempt to alleviate the impact of PCI on plant capacity. Design remedies have addressed the mechanical-chemical nature of PCI, namely reducing clad stresses, fuel temperatures, and/or fission product release. Operation remedies have emphasized reduced severity of the duty cycle through less use of control rods for achieving power maneuvers and power shaping. One of the most significant changes to

the LWR fuel design that is expected to reduce PCI damage was the increase in the number of fuel rods per assembly to reduce the power per rod. For PWRs, however, the principal reason for this change was not PCI alleviation, but to reduce the consequences of hypothetical accidents to acceptable conservative levels.

Early changes adopted by fuel vendors included fuel pellet shape, clad thickness, and metallurgical structure, all of which were intended to reduce clad stresses. Subsequent and current changes being evaluated address either or both (a) the thermal, and hence fission product, environment in the fuel rod, and (b) crack formation at the cladding inside surface /23,24/.

One other "simple" change recently introduced by BWR vendors is prepressurization (typically 0.3 to 0.5 MPa helium) of the fuel rods, which is the current practice in PWR designs. This step should stabilize the internal thermal environment (i.e., fuel-to-clad gap heat transfer), thereby eliminating the possibility of the sharp temperature rise and high fission product release that is sometimes observed in unpressurized fuel rods /4,10/.

Modifications to the fuel pellet itself that would reduce (or eliminate) fission product release also appear practical. Three that are being pursued are the annular pellet /25/, a large grain size fuel pellet (fabricated using Nb_2O_3 as an additive) in which the large grains delay the grain boundary saturation and release process, /23/ and a dual enrichment (or duplex) pellet which, by virtue of an outer enriched UO_2 region and an inner natural UO_2 core, operates at lower average temperatures and flatter temperature gradients for the same equivalent power /23,24/ (Fig. 8).
The mechanical properties of Zircaloy have been modified progressively over the years to respond to various concerns (creep collapse, fuel rod bow, etc.) and they seem to be optimized for overall performance in LWRs. Texture could perhaps be modified to make the I.D. surface more resistant to crack formation and earlystage propagation. A modification of the inner surface of the Zircaloy cladding would eliminate (or disperse) the locally high concentrations of alloying impurities (Fe, Cr, Ni), or impurities (Al, Si) at or near which cracks have been found to initiate /9/. Suitable heat treatments, combined with a general "clean-up" at the ingot, and pickling and grit blasting stages could

possibly achieve some significant improvements. Of the "remedies" that fall into this category, none alone, or in combination, appears likely to lead to a nil-capacity loss fuel. A modified design combination, such as a pre-pressurized fuel rod containing an annular, large grain size fuel pellet, when combined with controlled core operations using a power shape monitoring type of system, may well be more than adequate for PWRs in which power maneuvers are made by chemical shimming (with boron), or for base-loaded BWRs. For load-follow capacity in BWRs, however, which would make extensive use of the control rods, a more forgiving design must be sought. Since Zircaloy and UO_2, in contact, are basically incompatible, a barrier between the two fuel-rod components seems a logical remedy. There is some evidence which indicates that the I.D. surface oxide film itself could be an effective barrier to SCC if it remains intact, /26/but most vendors have opted for a barrier material. The Canadians have developed a graphite coating on the Zircaloy I.D., called CANLUB fuel, for their CANDU reactors; /27/ extensive data indicate an improvement in PCI resistance which is due, primarily, to a fission product "gettering" mechanism, rather than to relaxation of interface stresses /28/. The Canadians are now pursuing a siloxane coating which will likely provide improved chemical gettering properties /27,28/.

For LWR application a more acceptable barrier would be a metal on the cladding surface, since it is unlikely that a ceramic coating could survive a LWR fuel cycle (e.g., the discharge burnup of CANDU fuel is 1037 GJ/kgM compared to 2000 to 3000 GJ/kgM). It is generally believed that the BWR duty cycle will necessitate that the barrier be both impervious to iodine attack and sufficiently plastic to relax interfacial stresses in the cladding. Two candidates that are receiving worldwide attention are copper (plated as a 5-10 μ layer on the inner surface) and zirconium (coextruded with the Zircaloy) /29/. Both laboratory PCI simulation tests and test-reactor ramp tests have confirmed the advantages of these concepts over conventional Zircaloy cladding in resisting cracking. The Cu- and Zr-barrier fuel rods survived ramps to ∿ 60 kW/m and 6-24 h holds at peak power, after 864 GJ/kgM burnup, wheras conventional rods failed by PCI-SCC in an hour or less. Fig. 9 shows the typical appearance of the (a) copper and (b) zirconium layers after ramping, compared to a (c) conventional cladding.

4. SUMMARY AND CONCLUSIONS

Mechanical and chemical interaction between the UO_2 fuel pellets and the Zircaloy cladding of LWR and HWR fuel rods can result in cladding failures. PCI failures tend to occur in rods that have been irratiated to significant burnup and then subjected to power increases. It is now generally agreed that this type of failure is due to SCC of the cladding. Cracking, usually on a radial plane, originates at the inside surface of the cladding by fuel thermal expansion during the power ramp and by chemical attack of aggressive fission products released rom the UO_2 fuel. Iodine is one of the prime suspects as the chemical substance involved in PCI-SSC failures.

The incidence of PCI failures can be kept acceptably low by using very slow rates of power change. However, this solution is expensive because of the substantial costs associated with the operation of the power plant at partial capacity throughout the long periods while the power is being slowly increased. Thus, there is an important need to understand and improve the SCC behavior of Zircaloy cladding so that increased operational flexibility and reduced costs can be achieved while maintaining the frequency of fuel failures at an acceptably low level.

References

J.T.A. Roberts, STURCTURAL MATERIAL IN NUCLEAR POWER SYSTEMS (1981), Plenum Press, New York

/1/ F. Garzarolli, H. Stehle, The Main Causes of Fuel Element Failure in Water-Cooled Power Reactors, At. Energ. Rev., 17, 31-128 (1979).

/2/ C.L. Mohr, P.J. Pankaskie, J.C. Wood and G. Hessler, PCI Fuel Failure Analysis, PNL-2755, NUREG/CR-1163 (December 1979).

/3/ P. Hofmann, J. Spino, Influence of simulated fission products on the ductility and time-to-failure of Zircaloy-4 tubing in LWR transients, KfK 3045 (1980).

/4/ N. Fuhrman, V. Pasuputhi, D.B. Scott, S.M. Temple, S.R. Pati and T.E. Hollowell, Fuel Performance in Main Yankee Core 1, EPRI NP-218 (November 1976).

/5/ Determination and Characterization of Incipient Defects in Power Reactor Fuel Rods, NP-812, (July 1978).

/6/ G.R. Thomas, The Studvik InterRamp Project - An Intern. Power Ramp Experim. Program, Meeting on Ramping and Load-Following Behavior of Reactors, November 30 to December 1, 1978, Petten, The Netherlands.

/7/ P. Knudsen, C. Bagger and M. Fishler, Characterization of PWR Power Ramp Tests, in: Proc. of the Am. Nucl. Soc. Topical Meeting on Water Reactor Fuel Performance, May 9-11, 1977, St. Charles, Illinois, pp. 243-252.

/8/ B. Cox and J.C. Wood, Iodine-Induced Cracking of Zircaloy Fuel Cladding, in: Corrosion Problems in Energy Conversion and Generation, Electrochem. Soc., New York (1974), pp. 275-321.

/9/ D. Cubicciotti and R.L. Jones, Stress Corrosion Cracking of Zircaloy, EPRI NP-717 (March 1978).

/10/ J.T.A. Roberts, E. Smith, N. Fuhrman and D. Cubicciotti, On the Pellet-Cladding Interaction Phenomenon, Nucl. Technol. 35, 131-144 (1977).

/11/ J.T.A. Roberts, R.L. Jones, E. Smith, D. Cubicciotti, A.K. Miller, H.F. Wachob and F.L. Yaggee, An SCC Model for Pellet-Cladding Interaction Failures in LWR Fuel Rods, in: Proc. of the 4th Intern. Conf. on Zirconium in the Nucl. Industry, ASTM 681 (1979), pp. 285-305.

/12/ R.F. Mattas, F.L. Yaggee and L.A. Neimark, Iodine Stress-Corrosion Cracking in Irradiation Zircaloy Cladding, in: Proc. of the Am. Nucl. Soc. Topical Meeting on Light Water Reactor Fuel Performance, April 29-May 3, 1979, Portland, Oregon, pp. 128-140.

/13/ M.Peehs, J. Stehle and E. Steinberg, Out-of-Pile Testing of Iodine Stress Corrosion Cracking in Zircaloy Tubing under the Aspects of the PCI Phenomenon, in: Proc. of the 4th Intern. Conf. on Zirconium in the Nucl. Industry, ASTM 681 (1979), pp. 244-260.

/14/ B.C. Syrett, D. Cubicciotti and R.L. Jones, Some Observations on the Influence of Texture and of Second-Phase Particles on Iodine SCC of Unirradiated Zircaloy, in: Proc. of the Am. Nucl. Soc. Topical Meeting on Light Water Reactor Fuel Performance, April 29 to May 3, 1979, Portland, Oregon, pp. 113-127.

/15/ Liv Lunde and Ketil Videm, The Influence of Environmental Variables and Irradiation on Iodine Stress Corrosion Crack Initiation and Growth in Zircaloy, paper presented at IAEA Specialists Meeting on Water Reactor Fuel Element Performance Computer Modeling, March 17-21, 1980 Blackpool, U.K.

/16/ W.J. Baley, C.L. Wilson, L.J. MacGowan and P.J. Pankaskie, State-of-the-Technology Rev. of Fuel-Cladding Interaction, Battelle Northwest Laboratory Report COO-4066-2, PNL-2488 VC-78 (December 1977).

/17/ E. Rolstad and K.D. Knudsen, Studies of Fuel-Clad Mechanical Interaction and the Resulting Interaction Failure Mechanism, in: Fourth United Nations Intern. Conf. on the Peaceful Uses of Atomic Energy, September 6-16, 1971, Geneva, Switzerland

/18/ P.J. Fehrenbach, In-Reactor Measurement of Clad Strain, in: Proc. of the Am. Nucl. Soc. Topical Meeting on Light Water Reactor Fuel Performance, April 29 to May 3, 1979, Portland, Oregon, pp. 255-263.

/19/ J.H. Gittus, Theoretical Analysis of the Strain Produced in Nuclear Fuel Cladding Tubes by the Expansion of Cracked Cylindrical Fuel Pellets, Nucl. Eng. Des., 18, 69-82 (1972).

/20/ D. Cubicciotti, J.E. Sanecki, R.V. Strain, S. Greenburg, L.A. Neimark and C.E. Johnson, The Nature of Fission-Product Deposits inside LWR Fuel Rods, in: Proc. of the Am. Nucl. Soc. Topical Meeting on Water Reactor Fuel Performance, May 9-11, 1977, St. Charles, Illinois, pp. 282-294.

/21/ D. Cubicciotti, State of-the-Art Model for Release of Volatile Fission Products from UO_2 Fuel, EPRI Project RP 355-11 (1978).

/22/ D. Cubicciotti, A Quantitative Model for Volatile Fission Product Release from UO2 Fuel, EPRI RP 355-11 (June 1979).

/23/ J.T. A. Roberts and F. E. Gelhaus, Zircaloy Performance in Light Water Reactors, in: Proc. of the 4th Intern. Conf. on Zirconium in the Nucl. Industry, ASTM 681 (1979), pp. 19-39.

/24/ D.H. Locke, Pellet-Cladding Interaction for Water Reactors: Experience Testing and Evaluation, At. Energ. Rev., 15, 779-792 (1977).

/25/ F.W. Buckman, C.E. Crouthamel and M.D. Freshley, FCI Remedy Development in: Proc. of the Am. Nucl. Soc. Topical Meeting on Light Water Reactor Fuel Performance, April 29 to May 3, 1977, Portland, Oregon, pp. 158-168.

/26/ R.F. Mattas and F.L. Yaggee, The Effect of Zirconium Oxide on the Stress Corrosion Susceptibility of Irradiated Zircaloy Cladding, paper presented an Fifth Intern. Conf. on Zirconium in the Nucl. Industry, August 4-7, 1980 Boston, Massachusetts, ASTM 783.

/27/ D.G. Hardy, J.C. Wood and A.S. Bain, CANDU Fuel Performance and Development, paper presented at the 18th Annual Intern. Conf. of the Canadian Nucl. Ass., Nucl. Fuels and Recycle Session, Ottawa, June 14, 1978.

/28/ J.C. Wood, D.G. Hardy and A.S. Bain, Mechanistic Studies of Power Ramping Defects and Remedies, in: Proc. of the Am. Nucl. Soc. Topical Meeting on Light Water Reactor Fuel Performance, April 29 to May 3, 1979, Portland, Oregon, pp. 169-178.

/29/ D.S. Tomalin, R.B. Adamson, R.P. Gangloff, The Performance of Irradiated Copper and Zirconium Barrier-Modified Zircaloy Cladding under Simulated PCI Conditions, in: Proc. of the 4th Intern. Conf. on Zirconium in the Nucl. Industry, ASTM 681 (1979), pp. 122-144.

/30/ P. Hofmann, J. Spino; Determination of the critical iodine concentration for SCC failure of Zircaloy-4 tubing between 500 and 900°C, J. Nucl. Mat., 107 (1982) 297-310.

/31/ P. Hofmann, J. Spino; Chemical Aspects of iodine-induced SCC failure of Zircaloy-4 tubing above 500°C, to be published in the J. Nucl. Mat. (1982).

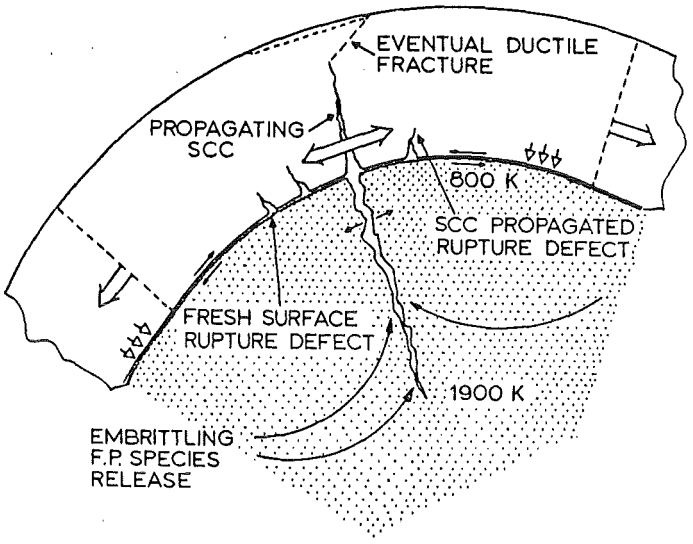

Fig. 1 : Schematic of PCI Zircaloy fuel rod failure mechanism.

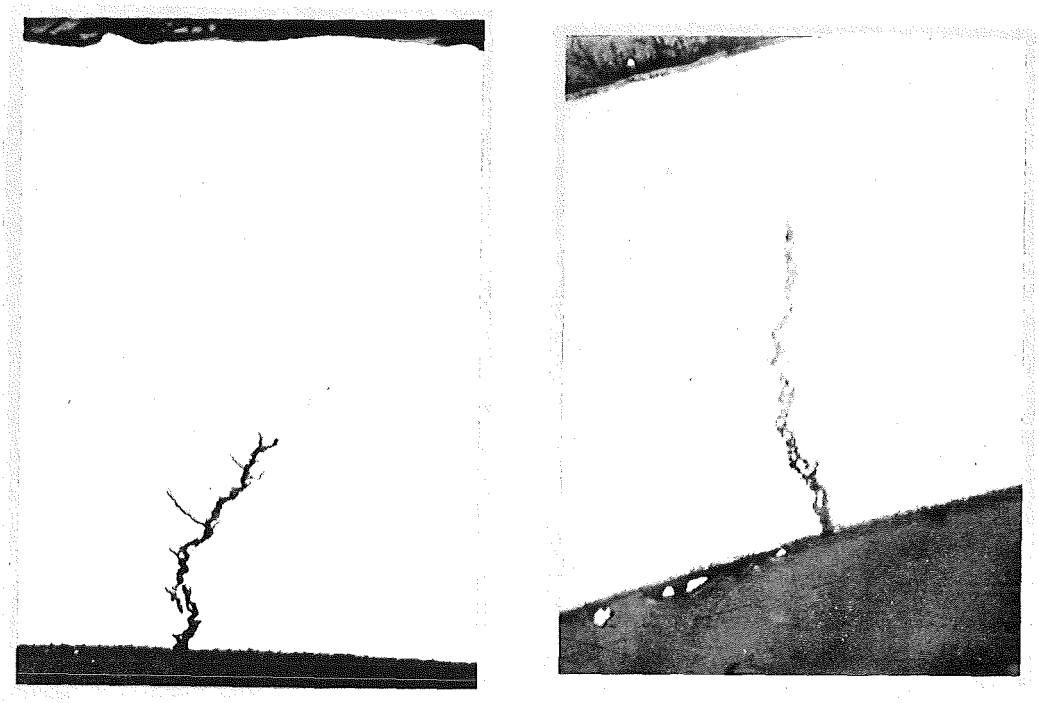

Fig. 2 : Partial through-wall crack in irradiated Zircaloy cladding caused by SCC (power reactor fuel rod).

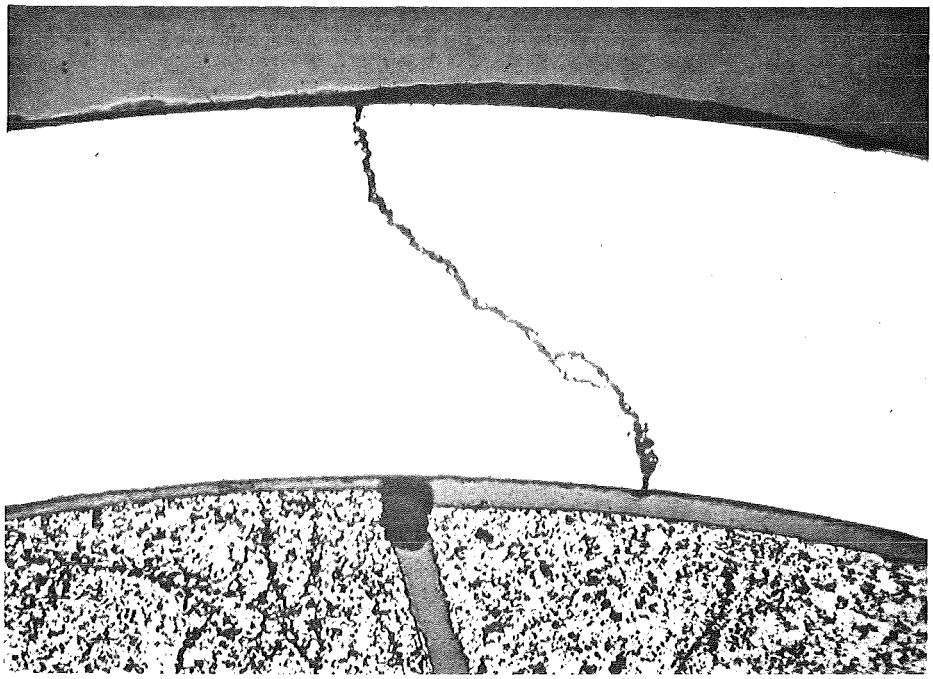

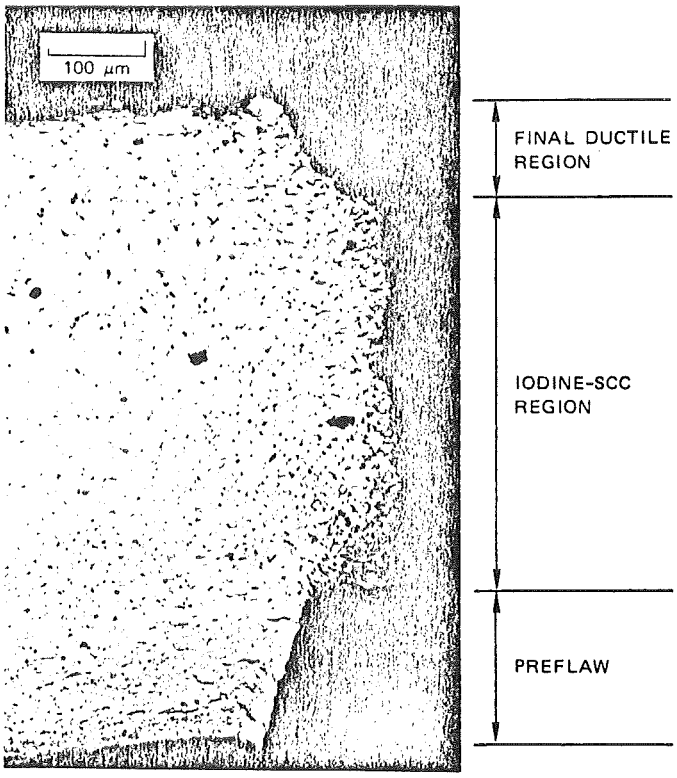

Fig. 3: A through-wall stress corrosion crack in the Zircaloy cladding of a fuel rod. Failure was induced by rapidly increasing power in a test reactor following irradiation of the fuel rod in a commercial reactor.

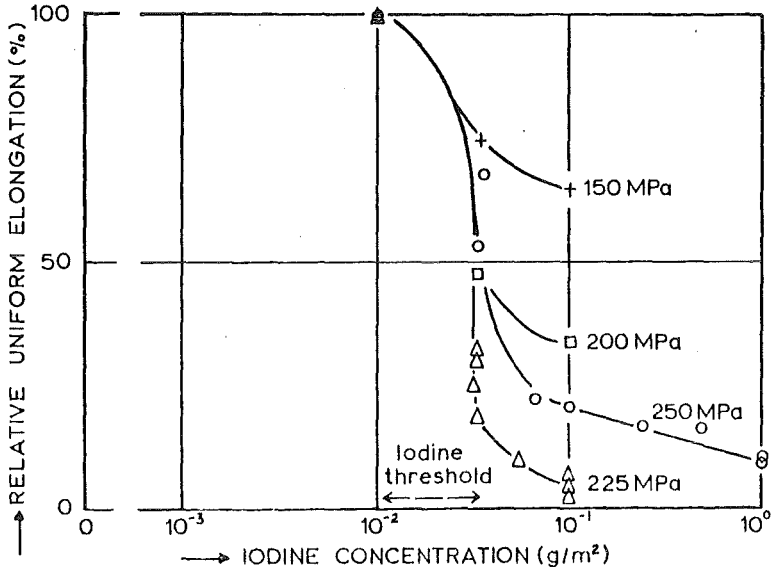

a

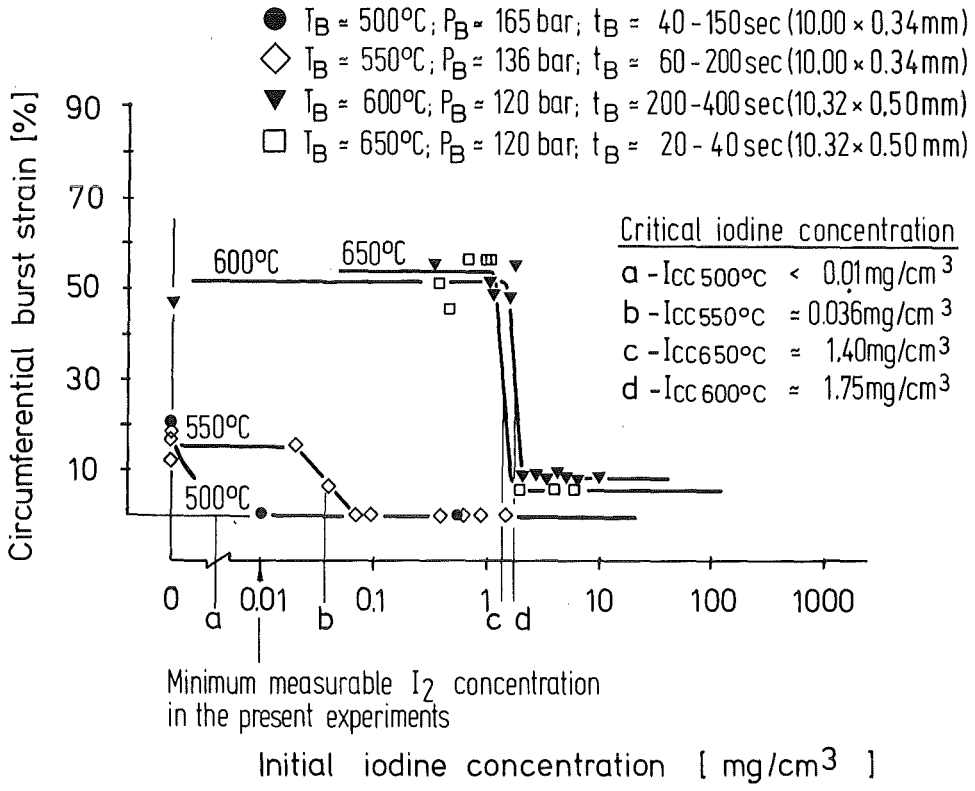

b

Fig. 4: Iodine concentration threshold for SCC of stress-relieved Zircaloy at 400°C (a), and for the temperature range 500 to 650°C (b).

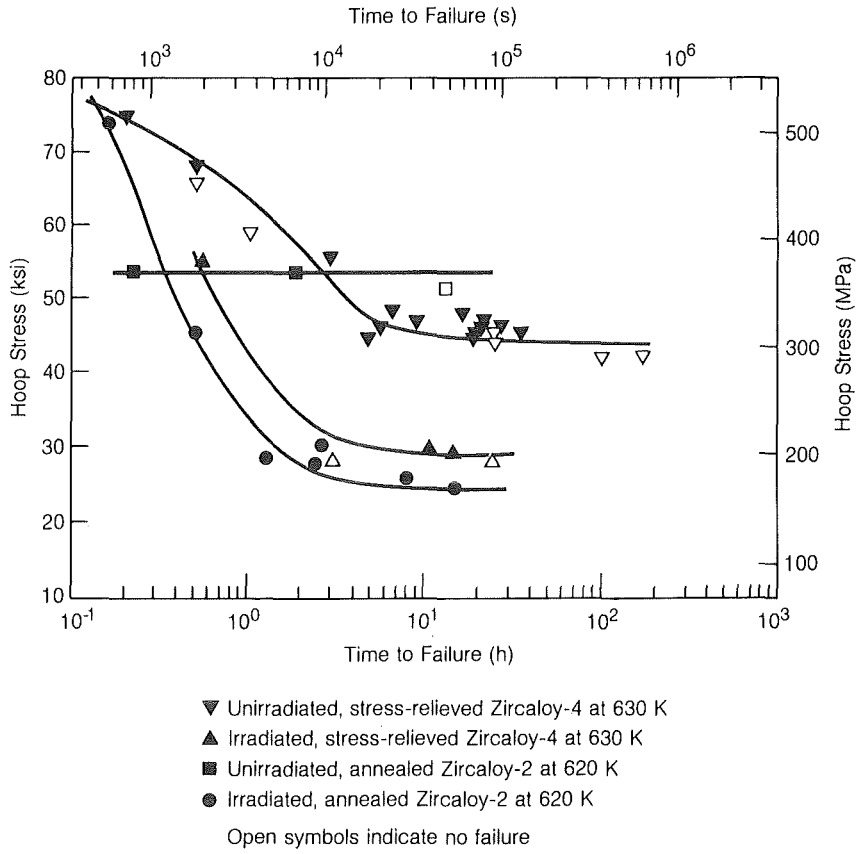

Fig. 5 : Effect of irradiation on the resistance of internally pressurized Zircaloy tubes to iodine-induced failure at 620-630 K.

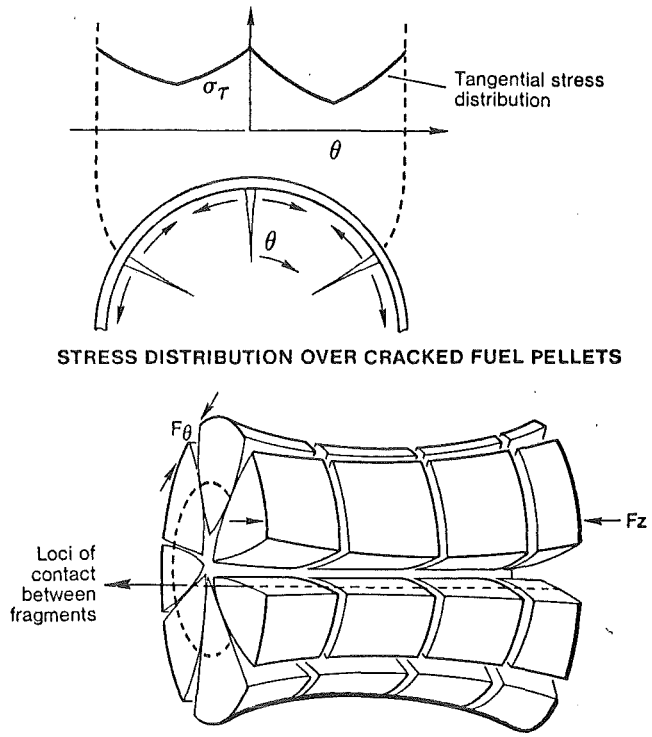

Fig. 6 : Theoretical pellet condition during irradiation

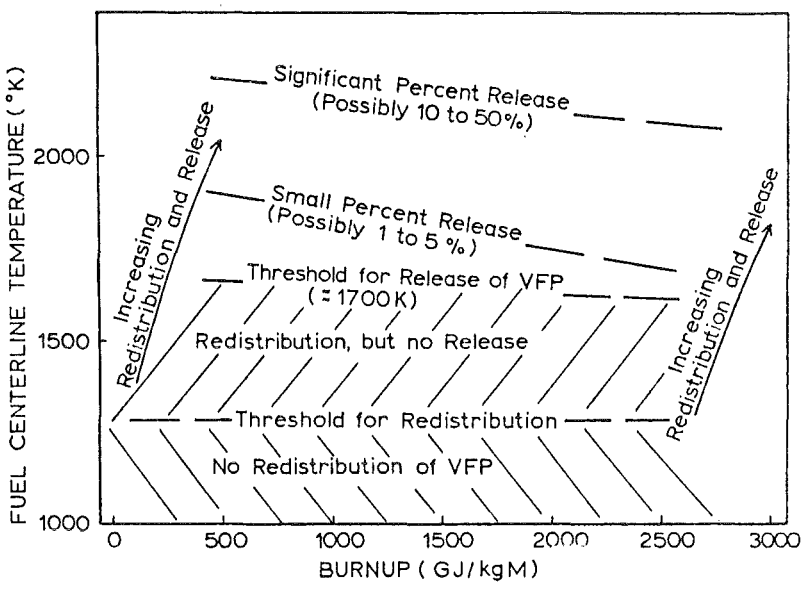

Fig. 7 : Schematic representation of redistribution and release behavior of volatile fission products (VFP) predicted by state-of-the-art model.

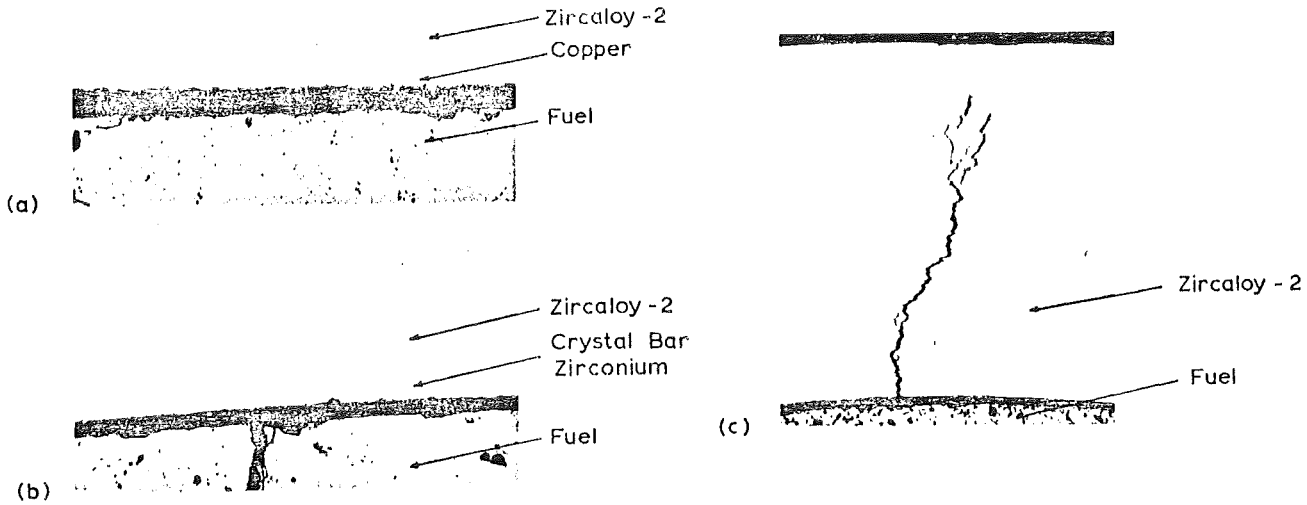

Fig. 9 : Typical appearance of (a) copper barrier, (b) Zr liner (in as-polished condition), and (c) reference fuel rod after ramp testing.

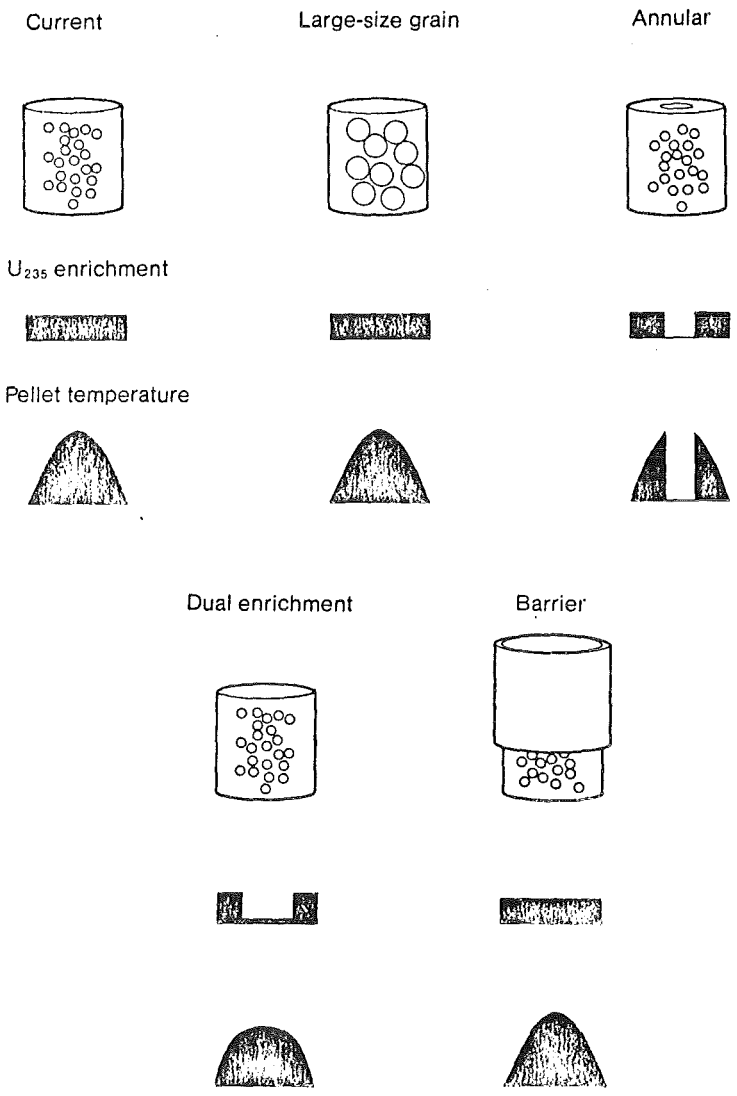

Fig. 8 : Modifying fuel rod designs to decrease the amount of aggressive fission products reaching the inner surface of the cladding appears promising as a means of preventing PCI failure.

Large-grain-size fuel should delay fission product release. Annular pellets reduce fuel temperatures, hence fission product release, by removing the hottest part of the pellet. Duel-enrichment pellets achieve these goals by surrounding an inner core of natural UO_2 with an outer ring of enriched UO_2. Another approach to preventing PCI failure is to place a physical barrier between the pellets and the Zircaloy cladding to prevent its attack by aggressive chemicals.

E. LWR FUEL ROD BEHAVIOR UNDER OFF-NORMAL CONDITIONS

1. INTRODUCTION

2. POWER COOLING MISMATCH ACCIDENT (PCM)

3. REACTIVITY INITIATED ACCIDENT (RIA)

4. LOSS OF COOLANT ACCIDENT (LOCA)

5. ANTICIPATED TRANSIENT WITHOUT SCRAM (ATWS)

6. SEVERE FUEL DAMAGE ACCIDENT (SFD)

7. CONCLUSIONS

E. LWR FUEL ROD BEHAVIOR UNDER OFF-NORMAL CONDITIONS

1. Introduction

Investigation of fuel rod behavior under off-normal conditions was initiated to determine the safety margins of licensing procedures, to identify overconservatisms and, where necessary, to formulate more precise criteria to achieve an even higher level of safety.

Numerous in-pile and out-of-pile experiments have been performed. Computer codes have been developed and tested against these experimental data. Initially, the work was performed only in the USA and West Germany; later Japan, England, Canada, and France started similiar programs.

The Power Burst Facility (PBF) reactor at the Idaho National Engineering Laboratory (USA) is the largest installation constructed for in-pile testing. The moste comprehensive experimental program concerning fuel rod behavior under off-normal conditions was performed in this reactor by EG&G, Idaho, Inc. Investigations in the other countries (except Japan) concentrated mainly on Loss Of Coolant Accidents (LOCA), particularly in West Germany. Fuel rod behavior under Reactivity Initiated Accident (RIA) conditions was studied primarily in Japan in the Nuclear Safety Research Reactor (NSRR), a swimming pool reactor.

The objectives of the PBF experimental program were:

- to investigate fuel rod failure under different types of accident or transient conditions,

- to identify the most important parameters and determine the threshold for fuel rod failure,

- to determine the extent of fuel rod damage, and

- to obtain experimental data for the development and verification of analytical models used to predict fuel rod and core behavior.

The types of accidents and transients considered here are the following:

- Power Cooling Mismatch Accident (PCM)
- Reactivity Initiated Accident (RIA)
- Loss of Coolant Accident (LOCA)
- Anticipated Transient Without Scram (ATWS)
- Severe Fuel Damage Accident (SFD)

Subsequent paragraphs will describe these accidents in detail, with special emphasis on the LOCA research which has been performed at the Kernforschungszentrum Karlsruhe.

2. Power Cooling Mismatch Accident

The PCM accident has been investigated primarily in the PBF reactor. The PCM test series was designed to parametrically evaluate the behavior of previously unirradiated fuel rods, with cladding temperature, fuel rod power, and time in stable film boiling as the primary variables. Fuel rod power, cladding temperature, and fuel rod internal pressure are the most important variables influencing the failure mode. The Irradiation Effects (IE) test series was designed to investigate the effects of prior irradiation and rod design variables on the film boiling behavior of typical LWR rods. The specific variables investigated included cladding irradiation damage; rod internal gas composition and pressure; closure of fuel-to-cladding gap due to cladding creep, fuel swelling, and relocation of cracked pellet fragments; fuel density; and the presence of corrosive fission products.

2.1. Physical process

In a postulated PCM accident, Departure from Nucleate Boiling (DBN) can be caused by a coolant deficiency or a transient increase in reactor power. DBN increases cladding and fuel temperatures, and may result in cladding embrittlement and cladding and/or fuel melting.

2.2. Accident sequence

This type of postulated accident can be initiated by any one of several events. Examples of a perturbation in cooling are:

- pump failure
- leak in secondary system
- loss of load.

Examples of a power increase are:

- control rod withdrawal
- loss of a main coolant pump.

2.3. Failure mode

Film boiling operation produces high cladding temperatures within the film boiling zone. At elevated cladding temperatures, the system over pressure causes collapse of the cladding onto the fuel column, into pellet interfaces, and into chips on the pellet surfaces. In a PCM accident, the coolant pressure is always higher than the fuel rod internal pressure. The intimate contact between the fuel and the cladding at high temperatures results in a cladding-fuel reaction at the cladding inside surface. The elevated cladding temperatures also result in a cladding-steam reaction at the cladding outside surface. Both chemical reaction constribute to cladding embrittlement, which is the primary failure mode in a PCM accident. A typical fuel rod failure due to oxygen embrittlement is shown in Figure 1. Thermal stresses, produced in the cladding

(thermal shock) during rewetting of the rod from film boiling operation, resulted in brittle fracture of the cladding. Film boiling operation also produces high fuel temperatures which may reach the melting point of UO_2.

2.3.1. Cladding deformation

Within the film boiling zone, the cladding collapses onto the fuel stack due to loss of cladding strength at the elevated temperatures and the differential pressure (typically 7 MPa) across the cladding. The cladding flows into irregularities in the fuel stack, such as the gaps between pellets and chips in pellet surfaces, as shown in Figure 2. The cladding collapse into pellet interfaces is termed "waisting". Previously irradiated cladding behaved similarly to unirradiated cladding, and thus led to the conclusion that irradiation damage is annealed out at elevated temperatures.

2.3.2. Cladding-Fuel reaction

The collapse of the cladding onto the fuel stack produces intimate contact between the fuel and the cladding. The UO_2 is reduced by the Zircaloy and oxygen diffuses into the cladding to produce oxygen-stabilized α-Zr(O). This material is brittle and degrades the ductility of the cladding. In addition to the α-Zr(O) phase, a (U,Zr) phase is formed which is liquid above 1470 K. The interaction between the fuel and the cladding has been extensively studied in out-of-pile experiments from 1270 to 1970 K.

2.3.3. Cladding-Steam reaction

The reactions of Zircaloy with steam at the cladding outside surface produces a double layer of zirconium dioxide (ZrO_2). In addition, a layer of oxygen-stabilized α-Zr(O) is formed as oxygen from the ZrO_2 diffuses in the Zry. These layers on the cladding outside surface are brittle and degrade the ductility of the cladding. The cladding-steam reaction has been extensively studied in out-of-pile experiments from 1070 to 1870 K.

2.3.4. Fuel restructuring and fuel swelling

Fuel restructuring always occurs in the fuel pellets within the film boiling zone. Fuel melting can occur at the center of the fuel pellet, accompanied by the characteristic central void and surrounding ring of high density large grain fuel. Outside the large grain fuel region, equiaxed grain growth occurs with the grain size decreasing toward the pellet outside surface. Extensive fuel melting, up to about 80 % of the pellet radius, has been observed in the film boiling zone. Evidence of extrusion of molten fuel into pellet-to-pellet interfaces,into the fuel-cladding gap and into fuel cracks has been observed (Fig. 3). Contact of molten fuel with the cladding does not necessarily cause fuel rod failure. Fuel melting was caused principally by the large decrease in gap conductance which occurred when the fuel relocated and created large gaps in the fuel stack (between the remaining fuel and the cladding).

In Figure 4, fuel microstructures form the equiaxed grain growth regions of two previously irradiated fuel rods are compared. Both rods have similar burn-ups, but one rod was subsequently tested in film boiling. The density of fission gas bubbles at the grain boundaries is much greater in the fuel that was tested in film boiling. The additional gas bubble volume contributed to fuel rod swelling.

3. Reactivity Initiated Accident

The RIA is a design basis accident. The rapid injection of excess reactivity into a LWR core has long been recognized as a potential accident in which fuel rod failure can occur. Extensive cladding failure and the subsequent dispersal of fuel into the coolant could disrupt the core geometry to such an extent that the post-accident core coolability would be significantly impaired. Licensing requires that LWR's must be designed such that a worst-case RIA will not result in a radial average fuel enthalpy greater than 280 cal/g UO_2 at any axial location in any fuel rod. The RIA accident has been investigated primarily in the NSRR and in the PBF reactor. Fuel rod design variation tests have been conducted to study the influence of fuel rod internal pressure, radial gap width, gap gas composition, fuel enrichment, pellet shape, cladding wall thickness, cladding heat treatment, and various cladding materials on fuel rod behavior during a RIA transient.

3.1. Physical Process

During a very short power burst a certain amount of excess energy is generated. Since the time span is so short, essentially no time is available to remove the heat from the pellet via the cladding to the coolant. The amount of energy generated is generally small enough that fuel melting is prevented. Due to sharp fuel temperature increases, transient fuel swelling may occur as mentioned in section 2. The Zry tube may be embrittled by oxidation, and may melt.

3.2. Accident sequence

A RIA is caused by ejection of a control rod from the core.

3.3. Failure mode

Energy deposition in the fuel, and the consequent enthalpy increase is the single most important independent variable. The failure threshold for unirradiated fuel was an energy deposition of about 240 to 265 cal/g UO_2 and is relatively insensitive to cladding material heat treatment, fuel form, fuel material, and gap width. Prepressurization of fuel rods causes a reduction in the failue threshold for internal pressures $\geq$ 1.2 MPa. Rods prepressurized to 2.9 MPa failed in the range of 150 to 160 cal/g UO_2.

Cladding melting during the power excursion or cracking of embrittled cladding during cooldown is the apparent causes of failure of unirradiated fuel rods for tests in which the rods received a total energy deposition of 350 cal/g UO_2 or less.

Wall thickness variation occurred as the result of extensive plastic flow of the hot cladding prior to significant oxidation. An example of the variation in circumferential wall thickness is shown in Figure 5 for an unirradiated PBF fuel rod subjected to an axial peak enthalpy of 250 cal/g UO_2. The oxygen embrittled cladding was breached in a region of wall thinning, and partial fuel loss occurred. Figure 6 shows photographs of typical unirradiated fuel rods in which the total energy deposition ranged from 168 to 378 cal/g UO_2.

Unirradiated fuel rods subjected to total energy depositions in excess of about 350 cal/g UO_2 failed by cladding rupture prior to the attainment of cladding melting, and significant fragmention of the rods occurred. Internal pressure from UO_2 vaporization was shown to be the likely cause of these failures.

In tests with preirradiated fuel rods (burnups to 32 000 MWd/t), rod failures occurred at lower energy depositions in some cases than in similar unirradiated fuel rods, with little sensitivity attributable to the degree of burnup. Whereas unirradiated fuel rods failed due to cladding melting or cracking, irradiated rods failed due to extensive fission product-induced swelling of the fuel at high temperatures. The irradiated fuel showed considerable porosity (Fig. 7), which was due to the release, coalescence, and expansion of gaseous and volatile fission products within the fuel matrix.

Waterlogging, or water absorption within oxide fuel, could result during shutdown conditions in a fuel rod with damaged cladding. The failure threshold of waterlogged fuel was strongly dependent on cladding material and cladding heat treatment. Zircaloy clad waterlogged rods were found to fail by cladding rupture at total energy depositions as low as 60 cal/g UO_2. Although failure often produced high transient pressures (in the tens of MPa) in the test capsule, the pressure pulses were very narrow and did not contain sufficient energy to damage adjacent rods. Large radial cladding expansion and small, or negative, axial cladding expansion occurred.

4. Loss of Coolant Accident

The large break LOCA is a design basis accident. Possible fuel rod deformation during a LOCA is a main concern of LWR safety research. In particular, in the second heatup phase of this accident, after the coolant has escaped from the reactor pressure vessel and before the emergency core cooling systems (ECCS) reflood the core, there is some probability of failure for many fuel rods. Elevated cladding temperatures, which reduce the strength of the material, combined with an increase in stress caused by internal overpressure (rod fill gas and fission gas pressure) after system depressurization, may result in

rod ballooning and rupturing. Because of its potential to reduce the effectiveness of ECC, this fuel rod behavior has been the subject of extensive analytical and experimental research. Most of the experiments have been performed out-of-pile with electrically heated fuel rod simulators. However, since some parameters cannot be simulated adequately out-of-pile, experiments in a nuclear environment have also been necessary.

4.1. Physical Process

In a LOCA DNB occurs due to system depressurization. Cladding temperatures increase because of the fission product decay heat and the heat stored in the fuel pellets (the reactor has scrammed). Depending on the pressure difference across the cladding and on the temperature large plastic deformation may occur until the rod ruptures or is quenched by the emergency core cooling systems.

4.2. Accident sequence

A LOCA is caused by a large break in the primary coolant loop. The size of the break is a parameter. It is assumed that the emergency core cooling systems work properly.

4.3. Failure mode

Depending on the axial and azimuthal cladding temperature gradients, large plastic deformation may occur which can form cooling channel blockages. Such blockages would inhibit cladding rewetting within the blockage area. Cladding embrittlement due to steam oxidation or partial fuel melting due to insufficient cooling may occur.

4.4. LOCA studies at the Kernforschungszentrum Karlsruhe

Several important question with respect to cooling channel blockages are:

- when does cladding creep or deformation begin ?
- when does cladding fail ?
- what is the influence of neighboring rods ?

A large research program was initiated at KfK to answer these questions. The work has been divided into the following areas:

- Zry cladding behavior experiments at high temperatures in inert and oxidizing atmospheres (out-of-pile)
- single rod and bundle experiments using indirectly heated simulators (out-of-pile) under LOCA typical thermohydraulic boundary conditions
- single rod experimental (in-pile)
- subchannel blockage experiments (out-of-pile)
- code development (SSYST)

4.4.1. Zircaloy behavior

Depending on test temperature and pressure, failure strains of 50 % to 120 % have been observed in Zry cladding experiments in an inert atmosphere. Below 1090 K (the lower boundary of the α/β phase transition region), a characteristic bending of the specimens towards the side of rupture is observed (Fig. 8). In an oxidizing atmosphere, rupture strains are strongly reduced due to oxygen embrittlement of the cladding. The effect of oxygen can also be seen when tensile test specimens without external load are exposed to air at 1170 K. Oxidation stresses strain the specimens to a remarkable extent (Fig. 9), and the oxide skin inhibits extended necking (Fig. 10).

4.4.2. Fuel rod simulator experiments

The creep rate of Zry is extremly sensitive to temperature. Fuel rod simulator experiments have shown that local temperature perturbations, i.e. an azimuthal temperature gradient, can lead to a drastic reduction in strain. The cladding deforms only in the region of the hot spot and fails with a relatively small circumferential strain (Fig. 11). A small azimuthal temperature gradient results in a relatively large circumferential strain. Bundle experiments essentially show the same behavior as single rod experiments. In addition, bundle experiments also show the effect of coolant on subchannel temperature and consequently on strains. If the coolant is mainly dry steam, axial temperature gradients are large and azimuthal temperature gradients are small.

The circumferential deformation will therefore be large but only a short axial section will be affected. If the coolant is a two-phase steam-water mixture, axial temperature gradients are small and azimuthal temperature gradients are large. Therefore, a longer axial section will be effected but the circumferential deformation will be relatively small (Fig. 12).

4.4.3. In-pile experiments

To investigate the possible influence of a nuclear environment on fuel rod failure mechanisms, unirradiated as well as irradiated (2500 to 35 000 MWd/t_U) PWR-type test fuel rods were exposed to temperature transients simulating the second heatup phase of a LOCA. Loaded by internal overpressure, the cladding ballooned and ruptured. The burst data are not significantly different from results obtained out-of-pile with electrically heated fuel rod simulators, and do not show an influence of burnup. The fuel pellets in previously irradiated rods, already cracked during normal operation, crumbled completely in the regions with large cladding deformation (Fig. 13). Posttest examinations revealed cladding mechanical behavior and oxidation to be comparable to out-of-pile results, with relatively little fission gas release during the transient.

4.4.4. Subchannel blockage experiments

Flow blockages produced by ballooned claddings change the cooling mechanism downstream of the blockage. The increased flow resistance in the blocked region results in a reduction of the mass flow of the coolant. On the other hand, droplet breakup and atomization of the liquid phase occur at the blockage, which improve heat transfer for a given coolant mass flow. Which of these effects is more dominant depends on a number of boundary conditions, e. g., flooding rate, ratio of blocked to unblocked areas etc.

Within the FEBA program /5/ flooding tests have been performed under transient LOCA conditions on a 5x5 bundle with conical sleeves simulating the flow blockage. Fig. 14 shows cladding temperature transients in the blocked and unblocked regions for a flooding rate of 3.8 cm/s and a blockage ratio of 62 % in the blocked region. It is evident from the diagram that under the given conditions the effect of water droplet breakup, which improves the heat transfer, overcompensates

the degrading effect of mass flow reduction with the consequence that the cladding temperature downstream of the blocked region is somewhat lower compared to that in the unblocked region. Only at relatively low flooding rates of about 2 cm/s the cladding temperatures in the blocked and unblocked regions are almost the same.

Experimental results suggest that flow blockages up to about 90 % do not degrade emergency core cooling, not even at relatively low flooding rates.

4.5. Code development (SSYST)

SSYST generally considers a single fuel rod in R-Z geometry. In particular, SSYST includes the following fuel rod behavior models /7/:

- radial and axial heat transfer in the rod
- open and closed gap conductance using gas mixture conductivity and radiation for the open gap and the Ross and Stoute model for the closed gap
- cladding outside surface oxidation using Baker-Just reaction kinetics
- rod internal pressure considering dish, crack, and gap temperatures as well as the plenum temperature, with an optional model for gas flow
- rod mechanics assuming thermoelastic fuel and thermoelastic plastic cladding
- azimuthal variations of temperature, gap conductance, oxidation, and cladding creep due to fuel-cladding eccentricity
- subchannel thermal hydraulics using RELAP calculated mass flux to calculate the enthalpy rise and evaluate the appropriate heat transfer coefficients.

Burnup dependent initial conditions are provided through a link to COMETHE III-J [9]. Geometry, gas pressure and content, power distribution, and porosity data are transferred. Boundary conditions during the blowdown, refill, and reflood phases of a LOCA are provided through links to RELAP4/MOD5, [10], WAKO [11] and REFLOS [12]. Subchannel temperature and pressure, heat transfer coefficients, and normalized power history are usually transferred. A major goal of SSYST development is to model bundle behavior. Special subroutines have therefore been developed which construct probabilistic descriptions of bundle behavior using Monte Carlo methods.

5. Anticipated Transient without Scram

Anticipated nuclear power transients are deviations from normal plant operating conditions that result from system component malfunctions which may occur one or more times during the service life of a reactor and are normally accompanied by a control rod scram. They are distinguished from "accidents" which have a much lower probability of occurrence. Many of the anticipated transients may be postulated to occur with a failure of the automatic scram system and are then termed "anticipated transients without scram (ATWS)". Significient damage is not currently predicted to occur for any pressurized water reactor ATWS event. However, boiling transition and high cladding temperatures are predicted to occur for the most severe boiling water reactor ATWS events.

5.1. Physical process

During a power transient, excess energy is generated in the fuel which results in higher fuel temperatures. Due to the increased thermal expansion of the UO_2 fuel, Pellet-Cladding mechanical and chemical Interactions (PCI) may occur which can lead to fuel rod failure. Boiling transition and high cladding temperatures may cause cladding oxidation and embrittlement.

5.2. Transient sequence

An ATWS transient can be caused by any one of the following events:

- control rod withdrawal
- boron dilution
- loss of primary flow
- loss of electrical load (generator trip, turbine trip)
- loss of condenser vacuum.

5.3. Failure mode

The differential thermal expansion between the fuel and the cladding (thermal expansion of the fuel is larger than that of the cladding) causes strong pellet-cladding interactions. Therefore, at very fast power ramps the fracture strength of the cladding can be exceeded and the tubing may fail. In the presence of aggressive fission products such as iodine, the stressed cladding can fail far below its fracture strength due to iodine-induced Stress-Corrosion Cracking (SCC). SCC failure of the cladding occurs in a brittle mode.

6. Severe Fuel Damage Accident

The consequences of a severe accident are dependent up on the sequence of damage in the accident. Degraded core cooling accidents can take many paths depending on several key parameters, including heating rate, cooling rate, steam flow, peak temperature, fuel rod burnup, bundle size, and low melting temperature control and structural materials. The damage produced is expected to range from fuel rods with cladding totally oxidized to ZrO_2 and geometry altered only by localized ballooning and rupture of the rods during the heatup, to rods with the formation, relocation, and freezing of molten cladding and liquefied fuel, to the formation of rubble beds of fuel pellet fragments, oxidized cladding fragments, solidified molten fuel, solidified liquefied fuel and solidified spacer grid, control rod and structural materials. The Severe Fuel Damage (SFD) tests in the PBF reactor (which began in September 1982), combined with data from special separate effects tests and examination of the TMI-2 core, will significantly improve understanding of the behavior of a large LWR during a degraded core cooling event.

6.1. Physical process

DNB is overridden by coolant boil-off. Cladding temperature are elevated for a long period of time and melting may occur. Associated with the high temperatures are severe oxidation and embrittlement of the cladding.

6.2. Accident sequence

A possible SFD accident seuqence is a leak in the primary coolant loop and failure of the emergency core cooling system.

6.3. Failure mode

The failure mode depends on the cladding temperature rise rate. A fast heatup rate (> 5 K/s) results in cladding melting and runoff with some dissolution of UO_2 in the melt. A slower heatup rate results in a ZrO_2 shell within which cladding melting occurs, with substantial UO_2 dissolution. A very slow heatup rate ($\sim$ 0.5 K/s) results in complete oxidation of the cladding(no melting)and possible rubble bed formation by cladding failure due to embrittlement(Fig. 15). In all cases an almost complete loss of the original core geometry takes place. An important question in these accidents is whether the post-accident heat can be removed from the rubble bed.

7. Summary

This paper described the onset of fuel rod failure for different LWR accident and transient sequences. The results also apply to heavy water reactors (e.g., Artucha, Candu). Most of the PCM, RIA, LOCA, and ATWS research has been completed, but as a consequence of the TMI-2 accident, additional severe fuel damage investigations have been initiated. All research contributes to even safer reactors by giving vendors and utilities a better knowledge of failure limits and failure consequences.

References

/1/ P. Haas et al:
Response of unirradiated and irradiated PWR fuel rods tested under power cooling mismatch conditions
Nuclear Safety, Vol. 19, No. 4, July-Aug. 1978, 440-464

/2/ P. MacDonald et al:
Assessment of light water reactor fuel damage during a reactivity initiated accident
Nuclear Safety, Vol. 21, No. 5, September-October 1980, 582-602

/3/ P. Hofmann and S. Raff:
Verformungsverhalten von Zircaloy-4-Hüllrohren unter Schutzgas im Temperaturbereich zwischen 600°C und 1200°C
KfK 3168 (1981)

/4/ M. Bocek et al:
Untersuchungen zum mechanischen Verhalten von Zircaloy-Hüllmaterial bei einem LOCA
in KfK 2195: PNS Halbjahresbericht 1/1975, 203

/5/ F. Erbacher et al:
Interaction between thermohydraulics and fuel clad ballooning in a LOCA. Results of REBEKA multi rod burst tests with flooding
WRSIM November 6-9, Gaithersburg

/6/ E. Karb et al:
Untersuchungen zum Brennstabverhalten in der 2. Aufheizpahse eines LOCA
in KfK 2600: PNS Halbjahresbericht 2/1977, 373

/7/ R. Meyder:
SSYST-2 Eingabebeschreibung und Handhabung
KfK 2966 (1980)

/8/ S. Hagen et al:
Experimentelle Untersuchung der Abschmelzphase von UO_2/Zry-Brennelementen bei versagender Notkühlung
in KfK 2600: PNS Halbjahresbericht 2/1977, 416

/9/ P. Verbeck und N. Hoppe:
COMETHE III-J. A Computer Code for predicting mechanical and Thermal behavior of Fuel Pin.
Part I: General Decription. BN 7609-01 (1976)

/10/ Relap 4/mod 5:
A Computer program for transient thermal-hydraulic Analyis of Nuclear Reactors and related systems.
ANCR-NUREG 1335, Sept. 1976

/11/ Seidelberger, E.: unpublished

/12/ Kersting, E.:
Rechenprogramm REFLOS, Programm zur Berechnung des Wiederauffüll- und Flutvorganges GRS-A-163 (September 1978)

/13/ P. Hofmann et al.
LWR fuel rod behavior during reactor tests under LOCA conditions: Results of the FR2 in-pile tests.
J. of Nucl. Mat. 107 (1982) 55-77

/14/ P. Hofmann et al.
Behavior of LWR fuel elements under accident conditions
Internat. Conference on "Nuclear Power and its Fuel Cycle, IAEA-CN-36/124 (1977), Vol.2, 673-694

/15/ P. Hofmann,
Influence of Iodine on the Burst Strain of Zircaloy-4 Cladding Tubes under Simulated Reactor Accident Conditions,
J. Nucl. Mat., 87 (1979) 49-69

/16/ P. Hofmann, J. Spino,
Chemical Interactions between Simulated Fission Products and Zircaloy-4 at Elevated Temperatures, Including Influence on Ductility and Time-to-Failure,
J. Nucl. Mat., 102 (1981) 117-134

/17/ P. Hofmann, J. Spino,
Can One Expect Low Ductility Failure of Zircaloy-4 Tubing Due to Iodine-Induced SCC in a LOCA Transient ?
ANS Meeting on "REACTOR SAFETY ASPECTS OF FUEL BEHAVIOR", Sun Valley, Idaho, USA, August 2-6 (1981) 2/410

/18/ F.J. Erbacher,
LWR Fuel Cladding Deformation in a LOCA and its Interaction with Emergency Core Cooling,
Same Conference as /17/, page 2/100

A great part of this chapter was prepared by
Dr. R. Meyder, KfK (1981)

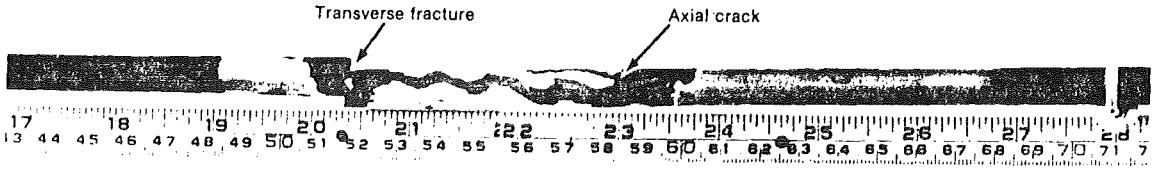

Fig. 1 : Fuel rod failure due to oxygen embrittlement (rod IE 007, test IE-1)/1/.

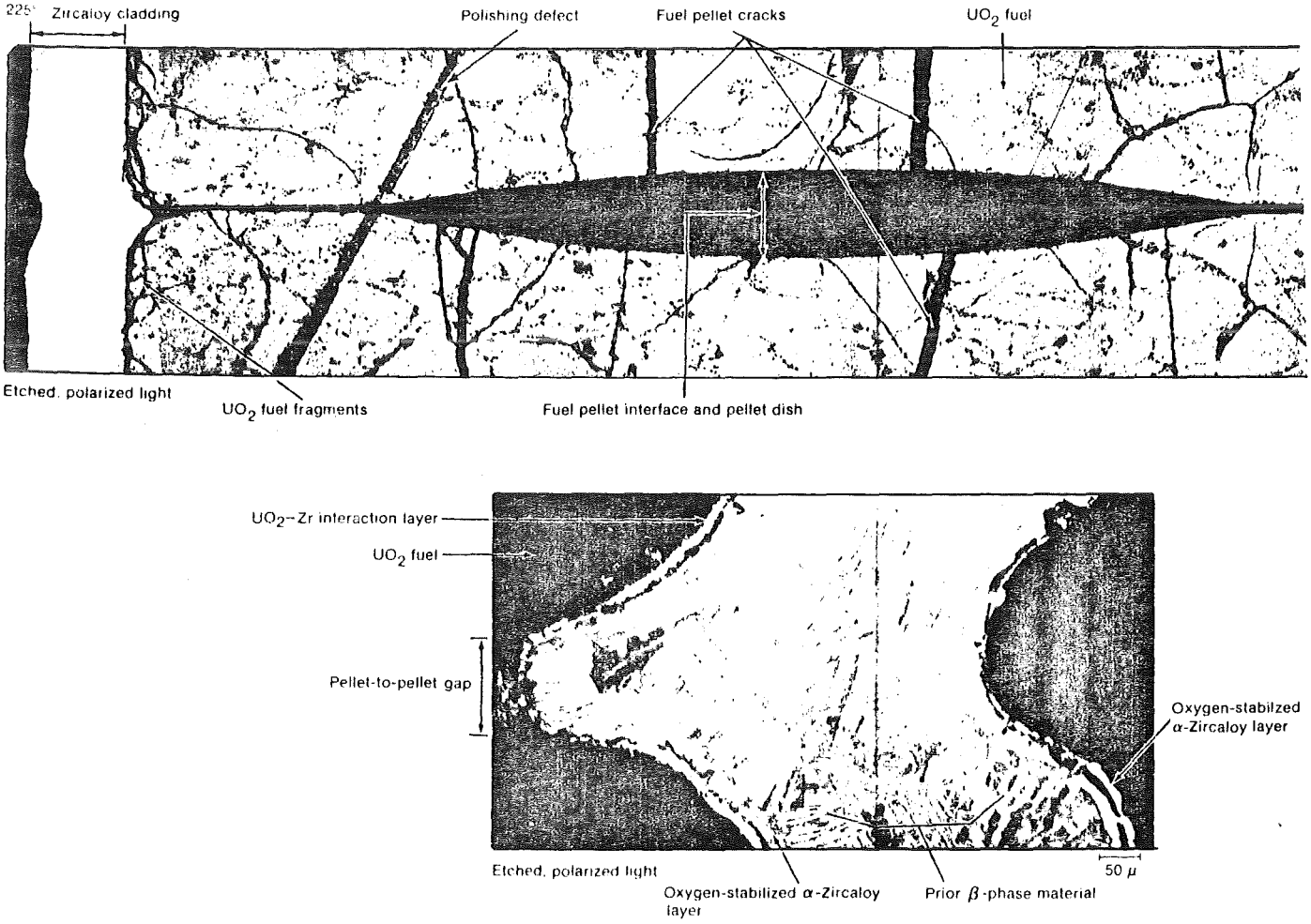

Fig. 2 : Example of cladding flow into a pellet-to-pellet gap (rod 7, test PCM-2A) /1/.

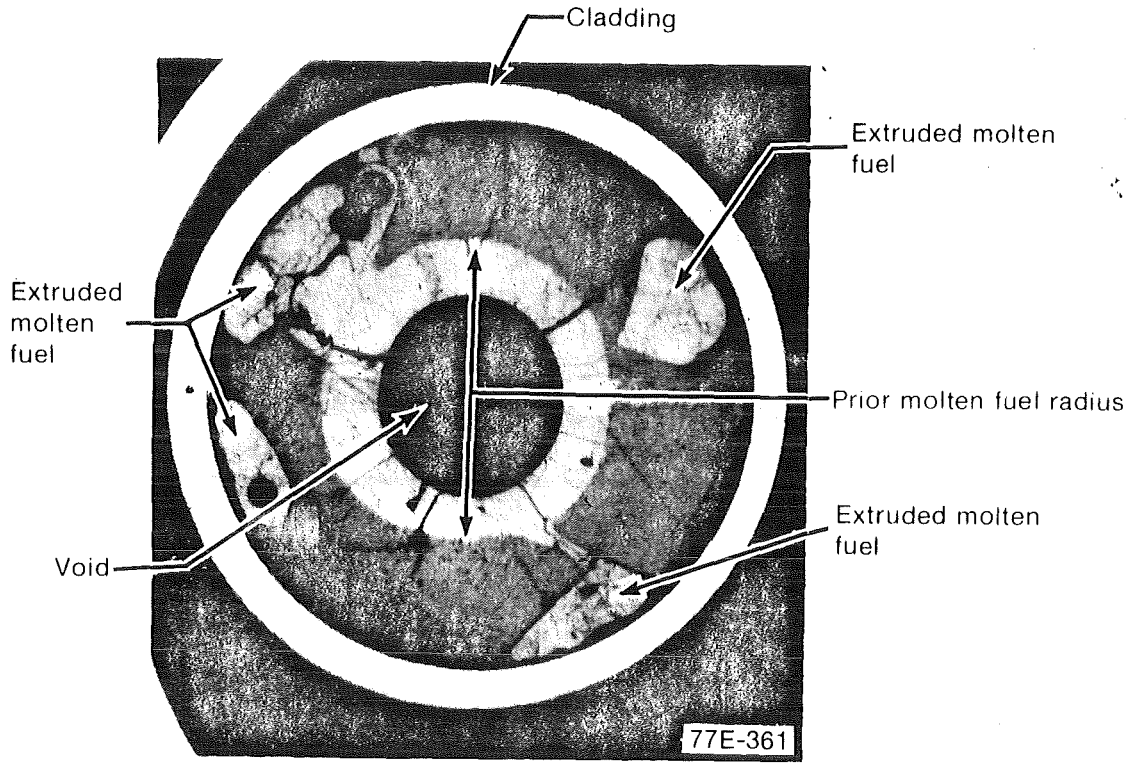

Fig. 3: Molten fuel extrusion above the film boiling zone in an irradiated fuel rod (rod IE016, test IE-3) /1/.

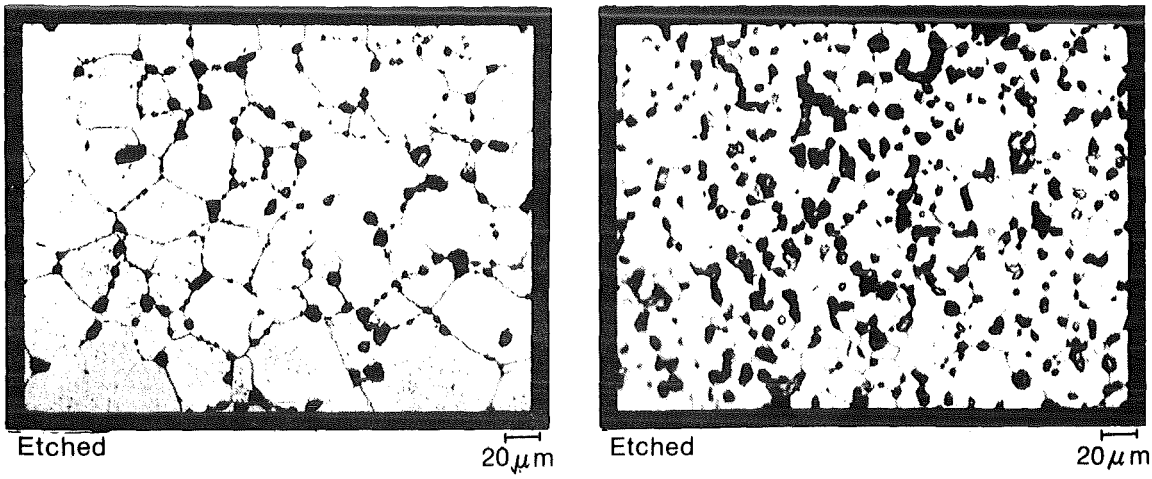

Fig. 4: Comparison of fuel microstructure from equiaxed grain growth regions of two irradiated fuel rods, one of which (rod IE 009, test IE-1) was tested in film boiling. Rod (a) was irradiated in the Saxton Reactor to 17000 MWd/t_U. Rod (b) was irradiated in the Saxton Reactor to 16000 MWd/t_U and then tested in the PBF /1/.

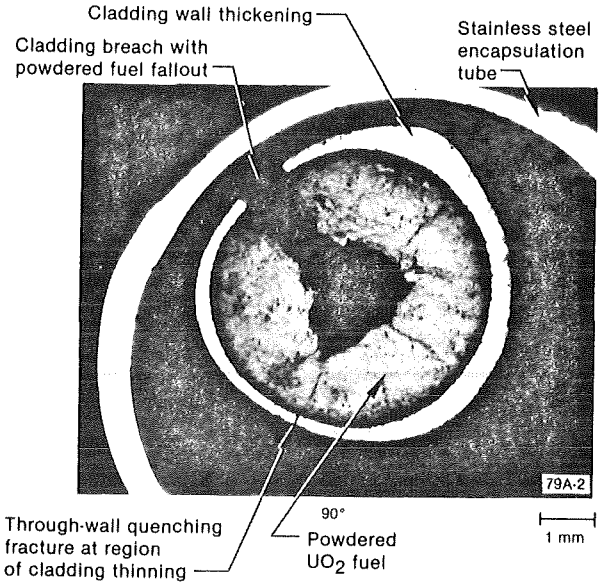

Fig. 5 : Cladding wall-thickness variation in the RIA-ST1 rod near the axial flux peak at the 0.446-m elevation (250 cal/g UO_2) /2/.

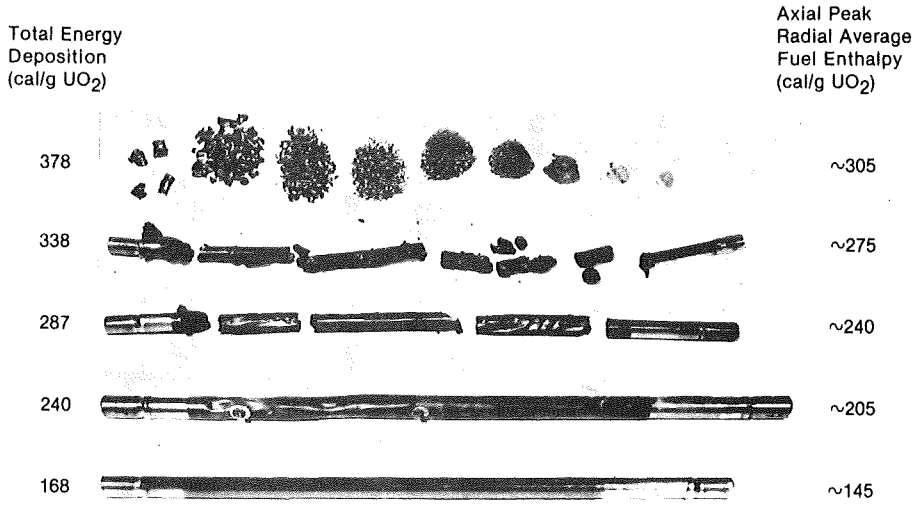

Fig. 6 : Posttest photographs of SPXM fuel rods tested in the SPERT program /2/ The total energy deposition varied from 168 to 378 cal/g UO_2.

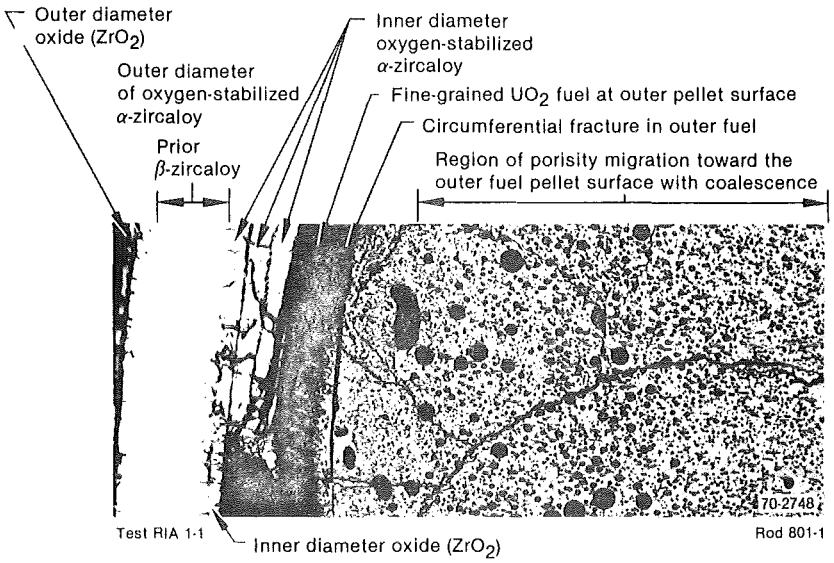

Fig. 7: Previously irradiated rod 801-1 cladding and pellet fragment in the blockage region near the peak power elevation (test RIA 1-1) /2/

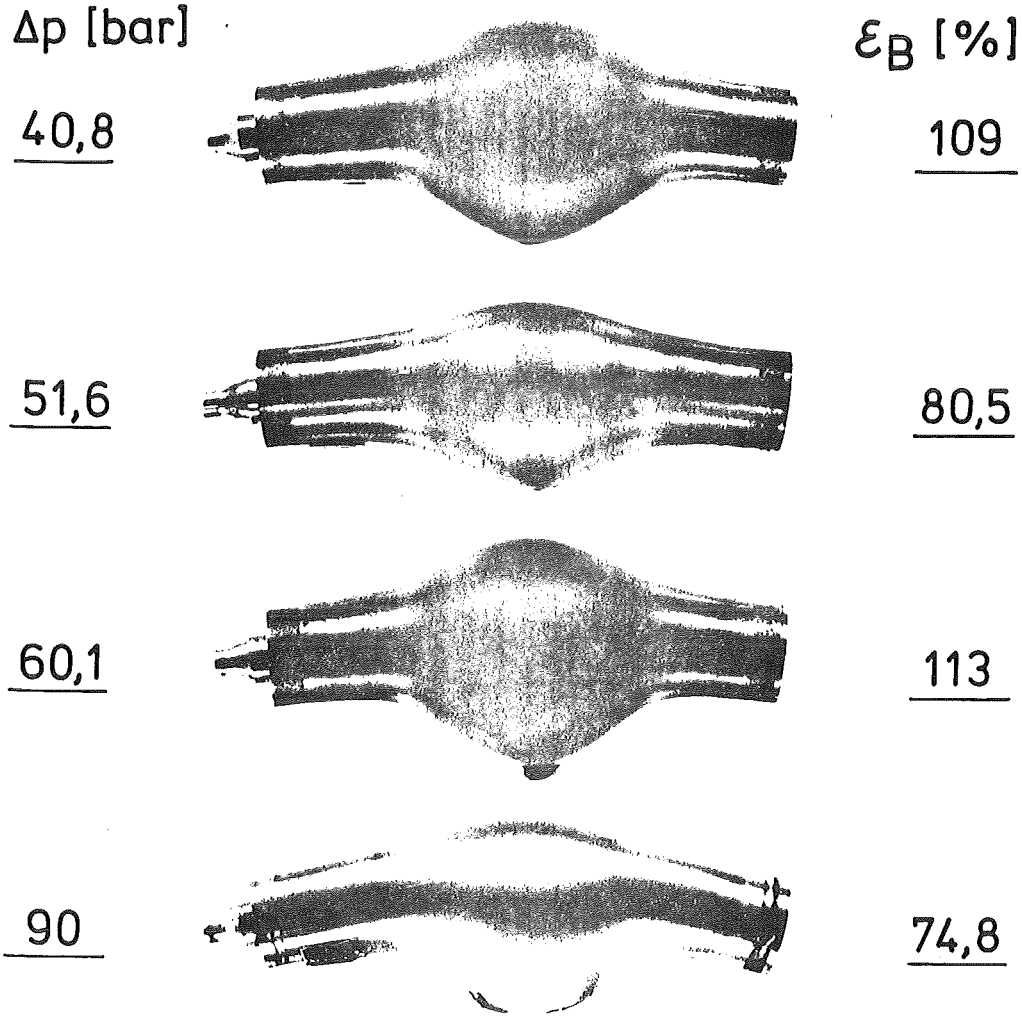

Fig. 8: Zry-4 tube specimens after rupture at 1070 K /3/.

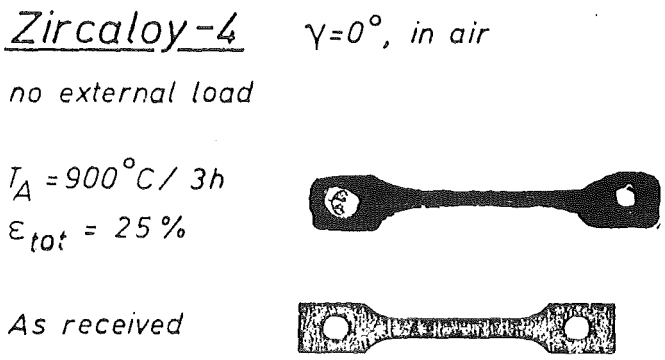

Fig. 9 : Tensile test specimen strained by oxidation stresses /4/.

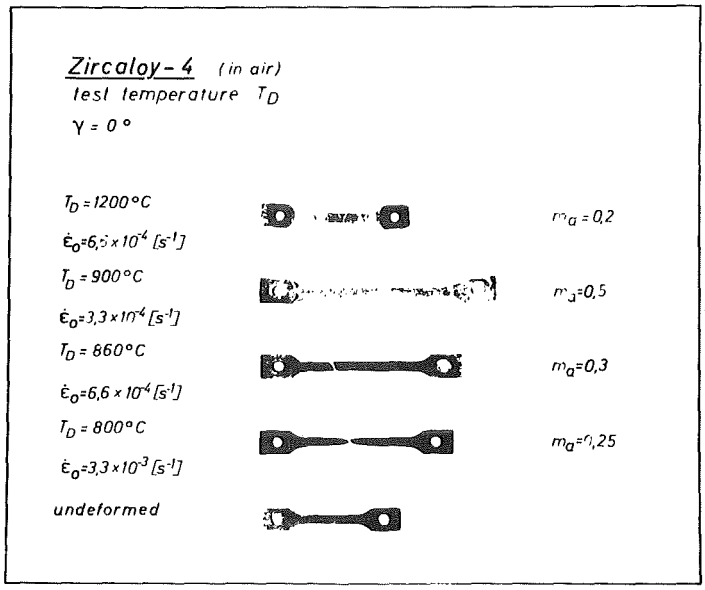

Fig. 10 : Tensile test specimens strained in an oxidizing atmosphere at various temperatures /4/.

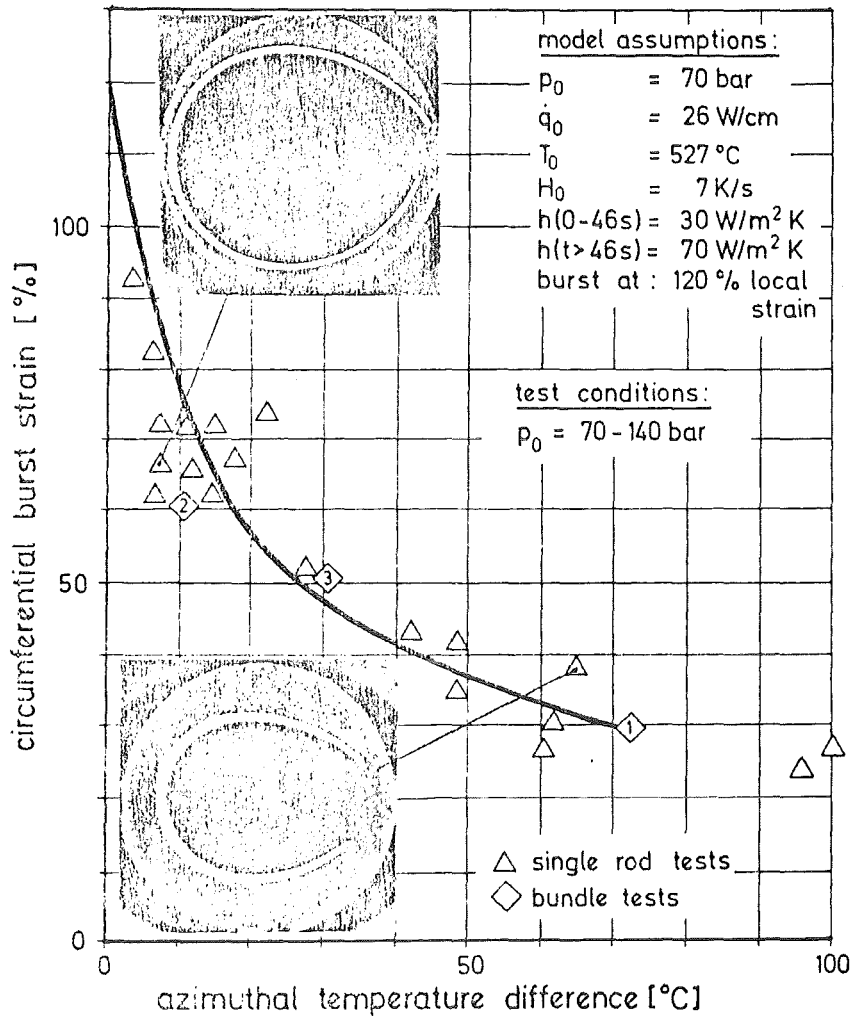

Fig. 11: Burst strain versus azimuthal difference (SSYST/AZI prediction with test results) /5/.

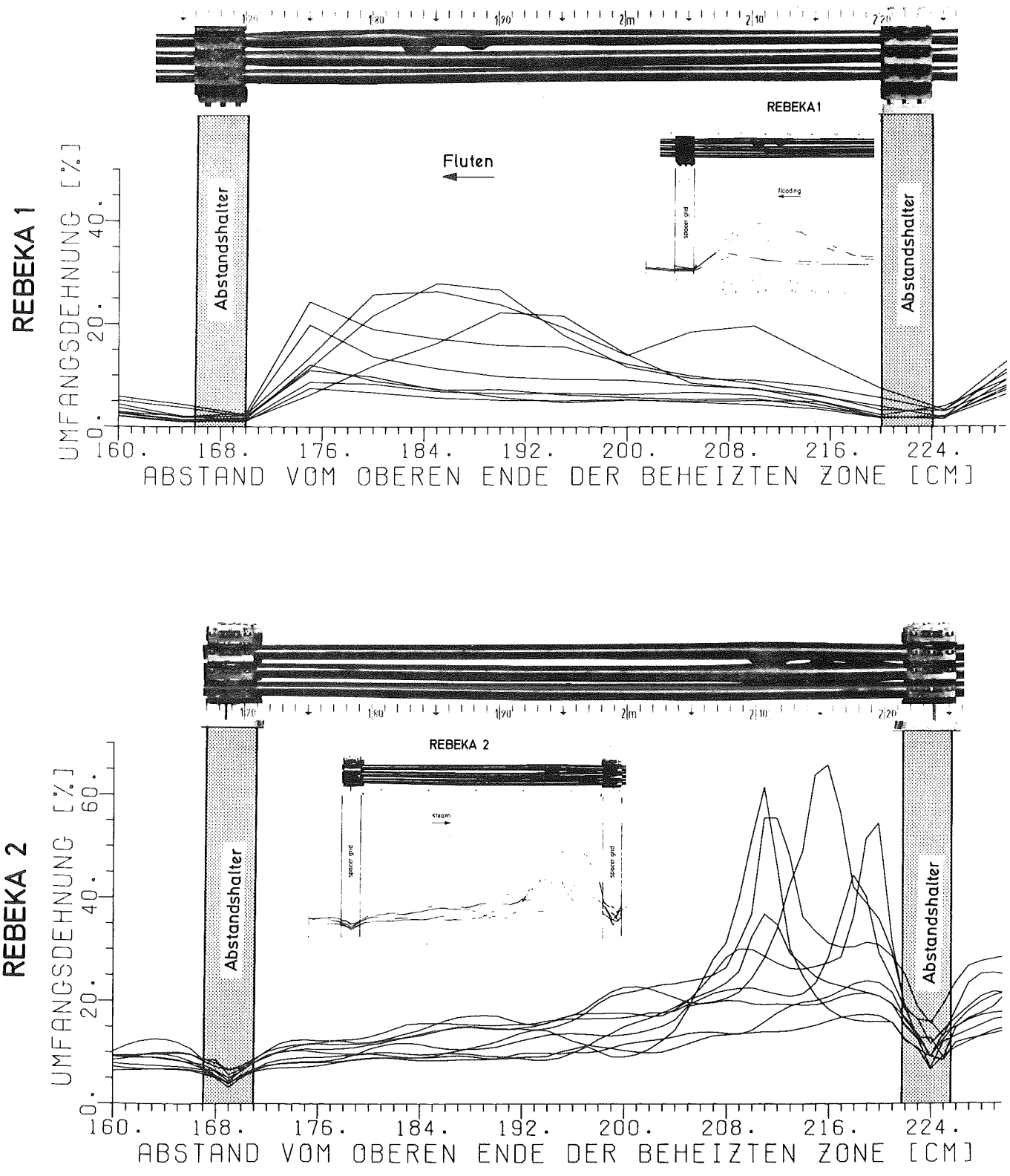

Fig. 12: REBEKA 1 and 2 axial deformation profile between the interior grid spacers /5/

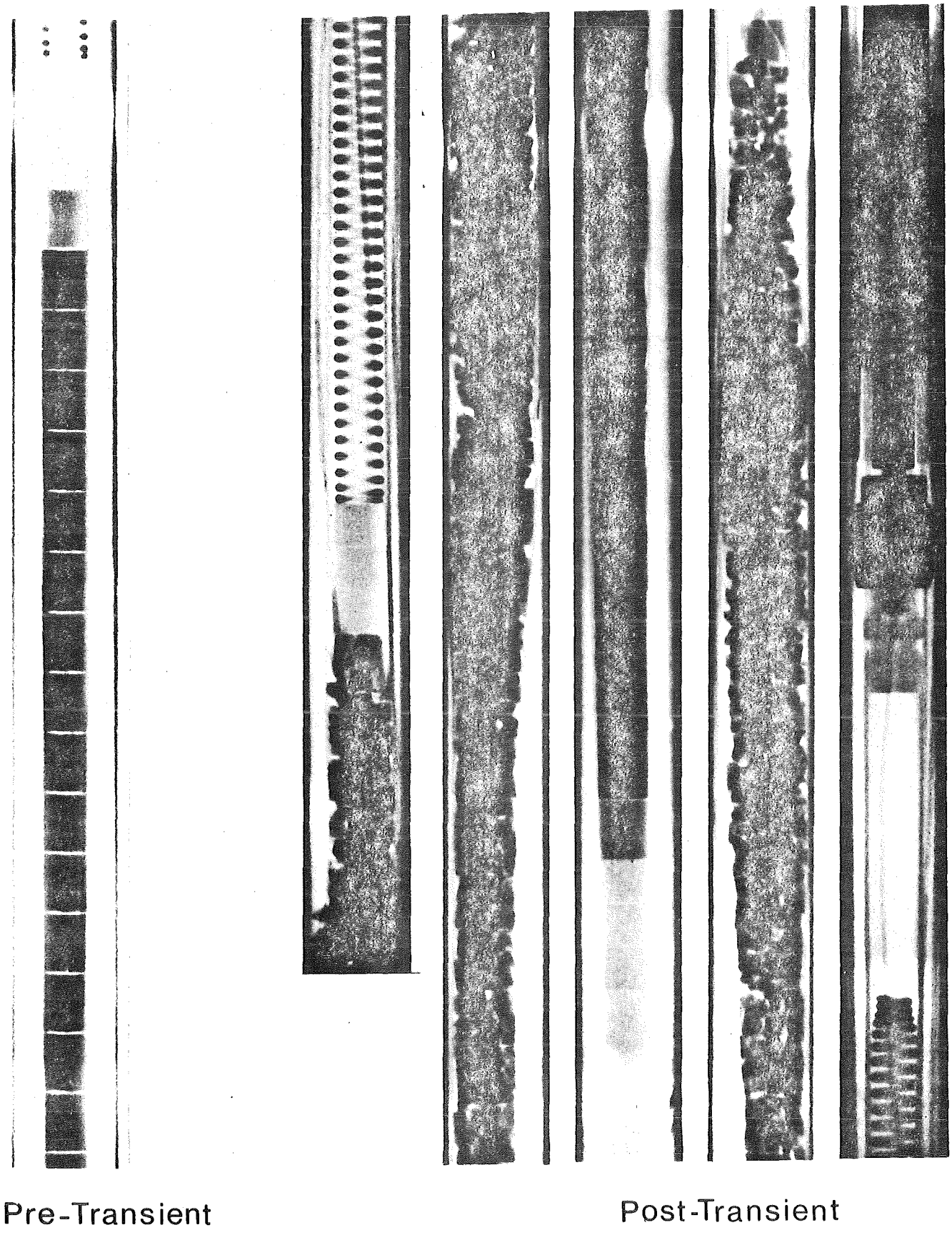

Fig. 13: Post test neutron radiography of rods with a burnup of 20 000 MWd/t_U /6,13/

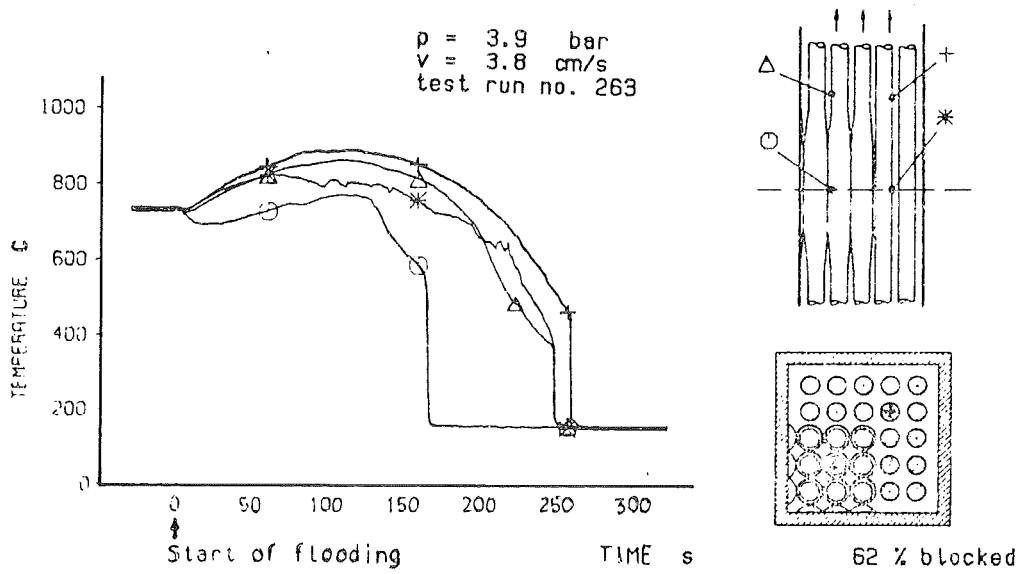

Fig. 14: FEBA flooding tests. Cladding temperatures in a partly blocked 25-rod bundle /5,18/.

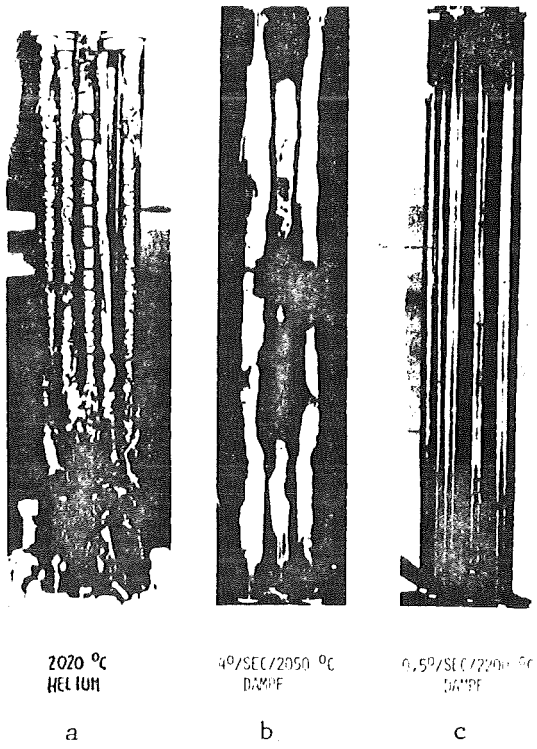

Fig. 15: Meltdown behavior of fuel bundles in (a) helium, (b) steam (4K/sec), (c) steam (0.5 K/sec) /8/.

F. LMFBR FUEL ROD BEHAVIOR UNDER NORMAL CONDITIONS

1. LMFBR Fuel rod Materials
2. Mixed Oxide Fuel Behavior
3. Cladding Behavior
4. Fuel-Cladding Mechanical Interactions
5. External Cladding Corrosion
6. Conclusions

F. LIQUID METAL FAST BREEDER REACTOR FUEL ROD BEHAVIOUR UNDER NORMAL CONDITIONS

1. LMFBR Fuel Rod Materials

The extensive experience with the thermal reactor core materials has provided the basis for Liquid Metal Fast Breeder Reactor (LMFBR) core materials development. However, the LMFBR fuel system must survive a much more hostile environment than the LWR fuel system with respect to temperature and fast neutron fluence. Typical fuel rod powers of 40 to 90 kW/m (compared to a maximum of $\sim$ 40 kW/m in LWRs) yield fast neutron fluences of $\sim 2 \times 10^{27}$ n/m^2 ($E > 0.1$ MeV), or $\sim$ 90 dpa, with maximum cladding temperatures of the order of 920 K (Fig. 1). These more extreme conditions are manifested in more profound chemical and microstructural changes in the fuel and cladding for instance, neither fission gas release approaching 100 % nor void swelling of cladding are observed in LWR fuel rods, but they are normal occurrences in some LMFBR fuel systems and must therefore be accounted for in design.

The current choice for a fuel system to contend with this environment is a uranium oxide, 25 ± 5 wt.% plutonium mixed oxide fuel, and austenitic stainless steel cladding. Both pellet (solid and annular) and packed particle (Vipac, Spherepac, etc.) fuel types have been seriously considered for the mixed oxide, and various stainless steels (types 304, 316, 1.4970, 1.4988, ferritic SS).

2. Mixed Oxide Fuel Behaviour

2.1. Fuel and Fission Product Interactions with the Cladding

Because of the higher power rating (40 to 60 kw/m) and corresponding higher fuel centerline temperatures, and higher burnups ($\gtrsim$ 8600 GJ/kgM) planned for fast-breeder fuels compared to LWR fuels, more attention has been focused on temperature gradient effects, such as development of microstructural and compositional gradients, and their influence on fuel temperature, fuel swelling, and fission product release.

Figure 2 illustrates the effects of the more extreme LMFBR thermal conditions. Exaggerated grain growth results from the dragging of grain boundaries as the as-fabricated pores move up the temperature gradient by a vaporization/condensation mechanism. This effect leads to the formation of a zone of columnar grains. Subsequently, the fission gas produced in the fuel pellet migrates to the grain boundaries, diffuses through the columnar grain boundaries, and, eventually, is released to the central void that has formed by the earlier porosity migration.

The extent to which this fuel restructuring occurs is, of course, determined by the fuel rod power level and, hence, the fuel temperature and temperature gradient. In at least 20 % of the core, the initially uniform, solid mixed oxide fuel pellet transforms to what is essentially a structure consisting of three zones, i.e., outer unrestructured; equiaxed, higher density; and fully dense, columnar zones, and an annulus.

This thermal effect is also manifested in oxygen diffusion and measureable segregation of plutonium and uranium atoms in these fuels. With respect to the former, oxygen diffusion can either be down or up the thermal gradient depending on whether the fuel is, respectively, hypo- or hyperstoichiometric; regardless, an O/M gradient is established in the fuel pellet. Plutonium segregation typically results in a local concentration increase of 35 to 50 % at the central-void edge, and no segregation is observed when a central void is not formed. This effect is important because the maximum allowable power level is constrained by the linear heat rating to incipient melting (typically "power-to-melt" is $\sim$ 60 kW/m at startup) and therefore segregation of fissile material toward the fuel centerline will lower the allowable power.

Fission gas relase from LMFBR fuels basically follows the same kinetics as for thermal reactor UO_2 when appropriate corrections are made for different diffusion coefficients and fuel temperatures. Mechanistic models for gas release in UO_2 and mixed oxide fuels are generally identical and provide reasonable predictions of the observed behaviour. High gas release in LMFBR fuel (100 % at 6910 GJ/kgM) is accommodated in the large plenum provided in the fuel rod.

The correlation between fuel swelling and available initial fuel porosity is also sufficiently well developed so that suitable fuel densities (of the order of 89 to 91 % TD) can be specified and fabricated to accommodate fission-product swelling without gross distortion of the cladding to design burnups.

Two types of fuel-cladding chemical reactions have been identified; the first is uniform oxidation (matrix attack) of the stainless steel, which results in a general decrease in the thickness of the cladding: the second involves the intergranular penetration by oxygen and fission products along the grain boundaries in the cladding. Matrix attack rarely exceeds a depth of 50 μm, however, intergranular attack, which is nonuniform in depth and sporadic in occurrence, may penetrate the entire thickness of the cladding. Nevertheless, it must be noted that no cladding failures have been attributed to this type of attack.

Fission products play important roles in fuel-cladding chemical interactions. Cesium is universally observed in the attack region and is usually associated with chromium from the cladding. Iodine is observed almost as frequently and is generally associated with cesium. Tellurium is observed less frequently, and numerous cladding attack regions have been observed in which tellurium has not been detected. The role of fission products in cladding attack has been extensively investigated in out-of-pile experiments, which show the cladding attack readily occurs in the presence of one or more of the following: cesium (in the presence of oxygen), Cs_2O, CsOH (liq.), I_2 and Te. If oxygen is not present, cesium is unreactive toward stainless steel (Fig. 3). The fuel and the remaining fission products do not promote intergranular attack separately or together (Fig. 4).

The cesium attack of stainless steel is controlled by the oxygen partial pressure in the fuel rod and the cladding temperature and most, importantly, the local temperature difference between the outer surface of the fuel and the inner surface of the cladding. Fuel O/M values near 2.0 and cladding temperatures above ∿ 810 K favor formation of cesium chromate; therefore, current practice is to utilize mixed oxide fuels with O/M in the range 1.94 to 1.97, which results in a fuel surface O/M of less than 2.0 and keeps the fuel-cladding attack below ∿ 20 μm at end of life (Fig. 5).

A long-term development thrust in this area is to either utilize lower O/M fuels (e.g., <1.94) or oxygen buffer/getter materials in the fuel rod. Fuel having an O/M of 1.90 and four different buffer/getter materials (V, Nb, Cr, Ti), incorporated either as coatings on the pellet surface, as layers at pellet-pellet interfaces, or as coatings on the cladding inside surfaces. Both approaches proved effective in reducing attack. The low O/M fuel exhibited no attack after 4320 GJ/kgM burnup, and two fuel rods with Nb and Cr coatings have successfully reached a peak burnup of 8640 GJ/kgM.

One potential problem with very low O/M fuel is the increased mobility of cesium within the fuel pellet column. Axial migration of cesium to the colder ends of the fuel column can be as detrimental to fuel rod performance as is radial migration to the fuel-cladding gap, primarily because cesium will react with the UO_2 insulator pellets, forming the larger-volume Cs_2UO_4, which locally strains the cladding. Additionally, the insulator pellets might fragment, and the central void may become restricted. Therefore, ideally one should choose a fuel O/M that would avoid both excessive radial and axial cesium migration-in other words, "tie up" the cesium in the fuel pellets. To assist in this goal, cesium buffers are also being tested, TiO_2, for example, when added to fuel reacts with cesium and avoids the formation of Cs_2UO_4. Also, it is possible that the niobium, used as an oxygen getter, also acts as an efficient cesium getter once it is oxidized to the + 5 valence state.

Despite the extra fuel swelling expected from fission gas bubble accumulation, the mechanical interaction between fuel pellet and cladding was considered to be less important than the chemical interactions because of two conteracting phenomena: first, stainless steel cladding is known to swell (increase specific volume and, hence, diameter) with increasing fast fluence; second, the plasticity (creep rate) of the mixed oxide is increased over UO_2 by the deviation from stoichiometry that results from the addition of plutonium (20 wt.% PuO_2 results in stoichiometries of 1.94-1.97), the plutonium content itself, and the higher fuel temperatures. As more data have been collected, however, at the higher burnups it has been shown that fuel swelling can overtake cladding swelling and that significant cladding hoop stresses can be generated. Also fission product accumulation in the fuel-clad gap can contribute significantly to cladding strain.

2.2. Control of the O/M ratio during Irradiation

Since oxygen activity appears to be a necessary condition for the occurrence of intergranular attack, its control in situ during burnup of the mixed oxide fuel rod is a useful means of preventing intergranular attack particularly late in the burnup period where fission product concentrations are highest and oxygen activity is at its peak. The oxygen activity in the fuel pin may be controlled by inserting a material which has a stronger affinity for oxygen than the cladding constituents (i.e., chromium). Several materials are suitable for this purpose, and the choice and placement of such depends on many factors other than chemical affinity.

Figure 6 shows the oxidation potential of several materials as a function of temperature. Similar relations for typical mixed oxide fuel compositions are superposed. The materials which have oxidation thresholds below that shown for stainless steel are useful as oxygen absorbers. Some materials have potential capable of reducing the oxide fuel to the metal. This occurrence need not happen, however, if the temperature is low and the oxygen absorber is present in limited quantities. Zirconium and titanium are known to react with UO_2 and produce a metallic phase containing uranium above 1200°C. The mixed oxide phase has a wider stoichiometry range than the UO_2 which should reduce the possibility of such a reaction. Niobium and tantalum have high melting points and do not form uranium alloys. Niobium has three oxidation states, NbO, NbO_2 and Nb_2O_5 - which are stable with respect to cladding oxidation. Pure chromium metal also will prevent cladding oxidation since its affinity, although close, is stronger than chromium dissolved in the stainless steel.

An absorber may be located at a position where the temperature is different from the fuel or from the hottest part of the cladding. In such cases the lower the absober temperature, the greater is its affinity for oxygen relative to the fuel. For instance, niobium oxidation at 650°C to Nb_2O_5 can reduce fuel at 900 to 1.97 and at 1500 to $\sim$ 1.91. The variation in oxygen potential, $\Delta \overline{G}_{O_2}$, with stoichiometriy of the fuel at 800°C is hown in Figure 7. Oxidation potentials for niobium and chromium as well as oxygen potentials for several fission products are indicated relative to stainless steel.

3. Cladding Behaviour

Production of defects in metals by fast neutron irradiation may lead to enhanced creep (from enhanced diffusion), grain matrix hardening (from the combined "barrier" action of defect clusters and voids), grain boundary embrittlement (from helium bubbles), and, swelling (again from voids). It is therefore considered that fuel assembly lifetime might be limited either by the strength and ductility of the fuel-rod cladding.

The principle cause of ductility loss in stainless steel at high temperatures (>820 K) is helium embrittlement. To reiterate, this is the formation of helium from n,α reactions and subsequent migration to grain boundaries and growth of bubbles under applied stress. An increase in grain-boundaries helium concentration is manifested in a reduction in uniform and total creep and tensile elongation, and as a reduction in stress rupture life. In addition, irradiation also introduces the possibility of crack propagation through locally heavily deformed regions in the matrix. This is the so-called "channel fracture" mechanism.

The fracture map in Fig. 8 shows the various fracture fields, and it can be seen that the intergranular fracture field covers a significant portion of the fuel-cladding operating regime. Channel fracture would be expected only at high stresses, but such locally high stress concentrations could develop in a PCI situation, as hypothesized for LWR fuel.
Important for fuel rod design strain limits is the fact that ductility does not approache zero but saturates at a low (1-2 % strain) but manageable value for normal operating conditions. Only in cases where specimens are fractured at significantly higher temperatures than at which they were irradiated - to simulate an off-normal temperature excursion, for example - did fracture strains fall to dangerously low levels of $\lesssim$ 0.1 %. The low ductility found in these tests has not resulted in a reduction in fuel rod life, however, since load-bearing capacity remains sufficiently high to meet goal lifetime requirements.

4. Fuel-Cladding Mechanical Interactions

Deleterions chemical interactions between fuel and cladding (FCCI) were observed. As shown in Fig. 5, significant cladding wastage is possible in current-design LMFBR fuel rods. This corrosion of austenitic stainless steel cladding by fission products degrades the mechanical properties and contributes to the reduction in life of cladding alloys. The strength reduction can be quantitatively explained by assuming that the effect of grain-boundary penetration is equivalent to the reduction in the tube-wall thickness of the specimen. As noted earlier, however, cladding ID corrosion can be minimized (a) with hypostoichiometric fuel, and (b) by maintaining cladding temperatures below $\sim$ 810 K, (c) by using oxygen absorber in the fuel rods (Chapter 2.2.).

Only recently has the potential for significant mechanical interactions (FCMI) emerged, as a result of more detailed analyses of fuel rod dimension changes during irradiation. The masking effect, of course, is the cladding swelling phenomenon, which causes dilation of the cladding in the absence of stress. In fact, in the reference design considerations it was estimated that a combination of cladding swelling and low fuel smeared densities would preclude any significant FCMI. However, with the trend to higher smeared densities and low-swelling cladding to improve burnup and breeding gain, the concerns about FCMI phenomena have reemerged.

Figure 9 indicates that the influence of fuel smear density (i.e., fuel pellet density and fuel-cladding gap size) on cladding strain is observed well before the start of significant cladding swelling, i.e., below 9500 GJ/kgM burnup and fluence levels below 6×10^{26} n/m^2 (E > 0.1 MeV). Fission gas pressure effects alone would only account for relatively small strains (0.1 to 0.3 % at 8640 GJ/kgM burnup). However, mechanical strains of up to 1 % have been achieved without cladding failure. Locally high cladding stresses might be caused by accumulation of cesium at the fuel-cladding interface.

Although it is apparent that steady-state FCMI effects have not given rise to cladding failures, the FCMI stress level may have significant effects on the margin to failure in subsequent overpower events. Fuel rod failures were generated by power increases in the range of 20 to 100 %. Calculated cladding deformations for the failed rods were 0.5 to 0.9 %, in contrast to 0.08 % for the unfailed rod. In the analytical studies, the LIFE-III code was used to assess cladding loads during a slow overpower event (a 10 % power increase over a one-hour period). Figure 10 summarizes the results, which indicate significant cladding stresses and strains.

The trend to higher fuel smear densities and low-swelling cladding alloys (ferritic SS) will accelerate the onset of fuel-cladding interaction.

5. External Cladding Corrosion

Sodium influences the structure and composition of the stainless steels in two important ways. First, sodium preferentially leaches out the chromium and nickel from the steels, with the latter being responsible for conversion of the original austenitic phase to ferrite. A 10- to 20-μm-thick ferrite layer forms at the outside cladding surface. Second, the transfer of interstitial elements, in particular carbon, in the liquid sodium/ stainless system can result in either carburization or decarburization of the steel, depending on the temperature and carbon activity (i.e., concentration) of the sodium. In contrast to fission product attack which is predominantly intergranular, external corrosion due to sodium is uniform. In general, the corrosion rate for Types 304, 316 and 1.4970 stainless steel reaches a steady-state value after an initial period of rapid metal loss. The steady-state corrosion rate increases exponentially with temperature and linearly with oxygen content and sodium velocity up to $\sim$ 3 m/s. The corrosion rate becomes independent of velocity at the higher values. The corrosion rate correlations for Type 316 stainless steel that are used for design calculations of fuel rod wall thinning in the LMFBR are shown in Fig. 11. These empirical relations refer to steady-state corrosion rates determined at locations of maximum corrosion, i.e., maximum upstream position. The downstream or positional effect, metallurgical condition of the material (annealed

or cold-worked), and minor variations in the nickel, chromium, niobium, or titanium contents of the stainless steels have relatively little influence on the corrosion rates in comparison with the temperature, oxygen content, and velocity of the sodium. The carburization/decarburization and the sodium leach-out-phenomena can both influence the mechanical properties of stainless steel, but all indications are that these effects are of minor significance to cladding integrity. For instance, the ferrite layer is typically included in the overall cladding wastage allowance (i.e., it is treated simply as a reduction in load-bearing capacity), and the effects of carburization/decarburization on important cladding creep and strength parameters are small ($\lesssim$ 10 %) compared to the effects of irradiation, and are included implicitly in the "safety factor" applied to the design curves. Coolant corrosion is not considered a limiting factor in the performance of LMFBR fuel.

6. Summary

In a LMFBR fuel rod more profound chemical and microstructural changes take place in the fuel and the cladding due to the higher temperatures, the fast neutron fluence, and the higher burnup compared to a LWR fuel rod.

In oxide fuels the nuclear fission causes an increase in the oxygen potential in the pin, as the fission products formed bind less oxygen than is released. Above a critical oxygen potential, oxidation of the cladding takes place which is accellerated by the fission products, especially by cesium. This is very dangerous, as it can take place preferentially along the grain boundaries of the cladding material. However, the initial fuel O/M ratio cannot be selected so low that it can prevent the dangerous Cs reactions with the steel cladding at high burnups also. In oxide fuel pins, therefore, strong chemical interactions with the cladding material can only be prevented by the use of getter materials in the fuel pin, which getters (absorbs) the excess oxygen and some of the reactive fission products.

Under steady-state condition cladding failures are acceptable small. However, fuel cladding failure can occur by strong power increases due to mechanical interactions between the fuel and the cladding.

Sodium Coolant corrosion of the stainless steel cladding is not a limiting factor in the performance of LMFBR fuel rods.

References

J.T.A. Roberts
Structural Materials in Nuclear Power Systems,
Plenum Press,New York (1981)

D. Olander,
Fundamental Aspects of Nuclear Reactor Fuel Elements,
Technical Information Center, ERDA, TID-26711-P1 (1976)

/1/ F.A. Nickols
Transport Phenomena in Nuclear Fuels under Severe Temperature Gradients,
J. Nucl. Mat., 84 (1979) 1-25

/2/ D.C. Fee, C.E. Johnson
Fuel-cladding Chemical Interaction in U-Pu Oxide Fast Reactor Fuel Pins,
J. Nucl. Mat., 96 (1981)

/3/ O. Götzmann, P. Hofmann, F. Thümmler
Attack upon the Cladding of Oxide Fuel Pins by Fuel and Fission Products,
J. Nucl. Mat. 52 (1974) 33-50

/4/ P. Hofmann
Studies on the Reactivity of Steels with Simulated Fission Products in the Presence of UO_2, $(U/Pu)O_2$ and UC and Possible Ways of Improving the Compatibility Behavior of Oxide Fuel Pins, KfK 1831 (1974)

/5/ E.A. Aitken et al.
A Thermodynamic Data Program Involving Plutonia and Urania at High Temperatures
GEPA - 12389 (1973)

/6/ O. Götzmann, P. Hofmann
Mechanical Properties of Austenitic Steels after Corrosion
by UO_2 and Fission Product Elements
J. Nucl. Mat. 59 (1976) 192-198

/7/ S.A. Shiels et al.
The In-Sodium Corrosion Behavior of Candidate Commercial
Fuel Cladding and Duct Alloys,
HEDL TME 77-71 (1978)

/8/ Schäfer, Hofmann;
Tensile Properties of 1.4970 Austenitic Stainless Steel after
Corrosion Caused by UO_2 and Simulated Fission Products,
J. Nucl. Mat., 67 (1977) 88-96

/9/ K. Ehrlich,
Irradiation Creep and Interrelation with Swelling in Austenitic
Stainless Steels,
J. Nucl. Mat., 100 (1981) 149-166

/10/ B. Lindemer, M. Besmann, C.E. Johnson,
Thermodynamik Review and Calculations - Alkali-Metal Oxide
System with Nuclear Fuels, Fission Products, and Structural Materials
J. Nucl. Mat., 100 (1981) 178-226

/11/ H. Hoffmann,
Crack Formation, Crack Healing and Porosity Redistribution
During Irradiation of UO_2 and $(U, Pu)O_2$
J. Nucl. Mat., 54 (1974) 9-23

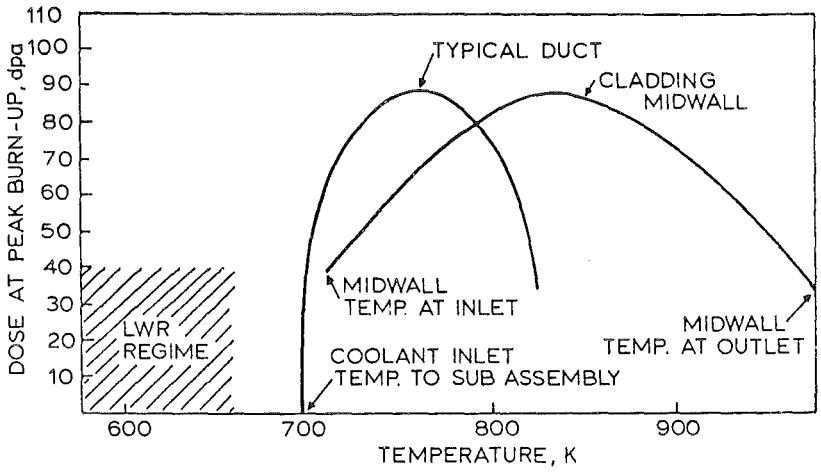

Fig. 1: Typical radiation dose-temperature profiles for LMFBR cladding and duct at 8640 GJ/kgM, compared to LWR cladding conditions. 1 dpa = 2×10^{25} n/m^2 (E > 0.1 MeV).

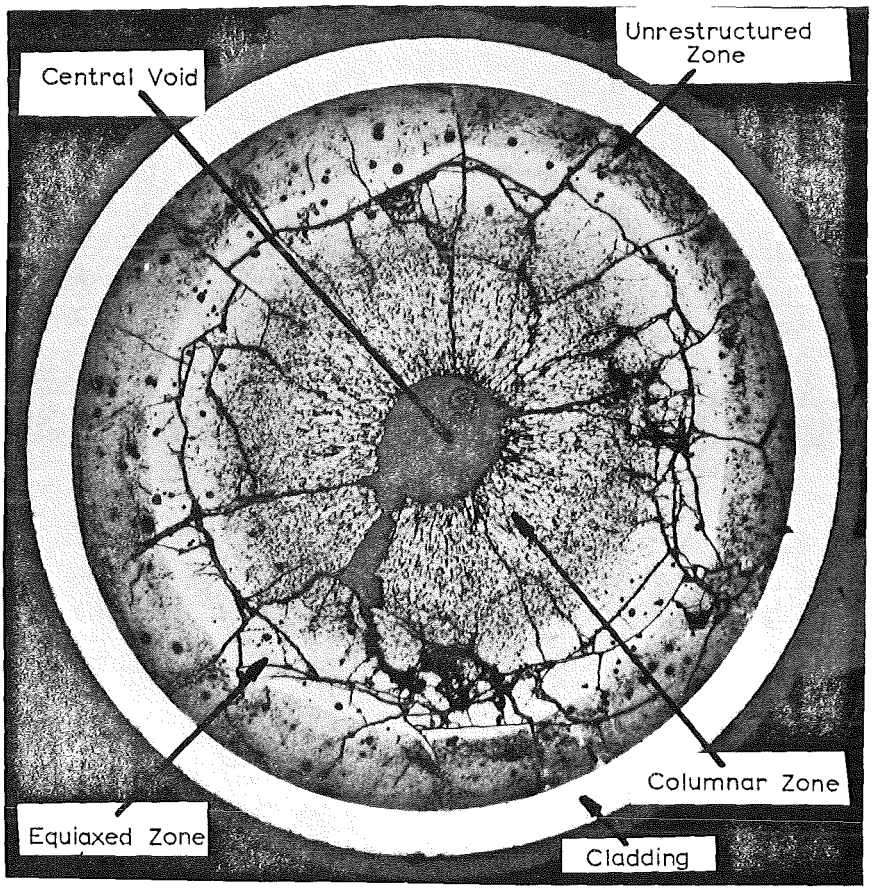

Fig. 2: Cracking and structural changes in LMFBR mixed oxide pellet.

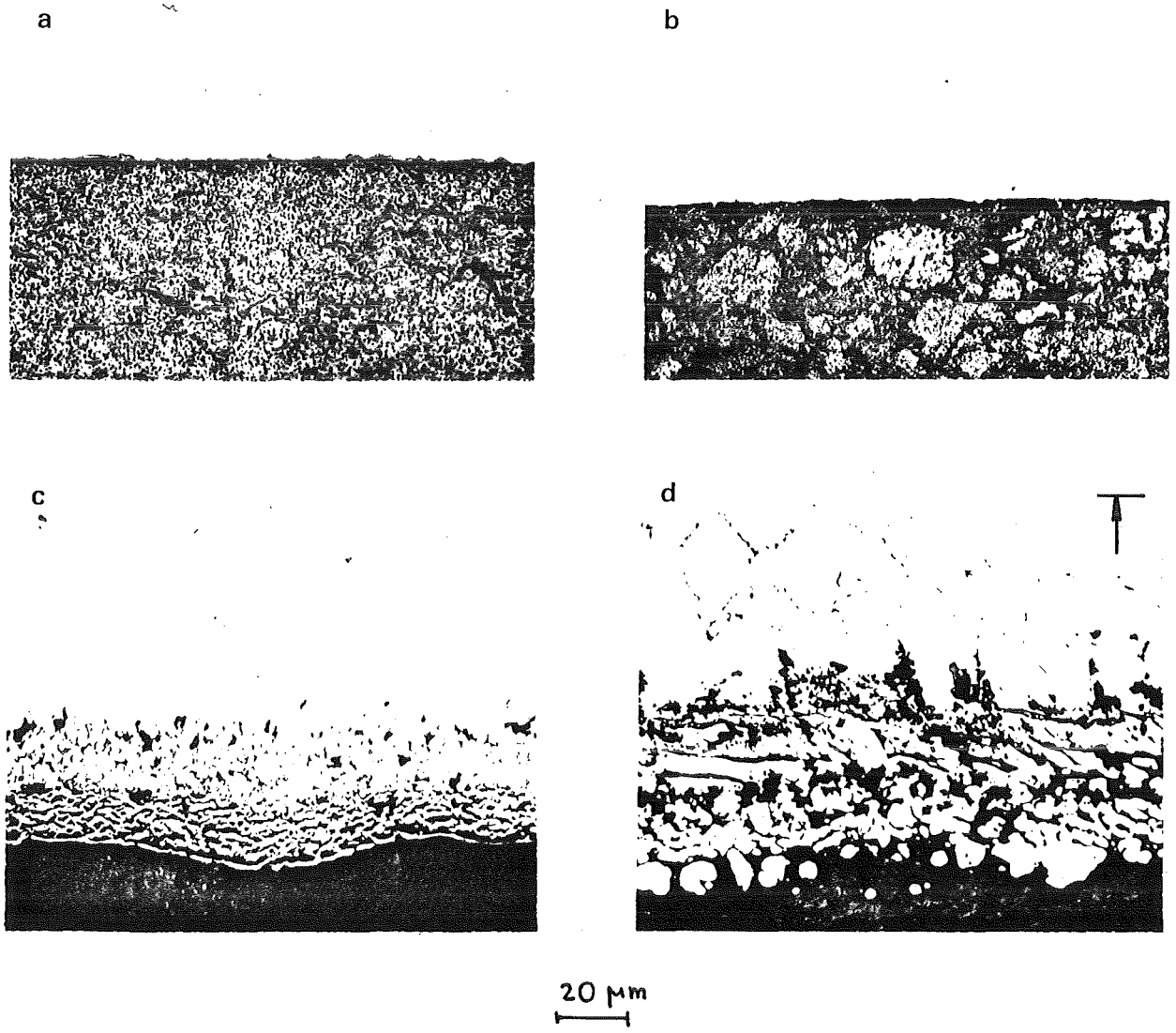

Fig. 3: Dependence of cesium reactions with 1.4988 steel on O/U ratio of the fuel (simulated burn-up: 10 at.%), temperature: 800°C, annealing time: 1000 h

a) $UO_{2.08}$ b) $UO_{2.00}$ + Cs

c) $UO_{2.04}$ + Cs d) $UO_{2.08}$ + Cs

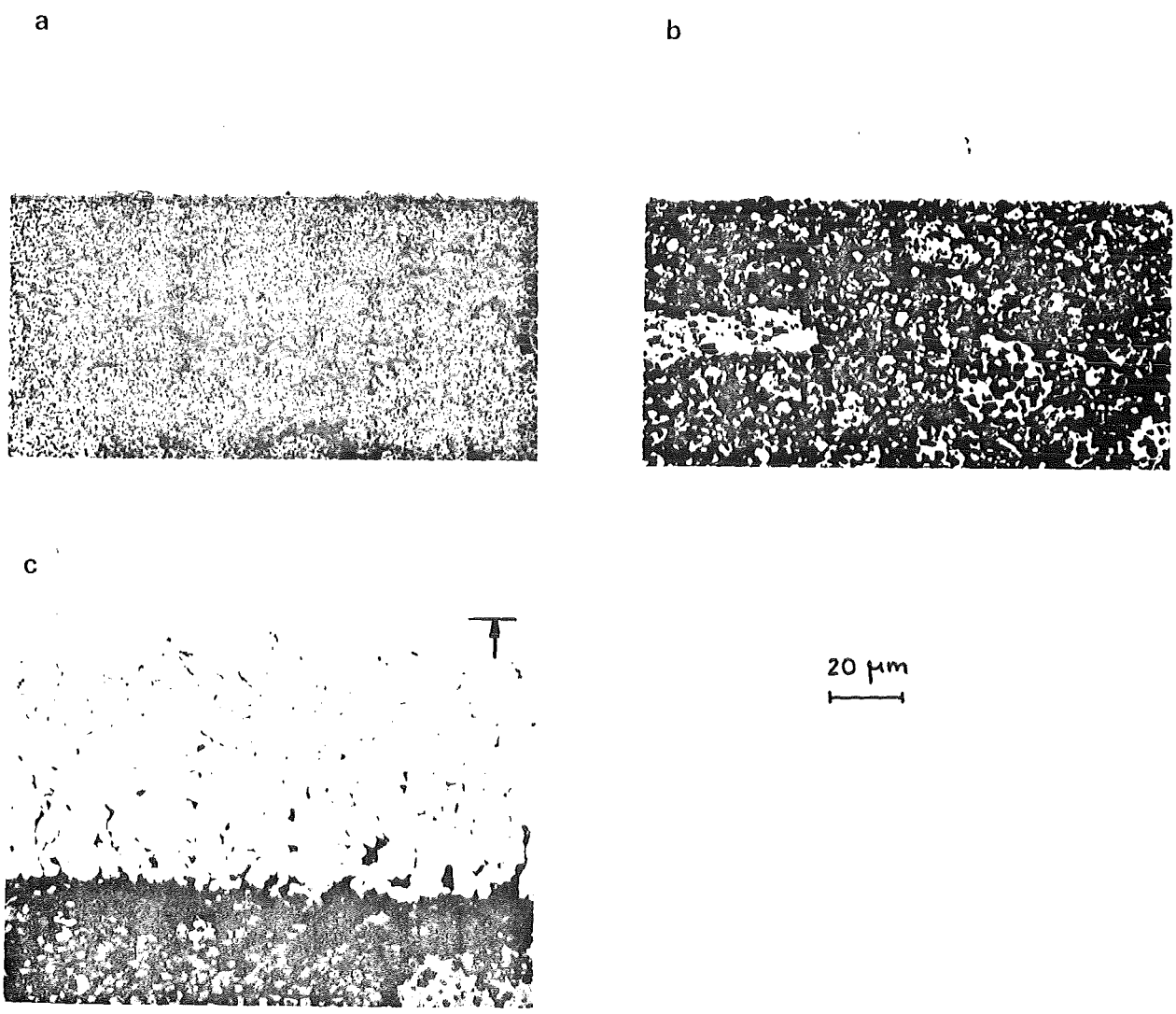

Fig. 4: Influence of Cs, I, Se, Te on the compatibility behaviour of oxide pins (simulated burn-up: 10 at.%); temperature: 800°C, annealing time: 1000 h

a) $UO_{2.08}$

b) $UO_{2.08}$ + Mo + Ru + Pd + BaO + ZrO_2 + CeO_2 + Nd_2O_3

c) $UO_{2.08}$ + Mo + Ru + Pd + BaO + ZrO_2 + CeO_2 + Nd_2O_3 + Cs + I + Se + Te

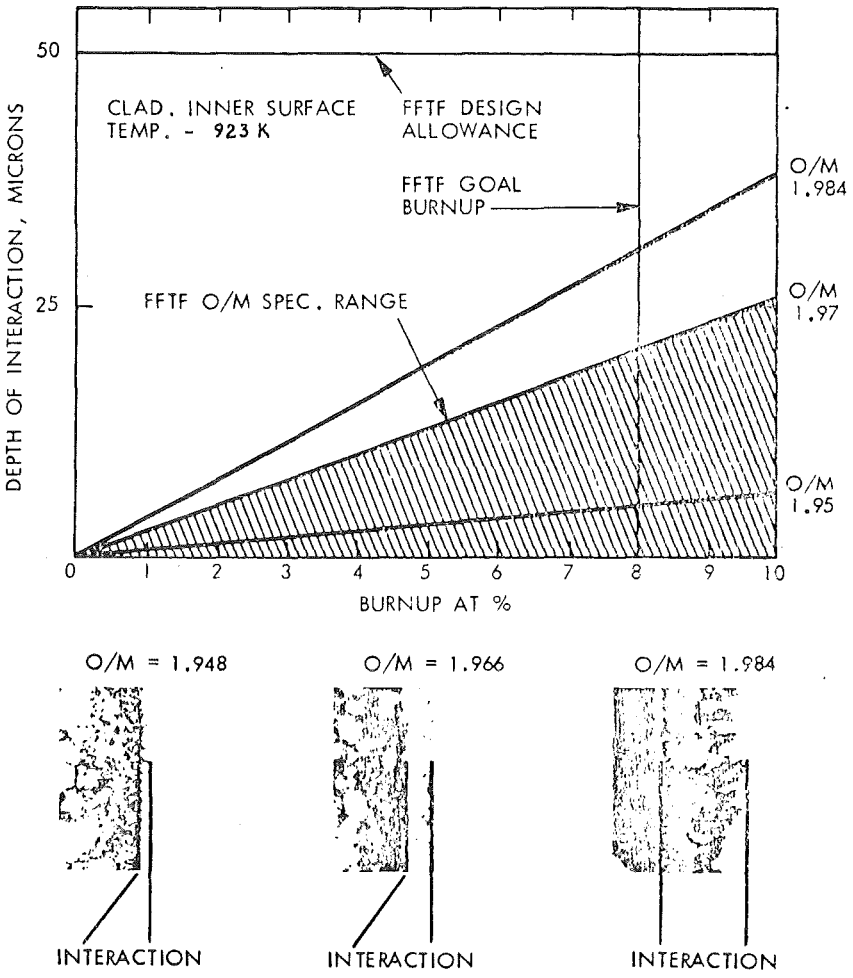

Fig. 5: Fuel-cladding chemical interaction (FCCI) in mixed oxide fuel irradiated in EBRII.

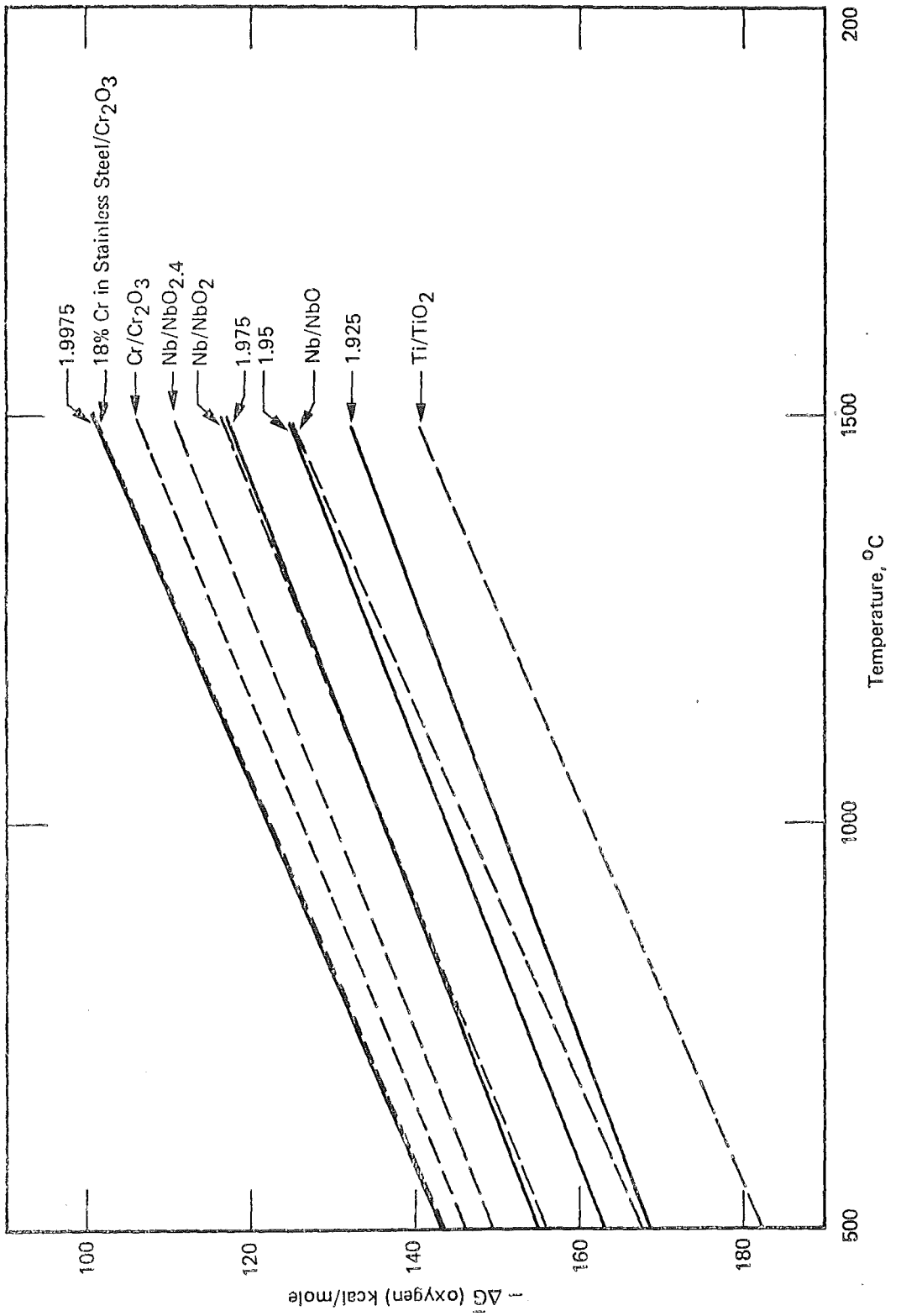

Fig. 6: Oxidation potentials for various fuel compositions $(U_{0.75}Pu_{0.25})O_{2-x}$ and various oxygen absorbers as a function of temperature

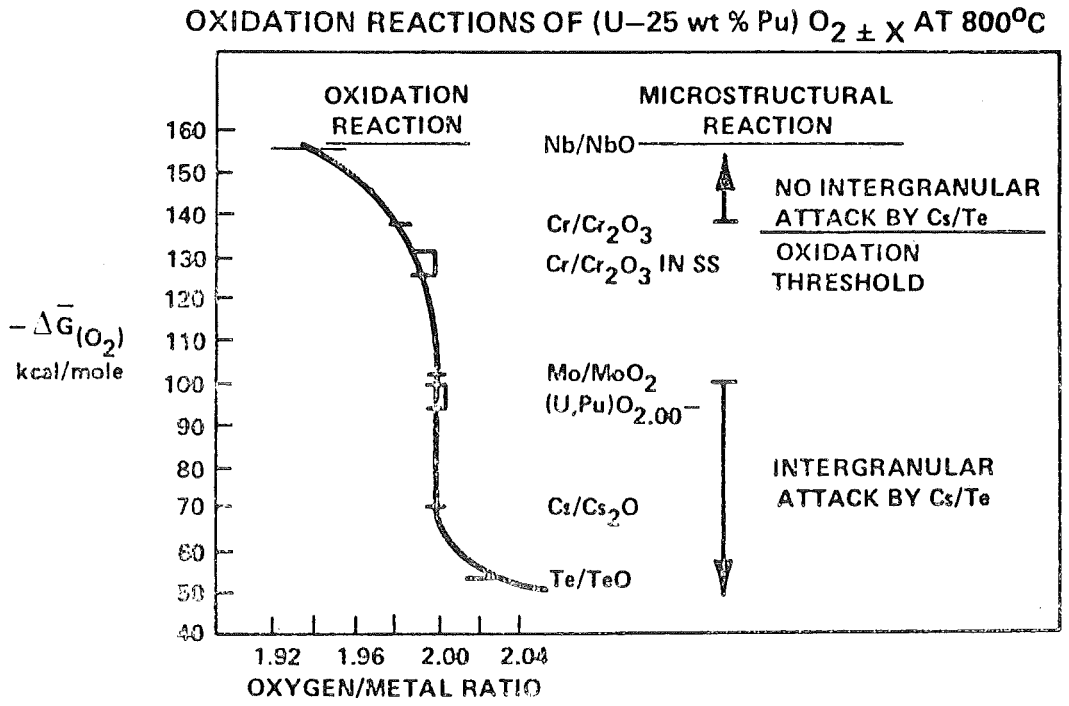

Fig. 7: Oxygen potential versus O/M of oxide fuel at 800°C relative to oxidation couples for various elements

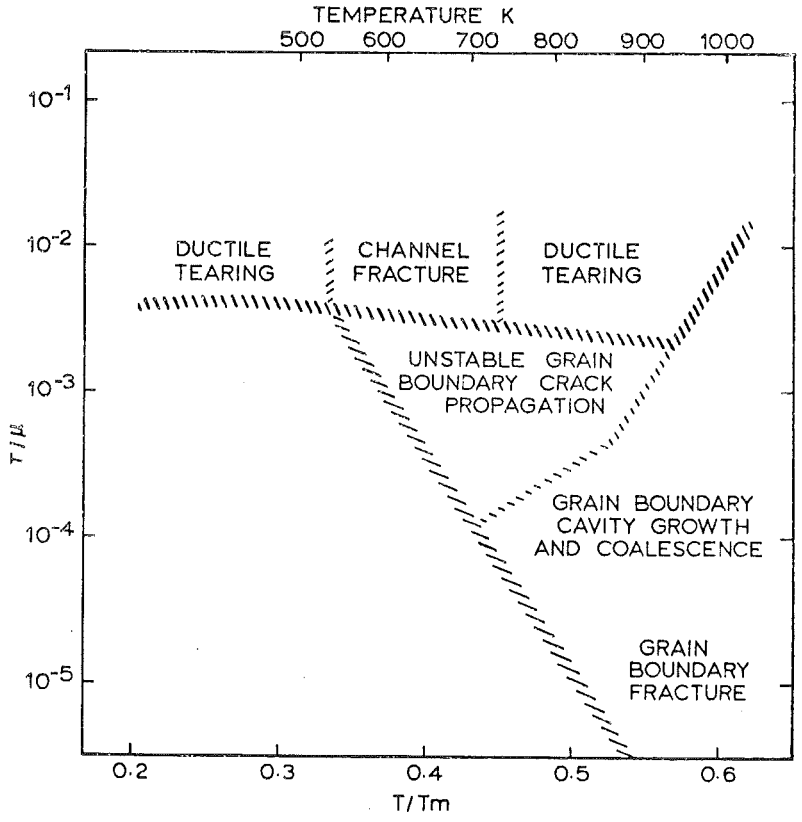

Fig. 8: A fracture map for austenitic stainless steel: schematic representation of the fracture behaviour after irradiation to high fast neutron fluences as a function of normalized stress and temperature

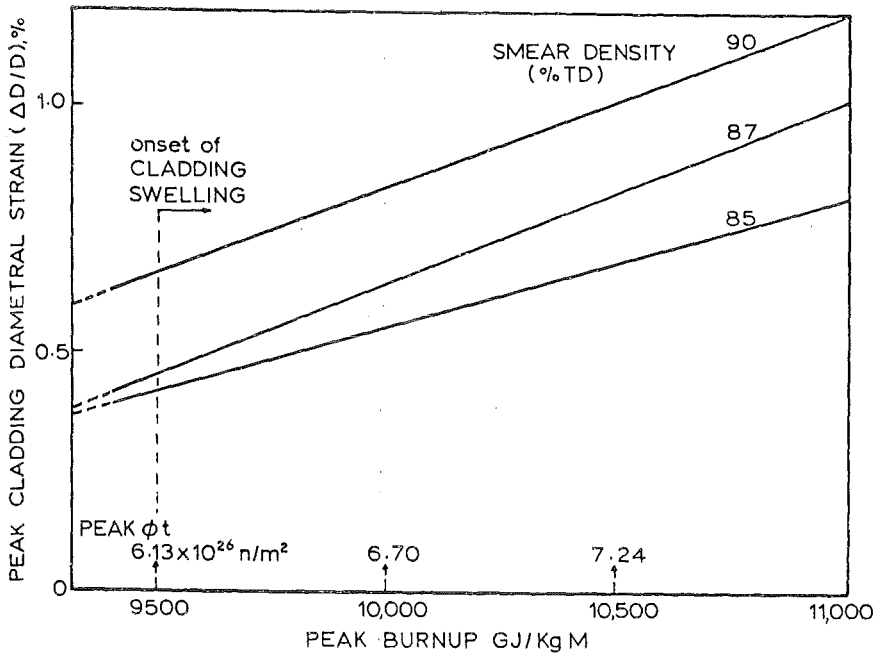

Fig. 9: Maximum cladding strain as a function of fuel smear density for stainless steel fuel rods irradiated in EBR-II

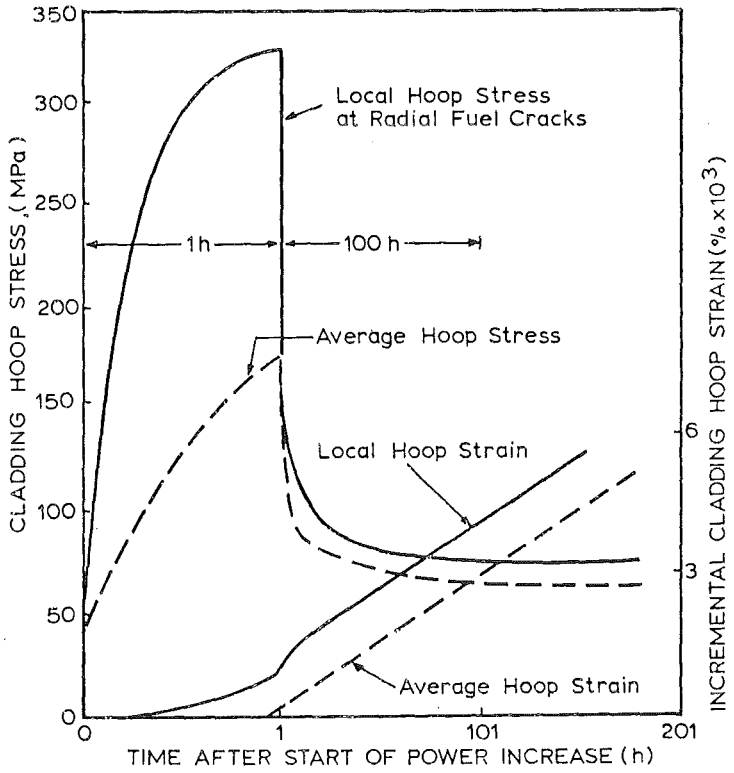

Fig. 10: Cladding stress and strain history following a 10 % increase in power for a mixed oxide fuel rod

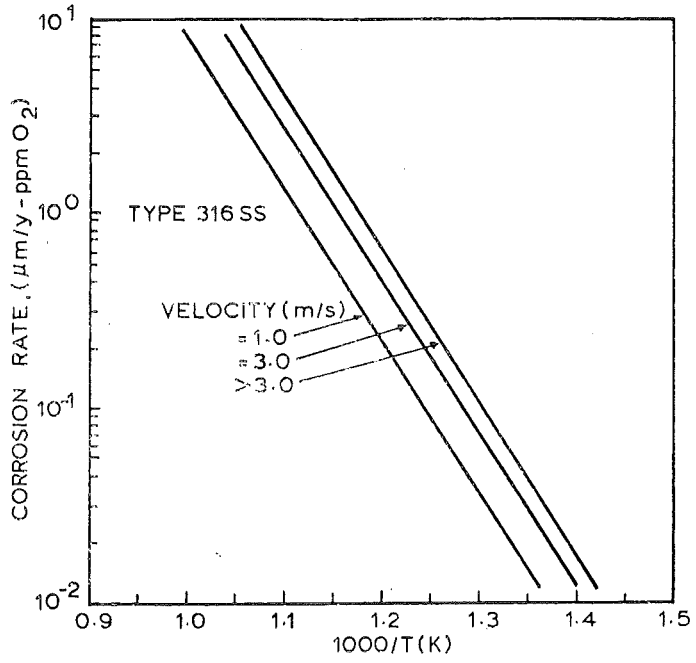

Fig. 11: Effect of temperature on the corrosion rate of Type 316 stainless steel in flowing sodium

G. LMFBR FUEL ROD BEHAVIOR UNDER OFF-NORMAL CONDITIONS

1. General considerations

2. Fast reactor accident scenarios

3. The loss-of-flow without scram accident (LOF)

4. The transient overpower without scram accident (TOP)

5. Fuel behavior phenomena in fast reactor accidents

6. Conclusions

6. LMFBR FUEL ROD BEHAVIOR UNDER OFF-NORMAL CONDITIONS

1. General Considerations

Fuel effects enter into fast reactor safety considerations many ways, with important effects in events over the full spectrum of severity ranging from operational transients to hypothetical core disruption accidents (HCDAs). At the less severe end, the behavior of the fuel relative to normal failures and its response to abnormal operational transients is of key importance. In more severe accidents, fuel behavior has key importance in accident energetics and debris coolability.

The principal goal of the designer of fast reactor fuel elements (but also for LWR fuel rods) is to ensure that goal burnup can be achieved without an unacceptable number of fuel pin failures. There is a safety incentive in minimizing or eliminating failures in normal operation. First, failure of cladding represents failure of one of the barriers to fission product release. Second, release of fission products from failed fuel will create an additional source of radiation exposure to plant personnel during operation and maintenance. Third, fuel failures represent a local fault with a potential for propagation into more widespread fuel disruption.

Reliable systems for removal of decay heat following shutdown must be provided. Should decay heat not be removed, the core will eventually melt.

While the fuel behavior under normal operation and off-normal transients, with and without cladding breach, and fuel behavior during loss-of-shutdown heat removal are important problems, the most important fuel behavior concerns are associated with unprotected transients potentially leading to core disruption and significant energy release. Fuel behavior, especially fuel dynamics effects related to reactivity, is a crucial issue in core disruptive accidents. Fuel behavior determines wheter the accident remains small and self limiting or whether it progresses, perhaps leading to full core disruption and then possibly to energetic disassembly. Because of the important reactivity effects, fuel behavior considerations in fast reactors significantly differ from those of light water reactors. It is necessary to know in considerable detail the motion of the fuel to a degree not required in light water reactor considerations.

In addition to reactivity, the major fuel disruption effect relates to the coolability of the core. Should significant core disruption occur, the fuel behavior to a considerable degree determines the debris behavior. It establishes whether the core debris can be cooled in place or whether containment integrity is threatened.

2. Fast reactor accident scenarios

Fast reactor accidents generally may be placed into one of three categories

- transient undercooling
- transient overpower
- local faults

Transient undercooling would include such initiators as pump coastdown, with and without scram, and loss of shutdown heat removal. Transient overpower would include various reactivity insertions, with and without scram. Local faults includes fuel pin failures, flow blockages, local cooling faults or debris accummulations, and the like.

In general, so long as the scram systems are assumed to work as designed, the transient undercooling and overpower accidents are quite benign in their effects on intact fuel. There is, of course, an issue with respect to fuel performance that is, to what extent is the fuel lifetime shortened or the probability of failure increased due to the transient. Evaluation of damage to fuel from operational or anticipated transients involves considerations of fuel-cladding mechanical interaction, fission-gas release, cladding response to loading and temperature, and cladding failure criteria.

Should the scram system fail to terminate an undercooling or overpower transient, some degree of core disruption is inevitable, because the only means of rendering the reactor permanently subcritical is by redistribution of fuel to a less reactive configuration. Generally, removal of some amount of fuel from the core region will be required.

3. The loss-of-flow without scram accident (LOF)

The postulated LOF accident sequence begins with a coastdown of the main coolant flow coupled with failure of the scram systems. During flow caost-down, there will be reactivity changes due to sodium density decrease. Doppler feedback, axial expansion of fuel, and possible grid plate expansion or relative motion of fuel and control rods. While it appears to be possible, in a properly designed system, to obtain sufficient negative reactivity feedback to avoid boiling, boiling will occur in the general case.

A typical LMFBR core will have a positive sodium void coefficient of reactivity, so boiling will produce a power rise and additional voiding. Reactivity insertion from boiling will be counteracted by axial expansion of fuel and by Doppler feedback. Cladding will melt and may be removed from the core due to hydrodynamic forces, producing an additional positive reactivity insertion.

Fuel dispersal in voided channels is a key branch point in the LOF accident sequence. If the fuel motion is such as to remove reactivity with a sufficient rate and magnitude, the accident will be non-energetic, at least in the initiating phase. Permanent subcriticality would require that fuel be removed well beyond the subassembly boundaries so that it could not return to the core.

A list of the most important fuel-related phenomena in alaysis of the loss of flow without scram accident includes:

- Axial expansion of solid fuel.
- Early fuel dispersal in voided channels.
- Fuel pin failure and fuel motion in unvoided channels – elevated power and reduced flow.
- Freezing and plugging of flow channels by fuel.
- Boil-up of molten fuel-steel mixtures.
- Fission product and fuel vapor effects in disassembly.

The status of knowledge of these phenomena will be assessed in chapter 5.

4. The transient overpower without scram accident (TOP)

The other accident to which major attention has been focused in fast reactor safety and licensing is the transient overpower without scram. It is assumed that a reactivity input of prescribed magnitude is introduced and not terminated by scram systems. The reactivity addition produces a power rise which eventually results in fuel pin failures in some subassemblies. Pin failures typically occur without coolant boiling, but with substantial fuel melting. It is thought that cladding failure will occur somewhat above the core midplane, and that molten fuel will move from the interior of the failed pins into the channel. Relocation of fuel from the pin to the failure site, along with subsequent dispersal in the channel is a mechanism for producing permanent subcriticality. Since the heat removal capability of the system is not compromised, the accident is terminated so long as the damaged assemblies are coolable. Generally, sweepout of molten fuel in the channel will enhance the negative reactivity effects and promote coolability. Freezing in place would have the opposite effect.

The fuel-related phenomena encountered in transient overpower without scram accident analysis are confined to the initiating phase. They are:

- Prefailure axial motion of molten fuel.
- Fuel pin failure and fuel motion in unvoided channels - elevated power and full flow.

The status of knwoledge of these phenomena will be addressed in the next chapter.

5. Fuel behavior phenomena in fast reactor accidents

5.1. Axial expansion of solid and molten fuel

Axial expansion of solid fuel during the early stages of an LOF accident can materially contribute to the total negative reactivity feedback, thereby reducing the net reactivity later in the transient. During the flow coastdown,

the power remains essentially constant and cladding expands away from the fuel. Later in the transient when void reactivity drives the power up, the fuel will again contact cladding. Two extreme conditions seem possible free standing fuel and fuel and cladding locked together.

It has been postulated that axial motion of molten fuel within intact cladding could provide a mechanism for shutdown of a TOP transient without cladding failure, thereby removing post-transient coolability as an issue. This mechanism is of particular interest in cores having annular pellet fuel, since a clear path would probably exist for fuel ejection to the plenum.

5.2. Early fuel dispersal in voided channels

Early fuel dispersal in voided channels is a central issue in evaluation of the initiating phase of the LOF accident. If early dispersal can be shown to be effective in producing permanent shutdown and if decay heat removal capability is intact, the LOF can be terminated without the need to consider either a transition phase or disassembly.

Important factors in the timing of fuel disruption and the nature of the disrupted fuel include the thermal history, (temperature, radial temperature distribution, time at temperature) of the fuel pin segment, the character of the fuel (burnup, irradiation power, level), and the nature of any restraint to disruption (presence of cladding, etc.). Disruption can be characterized as a thermal-mechanical process, in which macroscopic effects such as melting and cracking, as well as microscopic effects such as fission gas release, intergranular void formation, and grain boundary separation are likely to be important.

Once the fuel disruption process has begun, axial displacement of the mobile fuel can also begin. The displacement process appears to be basically hydrodynamic in nature, depending upon momentum exchange between expanding fission gas, streaming steel and/or sodium vapor, and mobile fuel to produce axial motion.

A number of different fuel disruption modes are possible. It is difficult to generalize with respect to a preferred mode without knowledge of the details of thermal history, fuel character, etc. At this time, it is thought that the most likely fuel disruption mode for lead subassemblies would involve a mixture of molten fuel, fission gas, and solid fuel fragments which have undergone some degree of swelling or grain boundary separation. Following disruption, the mixture will be propelled upwards by pressure gradients resulting from expanding fission gas, sodium vapor, and steel vapor streaming until stopped by a cladding blockage or fuel freezing and plugging in the bundle outlet.

5.3. Fuel pin failure and fuel motion in unvoided channels

Fuel pin failure and fuel motion in unvoided channels is an important issue in both LOF and TOP accident sequences. In the LOF sequence, primary interest is focused on low power fuel, failing under a rapid, high power transient with reduced flow in the subassembly of interest. In the TOP sequence, the focus is on high-power fuel subjected to excessive power, but with full subassembly flow. The transient may vary from a quasi-steady-state power rise with a period of several tens of seconds to a more rapid rise with a period of less than a second. The differences in the power and flow histories will influence parameters such as cladding temperature and its axial variation, fuel temperature distributions, fuel-cladding mechanical response, and hydraulic aspects of molten fuel-coolant interaction in the channel in important ways. However, the basic considerations are essentially the same in both scenarios. These include loading of the cladding by fuel and fission gas, eventually producing cladding failure, motion of fuel from within the pin into the coolant channel, interaction of the released fuel with sodium coolant, and motion of fuel and coolant following fuel release.

Determination of the time, location, and nature of cladding failure involves a complex thermal-mechanical calculation of the loads placed on the cladding by the fuel and the response of cladding to these loads. Important factors in the calculation include:

- Radial and transverse cracking of relatively low temperature fuel.
- Non-elastic behavior of high temperature fuel, including plastic deformation, fission-gas-induced swelling, and hot-pressing of residual porosity.
- Fuel melting, with accompanying volume expansion and liberation of retained fission gas.
- Cladding mechanical response to loading, including effects of irradiation on mechanical properties.
- Cladding failure criteria, including effects of loading, time, temperature, irradiation, and chemical (fission product) environment.

Failure is thought to be more localized in the TOP sequence, with fuel motion towards the failure and into the channel. Subsequent fuel motion will depend on the balance between inlet pressure, pressure in the interaction zone, fluid momentum, and fuel freezing. Expansion of the interaction zone will eject sodium from the channel with relatively little fuel motion in the channel. Location of failure is especially important in this case.

5.4. Freezing and plugging of flow passages

In order for fuel to be removed from the core, it must traverse restrictive flow passages above and/or below the core. This is a complex problem of flow of a material (fuel) which will be freezing on the walls of the flow passage, while at the same time melting the steel walls under the frozen steel crust. A complication is the possible presence of sodium film on the steel and contact between fuel and bulk sodium with consequent pressure generation. Typically, experiments show that a large mass of molten material can be relocated into pin bundle flow passages, but that freezing and plugging does take place. Clean sweepout of fuel beyond the bundle has not been generally observed. However, the presence of sodium has not resulted in flow reversal which would imply fuel reintroduction, either.

5.5. Fuel-steel pool boilup

In addition to freezing and plugging, pool boilup represents a key phenomenological issue of the transition phase. It is postulated that a mixture of fuel and steel will boil up promptly as the fuel becomes molten. For a system consisting of oxide fuel and stainless steel, the boiling point of the steel is nearly equal to the melting point of fuel, so that dispersive forces due to vapor will be available as soon as fuel can move. The density of the fuel-steel mixture will be less than that of the core, and will ensure subcriticality so long as the pool remains in a dispersed state. Important considerations in this analysis include flow regime modeling, phase transitions, energy exchange between fuel, steel, and system boundaries, and stability of boiling, heat-generating pools under open and bottled-up conditions.

6. Summary

Fuel behavior phenomena can importantly affect the course of fast reactor accident sequences in a variety of ways. In postulated loss of flow and overpower accidents without scram, these phenomena include time and location of failure, reactivity associated with fuel motion both early and late in the transients, the effects of fuel disruption on core coolability, and the potential for fuel recompaction phenomena.

Reference

R. Avery, L.W. Deitrich,
Fuel Effects in Fast Reactor Accident Analysis,
International Conference on "REACTOR SAFETY ASPECTS OF FUEL BEHAVIOR",
August 2-6, 1981, Sun Valley, Idaho, USA, Vol. I, p. 1/17

PARTE II:

El material y el accidente de fusión del núcleo (seguridad nuclear)

G. Ondracek

(Traducción U. Röser)

El material y la seguridad nuclear: el accidente de fusión del núcleo

Sumario

La fusión del núcleo resulta de pérdidas de refrigeración durante el funcionamiento de un reactor nuclear.

Los problemas de materiales ligados a un accidente de fusión del núcleo pueden resumirse en dos grupos:
primero se refiere a la estructura de las fases y componentes y el segundo a sus propiedades en cada una de las etapas del desarrollo del accidente. Los resultados esenciales obtenidos hasta ahora son que

- los fenómenos de fusión del núcleo son bifásicos durante la mayoría del tiempo en que se desarrolla el accidente,
- la fase oxídica de los materiales fundidos del núcleo se compone de $(U, Zr)O_2$, mientras que la fase metálica tiene una composición semejante a la del acero,
- los elementos de la fase metálica se oxidan en el órden Cr-Fe-Ni y se convierten en la fase líquida de óxido,
- los productos de fisión están repartidos heterogéneamente en las fases, donde al principio la mayoría de ellos, y más tarde todos excepto los metales preciosos, están disueltos en la fase líquida oxídica,
- la fase líquida oxídica del corio disuelve el hormigón que funde, mientras que su temperatura de solidificación baja,
- las fases líquidas oxídicas con componentes disueltos de hormigón y la fase líquida metálica de corio se segregan, estando la fase metálica bajo la fase de oxído,
- varias características de las fases líquidas de materiales fundidos del núcleo pueden determinarse aproximadamente por extrapolación de cálculos basada en experiencias y por extrapolación gráfica.

1. El desarrollo del accidente de fusión del núcleo

1.1 El sistema

Cuando el sistema de contención de p.ej. un reactor de agua a presión (fig. 1) se considera como sistema termodinámico, su estado está determinado por sus magnitudes de estado, a saber:

- la concentración de sus componentes determinada por las estructuras internas del núcleo,
- la temperatura que está dada por el calor de fisión o el calor residual,
- la presión que está dada por la atmósfera de vapor de agua presente.

La parte de los componentes que proporciona el "calor residual" es el combustible - fisionable - del reactor nuclear que está dentro de agujas de combustible reunidas en elementos combustibles (fig. 2).

Una parte de los núcleos nuevos más ligeros que se forman durante la fisión de un núcleo pesado dentro de un reactor nuclear (los productos de fisión, ver fig. 3) y también los núcleos nuevos que se forman por captura de neutrones (los productos de activación) son radiactivos; es decir que se desintegran y se transforman en nuevos tipos de núcleos (los productos de desintegración). Con esto, se emiten por una parte rayos radiactivos (rayos α, β, γ), por otra parte se produce en esta desintegración en cadena aquel "calor de desintegración" cuyo rendimiento térmico residual tanto como la radiactividad de todos los elementos combustibles en el núcleo del reactor disminuye primero rápidamente, y entonces más y más lentamente, proporcionalmente a la desintegración exponencial de todos isótopos radiactivos (con períodos de semidesintegración cortos y largos (ver fig. 5).

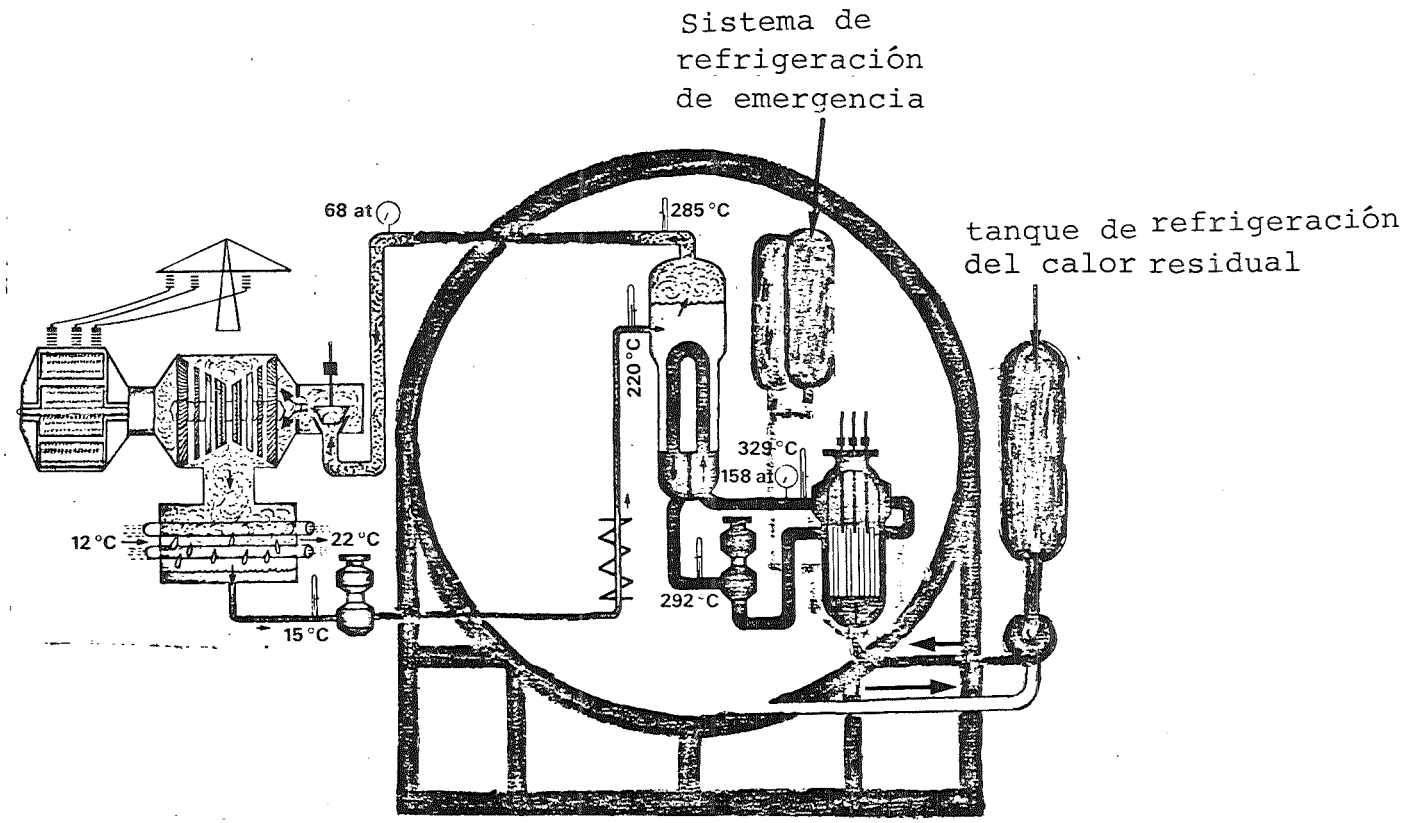

fig. 1: Esquema de un reactor de agua a presión

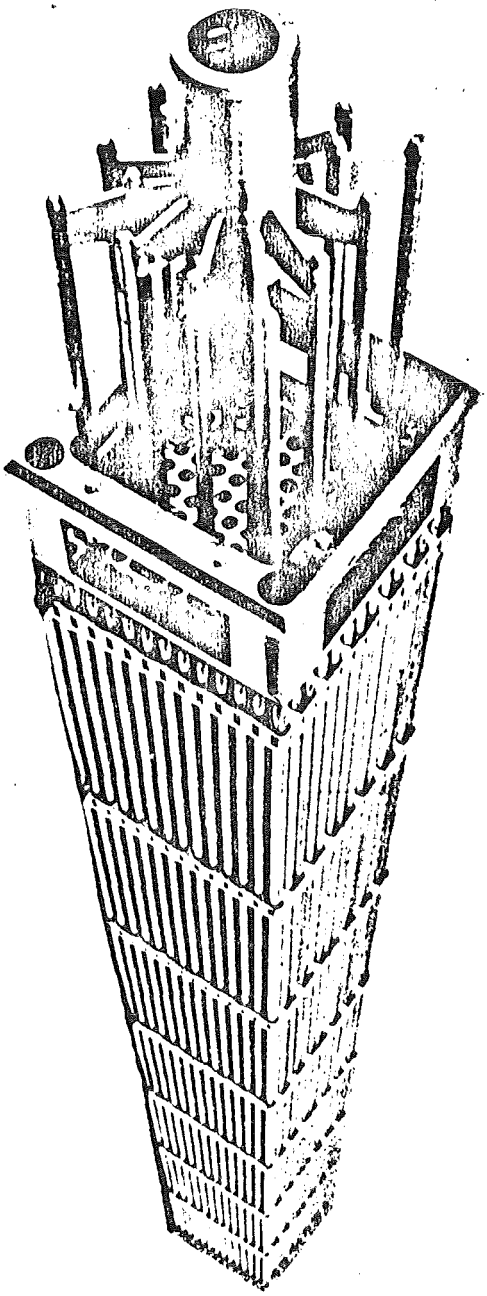

fig. 2: Elemento combustible de un reactor de agua a presión

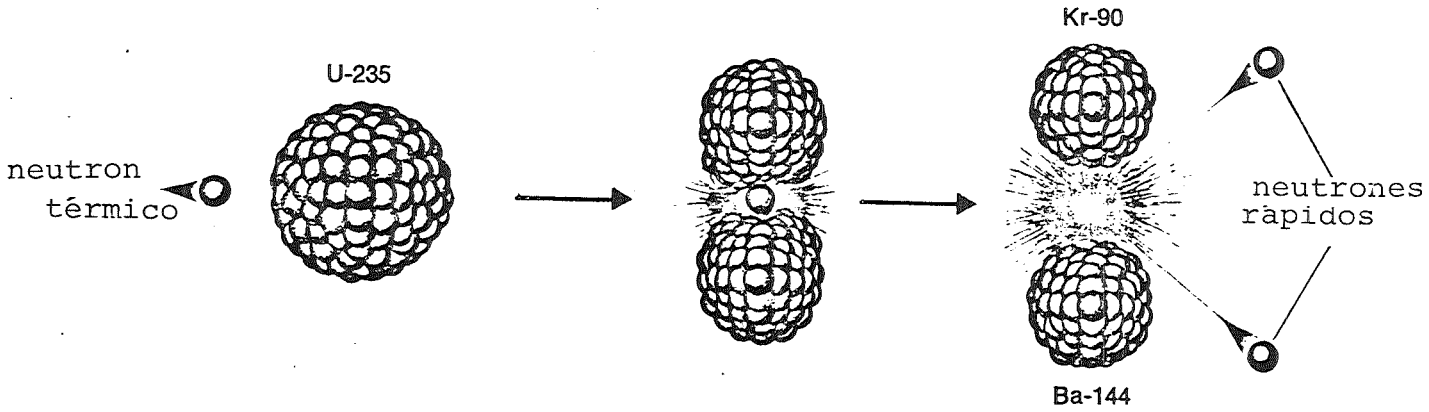

fig. 3: La fisión nuclear (esquema)

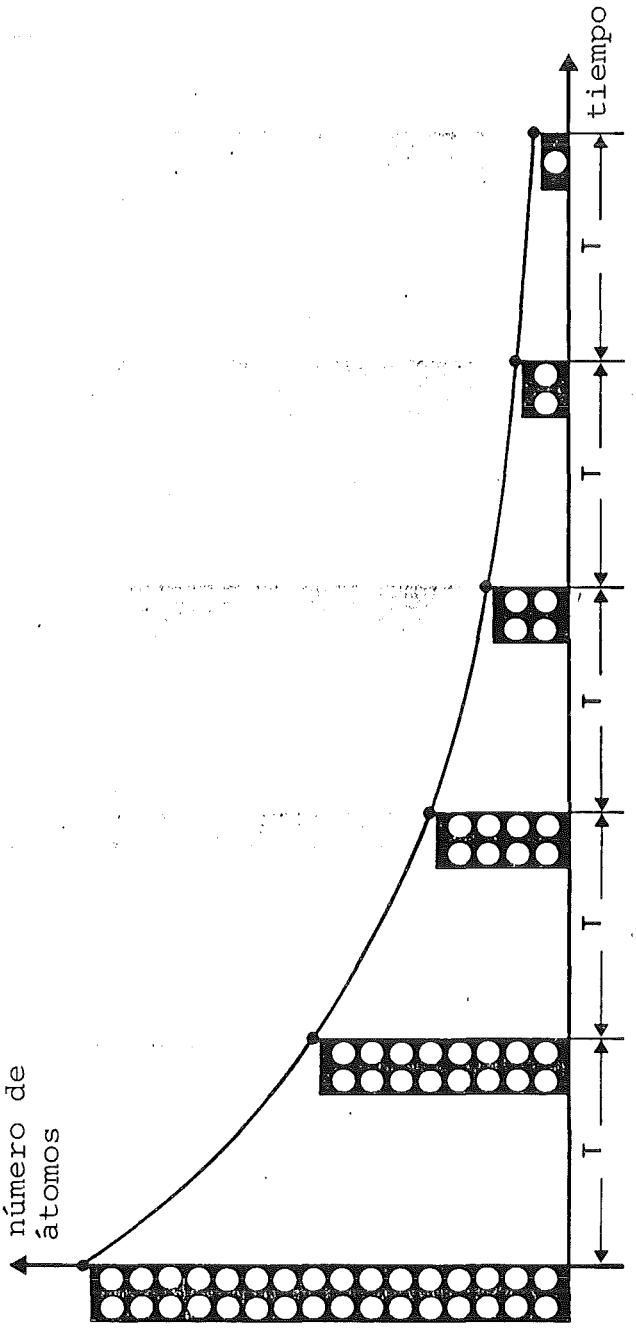

fig. 4: Períodos de semidesintegración

Con el aumento del tiempo de funcionamiento de los elementos combustibles en el reactor aumenta el calor residual, porque con esto aumenta también el número de los núcleos de productos de fisión producidos a partir de la parte fisionable del combustible. Para un reactor moderno de agua a presión (600 MW de potencia eléctrica bruta, 2,5 años de funcionamiento), el calor residual corresponde algunos minutos después de la interrupción de la fisíon nuclear a 100 Megawatt, y después de algunos meses quedan aproximadamente 20 Megawatt. Esta potencia térmica basta - sinó fuese evacuada de una manera adecuada a través de circuitos de refrigeración - para evaporar toda el agua contenida en el circuito primario dentro de algunas horas, lo que tiene como consecuencia un cambio dramático en función del tiempo, de las magnitudes de estado mencionadas del sistema y con esto un estado inestable del sistema: El accidente de fusión del núcleo del reactor.

Las condiciones extremas bajo las cuales podría ocurir tal accidente excluyen su estudio dentro de un ensayo integral real. Para describir su desarrollo con el tiempo se han por lo tanto elaborado modelos de simulación que describen sobre todo el cambio de la temperatura como variable de estado central en función del tiempo. Están basados generalmente en hipótesis pesimistas y constituyen representaciones inexactas de la situación real o representaciones exactas de un modelo irreal, es decir en todos los casos son aproximaciones.

El desarrollo de un accidente de fusión del núcleo del reactor puede subdividirse en los períodos siguientes:

- disparo del accidente,
- calentamiento y fusión total del núcleo del reactor, explosión de vapor y evaporación del agua residual,

- penetración de material líquido en la vasija de presión del reactor y liberación de productos de fisión arrastrados en aire o vapor (aerosoles),
- penetración de material líquido del núcleo del reactor en el hormigón.

Sobre
1.2 el disparo del accidente se hace la hipótesis pesimista que en un reactor de agua a presión con 4 circuitos primarios una de las tuberías de vapor se rompa y que sus dos extremidades estén completamente desacopladas hidrodinámicamente. El circuito primario de refrigeración (presión de agua 160 bar) se descarga de repente. Una onda de descargas de presión será inyectada en la vasija de presión. A este fenómeno de descarga de presión los expertos lo llaman "Blowdown" (laminado). Después de aproximadamente 6 segundos, la mitad del fluido primario ya se ha escapado. La presión ha igualmente disminuido hasta aproximadamente la mitad. El vapor que entra en la vasija de contención como un chorro hace aumentar la presión allí; pero no proporcionalmente a la masa de vapor, porque una gran parte del vapor se condensa en las paredes y estructuras de la vasija de contención y sale en forma de agua al sumidero del edificio del reactor. Después de medio segundo aproximadamente, debido a la caída de la presión del circuito primario se dispara la parada de emergencia. El blowdown está terminado después de 17 segundos aproximadamente.

En la vasija de contención existe entonces la presión máxima (aprox. 4,5 bar para 130 ^{o}C). A continuación disminuirá otra vez. Durante este tiempo dos elementos combustibles del reactor son refrigerados por la mezcla gotas de agua/vapor del agua primaria que sale. Pero esta refrigeración no basta para evacuar completamente el calor residual de los elementos combustibles. Por consiguiente las vainas se calien-

tan (de inicialmente ∿600 K a ∿1100 K después de 17 segundos). Al final del blowdown varios (p.ej. 8) de los llamados acumuladores comienzan inyectar agua boricada (en total 250 m^3) en los circuitos primarios (4). Este fluido está mezclado con boro, porque los núcleos atómicos de este elemento absorben particularmente bien los neutrones. De este modo se evita que en el combustible puedan fisionarse otros núcleos. El agua de los acumuladores no basta todavía para mojar de modo permanente el núcleo de reactor con agua. La evacuación del calor residual sigue haciendose por vapor y cada vez más también por radiación térmica. Las vainas de la agujas de combustible más calientes se ponen al rojo blanco (∿1300 K) y están en el interior bajo una presión de helio (aprox. 100 bar), que viene todavía aumentada por la presión de los productos de fisión gaseiformes en el entrehierro entre las pastillas de combustible y la vaina. Durante el funcionamiento normal de reactor, a la presión interior de la vaina se opone la presión cuasi doble del sistema del circuito primario. Pero después del blowdown la presión interior carga el material de vaina que además se hace más deformable con el aumento de la temperatura. La consecuencia es que después de 1,5 minutos las vainas más calientes (∿1000 entre 46.000 en total) se hinchan y revientan (ver fig. 5). Una parte de los productos de fisión gaseiformes bajo estas condiciones de estado en el entrehierro entre el combustible y la vaina de estas agujas penetra al fluido de vapor en el circuito primario y con esto al recipiente de seguridad.

Entretanto los acumuladores son vaciados, y el agua condensada (∿1300 m^3) se ha acumulado en el "sumidero del edificio". Cuando fallen los sistemas de refrigeración de urgencia por los cuales en un "circuito cerrado "se bombea agua del sumidero hasta el núcleo del reactor, comienza

1.3 el calentamiento y la fusión del núcleo del reactor, la explosión de vapor y la evaporación del agua residual

El accidente de fusión del núcleo del reactor resulta entonces

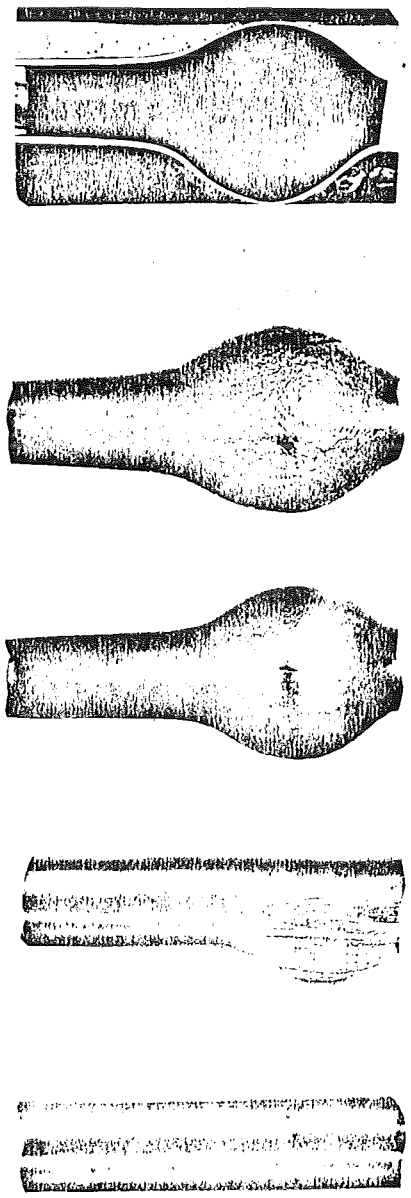

fig. 5: "Ballooning" de agujas combustibles

como consecuencia de la hipótesis poco probable que todo el sistema de refrigeración de un reactor de agua ligera falle al mismo tiempo. De este modo se calientan las agujas de combustible o partes de agujas insuficientemente refrigeradas, debido al calor residual, a lo cual hay que añadir todavía el calor de reacción exotérmico (con $\gtrsim$ 1700 K) procedente de la oxidación de vapor de agua de las vainas de Zircaloy.

Por esta adición de calor las partes de agujas de combustible que ya no están mojadas por agua se calientan hasta la temperatura de fusión del Zircaloy (aprox. 1900 ^{o}C) (después de $\sim$ 5 minutos). Sigue la fusión de las agujas de combustible (fig. 6) - y durante el calentamiento hasta la rotura de toda la estructura del núcleo del reactor - la formación de una masa del núcleo en fusión en la calota del fondo de la vasija de presión del reactor. Entonces se evapora toda el agua residual, la vasija de presión del reactor está (después de aprox. 1,5 horas) "resecada". Se tiene que mencionar aquí que la introducción de material en fundición en el agua residual por debajo de la estructura de soporte del núcleo puede dar lugar a la formación de una o varias llamadas "explosiones de vapor". Por explosión de vapor se entiende un intercambio de calor rápido y ligado con una liberación de energía mecánica. Podría originar una onda de choque de presión y producir más fragmentos del núcleo en el ambiente inmediato de la mezcla agua/material fundido del núcleo, que hacen que la vasija de presión y la vasija de contención del reactor sean prematuramente destruidos (1,5 horas después del principio del accidente).

La aparición de una explosión de vapor es bastante probable.

Una gran cantidad de materiales fundidos del núcleo entrará primero al agua residual de la calota inferior de la vasija de presión del reactor. Entonces el material fundido del

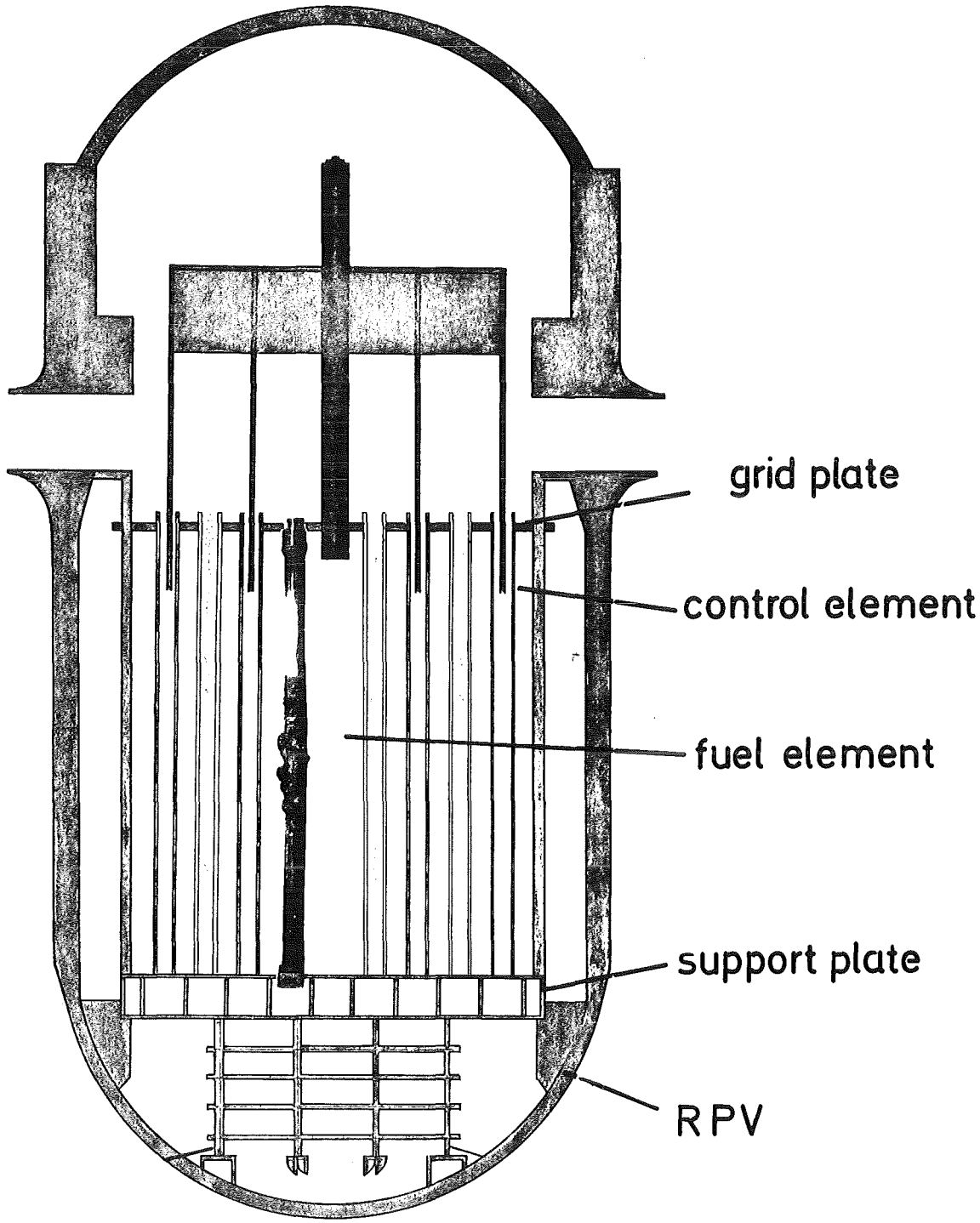

fig. 6: Fusión local de agujas combustibles

núcleo en parte se fragmentará groseramente en agua, de modo que los fragmentos, sin formar una piel solidificada, se rodeen de una película hirviente estable. Cualquier impulsión de presión local que puede aparecer por ejemplo cuando el material fundido incluye agua en la zona de la pared de la vasija de modo que ésta se evapora de repente, tiene que garantizar entonces que las películas de vapor de los fragmentos groseros de material fundido se rompan en la región suficientemente extendida, por lo que los fragmentos groseros vienen fragmentados a gotas de material fundido considerablemente más pequeñas. Estos fragmentos finos tienen que mezclarse inmediatamente con el agua ambiente. Estas son las condiciones de una explosión de vapor. Debido a la superficie considerablemente aumentada del material fundido, se produce una transmisión muy rápida de calor desde el material fundido finamente fragmentado al agua. El gran flujo térmico al agua ambiente origina la evaporación repentina y presiones extremamente elevadas localmente, que producen una onda de choques que se propaga y que por su parte origina otra fragmentación fina y otra producción de vapor. Finalmente las presiones interiores que aparecen durante la evaporación extremadamente rápida originan una aceleración del agua ambiente y también de materiales sólidos desde la vasija de presión del reactor hacia el exterior.

Con la hipótesis arbitraria que todo el núcleo del reactor fundido en el agua sobrante de la vasija de presión del reactor participe al mismo tiempo en una explosión de vapor (aprox. 170 t) se ha calculado que, a lo sumo, durante un accidente de fusión de núcleo entre 10.000, la vasija de contención podría destruirse por una explosión de vapor. En cambio, estudios experimentales y teóricos permiten decir que se fragmenta simultaneamente solamente una cantidad de material fundido (20 t) con la cual las transformaciones

de energía que aparecen no bastan para destruir la vasija de presión ni para poner en peligro la vasija de contención.

Después del calentamiento y de la fusión del núcleo del reactor, la explosión de vapor y la evaporación del agua sobrante,

1.4 el material fundido del núcleo del reactor se encuentra en la vasija de presión del reactor - liberación de productos de fisión

El calor residual producido en la masa del material fundido se evacua por conducción en la parte mojada de la vasija de presión del reactor. La parte no mojada se calienta por radiación térmica a partir de la superficie del material fundido. El transporte de masa y de energía en el material fundido desde su centro hacia las zonas marginales más frías se hace por convección natural. Se forman las llamadas "celdas de rodadura" (fig. 7). El calentamiento de la pared de la vasija de presión del reactor que está en contacto directo con el material fundido, así como el calentamiento de las estructuras no mojadas puede calcularse a través de la conducción del calor por convección y radiación térmica. En la masa fundida se alcanzan las temperaturas más elevadas durante todo el desarrollo del accidente de fusión del núcleo (aprox. 2700 K). Esto tiene como consecuencia que también aquí se produce la liberación máxima de productos de fisión. Por ello es razonable y comprensible que los estudios experimentales de la liberación de productos de fisión se han referido en primer lugar a este período del accidente de fusión del núcleo del reactor. Inexactitudes en la estimación debidas a la liberación en los períodos precedentes implican a lo sumo un desplazamiento de los lapsos de tiempo (de $\sim$ 2 h), lo que no tiene ninguna importancia para las consecuencias radiológicas de un accidente de fusión del núcleo.

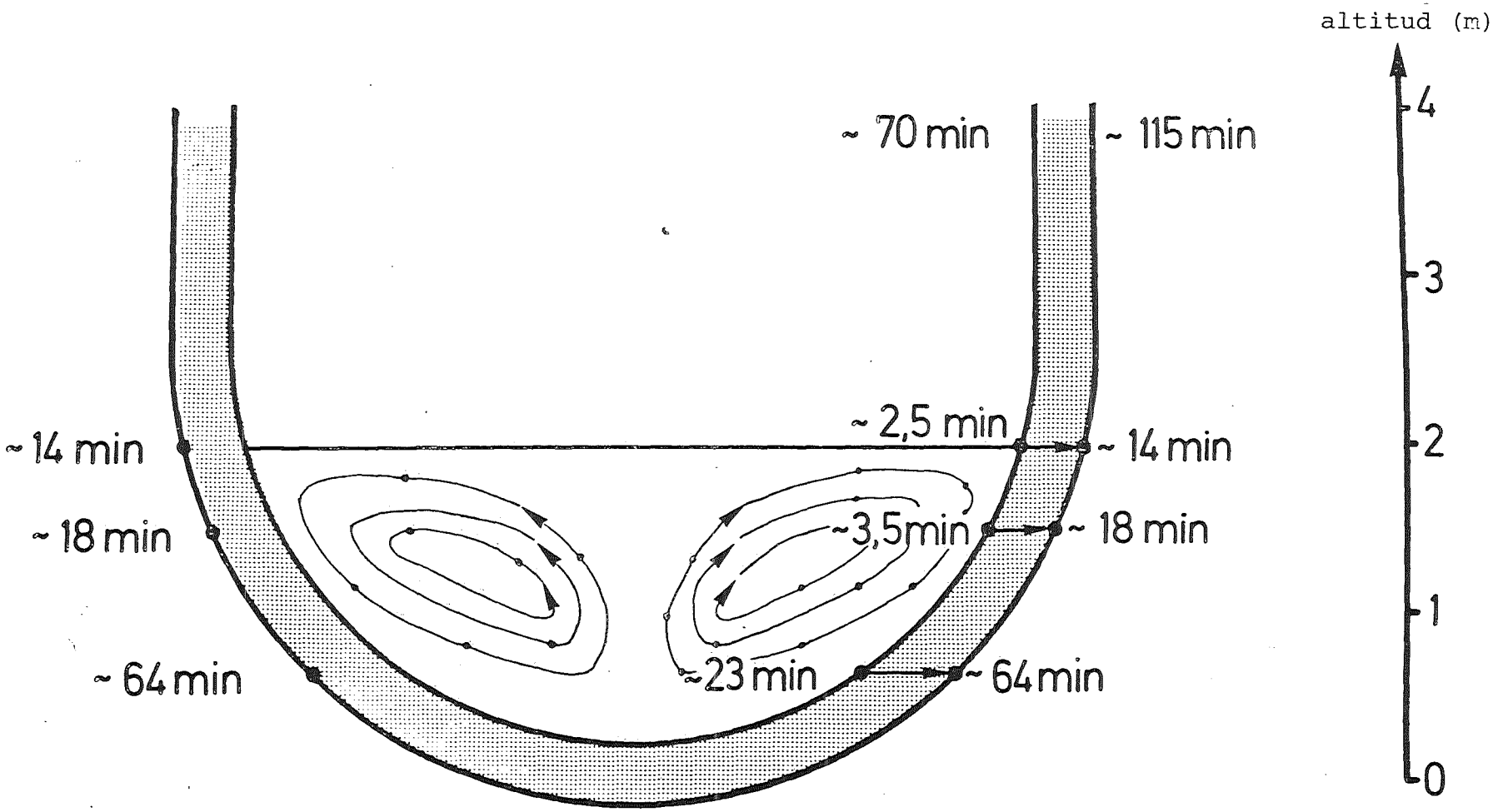

fig. 7: Convección en materiales fundidos del núcleo del reactor

Los productos de fisión y de desintegración radiactivos liberables a partir de un reactor de agua a presión (tiempo de funcionamiento 3 años; grado de quemado 37 GWd/t) representan solamente una pequeña parte (0,2% en peso) del inventario de una vasija de agua a presión. Pero cuando se toman en cuenta los componentes no radiactivos liberables del material fundido del núcleo, resulta integralmente una masa de partículas aproximadamente dos veces más grande, que penetra en forma de aerosoles (partículas arrastradas por vapor/aire) a la vasija de contención dentro de un período de apenas una hora. La mayor porción de masa (∿1,6 t) viene de las barras de regulación y control (Cd, In, Ag). Se compone casi totalmente de plata metálica. Siguen los constituyentes de acero liberados en forma de partículas (745 kg) que existen sobre todo en forma de óxidos, y el óxido de uranio (490 kg). La porción más grande en masa de las que siguen procede de los productos inactivos de fisión y de desintegración (aprox. 160 kg). Desde el material de vainas se libera un poco de estaño, pero sobre todo circonio en forma de óxido (80 kg). Entre los componentes radiactivos liberados en forma de partículas a partir del combustible (∿100 kg) la mayor parte es cesio-137.

Los gases de fisión, sobre todo xenon y krypton, se liberan completamente a partir del núcleo del reactor, como el yodo (18 kg). Bajo las condiciones arriba mencionadas el inventario de yodo es de 18 kg al principio del accidente. También esta masa se libera con un 100%. Es importante mencionar que solamente aproximadamente 800 g de esta masa forman parte del isótopo de yodo-131, que es el único isótopo de yodo que proporciona una contribución notable a los efectos radiológicos durante un accidente de fusión del núcleo.

Debido a los gradientes de temperatura que existen alrededor del material fundido del núcleo, la liberación no se hace en el órden de tiempo: Primero los productos de fisión facil-

mente volátiles y al final los difícilmente volátiles. Sinó el sistema de aerosoles liberados está bastante homogeneizado debido a procesos de coagulación y condensación.

Bajo las condiciones mencionadas, la liberación de masas de aerosoles activos e inactivos en forma de partículas puede determinarse de antemano con bastante exactitud. Asimismo puede estimarse que la vasija de presión del reactor falla 1,7 horas después del principio del accidente, 14 minutos después de la formación del material fundido, justamente por debajo de la superficie del baño líquido (ver fig. 7). Ahora comienza el último período del accidente,

1.5 la fusión del núcleo en el hormigón

Después de la falla de la vasija de presión del reactor, la masa fundida (∿50 t metal + ∿120 t de óxido compuesto de 102 t ≙ 60% en peso de combustible UO_2, 31 t ≙ 18% en peso de estructuras de acero, 32 t ≙ 19% en peso de vainas de Zircaloy, 2 t ≙ 1% en peso de barras de regulación y control, 3% ≙ 2% en peso de productos de fisión alcanza la fundación de hormigón del edificio de reactor (caverna con 6 m de diámetro; espesor de la fundación: 5 hasta 7 m, fig. 8). Después del fraguado y secado, el hormigón del reactor se compone de áridos (18% en peso, en la mayoría grava silícea con carbonato de calcio, agua libre en los poros del hormigón (∿4% en peso) y cemento (16% en peso, en la mayoría hidróxido de calcio). Es evidente que el hormigón fraguado a la temperatura ambiente se descompone térmicamente a temperaturas elevadas y que en la descomposición del hormigón se produce una formación considerable de vapor de agua (∿200 kg de agua por 1 m^3 de hormigón).

Cuando el material fundido del núcleo ha salido a la caverna de hormigón, la parte metálica de la masa fundida está abajo, y arriba se encuentra la parte de óxido que se compone sobre

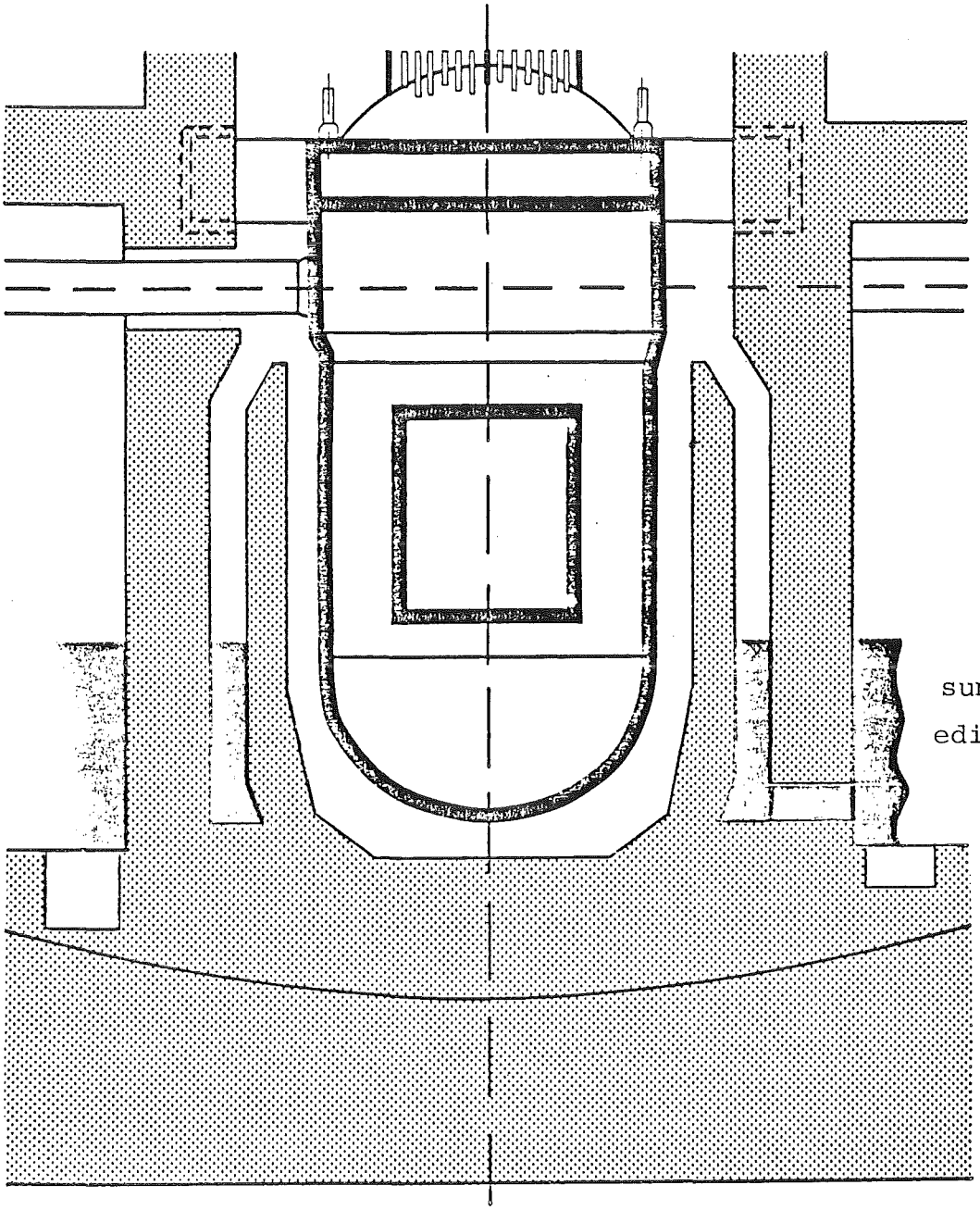

fig. 8: Cimiento de hormigón de un reactor de agua a presión

todo de óxido de uranio, circonio y cromo. La parte licuada de hormigón tiene un compartamiento semejante al de una masa líquida de cuarzo, porque se compone sobre todo de SiO_2. Los componentes fundidos del hormigón se mezclan con la fase de óxido de la masa fundida. De este modo, los productos de fisión que producen el calor residual vienen contínuamente diluidos, comparados con la masa fundida de óxido total. Debido al flujo térmico considerable que se evacúa desde la masa fundida hasta el hormigón, y porque al mismo tiempo se tiene que calentar el hormigón fundido hasta la temperatura del baño de masa fundida, la temperatura del material fundido del núçleo baja rapidamente. Por ello la temperatura de fundición el hormigón se disminuye dramáticamente. Al mismo tiempo los vapores de agua liberados durante la destrucción del hormigón atraviesan el baño de masa líquida en bandadas de burbujas de modo que aproximadamente la mitad del volumen del baño de masa líquida está gaseiforme. Como los áridos del hormigón contienen también carbonato de calcio, se libera además dióxido de carbono que pasa también por el baño de líquido en forma de gases. El vapor de agua pasa primero en forma de perlas por la masa líquida metálica inferior y la oxida. Las partes metálicas oxidadas se mezclan con la masa fundida de óxidos. En la reducción del vapor de agua sobra hidrógeno que pasa por la masa fundida de óxidos y que se libera en la vasija de contención. Entre el hidrógeno y el óxido de carbono puede producirse la llamada reacción agua/gas, lo que origina además la liberación de monóxido de carbono en la vasija de contención.

Hasta ahora no está exclarecido completamente si se puede excluir la posibilidad que la vasija de contención sea destruida por una detonación de hidrógeno.

La fig. 9 muestra el diagrama del sistema ternario de mezclas de aire - vapor de agua - hidrógeno. Para cada composición de mezcla dentro de la zona de encendido existe la posibilidad

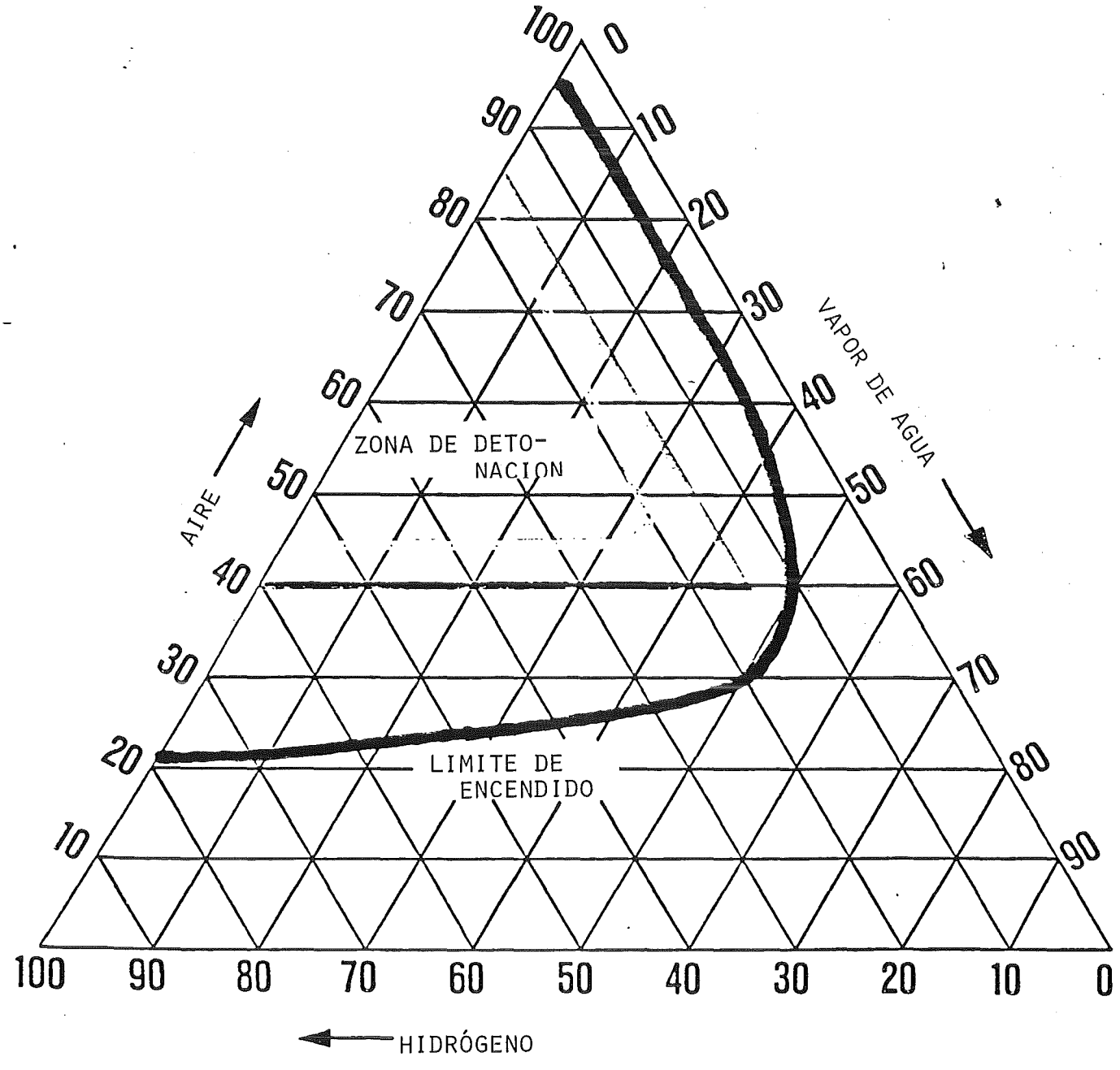

FIG. 9: DIAGRAMA DEL SISTEMA TERNARIO HIDRÓGENO-AIRE-VAPOR DE AGUA (% VOL.)

de una combustión explosiva y se produce la detonación. Tal detonación de H_2 en la vasija de contención. tiene bastante potencial para destruirla. Por otra parte, una combustión de H_2 iniciada a propósito ofrece la posibilidad de evitar la detonación. - Volvamos a la fusión del núcleo del reactor: Como en la fundación del reactor existen también capas espesas de armadura de acero, la masa fundida metálica viene reemplazada progresivamente por la armadura que funde.

El contorno siempre más grande de la caverna fundida de hormigón, la masa de baño de material fundido siempre más grande, su temperatura siempre más baja y el fluido de gas que disminuye contînuamente, originarán pronto los primeros fenómenos de solidificación en la masa fundida metálica y de óxido. Se libera entonces calor de solidificación, y la transmisión térmica al hormigón se disminuye debido a la formación de costras. Pero la disminución de la transmisión térmica al hormigón significa que el sistema se calienta de nuevo, debido al calor residual. Este cambio entre el enfriamiento y el calentamiento, es decir la solidificación y la fundición, se termina finalmente, cuando la fundación tiene el diseño correspondiente, por la "recuperación" ("core catching") del material fundido por solidificación completa, lo que puede tardar algunos meses - con hipótesis desfavorables aún años. En la fig. 14 hemos introducido la disminución de la temperatura efectiva de la masa fundida debido a la "dilución del hormigón" segun cálculos efectuados en 1a aproximación.

Con esto está parado el accidente de fusión del núcleo del reactor "hacia abajo". - En cambio, su control "hacia arriba" permanece sin solución hasta ahora. Afecta el aumento de la presión en la vasija de presión debido a los gases liberados y los vapores durante la interacción de la masa fundida con el hormigón hasta que la vasija de contención

de un reactor de agua a presión falle (∿9 bar). En este caso no podemos imaginarnos que la esfera de acero (ver fig. 1; diámetro 50 m; espesor de pared 4 cm) revienta como un globo, sinó se tiene que suponer que las juntas o soldaduras fallan progresivamente de modo que salgan justamente tantos vapores y gases a partir de la vasija de contención cuantos se producen por la destrucción del hormigón. Las primeras aproximaciones consideran que este fallo por sobrepresión comienza con 6 bar 2-5 dias después del principio del accidente. Durante este tiempo el sistema de aerosoles en la vasija de contención está sometido a fuertes mecanismos de separación. Las estimaciones de ingeniería indican que la masa de aerosoles liberada inicialmente está reducida después de 5 dias de 6 órdenes de magnitud, donde el yodo se separa en forma de yoduro de plata. Este "escenario" corresponde al estado actual de las consecuencias del accidente "hacia arriba".

En todos los períodos del accidente de fusión del núcleo del reactor intervienen problemas de material a través de dos grupos de problemas:

- la estructura material del sistema en el período estudiado del accidente,
- las propiedades de los componentes o respectivamente fases del sistema en el período considerado del accidente.

Cuales son las interacciones que tienen lugar entre los componentes del núcleo del reactor y cuales son las sustancias que se forman? Cual es la fase de la masa fundida polifásica que tiene la menor densidad y "nada" sobre la otra? Cual es la influencia del hormigón que con su fusión entra en la fase de óxido, sobre las temperaturas de fusión? Y cuales son las capacidades caloríficas, viscosidades o conductividades térmicas de las fases líquidas? Aquí la estructura material por una parte y las propiedades por otra están

estrechamente ligadas, porque cada cambio de la estructura material, según las condiciones de estado existentes, tiene como consecuencia un cambio correspondiente de las propiedades. - El estudio de estos problemas de material ha sido realizado con experiencias en escala de laboratorio bajo condiciones de accidente simuladas y mediante estimaciones teóricas y extrapolación a partir de los campos accesibles para la experiencia.

2. La estructura de los materiales durante el accidente de fusión del núcleo

Como la fusión del núcleo del reactor en el sentido propio no tiene lugar durante el primer período del accidente, estos problemas de material se tratan dentro del margen de la refrigeración de emergencia. En cambio en el segundo período del accidente (con aprox. 2100 K) comienza el proceso de fusión en la aguja combustible (ver fig. 6). En atmósfera oxidante o parcialmente oxidante la superficie exterior de las vainas de agujas combustibles de Zry-4 se oxida, en la superficie interior de la vaina de Zry-4 se produce una reacción con el combustible UO_2, que viene reducido parcialmente. El Zircaloy absorbe oxígeno y se funde.

La estructura material del sistema en el tercer período del accidente que ahora comienza está determinada por la formación de una masa en fusión del núcleo del reactor

- por interacción entre los componentes del núcleo y
- por interacción de los componentes del núcleo con la atmósfera de accidente.

La composición material de esta masa en fusión del núcleo puede variar (entre "A" y "E"), según los componentes del núcleo (UO_2, Zry, acero, Inconel, productos de fisión; se han despreciado los componentes de barras de control) que funden bajo tal atmósfera (vapor de agua, hidrógeno, oxígeno,

aire; no oxidante hasta completamente oxidante) (ver fig. 10). La fig. 11 muestra una de estas composiciones iniciales posibles sin tener cuenta de los productos de fisión. Su distribución y concentración determina la densidad del fuente de calor en las fases de fusión del núcleo y con esto el calor residual que por su parte determina el momento de la solidificación de la masa fundida - junto con el punto de fusión de las fases. - Conforme a las cantidades distintas de materiales de estructura fundidos bajo atmósfera no oxidante, parcialmente o completamente oxidante, pueden definirse seis casos límites de la composición material (ver fig. 10). Los materiales fundidos del núcleo formados según la composición inicial (corio A, E) y la atmósfera de accidente (no oxidante = corio AX1, EX1; parcialmente oxidante = corio AX2, EX2; completamente oxidante = corio AX3, EX3) son monofásicos oxídicos únicamente en el estado completamente oxidado (corio AX3, EX3), mientras que en los otros casos se componen de una fase fundida metálica y una de óxido (ver fig. 10).

Como ya lo predicen las entalpías libres de formación en la fig. 12 y lo confirman las experiencias, la fase fundida de óxido se compone inicialmente sobre todo de $(U, Zr)O_2$, donde entran por fusión componentes de acero siempre más oxidados (Cr_2O_3, FeO, NiO). En cambio la fase fundida metálica tiene una composición semejante a la del acero.

El carácter bifásico de las masas fundidas de corio tiene como consecuencia una distribución inhomogénea de los productos de fisión. Las tierras raras facilmente oxidables (ver fig. 12) se disolverán inmediatamente en la fase líquida de óxido, mientras que los productos de fisión Mo y Tc siguen solamente con el aumento del grado de oxidación - a semejanza de los componentes de acero. En cambio los productos de fisión con carácter de metal precioso (Ru, Pd, Rh) permanecen en la fase metálica, mientras que los productos de fisión con presión de vapor elevada, como los metales alcalinos y el yodo y

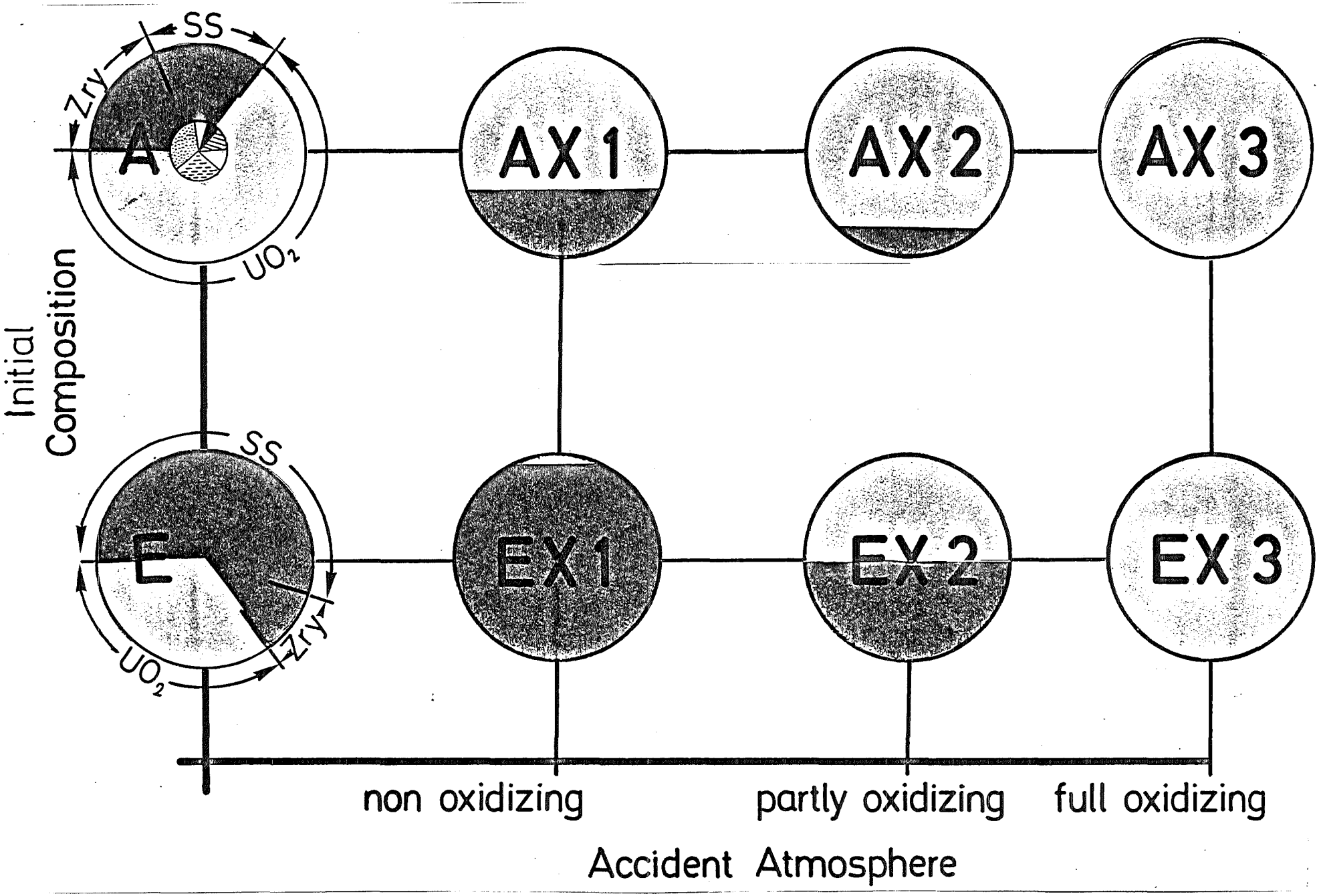

fig. 10: Casos límites de la composición de materiales de núcleo fundidos

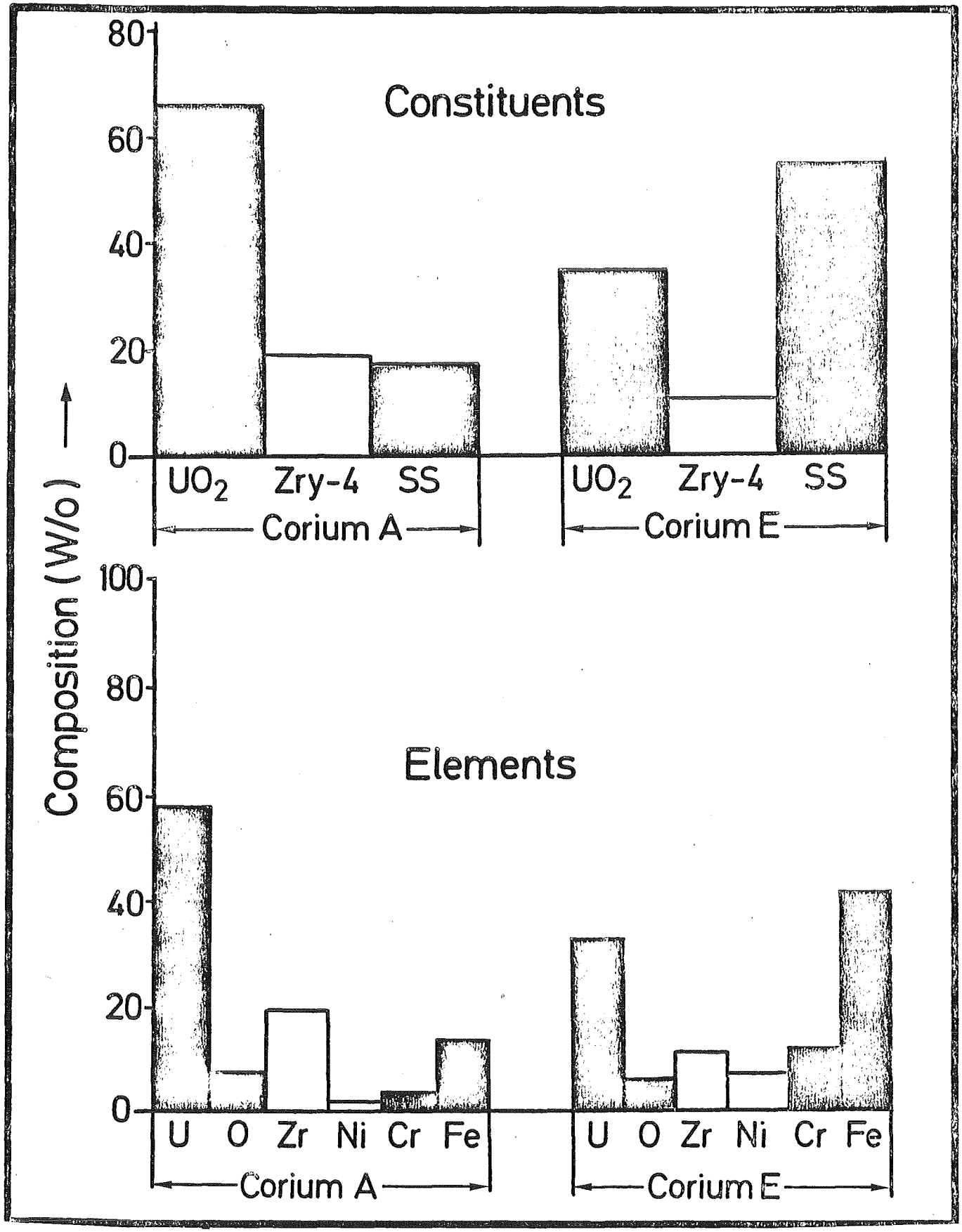

fig. 11: Composiciones iniciales del corio

telurio, se han probablemente volatilizado completamente antes que la fase líquida se haya formada.

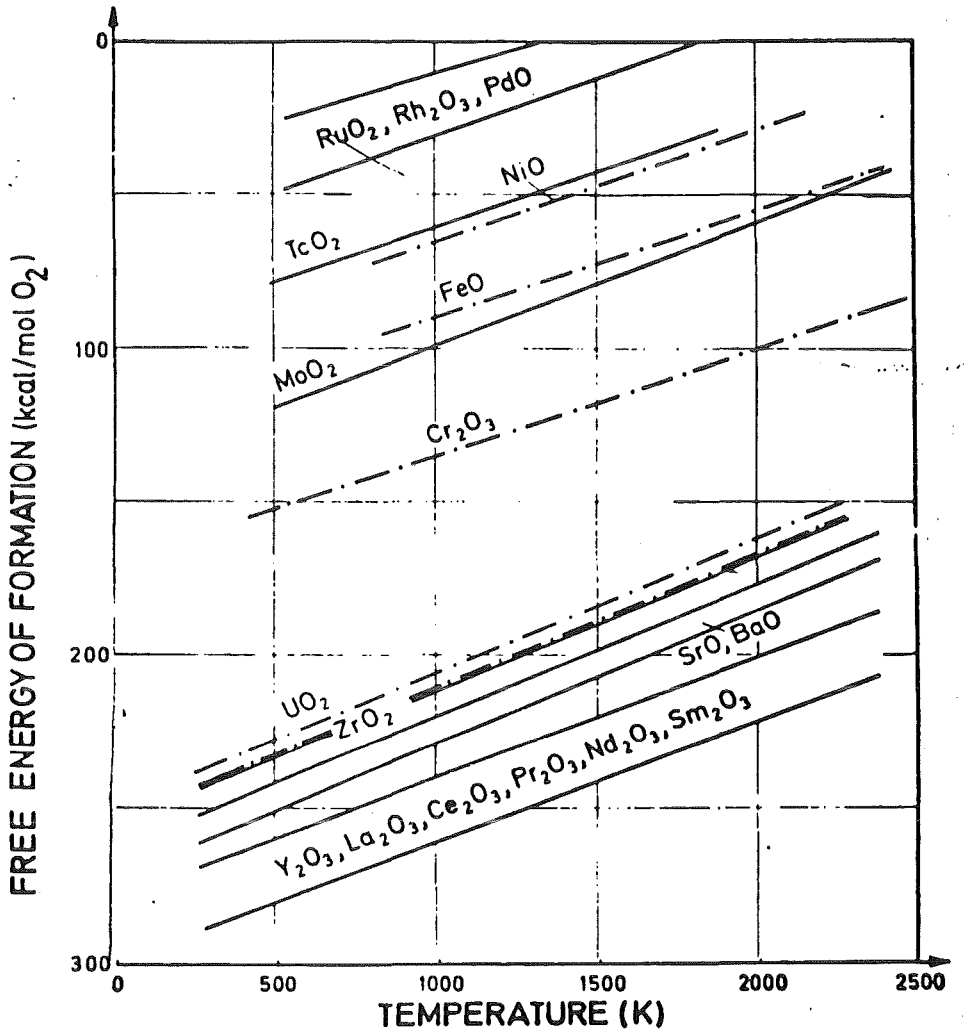

fig. 12: Entalpías libres de formación de los óxidos de los componentes del núcleo y de los productos de fisión

En las experiencias en que se basan estos resultados se han podido simular varios productos de fisión por elementos químicamente muy parecidos. Ce y Nd representan las otras tierras raras trivalentes, el estroncio representa también bario, molibdeno representa tecnecio. El rutenio substituye todos los metales preciosos, y solamente el zirconio se representa solamente por si mismo. Como lo hemos ya mencionado,

las concentraciones de productos de fisión se han introducido conforme a un grado de quemado triple (10%), para hacer resaltar más claramente su efecto.

Según los cálculos efectuados hasta ahora con códigos, hay que contar con un fallo de la vasija de presión del reactor poco después de la formación de la fase fundida del núcleo (ver fig. 7). Al principio de este cuarto período del accidente - material fundido del núcleo en el hormigón - la composición material de este cambia - se llama ahora corio (A+R)... y corio (E+R).... - como consecuencia de la fundición suplementaria del acero de la vasija de presión. Se tiene que suponer que un material fundido bifásico del núcleo entra ahora en interacción con el hormigón siliceo. Según los resultados experimentales obtenidos hasta ahora

- el hormigón cede su agua en tres campos de temperatura (fig. 13)
- el hormigón se funde en el campo de temperatura indicado en la fig. 13 por la curva DTA
- el hormigón se mezcla completamente con la fase fundida de corio oxídica

y forma una nueva fase fundida oxídica, cuyas temperaturas de líquidus y solídus calculadas aproximadamente están indicadas en la fig. 14 en función de la concentración de la fase de corio oxídica o respectivamente del componente de hormigón, junto con valores experimentales.

Para el cálculo se tomarían en cuenta como estados iniciales imaginables del material fundido del núcleo en el hormigón, los estados bajo atmósfera parcialmente o completamente oxidante después de la fusión completa de todas las estructuras interiores del núcleo (corio EX2, corio EX3). La zona de solidificación de la fase de óxido, en interacción con el

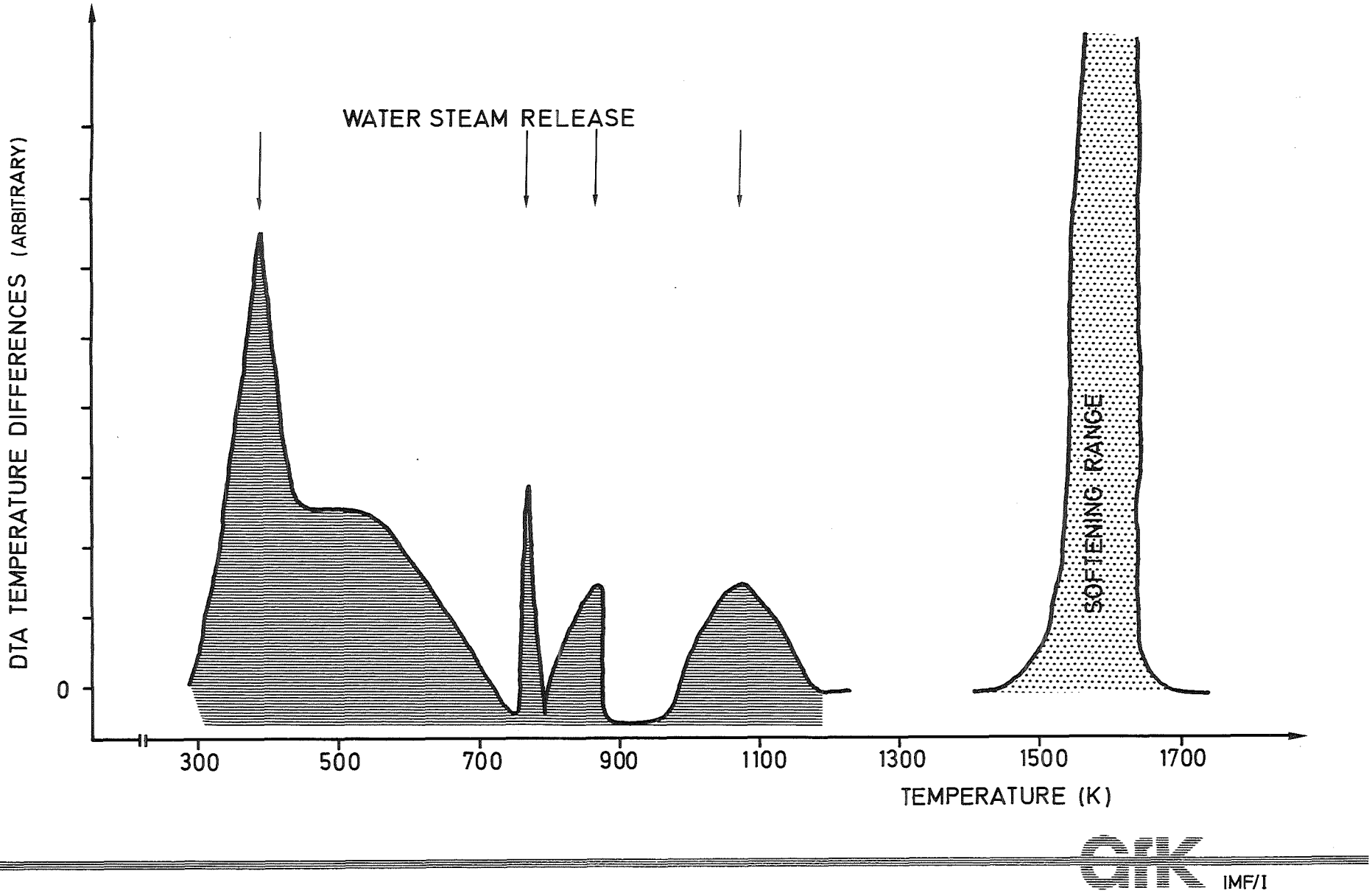

fig. 13: Campos de temperatura de la cesión de agua y de la fundición de hormigón de silicato

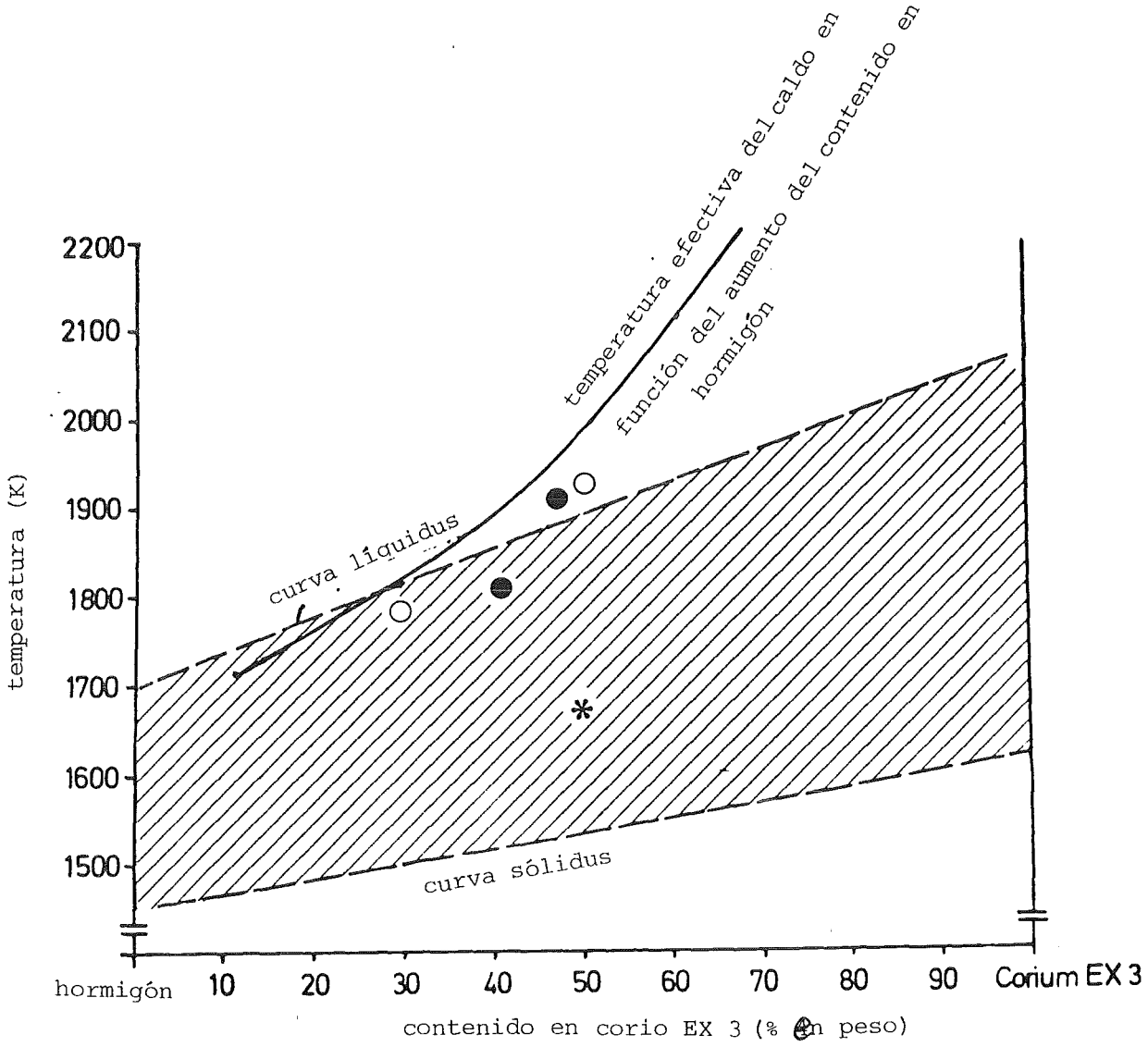

fig. 14: Campo de fusión estimado para caldos de hormigón-corio EX3 con valores de medida de probetas simuladas (o●+)

hormigón, del material fundido de corio EX2 es más alta que la del material fundido de corio EX3. Por ello la dilución del fuente de calor y el aumento de la temperatura de sólidus que intervienen como consecuencia de la interacción arriba descrita con el hormigón originarían para caldos de hormigón-corio EX2 en comparación con caldos de hormigón-

corio EX3 una solidificación más temprana, lo que vale probablemente también para la comparación con los caldos de hormigón-corio AX. Por consiguiente los caldos de hormigón-corio EX2 y respectivamente AX están quizás los casos reales, pero optimistas. Las consideraciones siguientes se harán de modo conservador y por esto se refieren al caso pesimista de caldos de hormigón-corio EX3.

Para estimar el campo de solidificación de caldos de hormigón-corio EX3 se considera en primera aproximación que

- los componentes hormigón y corio EX3 son completamente solubles en ellos,
- forman una solución ideal en el caldo y
- se puede despreciar la dependencia de la temperatura del calor de fusión de los componentes entre sus puntos de fusión.

Bajo estas condiciones las curvas de líquidus y sólidus siguen en primera aproximación según las relaciones de Schröder-van Laar:

$$C_{corio}(liqu.) = \frac{e^{n}-1}{e^{n}-e^{-m}} \qquad (1)$$

$$C_{corio}(sol.) = \frac{e^{n}-1}{e^{n+m}-1} \qquad (2)$$

$$n = \frac{\Delta H_{S\ hormigón}}{R}\left(\frac{1}{T} - \frac{1}{T_{S\ hormigón}}\right) \qquad (3)$$

$$m = \frac{\Delta H_{S\ corio}}{R}\left(\frac{1}{T_{S\ corio}} - \frac{1}{T}\right) \qquad (4)$$

[C = concentración de corio en porcentajes molares; ΔH_S = calor de fusión; R = 8.314 J/mol K; T_S = temperatura de fusión; T = temperatura]

Como el hormigón y el corio EX3 no tienen puntos de fusión, sinó campos de fusión, la curva de líquidus se calcula con las temperaturas de líquidus, y la curva de sólidus se calcula con las temperaturas de sólidus. Para ello, debido a la estimación conservadora buscada, se utilizan para el cálculo las máximas temperaturas conocidas de líquidus y las mínimas conocidas de sólidus. Estas hipótesis proporcionan temperaturas de solidificación mínimas y la máxima extensión del campo de fundición bifásico.

La composición material de los componentes da

- para el hormigón siliceo con cemento de Portland la "fórmula molecular"

$$Fe_{0,018}\ Ca_{0,08}\ Si_{0,84}\ Na_{0,05}\ K_{0,02}\ Al_{0,09}\ O_2$$

con el "peso molecular" medio de 48 g/mol y

- para corio EX3

$$U_{0,166}\ Zr_{0,139}\ Fe_{0,886}\ Cr_{0,252}\ Ni_{0,126}\ O_{2,443}$$

con el "peso molecular" medio de 168,6 g/mol.

Las máximas temperaturas de líquidus conocidas hasta ahora de los componentes extán

- para hormigón $\sim$ 1700 K y
- para corio EX3 según las últimas medidas de $\sim$ 2075 K

mientras que las temperaturas mínimas conocidas hasta ahora de sólidus son

- para hormigón $\sim$ 1450 K y
- para corio EX3 $\sim$ 1620 K.

Como calor de fusión para el hormigón se ha determinado

$$\Delta H_{S\ \text{hormigón}} = 210{,}6\ \text{J/g} \triangleq 10{,}1\ \text{KJ/mol}.$$

Se ha tenido que estimar el calor de fusión del corio EX3. Según análisis radiográficos el corio EX3 en el estado sólido se compone de por lo menos dos fases con red cristalina cúbica-hexaquisoctaédrica, es decir $(U_xZr_{1-x})O_2$ (tipo CaF_2) y Fe_3O_4 (tipo espinela). Para compuestos cristalizantes cúbicos-hexaquisoctaédricos del tipo NaCl y CaF_2 las entropías de fusión - análogamente a la regla de Richards para metales - están aproximadamente constantes y semejantes (ver fig. 15). El valor medio de la entropía de fusión para materiales cúbicos cristalizantes del tipo CaF_2, NaCl y espinela es por consiguiente

$$\Delta S_S \sim 21\ \text{J/mol K}.$$

A partir de

$$\Delta H_S = T_S \cdot \Delta S_S \qquad (5)$$

se tiene con los calores de fusión para T_S = 1620 K (temperatura de sólidus) y para T_S = 2075 K (temperatura de líquidus) un calor de fusión médio para el corio EX3 de

$$\Delta H_{S\ \text{corio EX3}} \sim 38{,}8\ \text{KJ/mol}.$$

Con esto conocemos todos los datos para la estimación por cálculo de las curvas de líquidus y sólidus para caldos de hormigón-corio EX3 según las ecuaciones 1-4. Se han programado las ecuaciones y se han calculado los programas con los datos siguientes:

- Estimación de la curva de líquidus (Ec. 1, 3, 4)

$\Delta H_{S\ hormigón}$ = 10,1 KJ/mol; $\Delta H_{S\ corio}$ = 38,8 KJ/mol;

$T_{S\ hormigón} = T_{liqu.\ hormigón}$ = 1700 K;

$T_{S\ corio} = T_{liqu.\ corio}$ = 2075 K.

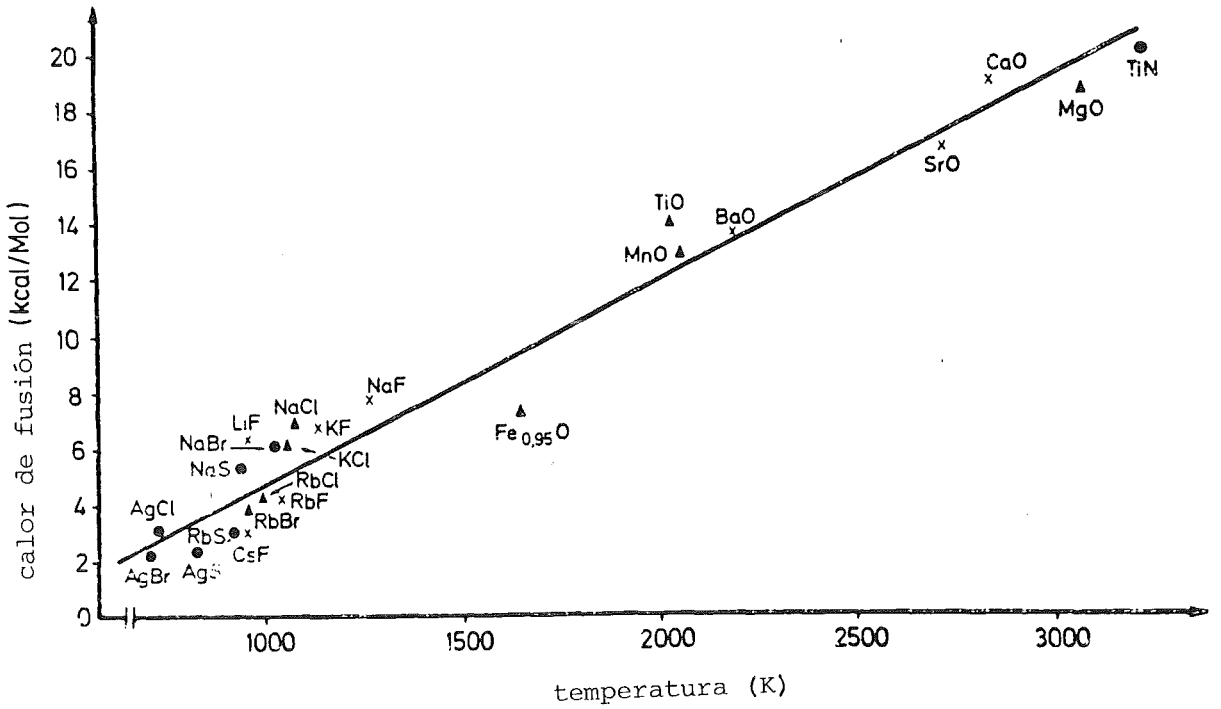

fig. 15: Regla de Richards para materiales cerámicos con red cúbica

- Estimación de la curva de sólidus (Ec. 2, 3, 4)

$\Delta H_{S\ hormigón}$ = 10,1 KJ/mol; $\Delta H_{S\ corio}$ = 38,8 KJ/mol;

$T_{S\ hormigón} = T_{sol.\ hormigón}$ = 1450 K; $T_{S\ corio} = T_{sol.\ corio}$ = 1620 K.

Para la comparación con datos de medida, las indicaciones de las concentraciones tienen que convertirse en porcentajes en peso:

$$G_{corio} = \frac{100}{1 + \frac{X_{hormigón} \cdot M_{hormigón}}{X_{corio} \cdot M_{corio}}} \qquad (6)$$

(G_{corio} = porcentaje en peso corio EX3; X = porcentaje molar; M = peso molar).

En la fig. 16 hemos representado gráficamente el resultado de esta conversión.

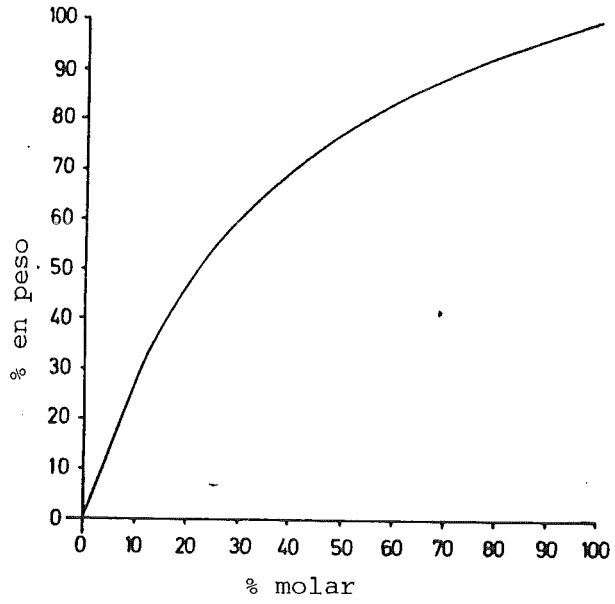

fig. 16: Conversión de porcentajes molares de corio EX 3 en caldos de hormigón-corio EX3 en porcentajes en peso de corio EX 3

temperatura de liquidus (K)	concentración de CorioEX3 (% mol)
1700	0.0
1719	1.2
1737	2.6
1756	4.1
1775	5.7
1793	7.6
1812	9.7
1831	12.0
1849	14.6
1868	17.4
1886	20.7
1905	24.4
1924	28.5
1942	33.3
1961	38.7
1980	45.1
1998	52.5
2017	61.2
2035	71.6
2054	84.3
2073	100.0

fig. 17: Representación gráfica de la conversión de porcentajes molares en porcentajes en peso del corio

temperatura de sólidus (K)	concentr. de Corio EX 3 (% mol)
1450	0.0
1458	1.7
1467	3.5
1475	5.4
1484	7.4
1492	9.6
1501	12.0
1509	14.5
1518	17.3
1526	20.3
1535	23.6
1543	27.3
1552	31.4
1560	36.1
1569	41.3
1577	47.4
1586	54.4
1594	62.7
1603	72.6
1611	84.8
1620	100.0

fig. 18: Temperaturas y concentraciones calculadas de la curva de sólidus de caldos de hormigón-corio EX3

Cuando se representan las temperaturas de líquidus y de solidus según las figuras 17 y 18 sobre las concentraciones de corio EX3 en porcentajes en peso según la fig. 16, se obtiene el campo de solidificación - rayado en la fig. 14 - para caldos de hormigón-corio EX3. La fig. 14 contiene también los valores de medida para los caldos ricos en hormigón, especialmente interesantes desde el punto de vista de la técnica de seguridad (> 50% en peso de hormigón), en los cuales se han simulado por una parte el componente de corio de óxido de uranio, zirconio e hierro (x), y donde por otra parte este componente se componía solamente de dióxido de uranio y zirconio (oo). Aunque estas composiciones discrepen en parte considerablemente de la del componente corio EX3, las temperaturas medidas para el principio de la fusión están dentro o inmediatamente cerca del campo de fusión calculado.

Como lo dejan esperar las determinaciones de densidad descritas más tarde, y como lo muestran las experiencias, la nueva fase fundida oxídica se coloca sobre la fase líquida metálica semejante al acero. Debido a las diferencias de mojabilidad esta colocación es más inequívoca para experiencias en crisoles de tungsteno (fig. 19) que para experiencias en crisoles de óxido de torio (ver también cap. 3, energías de superficies límites). Se supone que estos últimos reproducen de modo más realista las condiciones reales en el accidente de fusión del núcleo, porque la fase fundida oxídica moja el hormigón.

Esta estructura material en el cuarto período admite la conclusión que el proceso de destrucción del hormigón está controlado térmicamente (fusión del hormigón). La fase fundida oxídica que puede iniciar el principio de la fusión del hormigón y disolver sus componentes, lo ataca menos fuertemente que la fase metálica. Por ello, los resultados de erosión de experiencias en gran escala, donde se han colado caldos de acero en hormigón, pueden considerarse como apropiados para la simulación. Aquí siempre hay que tener en cuenta que

partimos de un hormigón de cemento hidratado, es decir que el empleo de hormigones aglomerados de otra manera (hormigón bituminoso o de resina artificial) no está tomado en consideración provisionalmente.

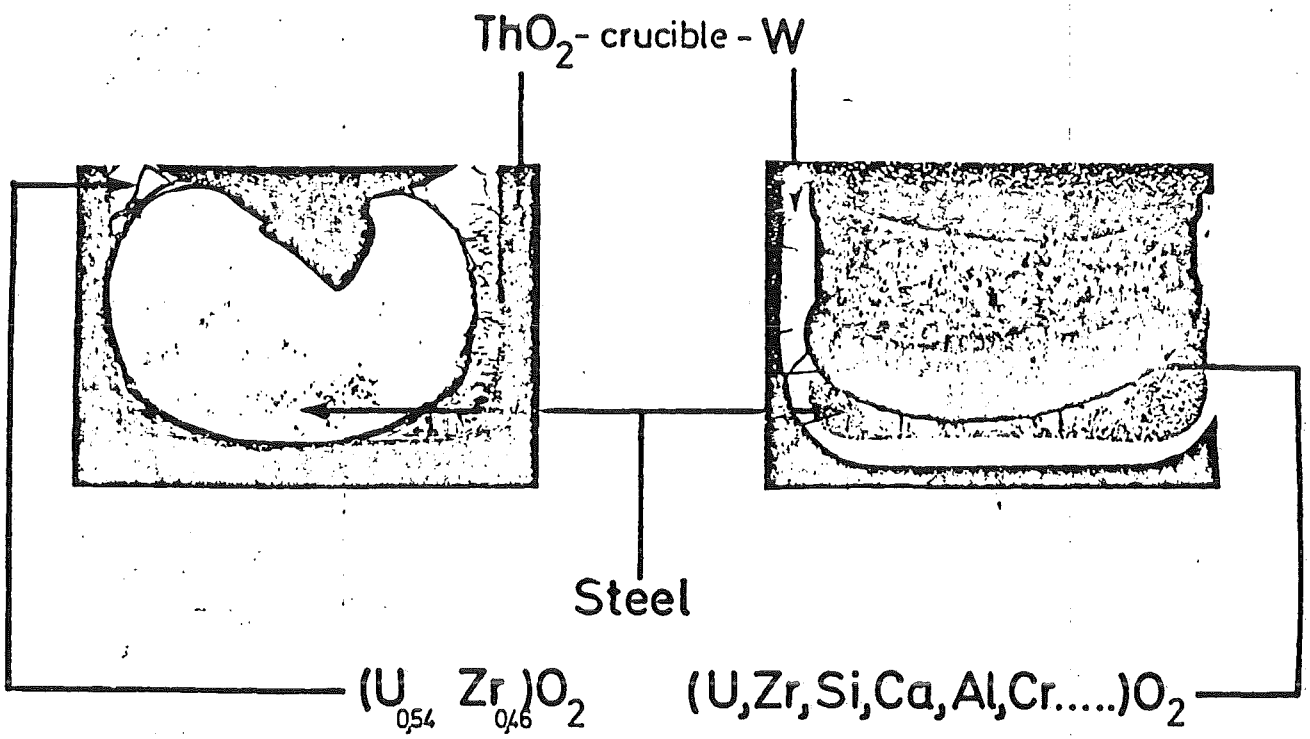

fig. 19: Disposición geométrica de la fase oxídica y metálica en

- caldos de corio (AX2+R) + hormigón en crisoles de ThO_2 (a)
- corio EX2 en el crisol de W (b)

3. Propiedades de fases fundidas y componentes del núcleo

3.1 Propiedades esenciales para el accidente

En los programas de cálculo mencionados en la primera parte para la descripción del desarrollo con el tiempo de un accidente de fusión del núcleo, el cámbio de la temperatura como variable de estado toca un papel decisivo. Determina el prin-

cipio del período de fusión así como la solidificación posible de fases fundidas del corio en la vasija de presión del reactor o del caldo de corio, corio Ax, EX+R + hormigón. La temperatura que existe en un momento determinado en un lugar determinado está determinada por los balances térmicos entre fuentes de calor (calor residual de los productos de fisión y calores de interacción exotérmicos) y los sumideros de calor (capacidades caloríficas de los componentes del núcleo y de las fases fundidas de corio, transporte térmico por radiación, conducción y convección, calores latentes como p.ej. calores de fusión y de evaporación). El conocimiento de la propiedades de los componentes y fases en los diferentes períodos del accidente, como p.ej. las energías superficiales, densidades, coeficientes de dilatación y viscosidades está por consiguiente necesario para el estudio del accidente.

Como la medición de las magnitudes bajo las condiciones de estado del accidente de fusión del núcleo es cuasi imposible, pero por lo menos dificil, costosa e imprecisa, su determinación se apoyó sobre estimaciones por cálculo y extrapolaciones gráficas que describirimos más en detalle en lo que sigue.

3.2 Energías de superficies límites de caldos metálicos de UO_2 y densidades de fases fundidas del núcleo

3.2.1 Bases

Cuando las superficies de una fase oxídica (α) y metálica (β) entran en contacto (fig. 20a), en el punto x_o accionan de conjunto tres tensiones de superficie límite: la tensión superficial de la fase de óxido ($\gamma_{\alpha G}$), la tensión superficial de la fase metálica ($\gamma_{\beta G}$) y la tensión de superficie límite de fase ($\gamma_{\alpha\beta}$). Para el estado de equilibrio se tiene - según el paralelogramo de fuerzas - la relación de Young-Dupré:

$$\gamma_{\alpha\beta} = \gamma_{\alpha G}\cos\phi_\alpha + \gamma_{\beta G}\cos\phi_\beta \qquad (7)$$

En el caso del borde de grano dentro del óxido ($\gamma_{\alpha G} = \gamma_{\beta G}$) resulta de la ecuación (7):

$$\gamma_{\alpha\alpha} = 2\ \gamma_{\alpha\beta}\cos\phi_P \qquad (8)$$

Si el borde de grano se termina en la fase metálica (β) (fig. 20b), y

$$\gamma_{\alpha\alpha} = 2\ \gamma_{\alpha G}\cos\phi_K \qquad (9)$$

Si el borde grano se termina en la superficie (fig. 20c).

Cuando la fase metálica fundida se encuentra como gota tendida en la fase de óxido plana y paralela, como lo muestra la fig. 20d, resulta de la ec. (7)

$$\gamma_{\alpha G} = \gamma_{\alpha\beta} + \gamma_{\beta G}\cdot\cos\phi_S \qquad (10)$$

A partir de la ec. (10) se tiene en combinación con la Ec. (8) y (9)

$$\gamma_{\alpha G} = \gamma_{\beta G}\ \frac{\cos\phi_S\cos\phi}{\cos\phi_P - \cos\phi_K} \qquad (11)$$

Con este sistema de ecuaciones (ecs. 8-11) se han determinado las energías de superficies límites entre fases de óxido y metálicas que estudiaremos en lo que sigue, donde en los casos más complicados teníamos que pasar por las etapas siguientes:

- determinación de la energía superficial de un metal líquido ($\gamma_{\beta G}$)
- determinación de los ángulos de contacto (ϕ_S, ϕ_K, ϕ_P, ver fig. 20)

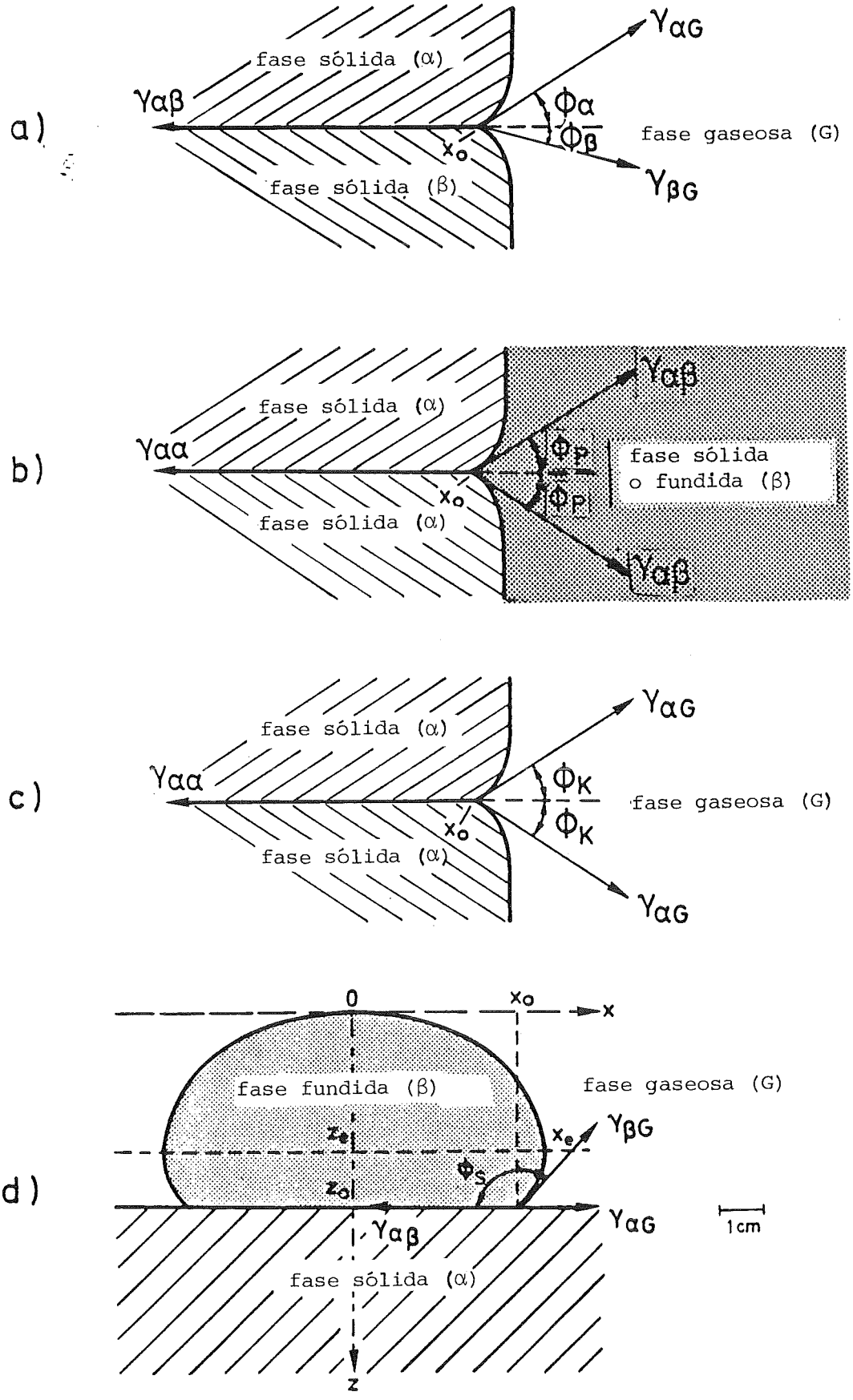

fig. 20: Energías de superficie límite y tensiones de superficie límite

- cálculo de la energía superficiál del óxido sólido según la ec. (5), entonces de la energía de borde de grano según la ec. (9) y con esto de la energía de superficie límite según la ec. (8).

Todas las energías de superficies límites y ángulos de contactos son independientes de las magnitudes de estado temperatura y composición química, aunque esta última esté dada por el sistema óxido-metal, pero pueda estar influenciada por la composición de la atmósfera ambiente y por elementos trazas tensioactivos.

Como los hemos indicado arriba, la primera etapa de la determinación de la energía de superficie límite de fases entre el óxido y el metal consiste en la determinación de la energía superficial del metal líquido ($\gamma_{\beta G}$ en la ec. (11)) en la disposición de una gota tendida (fig. 20d), que se realiza en aparatos de mojadura conocidos (fig. 21). La energía superficial resulta entonces - en el supuesto de que las condiciones de estado sean constantes - del peso de la gota (G) y de las dimensiones de su silueta (x_e, z_e, x_o, z_o; fig. 20d) mediante la ecuación

$$\gamma_{\beta G} = \frac{G \cdot b^2}{V \cdot \beta} = \frac{g \cdot \rho \cdot b^2}{\beta} \qquad (12a)$$

con

$$\rho = \frac{G}{g \cdot V} \qquad (12b)$$

(g = acceleración de la gravedad; V = volúmen de la gota; b = radio de curvatura de la gota; β = factor de proporcionalidad; ρ = densidad de la gota fundida).

Se suponen aquí ángulos de contactos superiores a 90 grados (ver fig. 20d: $\phi > 90^o$) y una forma elipsoidal de rotación (eje de rotación z) de la gota.

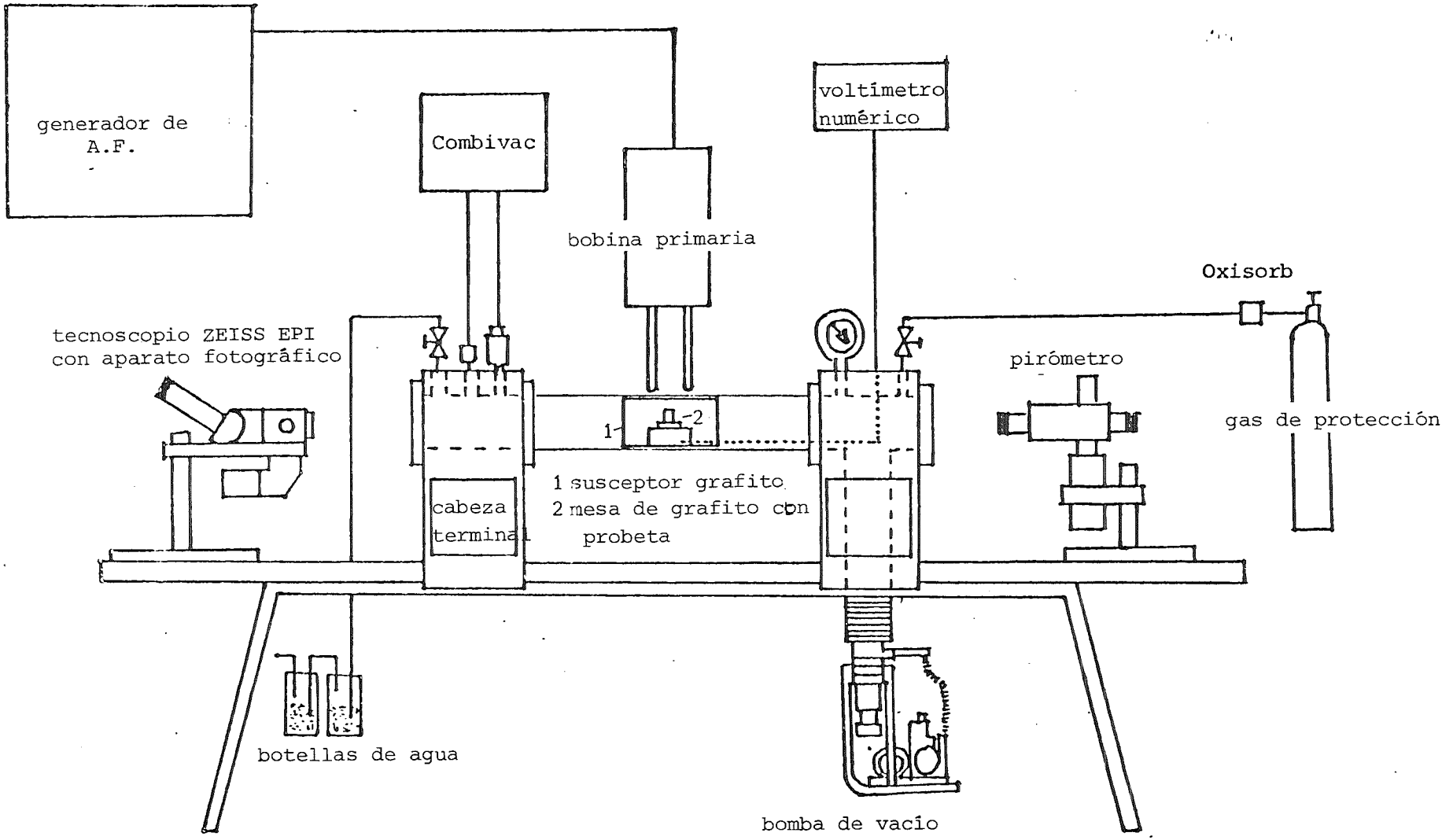

fig. 21: Esquema del aparato de mojadura

La determinación del factor de proporcionalidad (β) así como del volumen (V) y del radio de curvatura (b) de la gota a partir de sus dimensiones (x_e, z_e, x_o y z_o) se obtiene a partir de tablas representadas gráficamente en lo que sigue. La fig. 22 indica la relación entre el factor de proporcionalidad (β) y la relación de los tramos centrales (x_e/z_e). Para la gota representada en la fig. 20d se tiene

$$x_e = 2{,}9 \text{ cm} \qquad z_e = 2{,}2 \text{ cm}$$

$$x_e/z_e = 1{,}32 \text{ cm} \qquad \beta = 3{,}1$$

Los tramos centrales x_e, z_e están siempre atribuídos a un ángulo de contacto $\phi = 90^o$ (fig. 20d). Para esta pareja de valores ($\beta = 3{,}1$; $\phi = 90^o$) se tiene a partir de la fig. 23a, b:

$$\frac{x_e}{b_x} = 0{,}77 \quad \text{y} \quad b_x = 3{,}77 \text{ cm}$$

así como a partir de la fig. 24:

$$\frac{z_e}{b_z} = 0{,}58 \quad \text{y} \quad b_z = 3.79 \text{ cm}$$

y con esto $b = \frac{b_x + b_z}{2} = 3{,}78$ cm

Entonces resulta con $x_o = 2{,}5$ cm, $z_o = 3$ cm la relación

$$\frac{x_o}{b} = 0{,}66 \qquad \frac{z_o}{b} = 0{,}79.$$

Con estas relaciones y la expresión constante $\beta = 3{,}1$ resulta

- otra vez a partir de la fig. 23 y fig. 24 por interpolación y tomando el valor medio

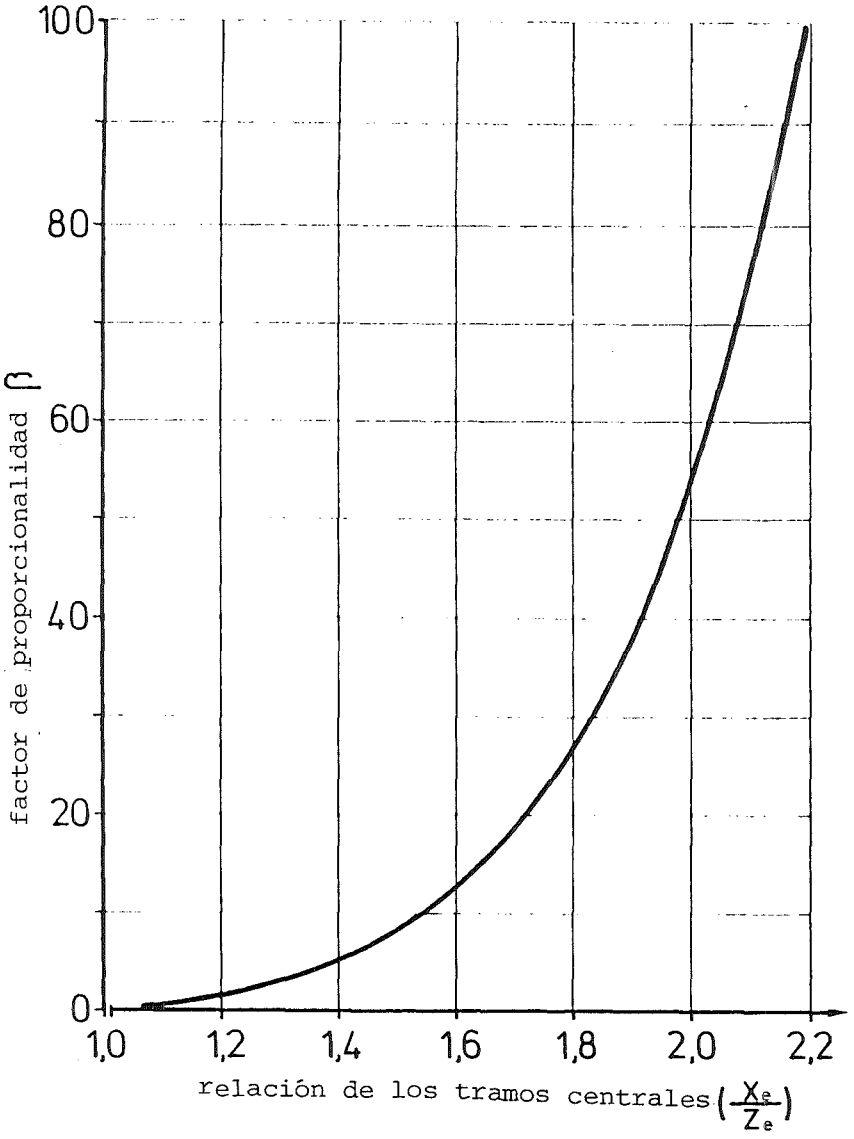

a

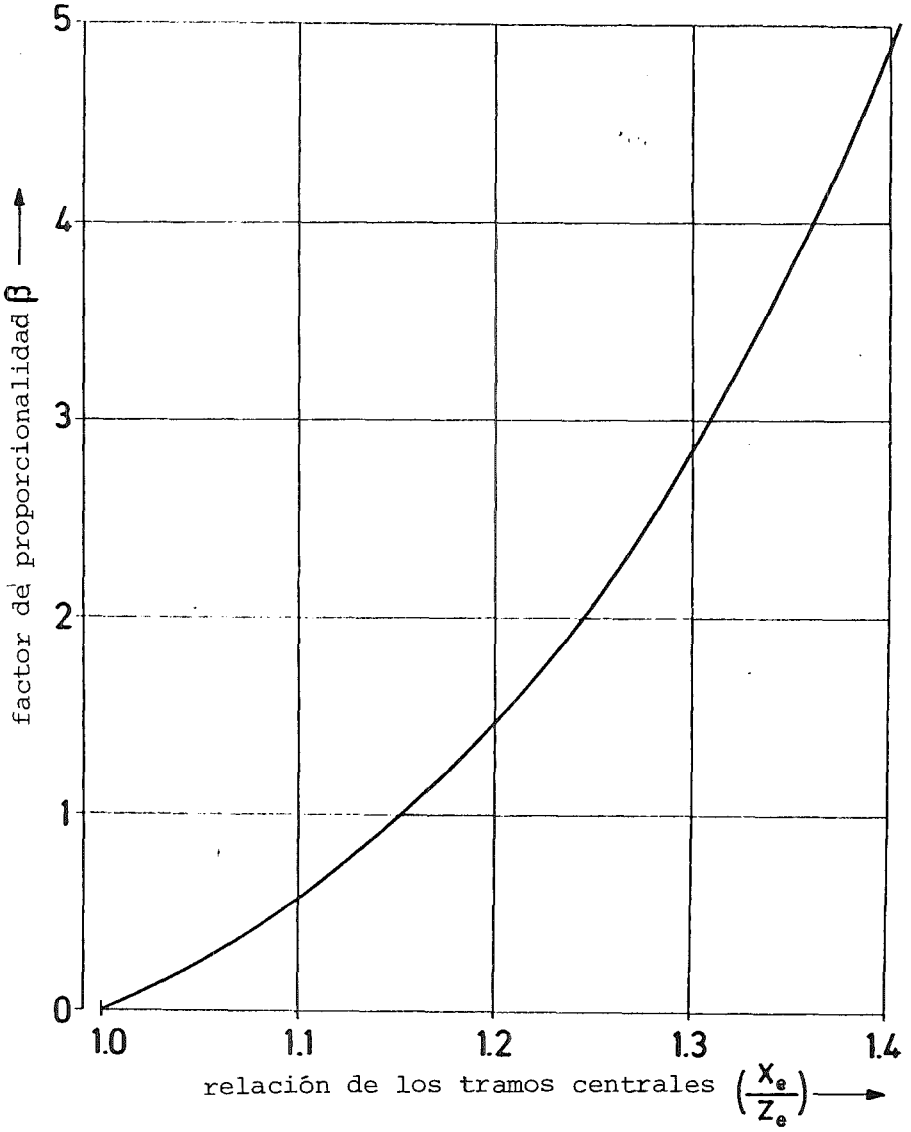

b

fig. 22: Factor de proporcionalidad (a:β = 1-5; b:β = 1-100) en función de la relación de los tramos centrales

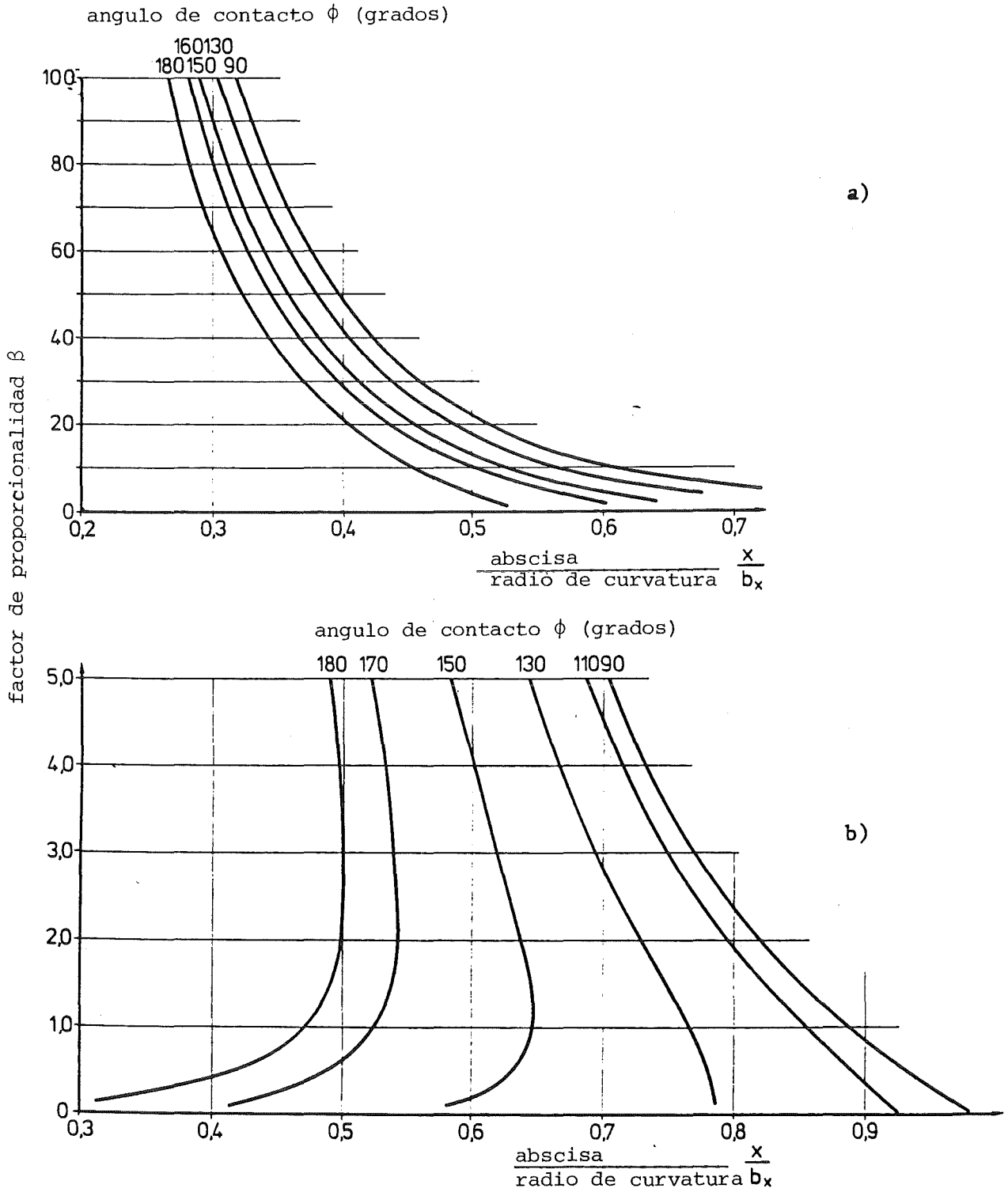

fig. 23: Factor de proporcionalidad, ángulo de contacto y abscisa normalizada

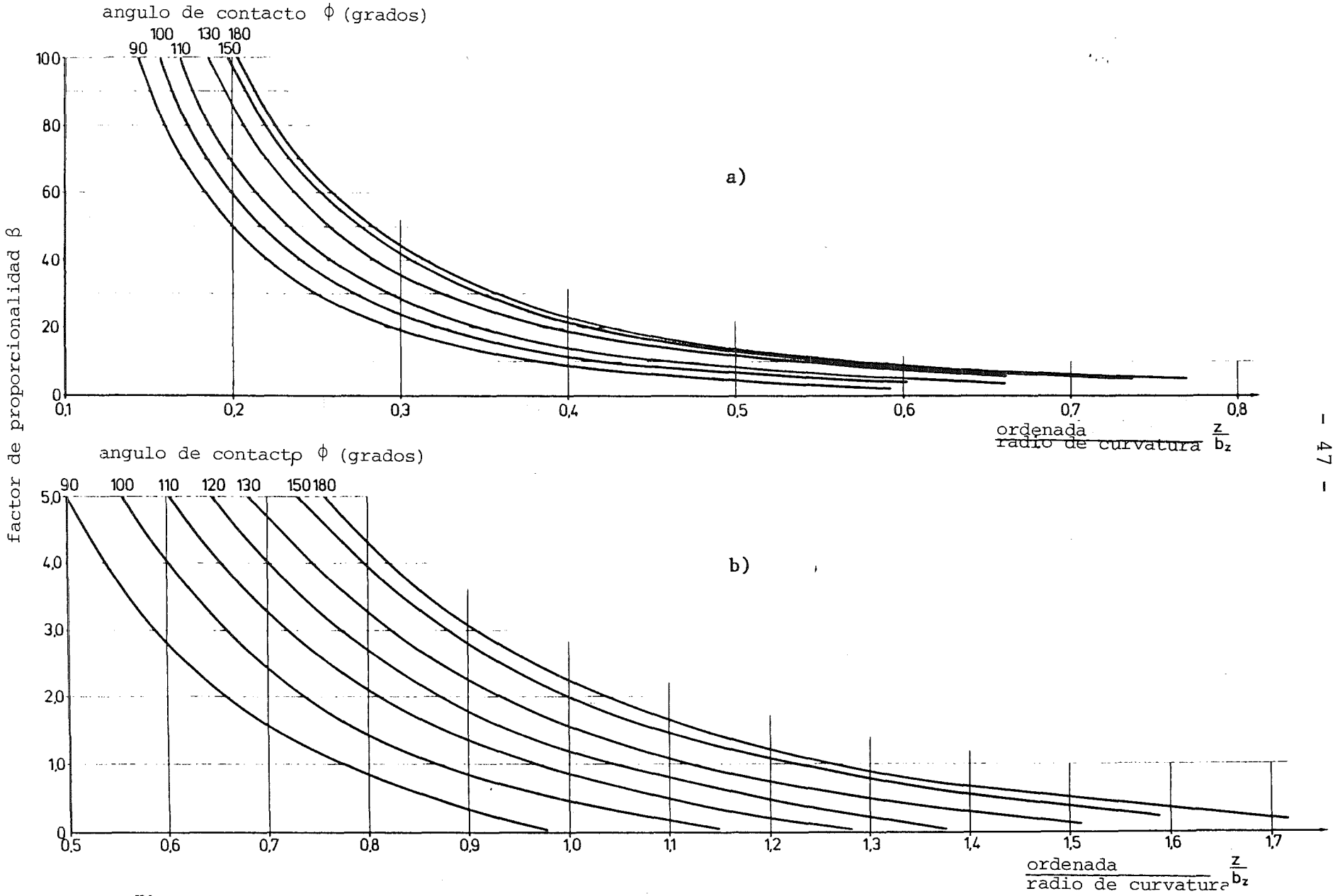

fig. 24: Factor de proporcionalidad, angulo de contacto y ordenada normalizada

- el ángulo de contacto $\phi_S = 133 \pm 7$,

lo que coincide con la fig. 20d.

Con la nueva pareja de valores ($\beta = 3,1$, $\phi_S = 133^o$) se obtiene a partir de la fig. 25 por interpolación

$$\frac{V}{b^3} = 1,12$$

y con b = 3,78 cm

$$V = 60,5 \text{ cm}^3.$$

El peso de la gota puede determinarse por pesada. Se conoce la aceleración de la gravedad (981 cm/s^2). Con esto disponemos de todas las magnitudes con las que se obtienen a partir de la ec. (12) la energía superficial - y la densidad - del caldo metálico.

Para determinar la energía superficial de la fase sólida de óxido se tiene que conocer según la ec. (11), además de la energía superficial de la gota metálica líquida ($\gamma_{\hat{\beta}G}$), tres ángulos de contacto (ϕ_S, ϕ_P, ϕ_K; fig. 9). El ángulo de contacto para la mojabilidad (ϕ_S; fig. 20d) puede ser superior o inferior a 90^o. Según la fig. 23 y fig. 24, ángulos de contacto superiores a 90^o ($\phi_S > 90^o$; fig. 20d) se obtienen conforme a los procedimientos de interpretación descritos.

Para ángulos de contacto inferiores a 90^o ($\phi_S < 90^o$) y un peso pequeño de la gota (pequeñas gotas) la influencia de la gravitación sobre la forma de las gotas es despreciable, y la gota puede considerarse como un segmento de esfera. En este caso el ángulo de contacto resulta de la ecuación de la tangente en un círculo.

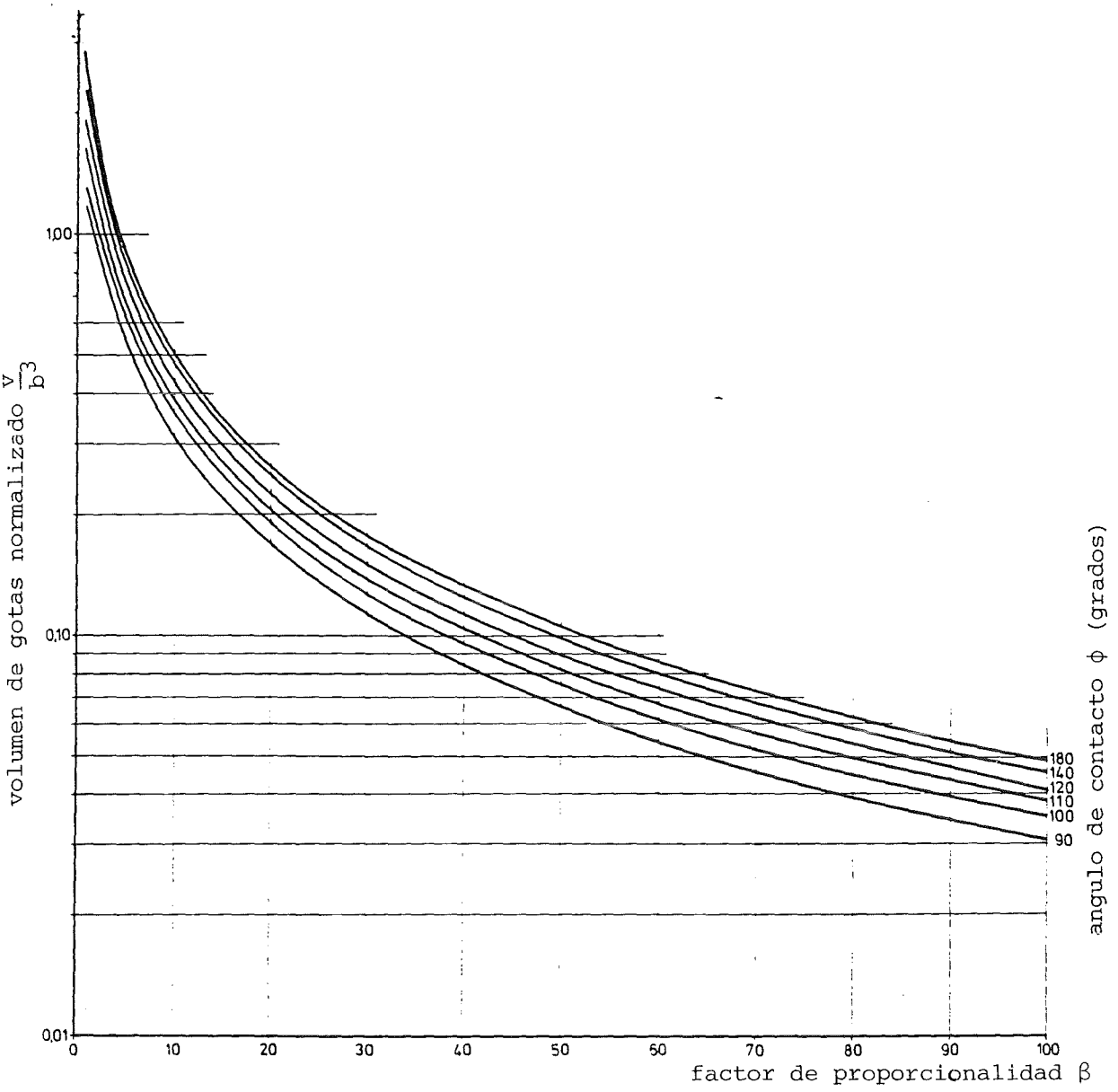

fig.25a: Volumen de gotas normalizado, angulo de contacto y factor de porporcionalidad

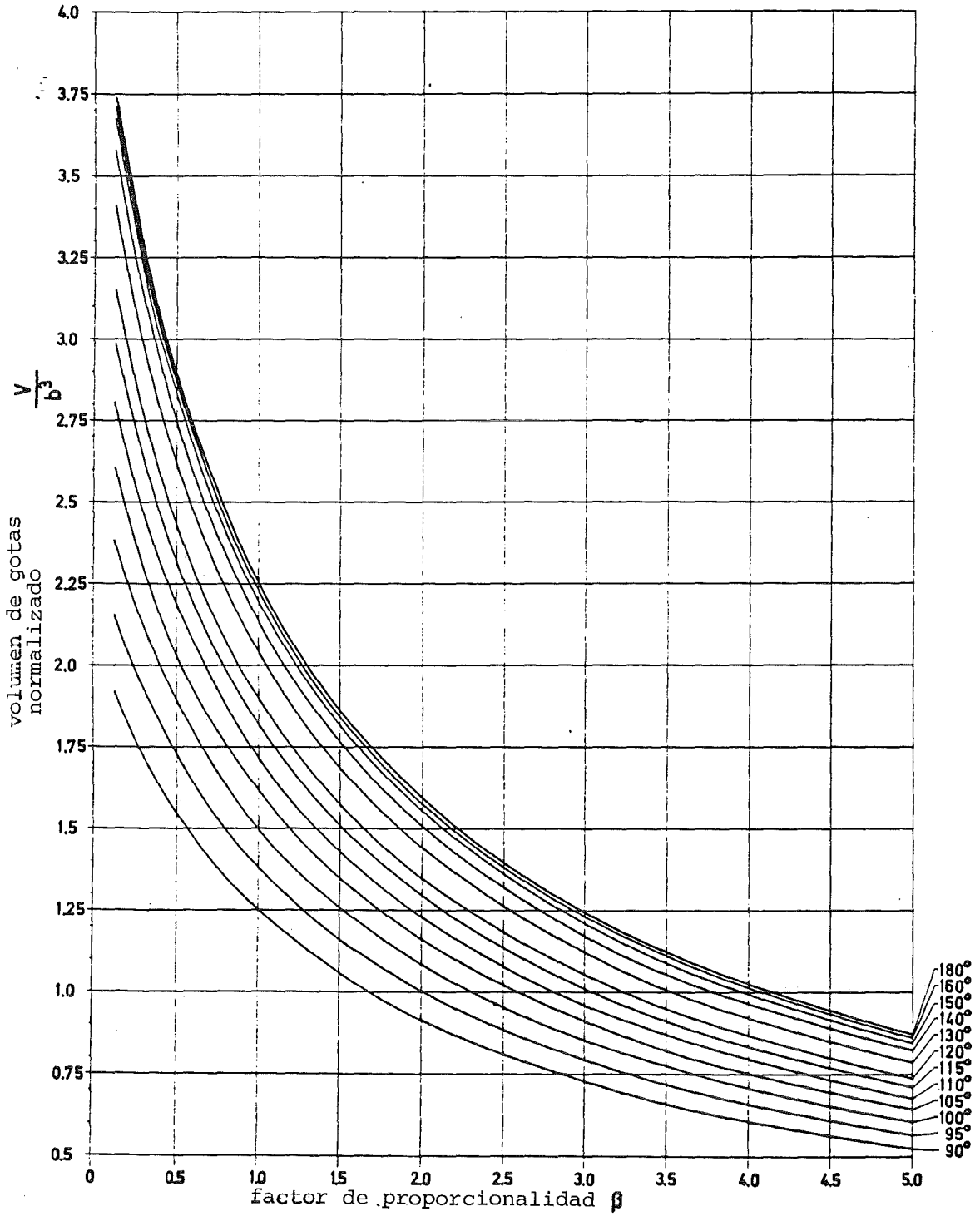

fig. 25b: Volumen de gotas normalizado, angulo de contacto y factor de proporcionalidad

Para determinar los ángulos de contacto del borde de grano de óxido frente a la fase metálica (ϕ_P; fig. 20b) y frente al ambiente gaseiforme (ϕ_K; fig. 20c), se enfrían rápidamente las probetas correspondientes después de un recocido isotérmico a largo plazo (congelación del estado de equilibrio isotérmico de las superficies límites), y se las preparan con métodos del análisis estructural (pulido, gravado al ácido) de modo que los bordes de grano se hagan visibles. Se miden los ángulos de aquellos bordes de grano que - según la fig. 20b, c - penetran en dirección aproximadamente vertical sobre la superficie. En el caso del ángulo de contacto de los bordes de grano que se terminan en las superficies, la preparación se hace paralelamente a la superficie. La obtención de la marcha vertical supuesta de los bordes de grano puede verificarse preparando por ambos lados probetas delgadas. Con este procedimiento los bordes de grano buscados penetran en dirección vertical referida a las probetas preparadas opuestas, y por ello tienen la misma posición local en ambas superficies. La medida se toma interferométricamente, teniendo franjas de interferencia rectilíneas sobre bordes de grano que penetran perpendicularmente a la superficie (fig. 26). Mediante el ángulo de desviación (α, fig. 27), la ampliación de la imagen, la distancia de las franjas de interferencia y la longitud de onda de la luz monocromática utilizada se obtienen los ángulos de contacto de los bordes de grano en superficies, cuya distribución de frecuencia sirve para determinar el ángulo de contacto medio (ϕ_K). Los ángulos de contacto de bordes de grano que tocan a una fase metálica sólida (ϕ_P; fig. 20b) están determinados en superficies de probetas perpendiculares a la superficie límite óxido-metal (ver fig. 27). Debido a la medida del ángulo en la superficie preparada de la probeta (fig. 20b), la marcha vertical supuesta frente a la superficie límite tiene entonces que ser garantizada aproximadamente en la superficie misma de la probeta así como en la dirección perpendicular

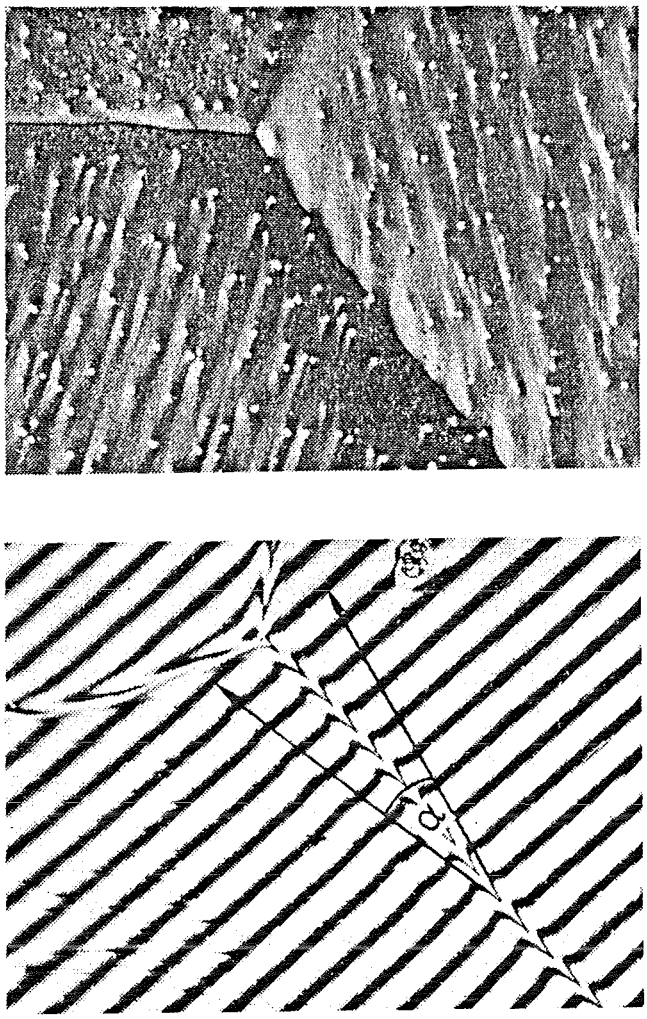

fig. 26: Bordes de grano de UO_2 (ampliado de 1075) después del recocido isotérmico a largo plazo (2173 K, 5 h, argón) sin (arriba) y con (abajo) franjas de interferencia superpuestas

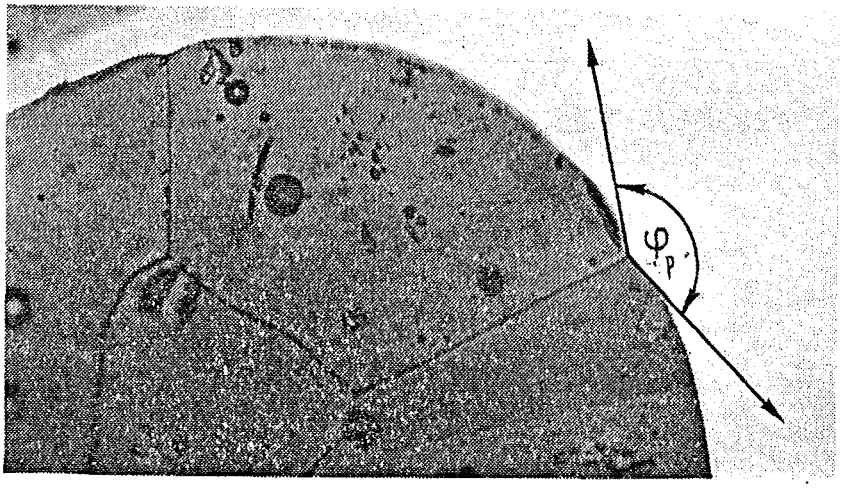

fig. 27: Angulos de contacto de UO_2-Cr (ampliado de 1000) después del recocido isotérmico a largo plazo (2023 K, 100 h, argón)

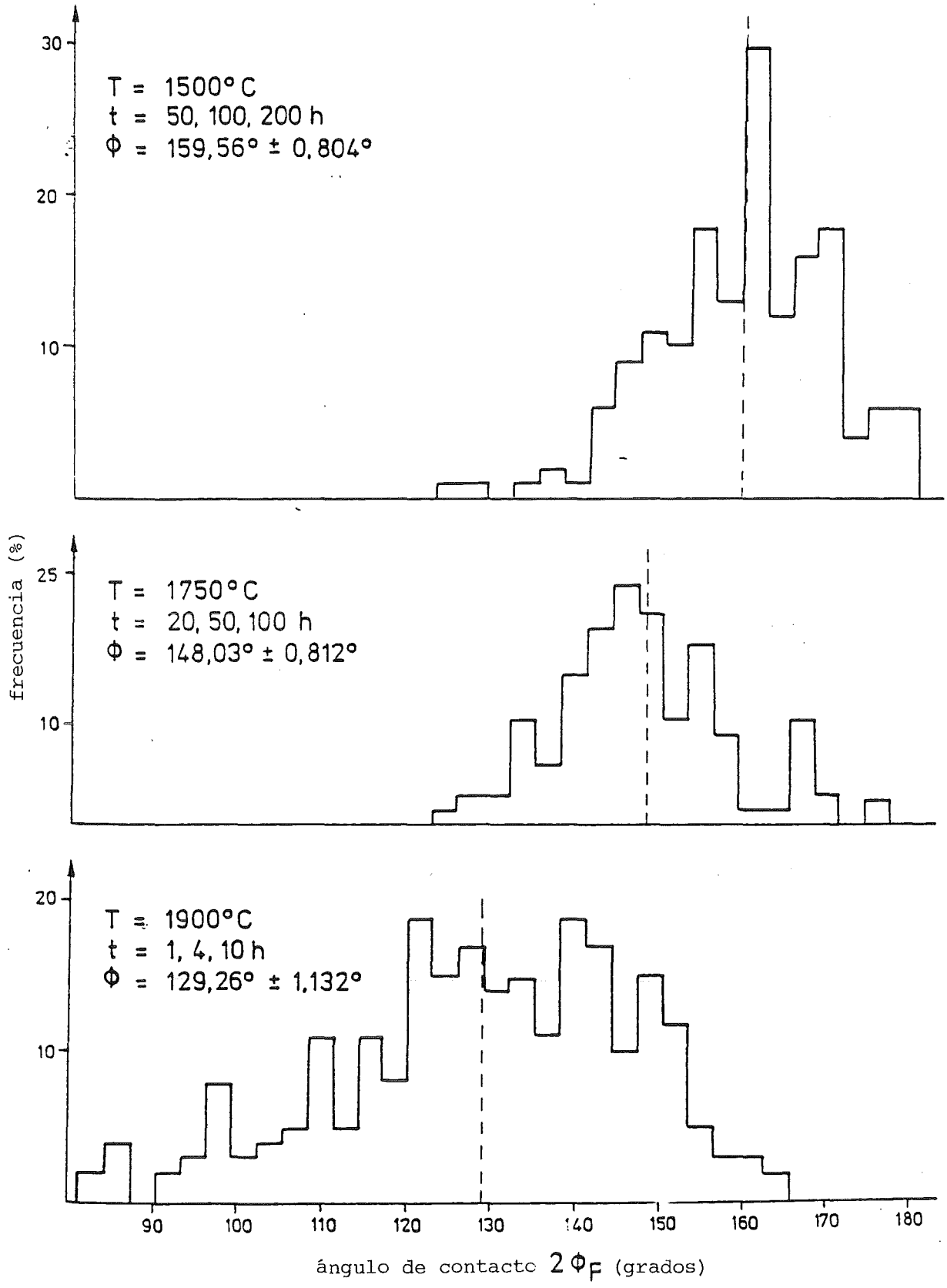

fig. 28: Histograma del ángulo de contacto UO_2-Cr Φ_p (valor medio en rayitas)

sobre ella. Se puede reconocer directamente en la superficie preparada de la probeta (fig. 27 ≙ 20b), y se tiene que examinar en la dirección perpendicular a ella mediante la preparación mencionada por ambos lados de probetas delgadas. Como lo hemos mencionado ya arriba para el ángulo de contacto en los bordes de grano, el ángulo de contacto medio en la límite de fase se determina a partir de la distribución de frecuencia de ángulos de contacto medidos en límites de fases (ϕ_p) (ver ejemplo de la fig. 28).

3.2.2 Resultados

Las fases o componentes respectivamente que aparecen en un accidente de fusión del núcleo de un reactor de agua liviana son acero, hormigón y corio EX3. Los caldos de acero no se mezclan con caldos de hormigón y corio EX3. En cambio el hormigón y corio EX3 son completamente mezclables en el estado líquido. Su disposición geométrica en el caldo está determinada por las funciones de temperatura de su densidad y tiene una influencia esencial sobre la destrucción - térmica y química - del hormigón. Por lo tanto, con el método de la gota tendida (fig. 29) se han medido las densidades de acero, corio y hormigón fundidos y algunas mezclas de corio-hormigón. Como soporte de las gotas se han empleado dióxido de uranio, nitruro de boro, tungsteno, carburo de hafnio, tántalo nitruro y tántalo carbonitruro de hafnio. Se han determinado las densidades en el estado sólido a partir de medidas de densidad según el principio de Arquimedes a la temperatura ambiente y con medidas dilatométricas.

En la fig. 30 están resumidos los resultados de las determinaciones de densidad. Según ellos, la densidad (ρ_s en kg/m^3) de todos los caldos disminuye en 1a aproximación linealmente con la temperatura (T en K), lo que puede describirse por las funciones siguientes:

para cero

$$\rho_S = 6,82 \cdot 10^3 - 10,25 \cdot 10^{-1} \ (T-1690) \qquad (13)$$

para corio EX3

$$\rho_S = 3,15 \cdot 10^3 - 5,77 \cdot 10^{-1} \ (T-1600) \qquad (14)$$

para hormigón

$$\rho_S = 1,86 \cdot 10^3 - 2,4 \cdot 10^{-1} \ (T-1550) \qquad (15)$$

Las lineas trazadas en rayitas en la fig. 30 caracterizan los campos de fusión. Comienzan para corio EX3 y hormigón con la temperatura de sólidus y se terminan con la temperatura de líquidus. Para todas las temperaturas se tiene

$$\rho_{acero} > \rho_{corio\ EX3} > \rho_{corio\ EX3\ +\ hormigón} > \rho_{hormigón},$$

de modo que se tiene que contar con una caldo polifásico dispuesto en capas, en que el acero líquido se encuentra abajo, mientras que el hormigón líquido está arriba.

Los coeficientes de dilatación que determinan las densidades en el estado sólido cerca del punto de fusión pueden estimarse facilmente a través de las relaciones representadas en la fig. 31a y b entre el punto de fusión y el coeficiente de dilatación térmica.

Las energías de superficie límite de los sistemas UO_2-Co, UO_2-Cu y UO_2-Fe se han determinado mediante medidas del ángulo de contacto según la ec. (7) (ϕ_p; fig. 20b) y la energía de borde de grano para el dióxido de uranio según la ecuación

$$\gamma_{UO_2-UO_2} = 0,839 - 0,1926 \cdot 10^{-3} \cdot T[J/m^2] \qquad (17)$$

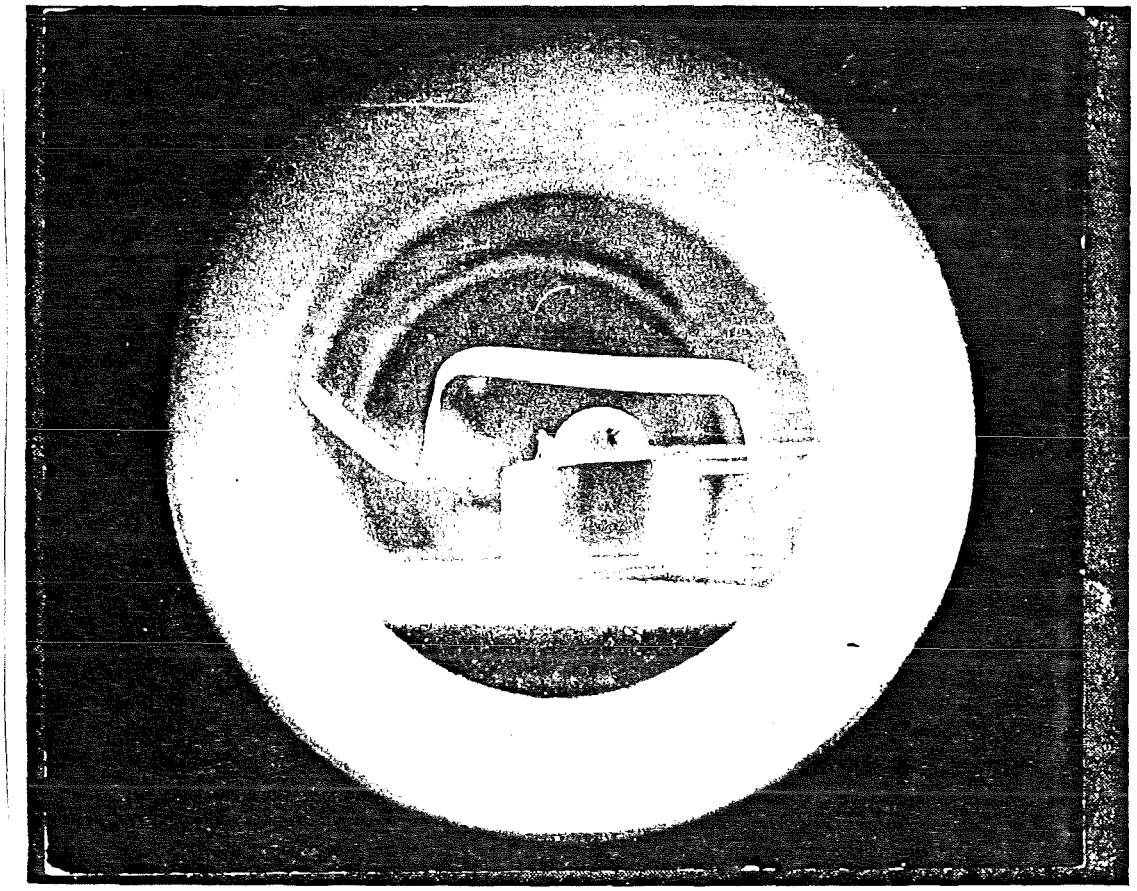

fig. 29: Gota tendida en un dispositivo experimental (acero sobre UO_2)

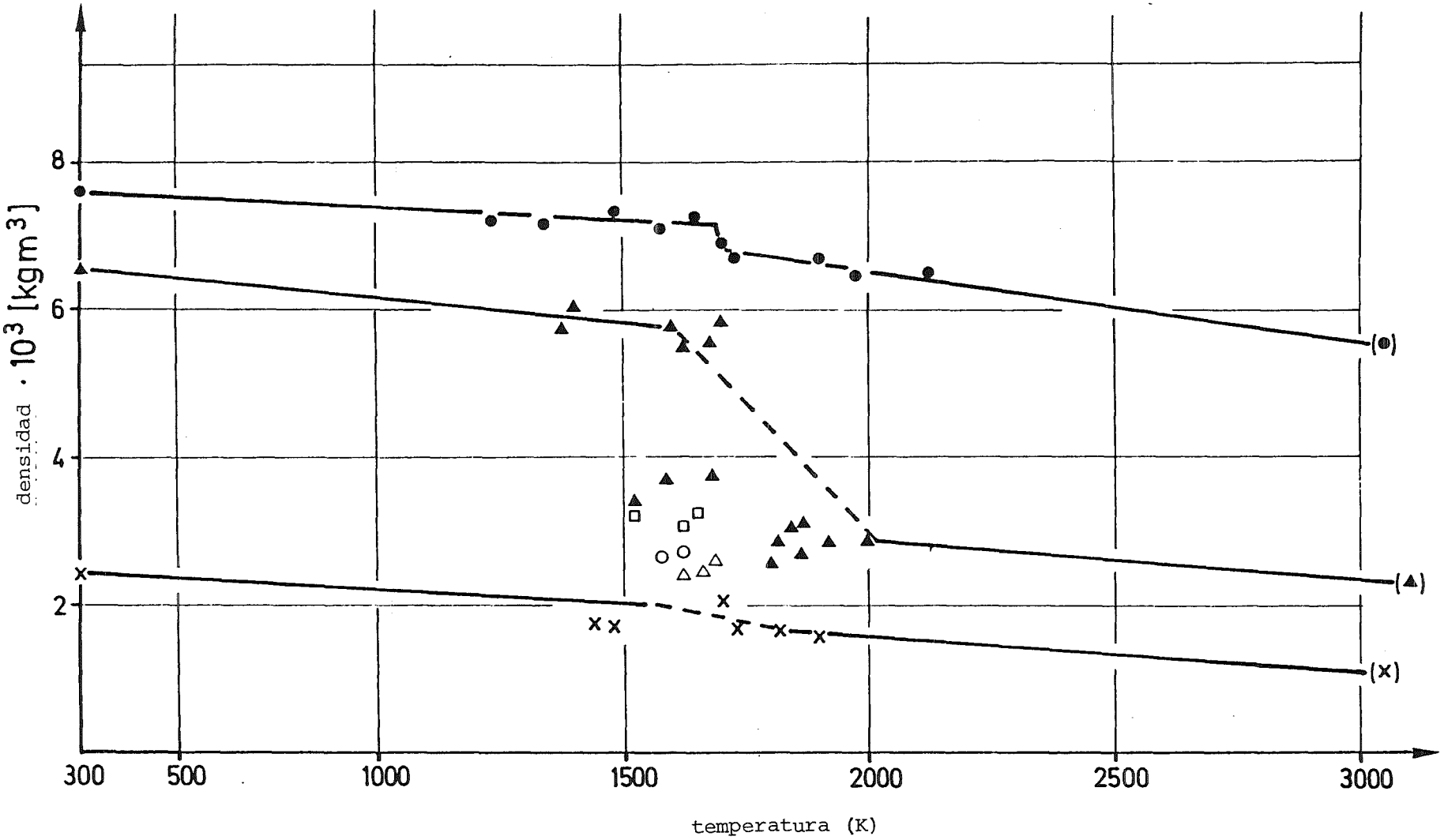

fig. 30: Funciones de temperatura de la densidad de acero, corio EX3, mezclas de corio-hormigón y hormigón

- ● acero 1.4970
- ▲ corio EX3
- x hormigón
- ▫ corio EX3+hormigón (75% vol.)
- ○ corio EX3+hormigón (50 % vol.)
- △ corio EX3+hormigón (25 % vol.)

} solidificado

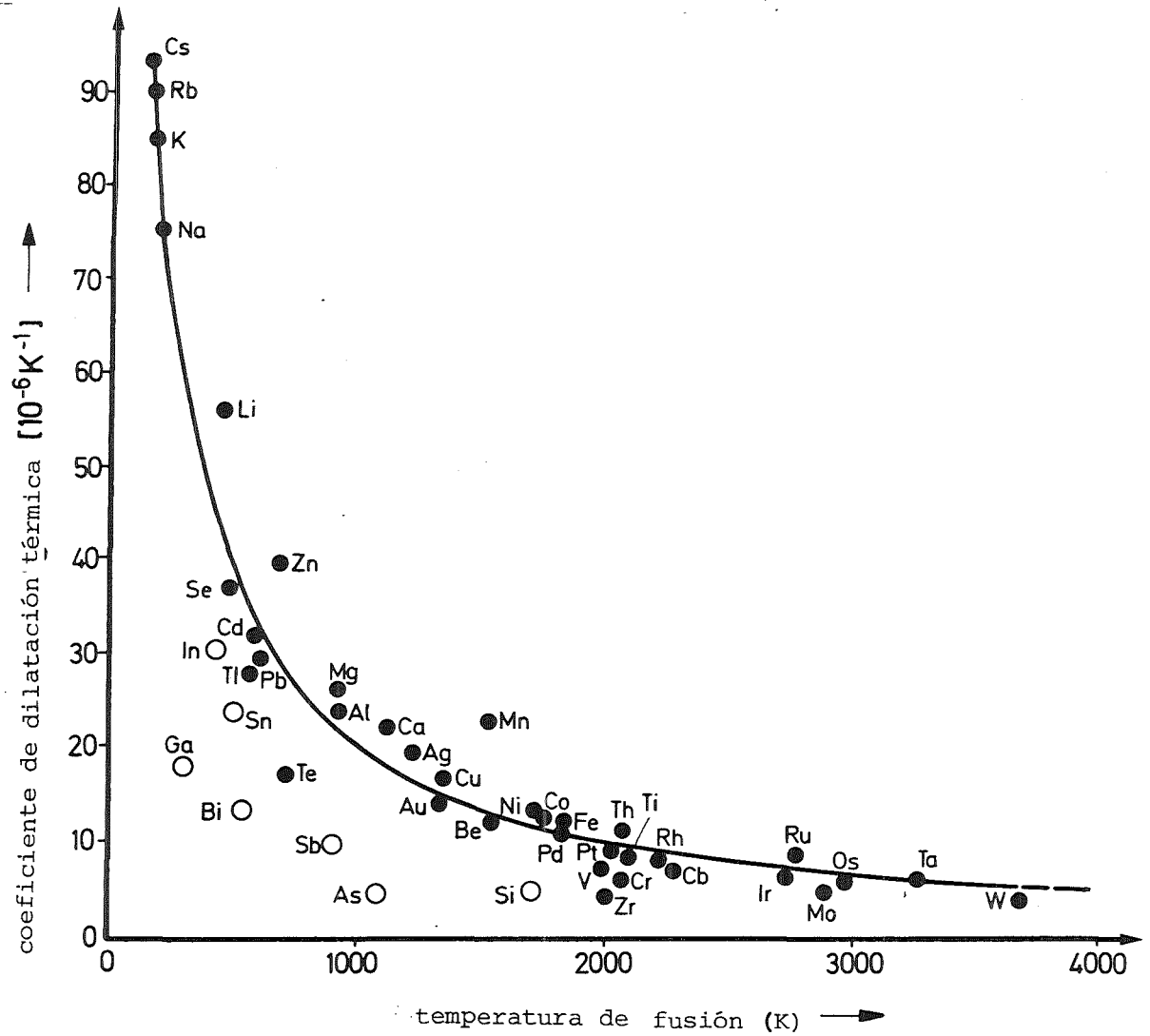

fig. 31 a: Coeficiente de dilatación y punto de fusión de metales o redes cúbicas y hexagonales, o otras redes

La ec. (17) se ha determinado de la manera descrita, es decir la medida de todos los ángulos de contacto (ϕ_S, ϕ_P, ϕ_K; fig. 20) y la energía superficial del metal líquido ($\gamma_{\beta G}$) según la ec. (11) y la ec. (9).

Para determinar las energías de superficie límite en los sistemas UO_2-Bi, UO_2-Na y UO_2-Pb, se han utilizado las energías superficiales de los metales líquidos y sus ángulos de contacto con el dióxido de uranio sólido a partir de la literatura. Se han calculado las energías superficiales del dióxido de uranio sólido mediante la ecuación

$$\gamma_{UO_2\text{-}G} = 1{,}507 - 0{,}3457.10^{-3}\ T\ [J/m^3] \qquad (18)$$

Con estos valores resultan de la ec. (10) las energías de superficie límite correspondientes.

Las energías de superficie límite de los sistemas UO_2-Ni y UO_2-acero (SS 1.4970) se sabían por publicaciones sobre trabajos anteriores.

En la fig. 32 están resumidos los resultados para caldos metálicos de UO_2 ($T_{S\ UO_2} > T > T_{S\ metal}$). En cada primera línea respectiva de cadá sistema en la fig. 32 se ha indicado la energía de superficie límite en el punto de fusión del metal ($T/T_S = 1$), extrapolada a través de rectas de compensación a partir de los otros valores de medida. Todos los valores se refieren a ensayos con $UO_{2.006}$ bajo atmósfera de argón (O_2 < 10 vpm; H_2, N_2 < 20 vpm). Cuando se representan las energías de superficie límite para caldos metálicos de UO_2 sobre la temperatura homóloga referida al punto de fusión del metal respectivo (fig. 33), resulta que

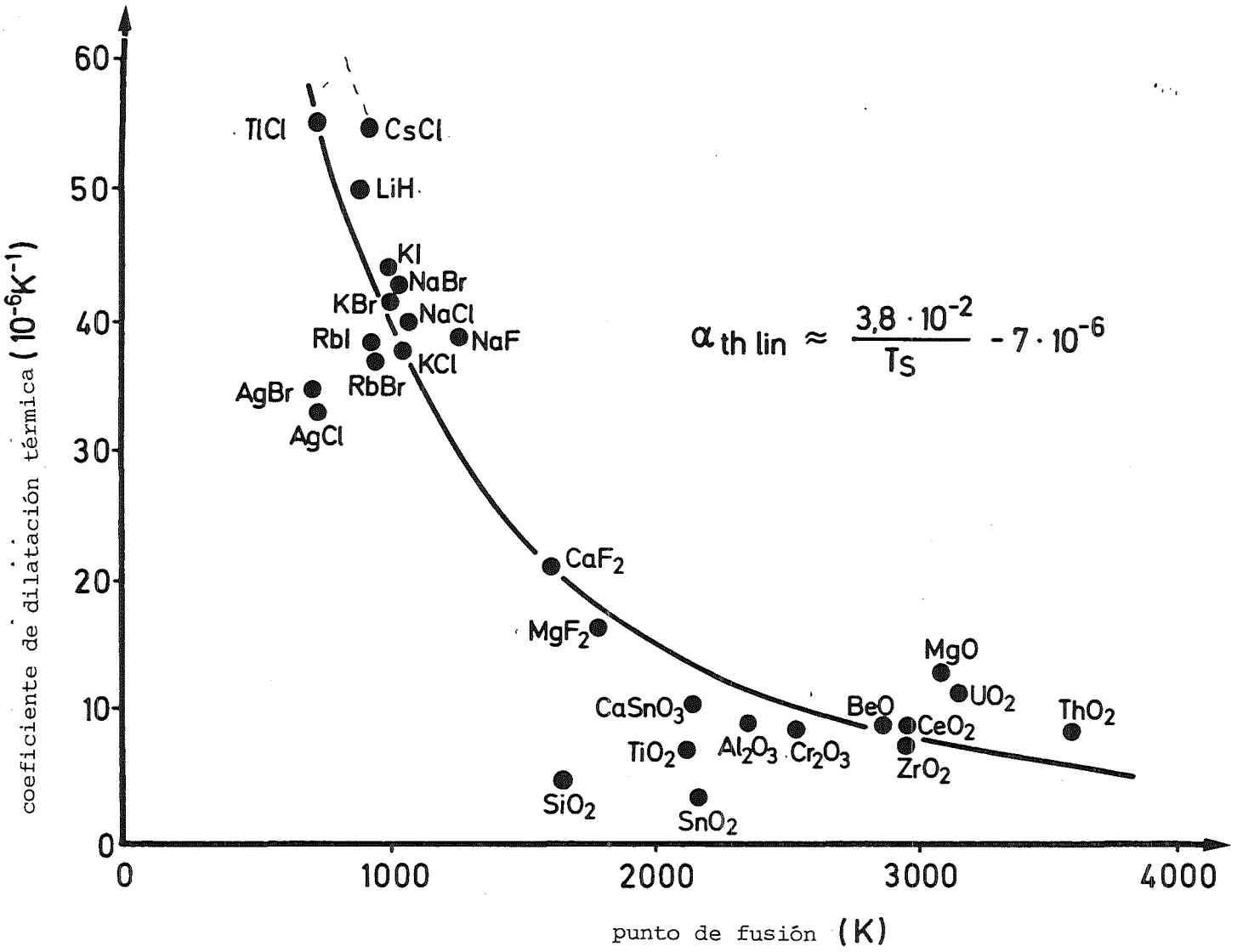

fig. 31 b: Coeficiente de dilatación y punto de fusión de materiales cerámicos

sistema	temperatura T [K]		energía de borde de grano $\gamma_{\alpha\alpha}$ de UO_2 [J/m²]	energía superficial		ángulo de contacto (grados)		energía de superficie límite $\gamma_{\alpha\beta}$ caldo metal UO_2 (J/m²)		coeficiente de temperatura de la energía de superficie límite $d\gamma_{\alpha\beta}/d(T/T_s)$ con $T > T_s$ [J/m²]
	T	T/T_s		$\gamma_{\alpha G}$ de UO_2 [J/m²]	$\gamma_{\beta G}$ de caldos met. [J/m²]	ϕ_s	ϕ_ρ	para T	para T_S(extrapolado)	
UO_2-Co	1768	1							1.582	-4.167
	1823	1.0311	0.488				160.5	1.441		
	1923	1.0877	0.469				159.1	1.293		coeficiente de correlación
	2023	1.1442	0.449				149.8	0.862		R = -0.961
	2123	1.2008	0.430				148.8	0.799		
UO_2-Cu	1356	1							1.586	-1.654
	1673	1.2338	0.517				155.1	1.199		
	1873	1.3813	0.478				151.0	0.955		
UO_2-Fe	1809	1							1.459	-2.923
	1873	1.0354	0.478				159.7	1.356		
	2073	1.1459	0.440				155.4	1.033		
UO_2-Bi	544	1							1.635	-0.360
	653	1.2004		1.281	0.377	138.5		1.563		
	1515	2.7849		0.983	0.248	92.0		0.992		
UO_2-Na	370	1							1.627	-0.447
	473	1.2784		1.343	0.181	145.0		1.491		
	573	1.5486		1.309	0.171	119.0		1.392		coeficiente de correlación
	673	1.8189		1.274	0.160	91.0		1.277		R = -0.995
	773	2.0892		1.240	0.152	42.0		1.127		
UO_2-Pb	600	1							1.660	-0.392
	683	1.1383		1.271	0.447	138.5		1.606		
	928	1.5467		1.186	0.432	127.0		1.446		
UO_2-Ni	1726	1							1.651	-2.119
	1773	1.0272						1.568		
	2023	1.1721						1.354		coeficiente de correlación
	2173	1.2590						1.060		R = -0.973
UO_2-acero (SS 1.4970)	1690	1							1.583	-3.503
	1690	1.0000		0.923	1.190	124.0		1.588		
	1840	1.0888		0.871	1.120	110.2		1.258		coeficiente de correlación
	1930	1.1420		0.840	1.050	104.0		1.094		R = -0.999

fig. 32: Angulos de contacto, energías superficiales y de superficie límite obtenidos, en función de la temperatura para sistemas de UO_2-metal

sus funciones de temperatura lineales coinciden dentro del margen del campo de dispersión en el punto de fusión de los metales ($T/T_S = 1$); es decir que la energía de superficie límite entre UO_2 y los caldos metálicos estudiados está aproximadamente constante en el punto de fusión de los metales!

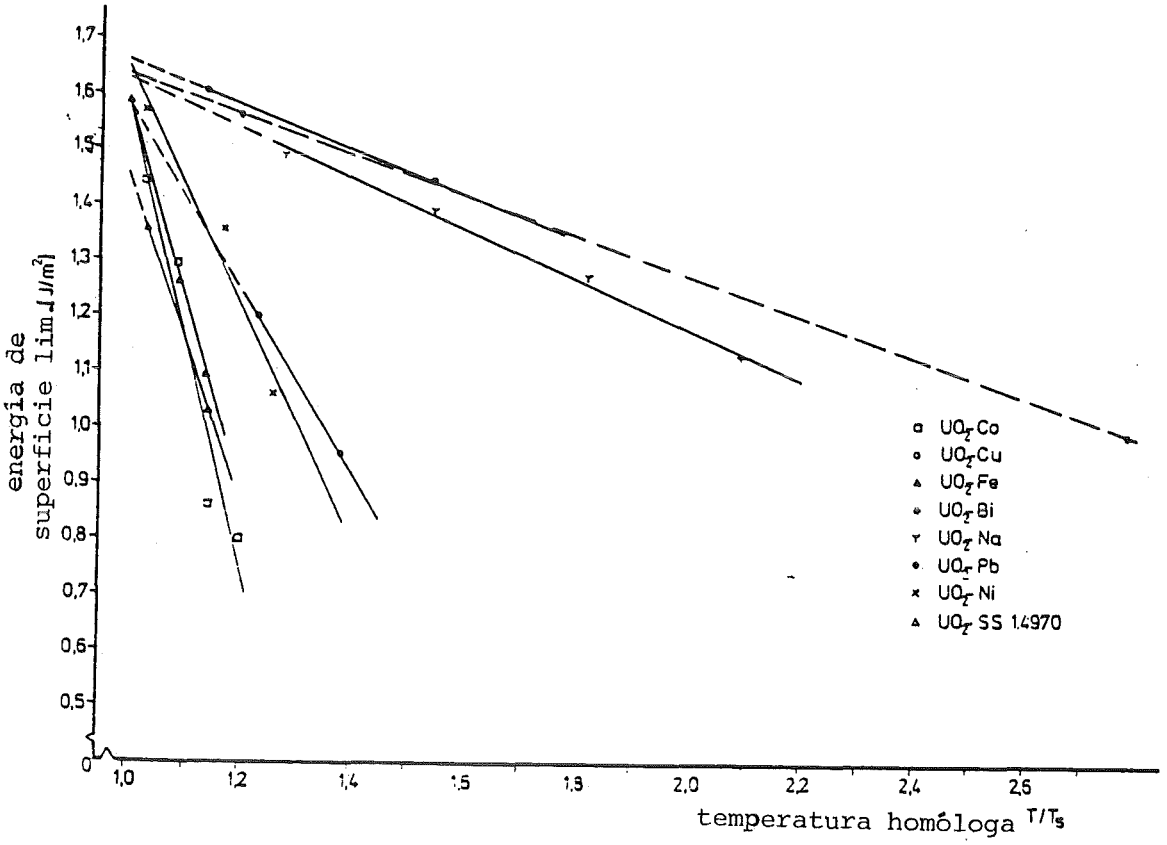

fig. 33: Marcha de las funciones de temperatura de las energías de superficie límite entre el dióxido de uranio y caldos metálicos

El valor medio de esta energía de superficie límite, calculado por un cálculo de compensación, está 1,68 ± 0,06 J/m^3. Con esto tenemos para la energía de superficie límite del dióxido de uranio frente a metales líquidos la función de temperatura siguiente:

$$\gamma_{UO_2\text{-caldo metálico}} = 1{,}68 - \frac{d\gamma}{d(T/T_S)} \cdot \left(\frac{T}{T_S} - 1\right) \; J/m^2 \qquad (19)$$

Los valores del coeficiente de temperatura $\left(\frac{d\gamma}{d(T/T_S)}\right)$ para los diferentes sistemas de UO_2-metal están indicados en la última columna de la fig. 32. Como se trata generalmente de valores extrapolados, se ha indicado en varios casos el coeficiente de correlación (para una extrapolación sin dispersión ± 1).

3.3 La capacidad calorífica y el calor de fusión del corio

se obtienen por simple extrapolación. Cuando se compilan las capacidades caloríficas disponibles para gran número de compuestos intermetálicos, compuestos metal-oxígeno, elementos y halogenuros (fig. 34), resulta una capacidad calorífica atómica media de 8,1 ± 1,4 c/g·átomo K o 33,9 ± 5,9 J/g·átomo K. Como se conoce la composición química de los diferentes caldos del núcleo, puede calcularse ahora aproximadamente su capacidad calorífica en el punto de fusión. - Ya hemos mencionado que los calores de fusión pueden estimarse a partir de los puntos de fusión (ver fig. 15).

Con un método semejante de extrapolación se han determinado algunas

3.4 conductividades térmicas del corio

La comparación de datos disponibles sobre la conductividad térmica en el estado líquido en el punto de fusión muestra que existen relaciones constantes para la conductividad térmica en el estado sólido y en el estado líquido en el punto

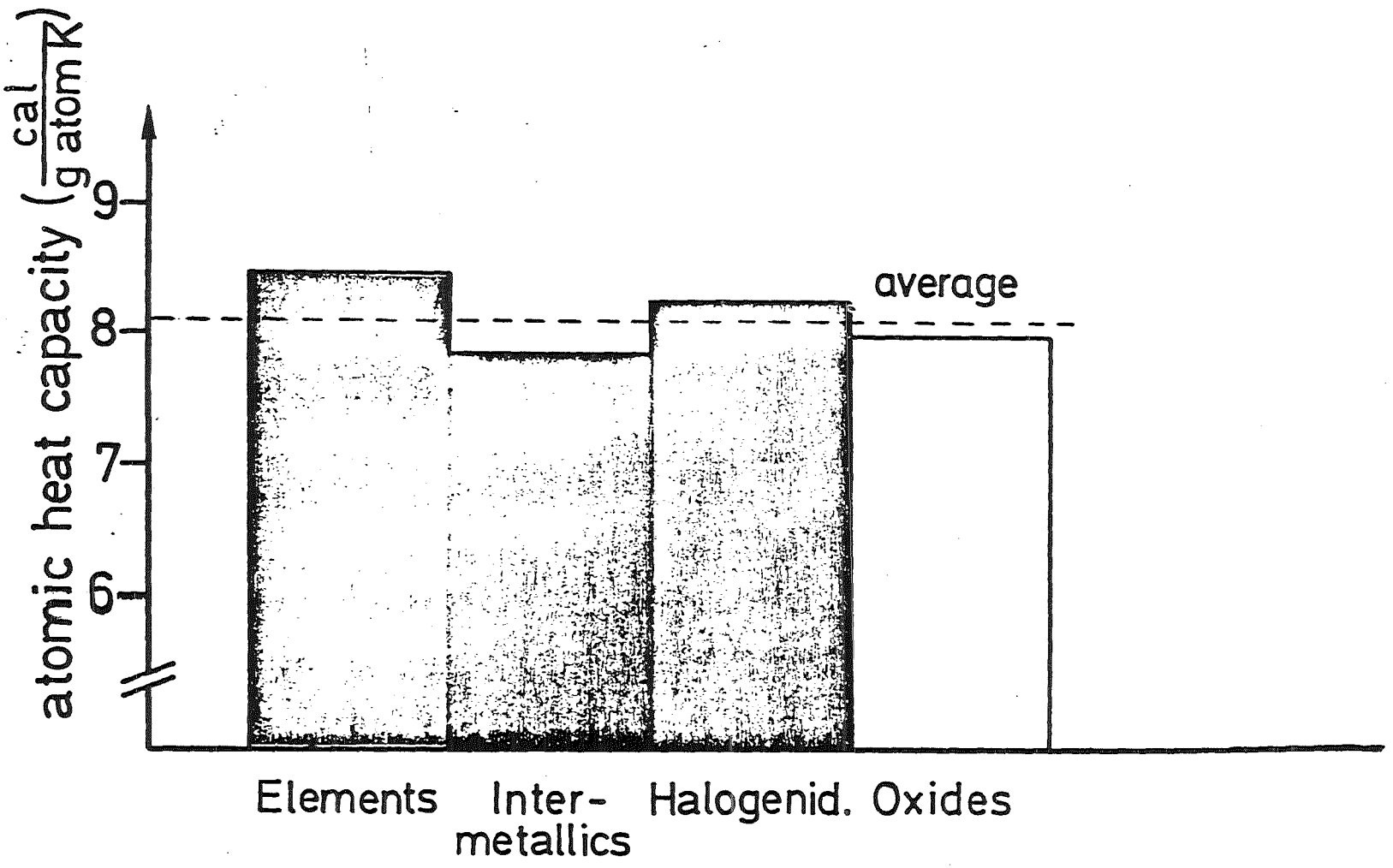

fig. 34: Capacidades caloríficas

de fusión, como p.ej. para metales cuyos átomos poseen 12 vecinos próximos en la red ($\lambda_{sólido}$: $\lambda_{líquido}$ = 2,0 ± 0,4). Un valor correspondiente para compuestos ionicos ($\lambda_{sólido}$: $\gamma_{líquido}$ = 1,16) puede utilizarse como primera aproximación también para óxidos, pero aquí se tiene que contar con mayores inseguridades que para metales. - Mediante estos coeficientes puede estimarse la conductividad térmica de fases líquidas de corio en el punto de fusión, si se conoce la conductividad térmica de las mismas en el punto de fusión en el estado sólido. Para determinar la conductividad térmica de la fase metálica de corio EX1, el corio ha sido preparado según las etapas tecnológicas representadas esquemáticamente en la fig. 35.

Las medidas de la conductividad térmica efectuadas (hasta 1200 K) sobre probetas de corio EX1 preparadas de esta manera (ver fig. 36) y su extrapolación al punto de fusión ($\lambda_{sólido}$ = 0,736 $\frac{J}{cm\ Ks}$ han proporcionado, con la aplicación del coeficiente (2,0) la conductividad del corio EX1 representada en la fig. 37. Una extrapolación correspondiente para acero proporciona aproximadamente la conductividad térmica de la fase metálica del corio EX2 en el estado sólido, semejante al acero,

$$\lambda_{sólido} = 0{,}736\ \frac{J}{cm\ Ks}$$

y mediante el coeficiente (2,0) se tiene la conductividad

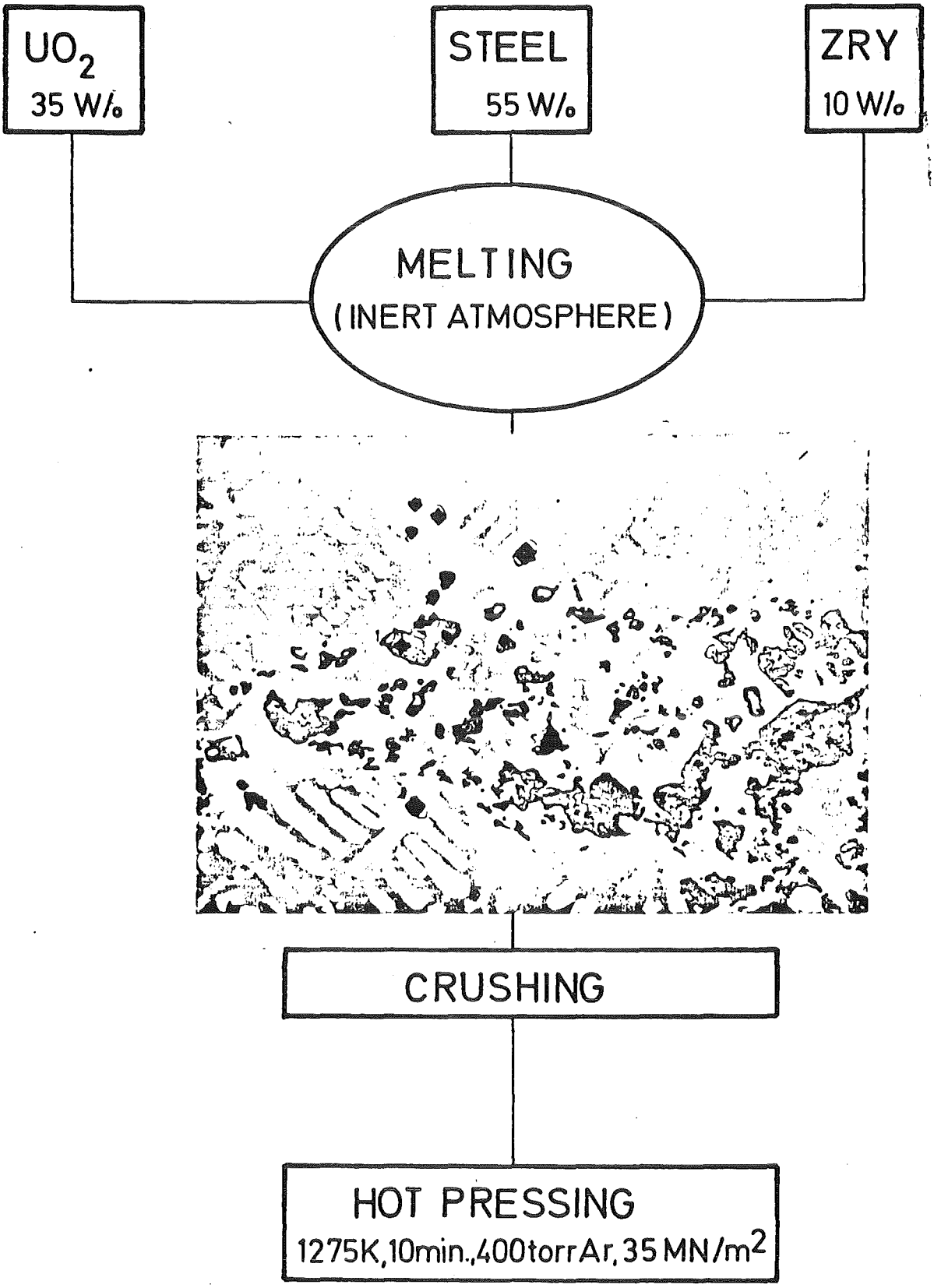

fig. 35: Fabricación de corio EX 1

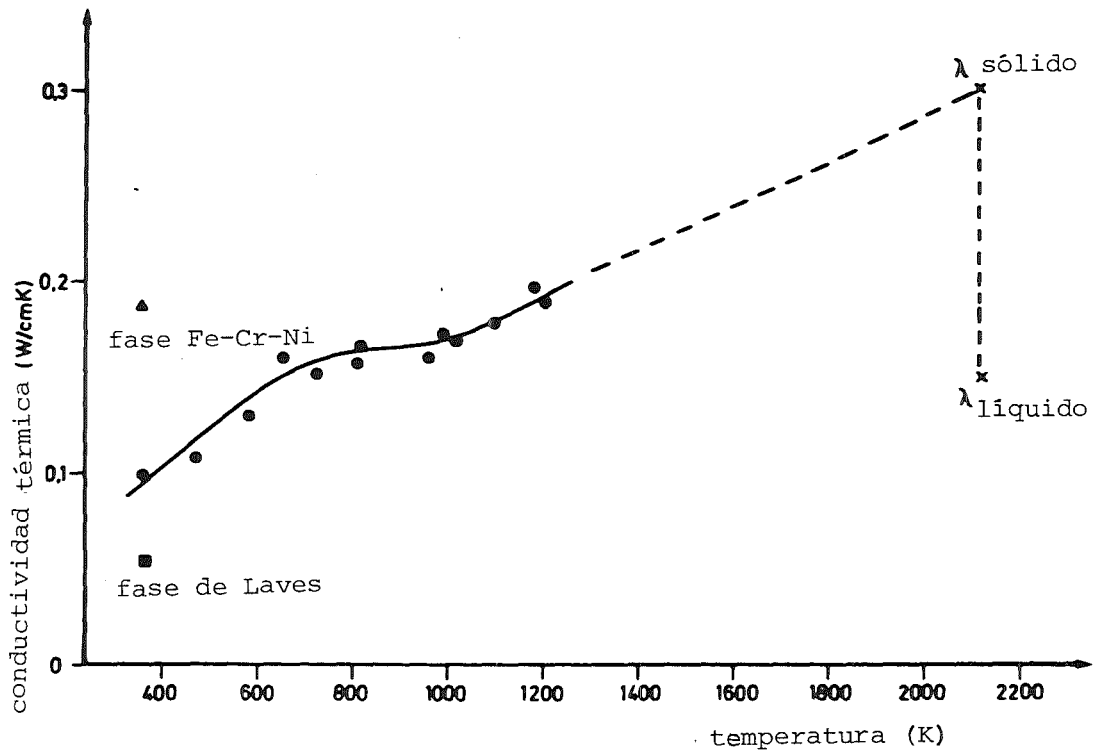

fig. 36: Conductividad térmica del corio EX 1

Corium Melt Type		Melting Point (K)	Heat Capacity at the Melting Point (cal/g K) (J/g · K)	Viscosity (cP) (mPa · s)	Thermal Conductivity (at the Melting Point) $\left[\frac{cal}{(cm\ K\ s)}\right]$ $\left(\frac{J}{cm \cdot K \cdot s}\right)$
AX1	Metal phase	~2275	0.085 (0.356)	3.4 (at ~2675 K) 5.4 (at ~2275 K)	
	Oxide phase	~2675	0.071 (0.297)	5.7 (at ~2675 K)	
EX1	Metal phase	~2275	0.129 (0.540)	5.4 (at ~2275 K)	0.049 (0.205)
	Oxide phase				
EX2	Metal phase	~1825	0.146 (0.611)	2.1 (at ~2675 K) 5.4 (at ~1875 K)	0.044 (0.184)
	Oxide phase	~2675	0.080 (0.335)	5.7 (at ~2675 K)	0.008 (0.033)
EX3		~2075	0.202 (0.846)	4.3 (at ~2075 K)	

fig. 37: Propiedades de fases de corio en el estado líquido en sus puntos de fusión

térmica de esta fase en el estado líquido (fig. 37). - La conductividad térmica de la fase de óxido $U_{0,54}Zr_{0,46}O_2$ del corio EX2 en el estado sólido ($\lambda_{sólido} \simeq 0{,}038 \frac{J\ J}{cm\ Ks}$) puede calcularse a partir de las conductividades térmicas de sus componentes UO_2 y ZrO_2 mediante una relación aplicable a cristales mixtos de conductores de fonones. De aquí se tiene con el coeficiente de la conductividad térmica para compuestos iónicos (1,16) en primera aproximación la conductividad térmica indicada en la fig. 37 de la fase de óxido del corio EX2 en el estado líquido.

3.5 Viscosidades del corio

Para la estimación teórica de la viscosidad en el punto de fusión se ha mostrado apropiada la ecuación de Andrade

$$\eta_S = 612 \cdot 10^{-4}\ V_M^{-2/3}\ \sqrt{T_S} \cdot A\ [cP] \qquad (20)$$

(A = peso atómico en g; V_M = volumen molar en cm^3; T_S = punto de fusión en K).

El peso atómico, el volumen molar y el punto de fusión del UO_2 proporcionaban p.ej. la viscosidad de UO_2 para 3123 K con 5,7 cP. Experiencias detalladas han proporcionado con un $UO_{2,03}$ (a la temperatura ambiente) en el punto de fusión una viscosidad de 4,6 cP. Las viscosidades calculadas para fases líquidas de corio están representadas en la fig. 38. En el cálculo se han tomado en cuenta dependencias de temperatura de los metales y el hecho de que caldos del núcleo poseen varios componentes. Entretanto se ha publicado un valor experimental para la fase metálica de un caldo de corio EX2 (6,8 cP), que confirma bien el valor calculado (5,4 cP, ver fig. 37) dentro del margen de los límites de error.

Literatura

Albrecht, H.; Wild, H.
"Investigation of Fission Product Release by Annealing and Melting of LRW Fuel Pins in Air and Steam"
ANS/ENS-Meeting on Reactor Safety Aspects of Fuel Behavior, Sun Valley (Idaho), August(1981)

Alsmeyer, H.; Müller, U.; Reimann, M.
"Wärmeübergang von Flüssigkeiten an abschmelzenden oder sublimierenden Körpern"
Chem.Ing.Techn. 54 (1982) 2

Bundesministerium für Forschung und Technologie (Auftraggeber)
"Deutsche Risikostudie - Kernkraftwerke"
Verlag TÜV Rheinland Köln. (1979)

Bunz, H.; Koyro, M.; Schöck, W.
"NAUA-Mod 3: Ein Computerprogramm zur Beschreibung des Aerosolverhaltens in kondensierender Atmosphäre"
KfK-Bericht 3154 (1981)

Eyink, J.
"Untersuchungen des Kernschmelzenunfalls unter Berücksichtigung des aktuellen radiologischen Kenntnisstandes"
BMI, Förderungsvorhaben SR 229 (1982)

Hagen S. et al.
"Phenomena and Material Behavior during Melt Down of PWR Fuel Rods"
Specialists Meeting on the Behavior of Water Reactor Fuel Elements under Accidents Conditions, Norway-Spatind (1976)

Hassmann, K.; Reimann, M.
"Analyses of Hypothetical Core Melt Down Accidents"
ANS/ENS-Meeting on Reactor Safety Aspects of Fuel Beahvior, Sun Valley (Idaho), August (1981)

Hennies, H.-H.; Hosemann, J.P.; Mayinger, F.
"Ablauf und Konsequenzen eines DRW-Kernschmelzenunfalls"
Atomwirtschaft 26 (1981), 3

Holleck,H.; Nazaré, S.; Ondracek, G.; Skokan, A.
"LWR Core Melt Down Accident - A Materials Viewpoint"
Topical Meeting on Thermal Reactor Safety
Sun Valley (Idaho), August (1977)

Hosemann, J.P.
"Wechselwirkungen mit der Containmentstruktur und Spaltproduktfreisetzung beim Kernschmelzenunfall"
Jahrestagung Kerntechnik '82, Mannheim, Mai 1982
Atomwirtschaft 27 (1982), 10

Klöckner, F. et al.
"Berechnungen zum Coreschmelzen unter vollem Primärkreisinnendruck"
BMFT, Förderungsvorhaben FB 150 387, März (1980)

Mayinger, F.; Jahn, M.; Reineke, H.; Steinberner, U.
"Numerische Berechnung der thermohydraulischen Vorgänge in einer Kernschmelze"
BMFT, Förderungsvorhaben RS 48/1, Abschlußbericht (1974)

Nazaré, S.; Ondracek, G.; Schulz, B.
"Property Determination of Corium"
nuclear technology 32 (1977), 239

Nikolopoulos, P,; Ondracek, G.
"Bestimmung der Dichten in Kernschmelzen"
atomwirtschaft - atomtechnik XXVI/12 (1981) 661

Nikolopoulos, P.; Ondracek, G.
"Interfacial Energies between UO_2 and Liquid Metals"
J. Nucl. Mat. 98 (1981) 306
Z. Werkstofftechnik 13 (1982) 60

Peehs, M.; Hassmann, K.; Hagen, S.
"Analysis of Hypothetical Core Melt Down Accident of a Pressurized Water Reactor"
Siemens Forschungs- und Entwicklungsberichte 8 (1979), 2

Peehs, M.; Skokan, A.; Reimann, M.
"The Behavior of Concrete in Contact with Molten Corium in the Case of a Hypothetical Core Melt Accident"
Nuclear Technology 46 (1979), 2

Perinic, D.; Mack, A.
"Entwicklung der Versuchsanlage BETA zur Untersuchung der Schmelze/Beton-Wechselwirkung"
KfK-Bericht 2572 (1979) und Jahrestagung Kerntechnik Mannheim, Mai (1982)

Rasmussen, N.C.
"Reactor Safety - An Assessment of Accident Risks in US Commercial Nuclear Power Plants"
USNRC, WASH-1400 (NUREG-75/014), Oktober (1975)

Reimann, M.; Hassmann, K.
"Analyse des Ablaufs hypothetischer Kernschmelzenunfälle" in PNS-Jahreskolloquium 1980, KfK-Bericht 3070, (1981)

Reimann, M.; Murfin, W.B.
"The WECHSL-Code: A Computer Programm for the Interaction of a Core Melt with Concrete"
KfK-Bericht 2890, (1981)

Schöck, W.; Bunz, H.; Kyoro, M.
"Messungen der Wasserdampfkondensation an Aerosolen unter LWR-unfalltypischen Bedingungen"
KfK-Bericht 3153, (1981)

Skokan, A.; Holleck, H.; Peehs, M.
"Chemical Reactions between Core Melt and Concrete and their Effects on the Course and Consequences of a Hypothetical Core Melt-Down Accident"
Nuclear Technology, 46 (1979), 2

Smidt, D.
"Reaktorsicherheitstechnik"
Springer-Verlag,(1979)

Snyder, A.Wm.
"A Current Perspective on the Risk Significance of Steam Explosions"
Jahrestagung Kerntechnik '82, Mannheim, Mai (1982)